# Structure-Function Studies on Type II $Na^+/P_i$ Cotransporters using Electrophysiological and Real Time Fluorometric Assays

**Dissertation**

**zur**

**Erlangung der naturwissenschaftlichen Doktorwürde**

**(Dr. sc. nat.)**

**vorgelegt der**

**Mathematisch-naturwissenschaftlichen Fakultät**

**der**

**Universität Zürich**


**von**

**Chiara Ghezzi**

**aus**

**Italien**


**Promotionskomitee**

**PD. Dr. Ian Forster**

**Prof. Dr. Heini Murer**

**Prof. Dr. Bruno Stieger**

**Prof. Dr. Gerhard Burckhardt**

**Zürich, 2011**

# TABLE OF CONTENTS

# SUMMARY

Reabsorption of inorganic phosphate ($P_i$) is mediated by secondary-active $P_i$ cotransporters that catalyzes uphill $P_i$ transport using the $Na^+$ electrochemical gradient. In mammalian cells, three isoforms of the so-called type II cotransporters are presently known: NaPi-IIa and NaPi-IIc, expressed at the brush border membrane of renal proximal tubules, and NaPi-IIb, expressed mainly in the intestine, lung, testis and liver. All three isoforms preferentially transport divalent $P_i$ ($HPO_4^{2-}$). NaPi-IIa/b are electrogenic with a $Na^+$:$P_i$ stoichiometry of 3:1, which results in the translocation of one net positive charge per transport cycle. NaPi-IIc has a $Na^+$:$P_i$ stoichiometry of 2:1; it is electroneutral and mutations in the gene have been directly associated with an hereditary disease: hypophosphatemic rickets with hypercalciuria (HHRH).

All NaPi-II proteins are assumed to be functional monomers and the current secondary structure model of the protein comprises 12 transmembrane domains; both C- and N- termini are localized intracellularly and a large extracellular loop separates the protein into two halves. The 3-D structure of NaPi-II proteins has not been determined due to the lack of a crystallographic structure, so our structural information relies solely on the application of indirect structure-function methods such as the substituted cysteine accessibility method (SCAM) and voltage clamp fluorometry (VCF). The rational of VCF is that a protein can be labeled at a particular position using a fluorophore. The fluorescence emitted by the fluorophore depends on its micro-environment so that a change in the fluorescence, induced by changes in membrane voltage or substrate concentration, reflects local conformational changes in the protein. This technique can be used to study the putative conformational changes that occur in the protein during the transport cycle.

The first study reported in this thesis focuses on the electroneutral NaPi-IIc and the determination of its substrate binding order. The 2:1 $Na^+$: $HPO_4^-$ stoichiometry observed for NaPi-IIc would suggest that it lacks one of the three $Na^+$ interactions proposed for NaPi-IIa/IIb. However, direct experimental evidence to support this conclusion was lacking.

Moreover, only limited kinetic information (apparent substrate affinities) was available and, in particular, the substrate binding order was not definitively established. We therefore addressed these issues first by determining the substrate binding order using traditional tracer uptake and efflux methods and second by using the VCF technique to study

putative conformational changes during substrate interactions on individual *X. laevis* oocytes. Unexpectedly, we show that also in the electroneutral NaPi-IIc the three $Na^+$ binding sites are present. Two of these sites are fully functional and contribute to the stoichiometry of 2:1, whereas one $Na^+$ ion is proposed to interact with the protein, but is not released inside the cell. On the basis of our results we cannot conclude if the interaction of this $Na^+$ necessary for the binding of the other substrates, but they do strongly suggest that the same interaction sites are conserved for electrogenic and electroneutral proteins. Moreover, this demonstrates, as already observed for other transporters, that the transport stoichiometry is not necessarily equal substrate binding stoichiometry.

The second study focuses on a common structural feature of all members of the NaPi-II family . Analysis of the primary sequence of NaPi-II proteins has shown the existence of regions with a high level of sequence similarity. These are believed to form two re-entrant loops that were proposed to be involved in translocation of both $Na^+$ and $P_i$. The recent crystallization of other $Na^+$-coupled co-transporters as led to the identification of an analogous common structural feature, namely a two-fold symmetry that allows interaction of substrates from either side of the membrane, in accord with the commonly accepted alternating access model for carrier-mediated transport. The presence of re-entrant loops and the observation that the two halves of the protein can move in a symmetrical way suggests that the same structural arrangement is also maintained in NaPi-II. To demonstrate localized interactions between the two re-entrant loops we introduced novel cysteines in the two regions and monitored conformational changes in the protein using VCF. The observation that fluorescence behaviour of the double mutants is different from that of the single mutant suggests a localized interaction between the two re-entrant loops. This localized interaction was further confirmed by using cross-linking reagents that promote the formation of a disulphide bridge between the novel cysteines. Treatment of the double mutant with these substances resulted in a decrease of $P_i$-induced current that it is not observed with the wild-type (WT) protein, or single mutants and indicates that the conformational changes associate with the translocation of the substrate are blocked.

# ZUSAMMENFASSUNG

Die Rückresorption von anorganischem Phosphat ($P_i$) erfolgt durch sekundär-aktive $P_i$ Cotransporter. Diese katalysieren den Transport von $P_i$ gegen dessen Konzentrationsgradienten indem sie den $Na^+$-elektrochemischen Gradienten nutzen. In Säugetierzellen sind bisher drei Isoformen der sogenannten Typ II Cotransporter bekannt: NaPi-IIa und NaPi-IIc, welche in der Bürstensaummembran der proximalen Tubuli der Niere expremiert werden, und NaPi-IIb, welches hauptsächlich in Darm, Lunge, Hoden und der Leber expremiert wird. Alle drei Isoformen transportieren bevorzugt divalentes $P_i$ ($HPO_4^{2-}$). NaPi-IIa/b sind elektrogen mit einer $Na^+$:$P_i$ Stöchiometrie von 3:1, was in dem Net-Transport einer positiven Ladung pro Transportzyklus resultiert. NaPi-IIc hat eine $Na^+$:$P_i$ Stöchiometrie von 2:1, ist elektroneutral und Genmutationen wurden direkt mit einer Erbkrankheit assoziiert: hypophosphatische Rachitis mit Hypercalciuria (HHRH).

Alle NaPi-II Proteine sind vermutlich funktionelle Monomere. Das gegenwärtige Sekundärstruktur-Model des Proteins beinhaltet 12 Transmembrandomänen, mit intrazellulären Lokalisation von sowohl C- als auch N-Terminus. Ein grosser extrazellulärer Loop trennt das Protein in zwei Hälften. Die 3D-Struktur von NaPi-II Proteinen wurde aufgrund einer fehlenden kristallographischen Struktur nicht bestimmt. Daher bauen unsere strukturellen Informationen alleinig auf Anwendung indirekter Struktur-Funktionsmethoden wie “substituted cysteine accessibility method” (SCAM) und “voltage clamp” Fluorimetrie (VCF).

VCF ermöglicht es, ein Protein an einer bestimmten Stelle unter Verwendung eines Fluorophores zu markieren. Die Fluoreszenz, welche vom Fluorophor emittiert wird, hängt von dessen Mikroumfeld ab, so dass seine Veränderung der Fluoreszenz, induziert durch Veränderungen der Membranspannung oder Substratkonzentration, lokale Konformationsänderungen im Protein wiederspiegeln. Diese Methode kann verwendet werden um die mutmasslichen konformellen Veränderungen, welche im Protein während des Transportzyklus` stattfinden, zu untersuchen.

Die erste Studie der vorliegenden Dissertation legt seinen Fokus auf den elektroneutralen Transporter NaPi-IIc und die Ermittlung der Reihenfolge in welcher seine Substrate gebunden werden. Die beobachtete 2:1 $Na^+$:$HPO_4^{2-}$ Stöchiometrie von NaPi-IIc würde darauf hindeuten

dass NaPi-IIc eine der drei $Na^+$-Interaktionen, welche für NaPi-IIa/IIb vorgeschlagen wurden, fehlt. Allerdings fehlte bis anhin der direkte experimentelle Beweis um diese Aussage zu unterstreichen. Darüber hinaus standen nur begrenzte kinetische Informationen (apparente Substrataffinitäten) zur Verfügung. Vor allem die Reihenfolge, in welcher die Substrate binden, war nicht endgültig etabliert. Deswegen haben wir diese Punkte untersucht, zuerst durch Bestimmung der Substratbindungsreihenfolge mittels traditionellen Tracer-Aufnahme und Efflux-Methoden, und des weiteren durch Nutzung der VCF-Technik, mit welcher putative konformelle Veränderungen während Substratinteraktionen in individuellen *Xenopus* Oozyten untersucht werden können.

Unerwartenderweise konnten wir zeigen dass auch im elektroneutralen NaPi-IIc die drei $Na^+$ Bindungsstellen vorhanden sind. Zwei dieser Stellen sind komplett funktional und tragen zu der 2:1-Stöchiometrie bei, während vorgeschlagen wird dass ein $Na^+$-Ion mit dem Protein interagiert, aber nicht in die Zelle entlassen wird. Basierend auf unseren Ergebnissen können wir nicht folgern ob die Interaktion dieses $Na^+$ notwendig für die Bindung der anderen Substrate ist, aber sie unterstreichen die Vermutung, dass die gleichen Interaktionsstellen für elektrogene und elektroneutrale Proteine konserviert sind. Darüber hinaus demonstriert dieses Ergebnis dass die Transport-Stöchiometrie und die Substratbindungsstöchiometrie nicht notwendigerweise gleich sind. Dies wurde auch schon für andere Transporter gezeigt.

Der Focus der zweiten Studie lag auf einer allgemeinen Charakterisierung aller Mitglieder der NaPi-II Familie. Eine Primärsequenzanalyse der NaPi-II Proteine zeigte die Existenz von Regionen mit einem hohen Anteil an Sequenz-Similarität. Es wird davon ausgegangen dass diese zwei Wiedereinstiegsloops formen, und es wird vorgeschlagen, dass diese in der Translokation von sowohl $Na^+$ als auch $P_i$ beteiligt sind. Die kürzliche Kristallisierung anderer $Na^+$-gekoppelten Cotransportern führte zu der Identifizierung eines entsprechenden gemeinsamen strukturellen Merkmals, einer zweifachen Symmetrie welche eine Substratinteraktion von beiden Seiten der Membran ermöglicht, was im Einklang mit dem gemeinhin akzeptierten „alternating access“ Model für Carrier-vermittelten Transport steht. Die Existenz von Wiedereinstiegsloops, und die Beobachtung dass die beiden Hälften des Proteins sich auf symmetrische Art und Weise bewegen, könnten darauf hin deuten dass das gleiche strukturelle Arrangement in NaPi-II beibehalten wurde.

Um lokalisierte Interaktionen zwischen den beiden Wiedereinstiegsloops zu zeigen, haben wir neue Cysteine in die zwei Regionen eingeführt und konformelle Veränderungen im

Protein unter Verwendung von VCF aufgenommen. Die Beobachtung, dass sich das Fluoreszenzverhalten der Doppelmutanten von dem der Einfachmutanten unterscheiden lässt, lässt auf eine lokalisierte Interaktion zwischen den beiden Wiedereinstiegsloops schliessen. Diese lokalisierte Interaktion wurde im weiteren durch Verwendung von Querverlinkungs-Reagenzien bestätigt, welche die Bildung von Disulfidbrücken zwischen den neuen Cysteinen fördern. Eine Behandlung der Doppelmutante mit diesen Substanzen führt zu einer Abnahme des $P_i$-induzierten Stromes. Dies konnte weder unter Verwendung des Wildtyp (WT)-Proteins, noch unter Verwendung der Einfachmutanten beobachtet werden. Dadurch konnte gezeigt werden, dass die konformellen Veränderungen die mit der Translokation des Substrates verbunden sind, blockiert sind.

# CHAPTER 1

# INTRODUCTION

## 1.1 Membrane transport proteins

The phospholipids bilayer that surrounds all living cells constitutes a barrier that prevents the movement of ion and polar molecules between the intra- and extracellular compartments. Yet the cell needs to import from the external environment all the substances that are necessary for its survival, i.e. amino acids, sugars, and export toxic substances or products of metabolic pathways. Moreover the selective passage of solutes as well as water across these barriers is an essential requirement to maintain different compartmental ionic compositions and osmotic balance, ensure the regulated movement and signaling molecules between compartments and initiate, maintain or terminate a multitude of essential cellular processes.

Small molecules, like $CO_2$ or $O_2$ can cross the membrane by *simple diffusion* following the concentration gradient, whereas for other molecules cells have developed specific systems to allow their movement.

Transport of inorganic ions and small polar molecules is mediated by specialized integral membrane proteins, which can be classified as *channels* and *carriers*.

The channel class includes pores and ion channels (Fig. 1). *Pores* constitute an aqueous transmembrane conduit that is always open. Typical examples of this sub-class are porins, found in outer membrane of gram-negative bacteria, and aquaporins, that allow the permeation of water or glycerol and are widely distributed throughout all forms of life.

*Ion channels* are next in order of functional complexity. They comprise one or more subunits that assemble to form a highly permeable pathway across the hydrophobic interior of the membrane. Two features distinguished channels from pores: the presence of a gate and a selectivity filter. Channels can exist in two different functional states: closed or open.

The conformational transition from one state to the other is referred to as gating and is controlled by sensors that respond to external factors like changes in membrane potential, second messengers (i.e. $Ca^{++}$), mechanical forces or binding of specific ligands.

When the channel is open, the direction of ion flux is determined by the electrochemical gradient and ion permeation is determined by the presence of selectivity filters as for pores. Ion selectivity filters are usually specific stretch of amino acids (e.g. "TVGYG" sequence found in voltage-gated potassium channels [1]) localized near the extracellular side of the pore. They allow the discrimination between type (anion or cation), size/valency (i.e. $Na^{+}$, $K^{+}$, $Ca^{++}$) and charge of permeant ion.

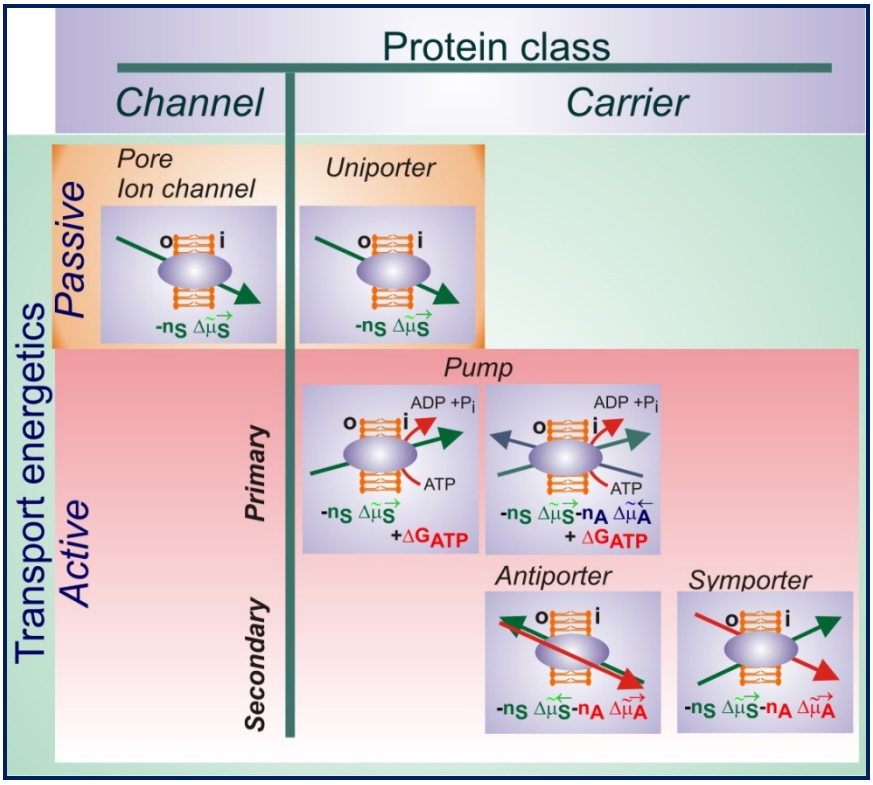


***Figure 1 Classification of membrane transport proteins.***

*Comparison of the two main classes of membrane transport proteins, channels and carriers and the associated energetic constraints for vectorial flux of a solute S (from outside-o to inside –i). (For more details, see Forster 2009).*

*Carriers* differ from channels because they do not offer an open pathway across the membrane. They are considered to cycle between conformational states in which the substrate binding site is accessible either from the extracellular side or the intracellular side of the membrane. At a molecular level this sequence of events includes binding of the solute to the

carrier, occlusion of the bound solute, exposure and release of solute on the other side. The carrier then returns to the initial conformation ready for a new cycle to begin. A second feature that distinguishes carriers from channels is that the former display saturation with the respect of substrate concentration under physiological conditions. This is due to the former having a defined number of binding sites available and displaying slower rates of substrate translocation. Saturation is also observed in ion channels at non-physiological concentrations (e.g. Hille).

The carrier class can be divided into 3 subfamilies (Fig. 2):

- Uniporters: mediate the translocation of a single solute in one direction (i.e. glucose carrier GLUT1);
- Symporters (or cotransporters): bind two or more different solutes and transport them across the membrane in the same direction (i.e. lactose permease or glucose-$Na^+$ symporter);
- Antiporters (or exchangers): exchange one solute for another across the membrane (i.e. ADP/ATP exchanger).

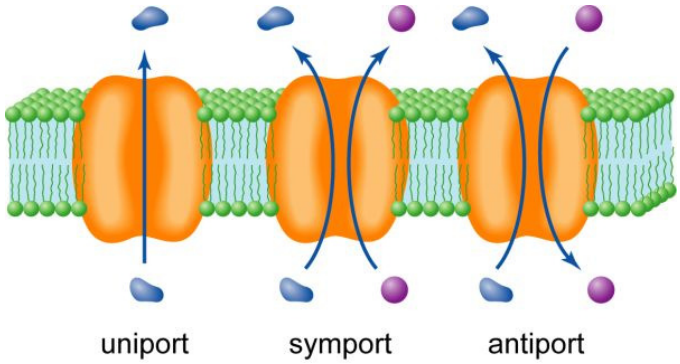


***Figure 2 Uniport, symport and antiport.***

*Schematic representation of the mechanism of translocation of solutes across the membrane for the three subfamilies of the carrier class (* www.uic.edu/.../bios100/lectures/diffusion.htm)

Membrane transport proteins can also be classified on the basis of the energetics of the transport process as passive or active systems (Fig. 1). In *passive* systems substances are moved down the concentration gradient from regions of greater concentration to regions of lower concentration.

In *active* systems such as members of the ATP-binding cassette (ABC) transporter family and ion pumps (ATPases), substances are moved against their electrochemical gradient and therefore can be concentrated. To satisfy thermodynamics, this process requires a source of

energy. In primary active transport, this comes from the hydrolysis of highly energetic pyrophosphate bonds (ATP, GTP). In secondary active transport the free energy provided by the translocation of a solute, mainly $Na^+$ or $H^+$ ions, along its electrochemical gradient is dissipated to promote the translocation of a second solute against its electrochemical gradient. Tertiary active transport combines two secondary active carriers, typically an antiporter and a symporter [2].

## 1.2 The ion channel-cotransporter controversy

Only in 1952, after introduction of the concept of cotransport as the mechanism that employs the electrochemical gradient of specific ions to concentrate specific substrate [3], was a clear distinction between channels and carriers made. The use of different theory to explain the transport activity of the two families, namely electro-diffusion for channels and enzyme theory for carriers, strengthened this distinction further.

The main experimentally observable difference between channels and carriers is the flux rate for the solute moving across the membrane: up to $10^8$ ions $s^{-1}$ in the case of channels and 10-50.000 particles $s^{-1}$ in the case of carriers. The principal reason for this difference is thought to be the rate limiting conformational changes accompanying the substrate translocation across the membrane in transporters and which is absent in channels.

The strict distinction between channel and carrier has become blurred in the last decade with the introduction of high-resolution electrophysiology techniques (such as patch clamp) that demonstrate the existence of channel-like currents also in cotransporters (as discuss below). Many cotransporters characterized exhibit channel-like properties: glutamate and dopamine cotransporters for example can behave like chloride channels [4]; GABA, serotonin and norepinephrine cotransporters behave like sodium and lithium channels [5] [6] [7].

On the other hand, Accardi, Miller, and colleagues showed that ClC-ec1, a membrane protein predicted to be a $Cl^-$ channel [8], is actually a $Cl^-/H^+$ exchanger [9] with a stoichiometry of $1H^+$:$2Cl^-$. Moreover, by making one mutation, the coupling to protons could be removed, leaving the basic channel behavior intact [10].

The significance of channel-like behavior in transporters is not yet completely understood but the existence of channels in transporters has implication for the therapeutic modulation of these molecules. For example the modulation of channel-like activity may provide an alternative therapeutic route to alleviate transport-associated disease conditions [11].

Taken together, these findings have therefore blurred the distinction between channels and carriers [3] and the obvious consequence is the necessity of revision the classical view with a less rigid distinction between the two families.

## 1.3 The SLC classification

Following the development of the expression cloning approach for transporters, numerous carrier proteins have been identified. The subsequent sequencing of multiple genomes and the establishment of the expressed sequence tag (EST) approach, have further facilitated the identification and characterization of many additional transporter families. The increasing number of proteins identified led the Human Genome Organization (HUGO) to propose the SLC (SoLute Carrier) gene nomenclature in 2004 with the aim of standardizing the names of the genes encoding carrier

It is generally assumed that at least 5% of the human genes are transporter-related, consistent with the biological significance of transporters and their roles in cellular homeostasis. The SLC subfamily represent the major part of these genes whereas the "non-SLC" human transporter-related genes include those encoding ATP-driven transporters, channels, ionotropic receptors, aquaporins, channels subunits, auxiliary/regulatory transport proteins, etc. [12].

The SLC super-family includes approximately 350 genes that code for different membrane carriers and that are further subdivided in 48 families based on the molecule that the proteins can transport (Fig. 3). According to this classification, a transporter is assigned to a specific SLC family if it has at least 20-25% amino acid sequence identity to other members of that family. A complete list of the SLC transporter protein families is available on the web site http://www.gene.ucl.ac.uk/nomenclature/.

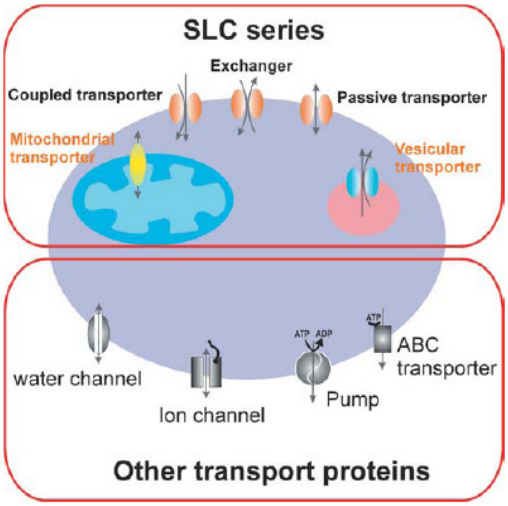


***Figure 3. The SLC family.***

*Cartoon showing a cell with solute carrier (SLC) and non-SLC transporters expressed in the plasma membrane or in intracellular compartments membrane [12] .*

The SLC proteins studied in this thesis are proteins belonging to the SLC34 gene family that codes for type II $Na^+$-dependent phosphate cotransporters (or NaPi-II). Since they promote the translocation of inorganic phosphate ($P_i$) inside the cell using the prevailing $Na^+$ gradient, according to the classification of membrane protein given above, they are secondary active members of the carrier class.

## 1.4 Functional characterization of carrier proteins

The most useful approach to study a secondary active transporter is to overexpress the protein in a convenient system that allows its study without significant contamination from endogenous membrane proteins.

Oocytes from the African frog *Xenopus laevis* represent one of the most widely used expression system for functional characterization of ion channels, receptors and transporters because [13]:

- they can be easily prepared and easily handled-a consequence of their large diameter of 1.1-1.3 mm;
- they express all the machinery necessary to efficiently translate proteins;
- they express only a small number of endogenous transport systems that gives a very low background compared to the heterologously expressed proteins;

- the high density of transporters in the cell membranes facilitates measurement of transport function that might be otherwise much lower in native tissue.

Overexpression of the transporters has given the possibility of extending the number of technical approaches, improving the quantity and the quality of experimental observations. Particular significant in this respect has been the possibility of using electrophysiological methods in the case of electrogenic processes. The most widely used techniques applied to study channels and electrogenic transporters at a functional level are patch clamp and two electrode voltage clamp (TEVC).

The TEVC (see Fig.4 for a scheme) allows the measurement of whole cell currents in response to change in membrane voltage or substrate. It uses two microelectrodes, one for recording the transmembrane voltage and one for passing current. The recorded membrane voltage is compared to the desired (command) voltage and a compensating current is automatically injected into the cell by an electronic feedback system.

A net charge movement across the membrane due to the collective activity of the transport proteins normally lead to a change in membrane potential. However, under voltage clamp conditions, the negative feedback system continuously injects a current into the oocyte that compensates this charge movement to keep the membrane potential at the desired value.

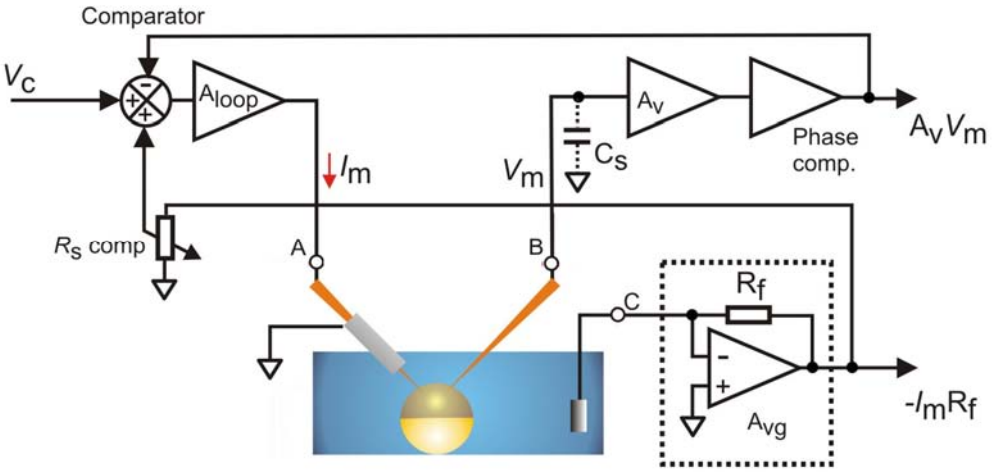


***Figure 4. A simplified scheme of a two-electrode voltage clamp (TEVC)***

*Schematization of a TEVC set-up. Membrane voltage is measured by the voltage electrode and compared to the command voltage($V_c$ ). This value is kept constant at the desired value by adjusting the current injected into the oocyte via the current electrode.*

Expression of the first cloned transporters in *X. laevis* oocytes and the investigation of their properties through electrophysiology have shown the existence of common features between transporters with different tissue localization and substrate specificity. In particular all electrogenic cotransporters, with some exceptions, are characterized by the presence of three currents: (i) transport-induced current, (ii) leak current and (iii) pre-steady state currents. The majority of the carriers, like the GABA transporter (GAT1) [14], the sodium-coupled glucose cotransporters (SGLT1) [15] or the type II $Na^+$ dependent Pi cotransporters (NaPi-II) [16], show, depending on extracellular solution conditions, all three currents. Other cotransporters appear to lack one or two of these components. For example the glycine transporter, GlyT1, shows only transport and pre-steady state current [17] [18] [19] [20] or the type III $Na^+$ dependent $P_i$ cotransporters Pit2 shows only transport current [21]. This may reflect the limitations of the TEVC measurement technique, or fundamentally different substrate translocation mechanisms.

*Transport related currents* (or steady-state currents) are recorded in presence of the specific substrate and the co-ions and are measured as a deflection from the baseline condition when membrane potential is clamped at a constant value (typically -50/-60 mV).
Their magnitude generally depends on membrane potential and substrate concentrations and can be measured in response to different intracellular or extracellular conditions (i.e. different substrates concentration, pH, membrane voltage or temperature).
Transport currents measured at each voltage can be plotted as a function of the membrane potential to obtain current-voltage (I-V) curves (Fig. 5) that allow the comparison of voltage dependence of kinetic properties of different proteins (i.e WT vs. mutant protein).
Manipulation of substrate concentrations over a wide range is useful to obtain information regarding substrate binding mechanism and substrate binding order. Fitting of the data with appropriate equations derived from enzyme kinetics allows determination of phenomenological parameters such as apparent substrate affinity ($K_{0.5}$), Hill coefficient (a measure of cooperativity of binding in case of multiple substrate interactions) and maximum transport rates. These parameters can be used as “kinetic” indices to compare different isoforms of a given carrier or compare the behavior of carrier mutants with that of the wild type protein.

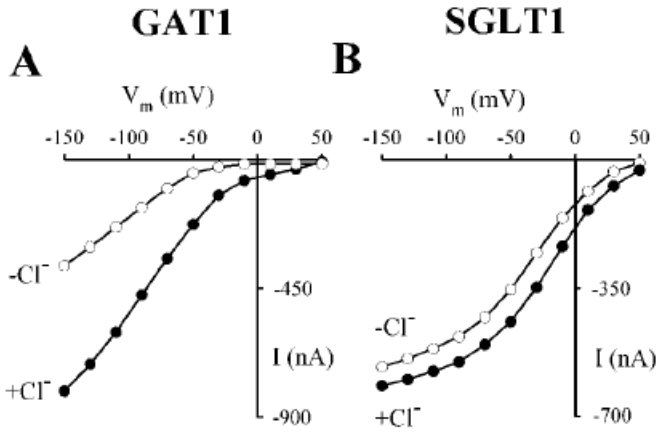


***Figure 5. Transport associated current in GAT1 and SGLT1.***
*Typical I-V data recorded from oocytes injected with GAT1 (A) or SGLT1 (B) in presence (full circles) or absence (empty circles) of chloride in the extracellular solution. The two proteins show a different voltage and substrate dependences. [22].*

*Presteady-state currents* are observed in almost all electrogenic co-transporters indicating that they are a distinctive feature of these proteins and their analysis has provided important clues to understanding the transport mechanism. Presteady-state currents are observed in response to rapid change of membrane potential and represent non-linear intramembrane charge movements. They can arise from two mechanisms that are not mutually exclusive:

- rearrangement of a charged or polar residues of the protein in the membrane field [23],[24];
- movement of ions that shuttle back and forth between the external solution and the open vestibule in the transporter facing the extracellular side [23], [25]

For some transporters, like SGLT1, a model has been proposed in which the charge movement is mainly determined by rearrangements in the protein [24] whereas for others, like rGAT1 [25], the movement of ions between extracellular space and the vestibule of the protein is the main contributor to charge movement.

The time integral of transient current represents the amount of charge that moves in the membrane electric field in response to the voltage change and it has been observed that the amount of charge moved in one direction when stepping the potential from a holding level ($V_h$) to the new value is equal to that moved in the opposite direction when the voltage is

returned back to $V_h$. The Q-V relationship that is obtained (e.g. Fig. 6) shows the amount of charge displaced as a function of membrane potential. This can be fitted using the Boltzmann equation to estimate the total charge movement (obtained from the hyper- and hypo-polarizing limits) and apparent valency (obtained from the maximum slope of the fitted function).

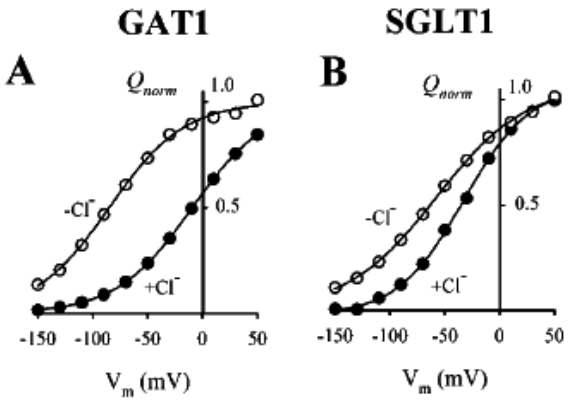


***Figure 6. Presteady-states currents in GAT1 and SGLT1.***

*Q-V curves obtained for GAT1 (A) and SGLT1 (B) integrating the presteady-state currents recorded at different membrane potentials. As observed for the transport associated curves, Q-V data are dependent on the composition of the extracellular solution [22].*

*Leak currents (or uncoupled currents)* represent a deviation from the tightly coupled electrogenic behavior and the strict dependence on the presence of both substrate and co-ions expected for ideal cotransporters. They appear to be quite ubiquitous and can be sub-classified in transport-dependent and transport-independent uncoupled currents.

Transport-dependent uncoupled currents are observed in presence of the substrate and the co-ions and manifest themselves as current in excess of those associated with the stoichiometric charge translocation.

Transport-independent uncoupled currents are observed in absence of the substrate and sometimes require the application of specific blockers to be characterized with any confidence, particularly as they are generally comparable in magnitude to endogenous oocyte currents.

## 1.5 Structural characterization of carrier proteins

The more direct way to obtain information about protein structure is to purify the protein, crystallize it and determine three-dimensional structure via X-ray diffraction. The aim of

protein crystallization is, therefore, to produce well-ordered protein mono-crystals without any inclusions and sufficiently large to diffract X-Ray beam.

For some time crystallization of transporter proteins has been a challenge because certain technical issues needed to be overcome. In particular, an intrinsic property of all membrane proteins is that they comprise hydrophobic and hydrophilic regions, which means that they are insoluble in aqueous buffer but they can be denatured in organic solvents. The consequence of this property is that it is more difficult to obtain sufficient purified protein necessary to grow diffracting crystals, compared with soluble proteins.

Two key breakthroughs toward the understanding of structural arrangement of membrane transport system were: (i) crystallization of potassium channel [1] in 1998 that proved the feasibility of the method for the studying of membrane proteins (ii) crystallization of the first secondary active transporter in 2002, the proton-driven multridrug efflux pump AcrB of the resistance nodulation cell division (RND) family from *Escherichia coli* [26].

Since then, a number of different transporters have been crystallized, see Table 1 for a summary, and the comparison of the structure of transporters with a different substrate specificity have, in particular, revealed the presence of a common membrane folding characterized by an internal two fold symmetry and discontinuous membrane helices.

| Protein | Family | Organism | Transport mechanism | Reference |
|---|---|---|---|---|
| Glycerol-3-phosphate/phosphate antiporter **GlpT** | Major Facilitator Superfamily (MFS) | *E.coli* | Exchanger | Huang Y 2003 |
| Proton coupled Lactose symporter **LacY** | Major Facilitator Superfamily (MFS) | *E.coli* | Cotransporter | Abramson J 2003 |
| Aspartate transporter **GltPh** | Glutamate transporter family | *P.H* | Cotransporter | Yernool D 2004 |
| $Na^+/H^+$ antiporter **NhaA** | NhaA family | *E.coli* | Antiporter | Hunte C 2005 |
| Leucine transporter **LeuT** | Neurotransmitter: sodium symporter (NSS) | *E.coli* | Cotransporter | Yamashita A. 2005 |
| Na(+)/galactose cotransporter **SGLT** | Solute:sodium symporter (SSS) | *V. parahaemolyticus* | Cotransporter | Faham S. 2008 |
| benzyl-hydabtion transporter **Mhp1** | Nucleobase:cation symporter | *M. liquefaciens* | Cotransporter | Weyand S 2008 |

***Table 1. Summary of relevant membrane transport proteins crystallized***

The glycerol-3-phosphate transporter, GltPh, is an antiporter that mediates the exchange of glycerol-3-phosphate for inorganic phosphate across the membrane. It belongs to the major facilitator superfamily that represents the largest group of secondary active membrane transporters in prokaryotic and eukaryotic cells.

GltPh was crystallized in the absence of its substrate and it was shown that the N- and C-terminal domains exhibit a presudo 2 fold symmetry along an axis perpendicular to the membrane (Fig. 7). Eight of the twelve transmembrane α-helices are arranged around a centrally located substrate translocation pore that is closed off at the periplasmic surface and the two harpin loops HP1 and HP2 may undergo alternating symmetry-related motions that open and close access to the substrate and ion binding sites [27].

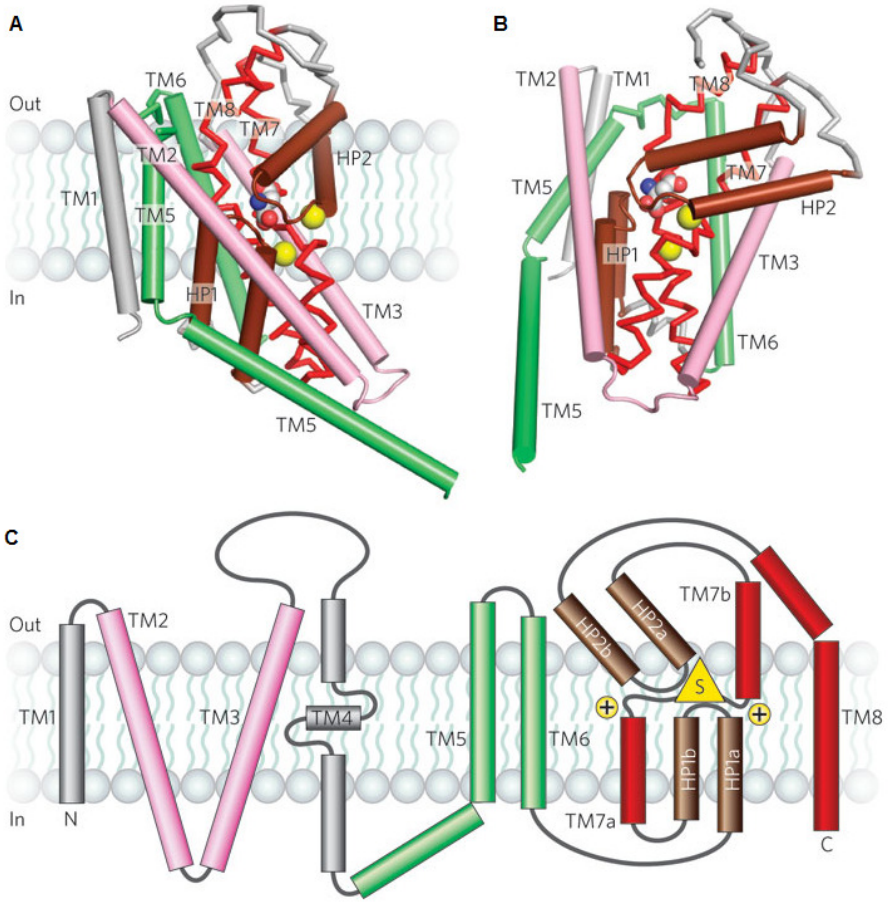


***Figure 7 Structure of the GltPh protein***.

*A) View parallel to the membrane of one subunit of the GltPh trimer. The core transmembrane helices of GltPh are shown, illustrating how the first six transmembrane segments surround the elements of the transporter machinery. The re-entrant hairpins (HP1 and HP2) .B) The same elements as viewed approximately perpendicular to the membrane. The bound substrates (carbon, grey; oxygen, red; nitrogen, blue) and sodium ions (yellow) are shown. C) Topology for GltPh with substrate and ions depicted as yellow triangle and circles respectively [28].*

The bacterial leucine transporter, LeuT, is one of the transporters that translocates amino acids in and out of bacterial cells and it is specialized in particular in the transport of small hydrophobic amino acids such as leucine and alanine. The transport is energized by the $Na^+$ ion gradient.

The 3-D structure of this protein has revealed that , even though LeuT shows a different fold from GltPh, it is possible to identify an internal two-fold-pseudo-symmetry axis running parallel to the membrane plane that related the first five transmembrane helices (TM1-TM5) to the second five helices (TM6-TM10) [29] (Fig.8).

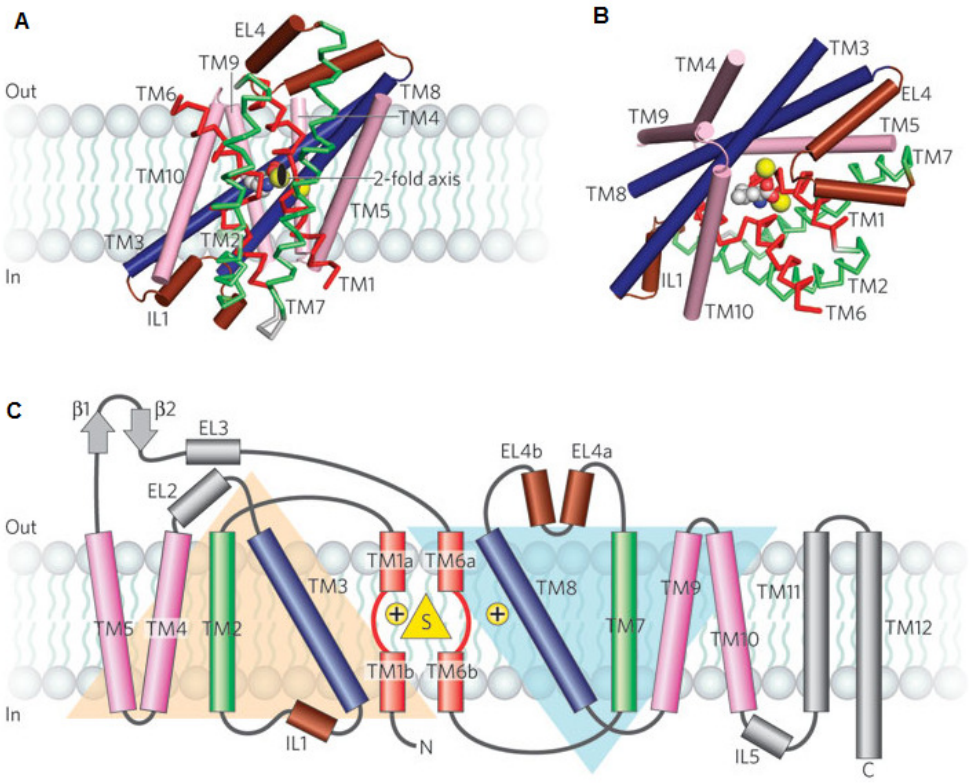


***Figure 8. Structure of LeuT protein.***

*A) View of the core 5+5 repeat structure for LeuT. Re-entrant, pseudo-two-fold related loops that either partly (EL4) or fully (IL1) occlude central binding sites are shown in brown. View is parallel to the membrane, B) View approximately perpendicular to the membrane, C) Topology diagram for LeuT with substrate and ions depicted as yellow triangle and yellow circles, respectively. The large beige and blue triangles overlap the five helix repeats related by the pseudo-two-fold axis of symmetry [28].*

Even more surprisingly, the fold observed for LeuT has been found in the subsequently reported structure of the galactose transporter vSGLT of the solute:sodium symporter (SSS) [30] family and of the benzyl-hydabtion transporter Mhp1 of the nucleobase:cation symporter [31].

Both vSGLT (Fig. 9) and Mhp1 contain the "5+5" inverted structural symmetry motif even though these transporters do not share significant amino acid sequence identity or have the same number of transport segment. The direct consequence of these observations is the hypothesis that secondary active transporters previously believed to belong to distinct

families, may also have LeuT-like folds and that different transporters can share common mechanism of transport (i.e. binding of substrates, conformational changes associated with the transport) [28].

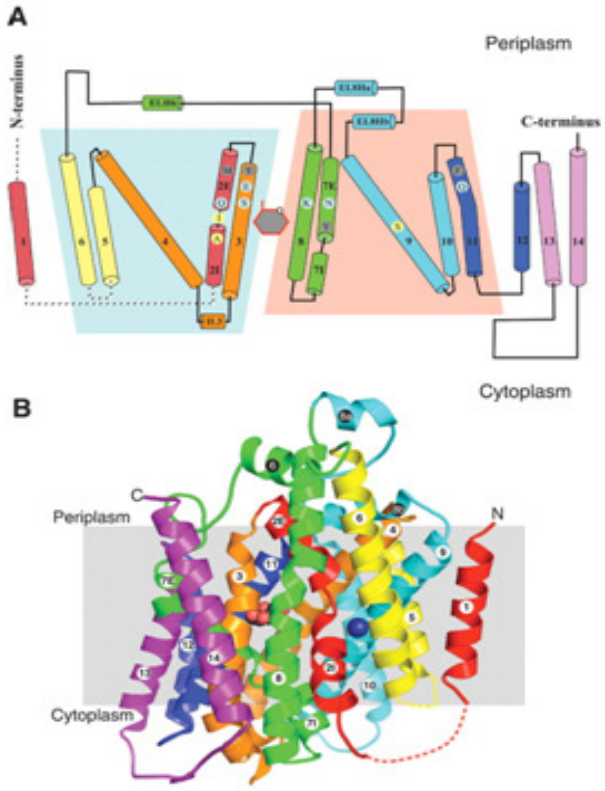


***Figure 9. Structure of vSGLT.***

*A) Topology model of vSGLT. The blue and red trapeziums represent the inverted topology of TM2 to TM6 and TM7 to TM11. The gray hexagon with red trim represents the galactose. Residues involved in sugar recognition, gate residues, and a proposed $Na^+$ site are shown in cyan, gray, and yellow circles. (B) Structure viewed in the membrane plane. The coloring scheme and numbering of α-helices is the same as in part A. Bound galactose is shown as black and red spheres for the C and O atoms. The proposed $Na^+$ ion is colored as a blue sphere. [30]*

The structures described above showed, moreover, that the two semi-halves of the protein define a central translocation pathway that contains the binding sites for substrate and ions. In particular, interruptions in the helical conformation seems to have a key role in the formation of the substrate binding sites. These interruptions exposes main-chain hydrogen-bounding partners and orient the helical dipoles to create a polar environment for coordinating substrate and ions within the lipid bilayer [29].

## 1.6 Structure-function studies

Despite the improvements of the crystallization technique, a large number of transporters remain to be crystallized. Moreover, to correlate the structure of a protein with its function is necessary to solve its structure in different conformational states but this is not always possible due for example to higher instability of certain conformations.

To obtain more information about structure of the proteins and correlate it to the mechanism by which they work, it is possible to take advantage of the specific molecular biology techniques. Generally point mutations are introduced in the protein and the effect is analyzed at a functional level. Two approaches that have become particularly useful to understand conformational changes in the protein are the substituted cysteine accessibility method and voltage clamp fluorometry.

The substituted cysteine accessibility method (SCAM) [32] has been widely used to map extracellularly or intracellularly accessible sites or to identify membrane-spanning segments that line the binding site crevice. To perform SCAM, residues are mutate one at a time to a cysteine. The mutant protein is then expressed in an heterologous expression system and assessed to determine if the Cys residues react with bulky thiol reagents such as metanethiosulfonate (MTS) compounds. This can be done biochemically (e.g. using MTS biotin) or functionally (assuming functionally important sites are labeled). In many cases the reaction of the engineered Cys with a sulfhydryl reagent in the binding-site crevice results in the alteration of the substrate binding thus the effect is visible as alteration in the transport associate current so that the MTS-Cys reaction can be observed in real time.

The validity of this approach is based in two important assumptions: (i) the site of perturbation coincides with the site of functional importance even though allosteric and structural artifacts due to the mutation itself and/or thiol binding cannot be easily excluded; (ii) free native cysteines do not become accessible as a result of mutagenesis, giving rise to a false positive result.

MTS based reagents can be selected by size, membrane permeability and superficial charge therefore using SCAM we can not only determine (i) if a site is functionally important but also (ii) if it is accessible and the extent of accessibility depending on the conformational state of the protein as well as (iii) the potential functional importance of the native residue for the transport cycle.

In the particular case of residues involved in substrate translocation it is possible to follow in real time the loss of activity of transport current, by keeping MTS concentration constant and applying the reagent for a known period.

The modification of the cysteine by the MTS reagent can be described in terms of a 3 state scheme (Fig. 10) and if the MTS reagents are used in excess this can be simplified to a pseudo 1$^{st}$ order reaction from which an effective order rate constant is obtained by fitting the data with a single decaying exponential function [32]. By keeping the assay conditions constant (i.e. concentration of MTS, membrane voltage), it is therefore possible to compare the accessibility of different residues and to create an "accessibility map". For example on the basis of periodicity in the accessibility is possible to obtain information about secondary structure such as the existence of α-helices or β-sheets. Moreover changing incubation condition, for example comparing the reaction rate in the presence or the absence of substrate, allow to assays for conformational changes occurring in the protein [32] [33].

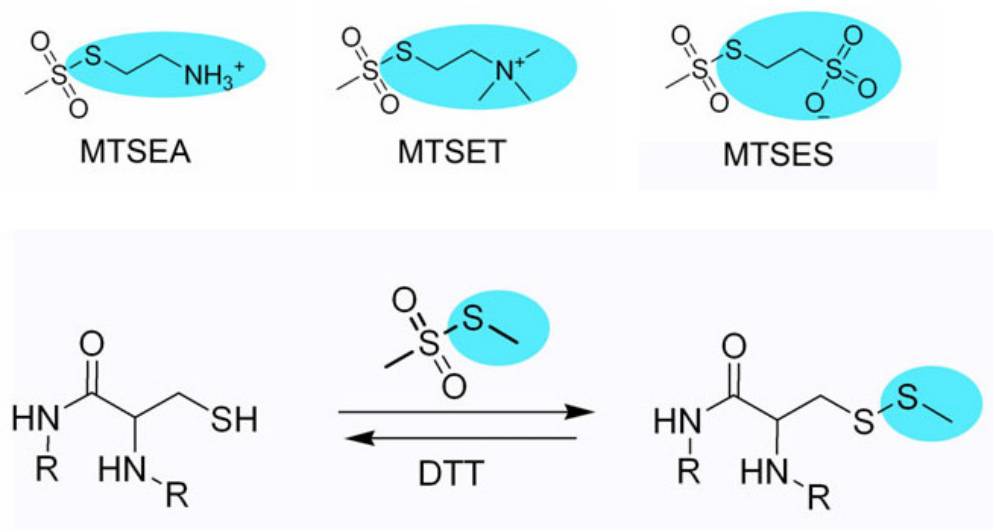


***Figure 10. Schematization of the mechanism of action of MTS reagents.***

*The side chain of a cysteine can interact with the sulfidryl group of the methanethiosulfonate (MTS) reagent and this lead to the formation of the disulphide bridge. The process can be broken using DTT reagents. The molecular structure of different MTS reagent is shown in the upper part of the figure (MJansen.ionchannels.googlepages.com).MTSEA: 2-aminoethyl MTS hydrobromide, MTSET: (2-(trimethylammonium)ethyl MTS bromide and MTSES: (sodium (2-sulfonatoethyl).*

The second approach that can be used to link structure of the protein to its function is voltage clamp fluorometry (VCF). This technique was developed by Isacoff and colleagues to study conformational rearrangement associated with potassium channels gating [34].

For the case of the *Xenopus* oocyte preparation, VCF usually combines the two electrode voltage clamp with fluorescence measurements to detect conformational changes at a local level. As already mentioned analysis of the presteady-state currents represents an indirect measure of voltage dependent conformational changes in the protein. One potential problem with the interpretation of presteady-state data is that the currents arise from many mobile charges distributed throughout the protein so we can obtain information only on global molecular rearrangements. This limitation is overcome by VCF that allows real-time recording of fluorescence changes of a fluorophore covalently attached to a selected site in the protein.

The rational of the technique is that the fluorescence emitted by the attached fluorophore is influenced by its local environment. Changes in substrate concentration in the extracellular solution or in membrane potential generally trigger conformational changes in the protein that will be reported by change in the fluorescence.

Different mechanisms have been proposed to explain the change in emitted fluorescence. For example, a change in fluorescence intensity can be due to: i) re-orientation of the fluorophore's transition dipole, ii) shift in the excitation spectrum of the dye can lead to changes in absorption at a particular excitation wavelengths and a corresponding change in emission, iii) changes in the hydrophobicity of the fluorophore's environment, iv) interaction with nearby protein residues that can quench the fluorophore [35].

To monitor local conformational changes it is necessary to label a specific site with the fluorophore (Fig. 11). Therefore the first step is the introduction of a point mutation in specific region of the protein. Since a variety of fluorophores are available for covalent linking between thiol groups generally is introduced a novel cysteine. As for SCAM, is moreover necessary that none of the native cysteine is accessible to the labeling with the fluorophore. Once the protein is labeled at the specific site of interest, emitted fluorescence is monitored in response to changes in membrane potentials or substrate concentration in the extracellular solution.

In contrast to presteady-state analysis, fluorescence changes can be rerecorded also from electroneutral partial reactions in response to change in substrate concentration (even in absence of variation in membrane potential) and like pre-steady state currents, fluorescence changes can be followed in real time.

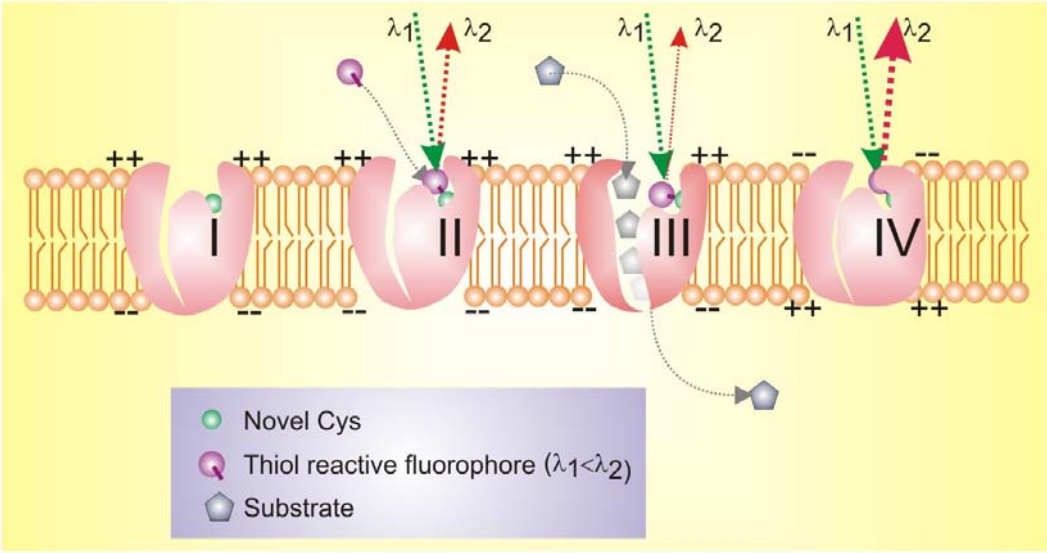


***Figure 11 Cartoon illustrating the basic principle of VCF***

*I-a novel cysteine is introduced at a conformationally sensitive site of the protein. II- with a fluorophore covalently linked to the cysteine, the emitted light intensity is a function of its microenvironment that can change depending on the substrate binding (III) or membrane potential (IV) (Forster, 2009).*

The instrumentation used in the studies reported in this thesis was modified from the original design by Drs. D.D.F. Loo and B.A. Hirayama, Dept. of Physiology, UCLA [24] (Fig 12). It comprises standard TEVC hardware and an oocytes recording chamber fitted with a transparent bottom, positioned above a fluorescence objective. The optical unit includes a dichroic mirror and filters for defining the excitation and emission spectra. A photodiode detects the light emitted by the preparation and the photocurrent is then converted to voltage using a low noise integrating patch clamp amplifier. An electrical shutter is used to isolate the light source from the preparation when not recording to reduce photobleaching of the fluorophore.

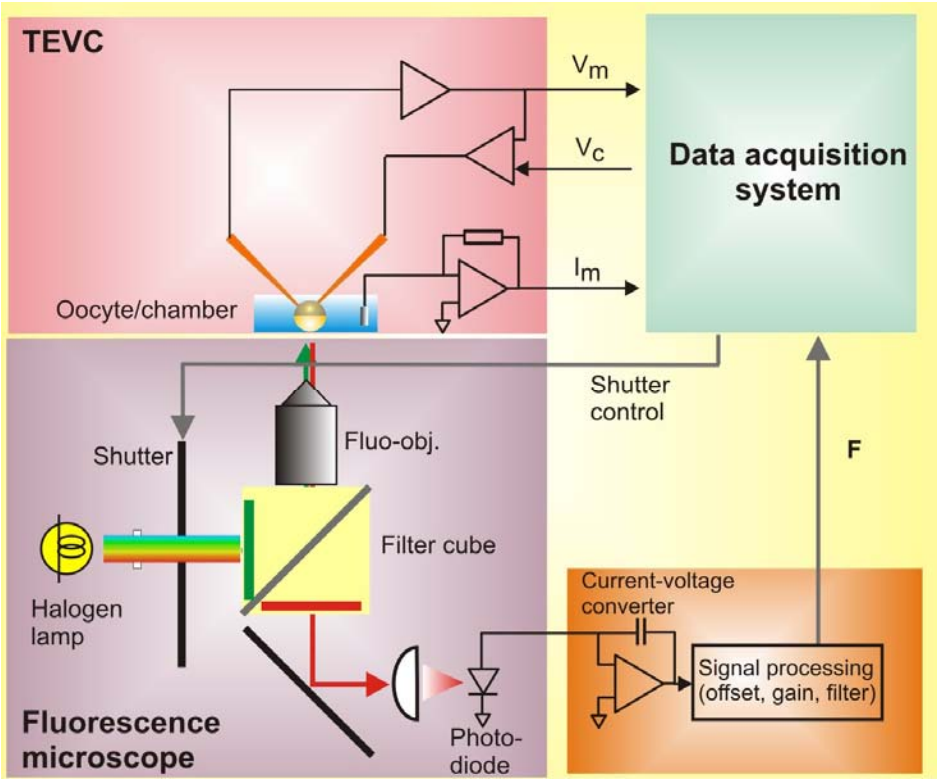


***Figure 10 Voltage Clamp Fluorometry set up.***

*VCF hardware comprises a conventional TEVC with oocyte mounted in a recording chamber with an optically transparent bottom. A basic fluorescent microscope allows the fluorophore excitation and the emitted light is measured using a photodiode connected to an integrating current-to-voltage converter (Forster, 2009).*

## 1.7 Kinetic models for secondary active carriers

A useful approach to understanding membrane transport mechanisms, both qualitatively and quantitatively, is to incorporate the experimental findings into a model that describes the essential features of the transport cycle.

To date the transport mechanism of a secondary active transporter has been described by means of two different models:

- Alternating access model (Fig. 11)
- Multi-substrate single file model (Fig.12).

The alternating access model considers a carrier like a gated channel, with a pore containing the binding site for the substrates and two gates that are never open simultaneously thereby preventing direct transmembrane solute movement.
When the external gate is open the first substrate can access its site. This induces a conformational change in the protein itself that in turn would expose other binding sites. Interaction of these with the specific sites leads to the "fully loaded carrier". The external gate would close and as a consequence the substrates remain trapped inside the central pathway. The instability connected with this event is proposed to lead to the opening of the internal gate allowing the release of solutes inside the cytoplasm of the cell. After substrates release the protein can return to its initial conformation ready for a new cycle to begin.

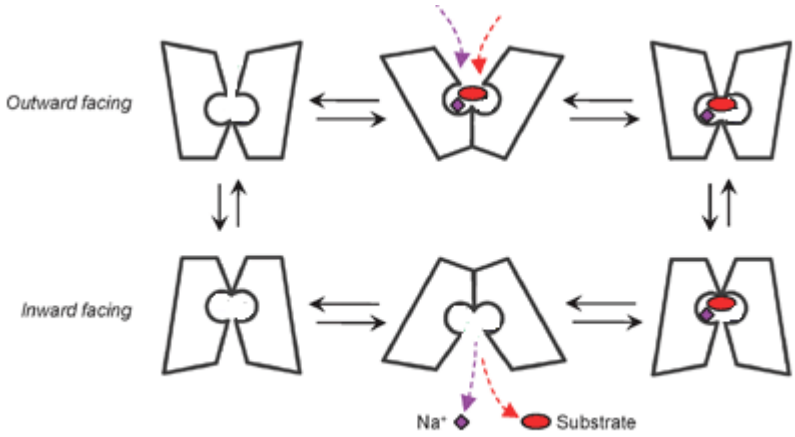


***Figure 11. Alternating access model.***
*Cartoon of the alternating access model showing the "outward" facing and "inward" facing conformation (Adapted from [36]*

The alternating access model can explain only some of the properties related to substrate permeation through the transporter, such as transport coupled currents with a strict coupling stoichiometry and transient (presteady-state) currents. However this model cannot give a satisfactory explanation for other kinetic transport features as uncoupled leak currents in absence of the substrate or variable stoichiometry. To account for these properties other models have been proposed, an example of which is, the multi-substrate single file model [37].

Here, the transporter is considered to behave as a channel with all binding sites linearly distributed through a pore structure and with both ends open to the external and

internal solution. After the substrate enters the protein it can move (or "hop") from one site to the next only if the latter is empty otherwise the substrate must wait until one of the surrounding sites is free. The movement of substrate can then continue up to its exit from the transporter and release in the cytoplasm (Fig. 12).

This model does not require large conformational changes as have been proposed to take place in the alternating access model. Instead the transporter is considered to form a pore that is always open and ready to translocate substrate in a defined direction depending on substrate availability.

The hypothesis of multi-substrate single-file transport has been tested and found to account quantitatively for the steady state data of ion-coupled transporter like GABA transporter, GAT1, sugar transporter, SGLT1 and serotonin transporter, 5-HTT. Moreover the transporter can explain, at least for GAT1 transient currents in response to voltage and concentration jumps [37]

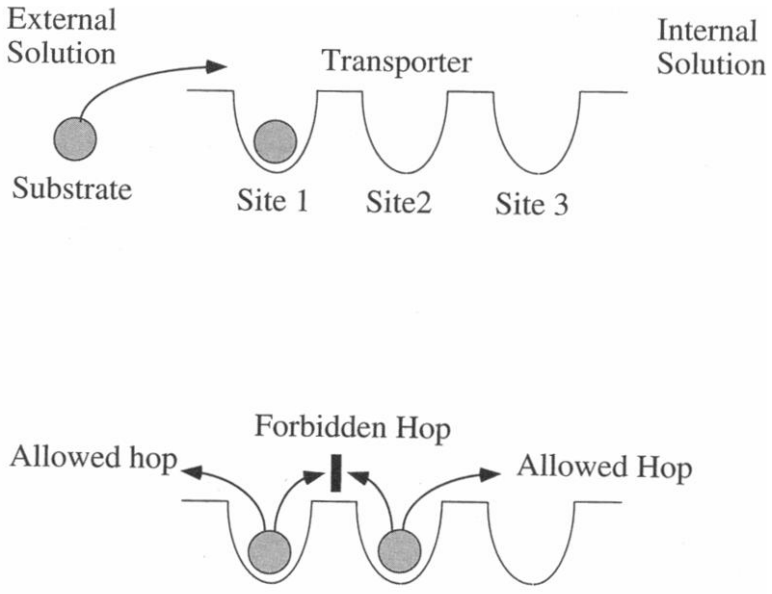


***Figure 12. Multi substrate single file model.***

*Scheme of the multi substrate single file model[37].*

Both models take in consideration the effect of membrane voltage, which strongly influence transport rate. An energy barrier separates binding sites and substrates must pass this to proceed in their movement through the membrane. The free energy associated with the barrier

can be modulated by the interaction among the charged substrates and the transmembrane electric field.

In the attempt to resolve difference between these two models, the behavior of the GABA transporter, GAT1, under different kinetic conditions [38-40] was compared using model predictions. This study favored the alternating access model and suggest the idea of two parallel substrate binding sites rather than a single pore-like structure [40]. Moreover the recent crystallization of different transporters in different conformational state (i.e. LeuT [29, 41] indicate a major role of the external and internal gates in the process of substrates translocation and further support the alternate access model.

Despite the increase numbers of techniques now available to study transport mechanism, our knowledge of molecular mechanisms underlying transport of substrates across the membranes is still limited. Many mechanistic questions still remain: what is the binding order of substrate interacting with the protein on the extracellular side of the protein, what is the sequence of events taking place on the intracellular side after the release of the substrates and what are the determinants of electrogenic behavior. We have attempted to answer some of these questions in the case of the $Na^+$-dependent Pi cotransporters family (NaPi-II) whose properties will be described in the next chapter.

# CHAPTER 2

# PHOSPHATE AND PHOSPHATE TRANSPORTERS

## 2.1 Phosphorus in living organisms

Phosphorus is an essential element of all living systems and plays a critical role in different physiological functions. It is involved in skeletal development and mineral metabolism and it is a major structural component of bones in form of calcium phosphate or hydroxyapatite. Phospholipids are major structural components of cell membranes, energy production and storage are dependent on phosphorylated compounds, such as adenosine triphosphate (ATP) and creatine phosphate. Nucleic acids (DNA and RNA) are long chains of phosphate-containing molecules. Different enzymes, hormones and cell-signaling molecules depend on phosphorylation for their activity. Phosphorus also helps to maintain normal acid-base balance by acting as one of the body most important buffers [42].

Phosphorus is present in virtually every fluid of the body. In human plasma, phosphorus exists in form of inorganic phosphorus or phosphate ($P_i$), lipid phosphorus and phosphoric ester phosphorus. Phosphate concentration range between 25.6 and 41.6 mg/l (corresponding to a concentration of 0.83-1.34 mM) and in mammalians most of it is contained in bones (10g/100g fat-free tissue) [43].

Given its roles in vital cellular process and its wide tissue distribution, it is important that the plasma phosphorus concentration is kept reasonably constant. Phosphorus (in the form of phosphate) is obtained from the diet and absorbed in the gut via a process that is efficient and minimally regulated. Absorbed phosphate is then transferred to the blood for its transport throughout the organism. For a state of phosphate balance, the amount of phosphate obtained with the diet (20 mg $\cdot kg^{-1} \cdot day^{-1}$) should be equal to the amount excreted in the urine (13 mg$\cdot kg^{-1} \cdot day^{-1}$) plus the amount excreted in the feces (7 mg$\cdot kg^{-1} \cdot day^{-1}$).

$P_i$ is freely filtered in the glomerolus and is then reabsorbed along the tubular part of the nephron, mainly in the proximal tubule of juxtamedullary nephrons with a higher rate in the S1 segmen [44].

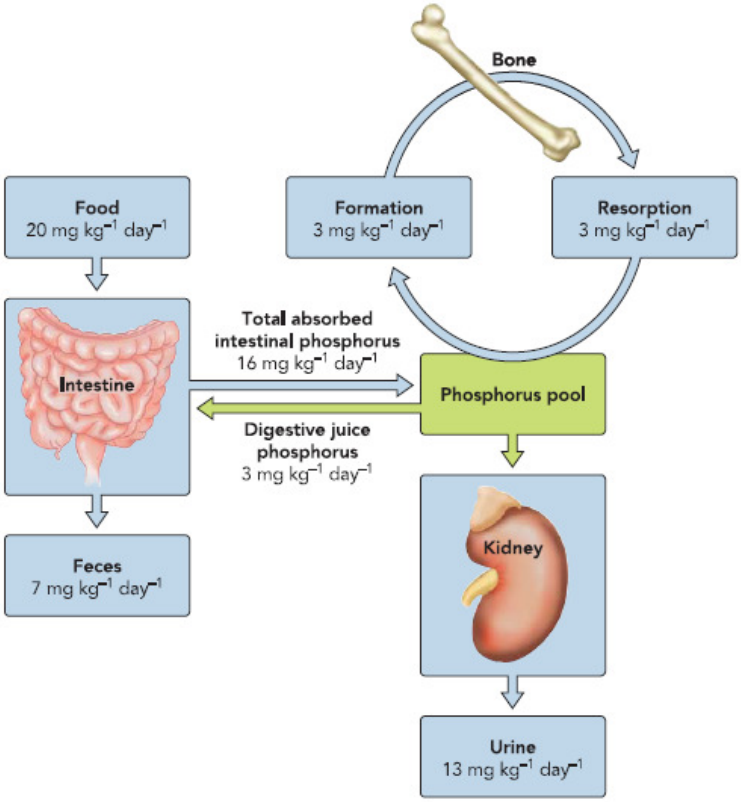


***Figure 13. Phosphorus homeostasis in healthy humans [43].***

The main site for regulation of its homeostasis is the kidney that can increase or decrease its reabsorbitive capacity to accommodate $P_i$ needs [45]. Renal excretion of $P_i$ in fact does not always operate at a constant rate, rather is continuously adjusted by various hormones and metabolic factors. Proximal tubular reabsorption is in particular regulated by at least 4 factors (see [46], [43] for a review):

- *dietary phosphate*: low $P_i$ diet can lead to increase of its re-uptake from the primary urine whereas a high $P_i$ uptake results in reduced proximal tubule reabsorption;
- *parathyroid hormone* (PTH): increase PTH levels in serum are associated with an increase in renal phosphate;
- *vitamin D*: exerts opposite effect than PTH. Decreased vitamin D levels cause decreased $P_i$ reabsorption, and in contrast to PTH, vitamin D can also regulate $P_i$ absorption in the intestine;

- *fibroblast growth factor-23*: is a secreted protein belonging to the phosphatonin family. Administration of FGF-23 to mice or rats induces phosphaturia and a serum reduction of vitamin D, whereas ablation of the corresponding gene results in a reduced phosphate excretion and elevated level of serum vitamin D.

## 2.2 Reabsorption of $P_i$ along the proximal tubules: $P_i$ cotransporters.

As already mentioned, the main site of $P_i$ reabsorption is the proximal tubule whereas there is no evidence for its reabsorption along the loop of Henle and the contribution of the distal tubular segments is yet unclear.

In the proximal tubule uptake of $P_i$ is:

(i) strictly dependent on the presence of $Na^+$ [47], indicating the absence of a paracellular transport pathway;

(ii) dependent on the presence of $Na^+/K^+$-ATPases localized at the basolateral membrane [48], that keeps intracellular $Na^+$ concentration low and indicates the involvement of a secondary active transport system.

Moreover the fact that $P_i$ is negatively charged indicate that this ion cannot cross the membrane by simple diffusion but it require the presence of specific membrane protein and an active transport system.

Three different families of transporters were originally considered to be involved in $P_i$ reabsorption in the proximal tubule: NaPi-I, NaPi-II and NaPi-III ( Fig. 14).

*NaPi-I*, (or SLC17A1), was identified using expression cloning studies using *Xenopus laevis* oocytes and localized at the brush border membranes of the proximal tubules [49] but further studies have shown that it is indeed an organic ion transporter so it is most likely not significantly involved in $P_i$ homeostasis [50].

*NaPi-II*, or SLC34 family, comprises three isoforms NaPi-IIa (or SLC34A1), NaPi-IIb (or SLC34A2) and NaPi-IIc (SLC34A3). NaPi-IIa and NaPi-IIc are localized at the apical side of proximal tubular cells and have not been found in any other segment of the nephron [51]. In normal dietary conditions, both proteins are highly expressed in the S1 segment and abundance decrease moving along the length of the proximal tubule.

The third member of the family, NaPi-IIb, has not been localized in the kidney but it is expressed in other epithelial tissues like intestine, where it is probably involved in $P_i$ absorption, salivary glands and liver [52].

NaPi-III, (SLC20), includes two isoforms commonly known as Pit1 and Pit2. They were originally identified as surface receptors for Gibbon Ape Leukemia Virus and Amphothopic murine retrovirus respectively [53] [54]. Further studies [55], based on the use of *Xenopus laevis* oocytes as expression system, showed that the two proteins are $Na^+$-dependent $P_i$ cotransporters. Analysis of expression levels have shown that Pit proteins have a widespread distribution (i.e. liver, heart, brain, placenta, lung, skeletal muscle, pancreas, spleen) indicating a housekeeping role for intracellular $P_i$ homeostasis. Initially it was supposed that Pit proteins were localized at the basolateral side of proximal tubular cells but recent experiment showed that Pit2 it is localized at the apical side [56] suggesting its role in regulation of $P_i$ homeostasis in the kidney.

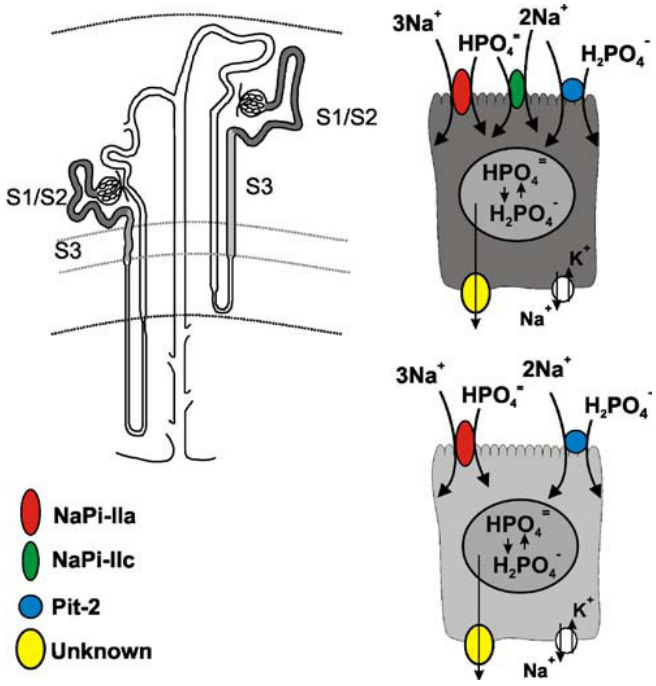


***Figure 14. Overview of the transporters involved in Pi reabsorption in the proximal tubule.***
*Cartoon shows NaPi-lla, NaPi-llc and Pit-2 localized at the brush borders of S1 and S2 segments of the proximal tubule cells, whereas NaPi-llc is absent in S3 segments [46].*

All the transporters described so far are localized at the apical membrane of proximal tubules cells; the pathway responsible for transport of Pi at the basolateral side is still unknown.

## 2.3 Secondary structure of NaPi-II proteins.

The secondary structure of NaPi-II proteins has been mostly based on studies using the rat isoform (rNaPi-IIa) as a model. Evidence from bioinformatic analyses supports, indeed, the idea that all three members share a common transmembrane topology.

The analysis of the protein hydropathy plots, based on the Kyte and Doolittle algorithm, suggests a secondary structure comprising twelve transmembrane domains (Fig. 15). Both N- and C- termini are localized intracellularly and the big extracellular loop connecting TM5 and TM6 contains two N-glycosylation sites.

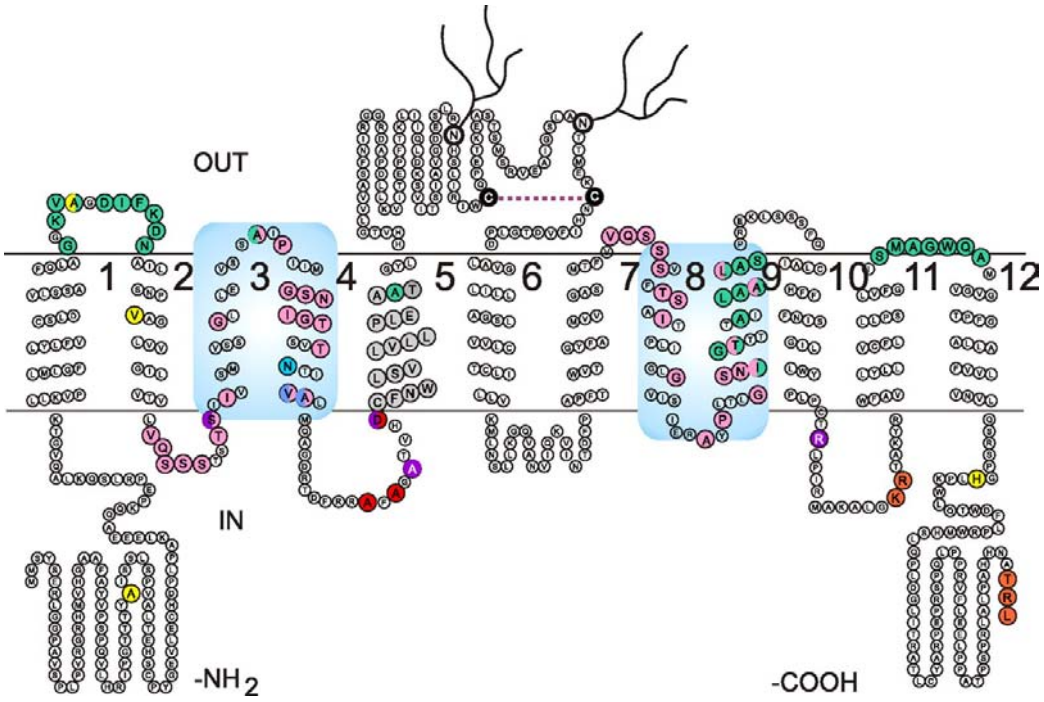


***Figure 15. Topological model proposed for rat NaPi-IIa.***

*According to the prediction NaPi-II protein display 12 transmembrane domains. The two re-entrant loop are indicated by light blue boxes. Two N-glycosylation sites have been identified in the large extracellular loop between TM5 and TM6 (Virkki, Murer, Forster 2007).*

An important structural feature of the NaPi-II primary sequence are two "repeat" regions in the N- and C-terminal halves of the protein. These repeats are preserved in all NaPi-IIa/b/c transporters in all organism suggesting an important functional role. According to the current

topology these two regions form two re-entrant loops that create the vestibule that allow the access of substrate from either side of the membrane [57].

## 2.4 Transport kinetics of NaPi-IIa and -IIb.

The initial characterization of NaPi-II proteins was performed in native brush border membranes [58] [59] [60]. On the basis of these studies, it was not possible to draw conclusions about some important characteristics such as electrogenicity vs electroneutrality, stoichiometry, preferred $P_i$ species and substrate binding order.
A more definitive kinetic characterization, was accomplished using the *X. laevis* expression system that allowed the expression and analysis of single isoform and the study of transport activity using both radioactive tracer uptake and two electrode voltage clamp (for a review see [61-64].

When expressed in oocytes, voltage clamped to hyperpolarizing potentials and perfused with 100 mM NaCl and $P_i$, NaPi-IIa and -IIb show an inward current (Fig. 16a). This transport associated current depends on the membrane potential and substrate concentration and it is only detectable with $Na^+$ ions in the extracellular solution [65]. To determine the stoichiometry and the preferred $P_i$ species translocated the relation between net charge (Q) translocated and the amount of radiotracer ($^{22}Na$ or $^{32}P$) uptake by transporters expressed in single oocytes was determined.
At pH 7.4 the ratio between the charge translocated and the $Na^+$ ions transported was 1:3 whereas the ratio Q: Pi was 1:1 [66]. These data are consistent with an electrogenic process in which one positive net charge is translocated inside the cell per transport cycle by both NaPi-IIa and NaPi-IIb. Moreover since the stoichiometry is independent of the external pH it was concluded that divalent $P_i$ is the preferred species co-transported.

The $P_i$-induced current ($I_{Pi}$) can be measured as a function of membrane potentials obtaining the typical I-V graph shown in figure 16b. The curve shows a sigmoidal shape with voltage independence at both positive and negative extremes. The absence of voltage dependence in these regions suggests that the transport cycle involves both voltage-dependent and voltage-independent partial reactions. $P_i$ induced current can be, moreover, measured as a function of $P_i$ concentration or $Na^+$ concentration present in the extracellular solution. At a given membrane potential, these data can be then fitted with the Hill equation and it is

possible to estimate the apparent affinity for the substrates. Both isoforms show an apparent affinity for $Na^+$ of about 50 mM (at 1 mM $P_i$) and an apparent affinity for $P_i \leq 0.1$ mM (for 100 mM $Na^+$).

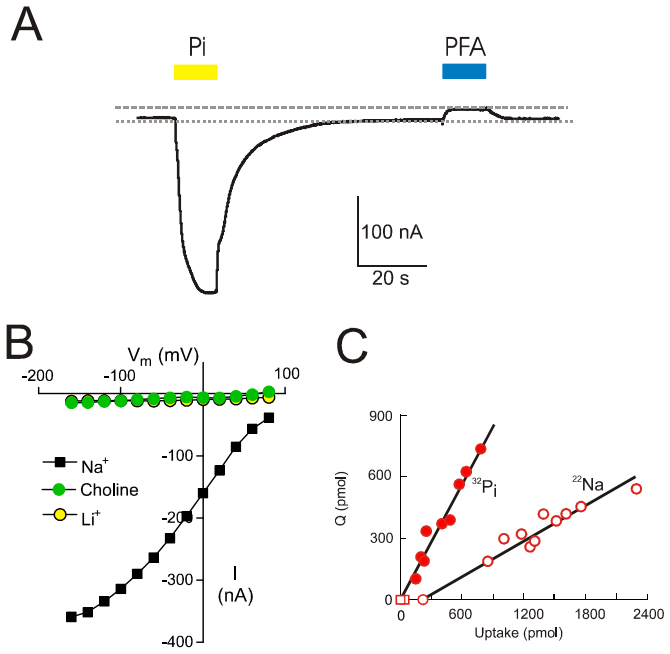


***Figure 16. Electrogenic properties of NaPi-IIa/IIb under voltage clamp conditions.***

*A) Representative recording obtained at a membrane potential of -50mV showing the inward $P_i$-induced current and the outward PFA-sensitive current, B) Representative I-V data showing $P_i$-induced current in presence or absence of external $Na^+$ . In 100 mM $Na^+$ (black squares) the I-V data show a sigmoidal form, whereas in 0mM $Na^+$ $I_{Pi}$ is suppressed indicating the strict $Na^+$ dependence of NaPi-II, C) Determination of the stoichiometry of NaPi-IIa and NaPi-IIb. Individual oocytes were voltage clamped and the charge (Q) and the amount of tracer substrate ($^{22}Na$ or $^{32}P$) taken up was assayed. The ratio Q:$P_i$ (filled symbols) is 1:1, the ratio Q: $Na^+$ is 3:1. These data indicate that the Na:$P_i$ stoichiometry is 3:1. (Modified from [63])*

A competitive inhibitor for brush border membrane $Na^+/P_i$ cotransport is phosphonoformic acid (PFA) [67]. Inhibition of $I_{Pi}$ is also observed in *X. laevis* oocytes expressing both NaPi-IIa or NaPi-IIb [68] indicating that the effect is directly due to interaction of PFA with the transporter.

Under voltage clamp conditions (-50 mV), PFA does not induce an inward current, which indicates that it is not a cotransported substrate. Instead, it induces a small upward deflection

of the holding current, which has been interpreted as evidence of the block by PFA of constitutive leak current through the transporter (Forster 1998 JGP)

As noted above, like other transporters belonging to the SLC family, NaPi-IIa/IIb show a leak current [69, 70]. In the absence of $P_i$, leak currents have been documented for electrogenic SLC34 proteins by using the inhibitor phosphonoformic acid or PFA. This current is generally small when compared with the transport mediated currents and therefore its analysis has been experimentally challenging.
As a first step it was necessary to demonstrate that this current is an intrinsic property of the transporter and not an artifact of the heterologous expression system.
Two experimental observations support this conclusion:

- the leak current correlates strongly with the $P_i$-induced current, indicating that it is also dependent on the number of active transporters inserted into the membrane;
- mutations introduced in the WT isoforms (NaPi-IIa and IIb) led to modification of the leak behavior or even to the uncoupling of leak and transport currents [71, 72].

Moreover, further studies on the NaPi-IIa isoform [69] have shown that:

- the leak current is mediated by $Na^+$ ions since a shift in the reversal potential of $I_{PFA}$ in response to a change in the extracellular sodium concentration was documented;
- the leak current magnitude shows a Michaelian dose dependence on external $Na^+$ suggesting the involvement of only one $Na^+$ ion.

These findings support the idea that a single $Na^+$ ion interacts with NaPi-IIa protein in absence of $P_i$ and that its translocation is blocked by the presence in the extracellular PFA.
The fact that leak current is present only in absence of saturating $P_i$ raises an important question: what is its physiological role? $P_i$ concentration along the renal proximal tubule is well above the $K_m^{Pi}$ so NaPi-IIa is constantly exposed to a $P_i$ concentration at which leak mode is inactive and is not expected to contribute to inward flux of $Na^+$. However, in the contest of structure-function studies leak current must be taken in account for the correct interpretation of the data and the development of a valid kinetic scheme.

As already mention above the voltage dependence of $I_{Pi}$ (Fig. 16b) is not linear indicating that the overall transport cycle must involve voltage-independent and voltage-dependent partial reactions. The latter have been identified from the analysis of presteady-state charge movements induced by rapid changes in the membrane potential.

Presteady-state relaxations have been observed for both NaPi-IIa and NaPi-IIb and a careful analysis has shown that they are dependent on the concentration of $Na^+$ ions present in the extracellular solution and they are strongly suppressed in presence of $P_i$ [73] [69].

Presteady-state currents are superimposed to the oocytes membrane capacitive currents so the first step of the analysis is the isolation of the carrier-dependent charge movement from the total transient. For this purpose the total transient is fitted with a multiple exponential function (usually 2 components) and the faster component (assumed to represent the linear oocyte charging component) is subtracted from the total transient.

This method is based on two assumptions: i) the curve fitting algorithm is considered to be accurate enough to resolve the components without cross-contamination, ii) the capacitive charging current is considered to be well described by a single exponential.

The reliability of this method is indeed challenged by two observations: i) the oocytes surface and variations in the electrical access resistance of the oocyte may result in inhomogeneous membrane clamping; ii) if the time constant of the carrier-related relaxation approaches that of the linear charging component, it is not possible to resolve the two components reliably (see Forster 2009 for more details).

Using the method described above it is possible to determine the total charge moved and obtain Q-V curves as shown in Fig 17 for the fNaPi-IIb isoform.

Three properties indicate that the presteady-state current represent the movement of a fixed number of mobile charges within the transmembrane electric field:

- the charge moved is balanced: the ON relaxation (changing the membrane potential from the holding value to the test potential) are equal to the OFF relaxation (changing the membrane potential from the test value to the holding level)
- the charge displaced shows saturation at both positive and negative membrane potentials;
- the charge moved is independent of the holding potential indicating that the process is memoryless.

Q-V curves are generally sigmoidal as expected for a saturable system and can be parameterized by fitting with the Boltzmann equation:

$$Q(V)=Q_{max}/(1+ \exp (V_{0.5}-V)ze/kT)+Q_{hyp}$$

where:

Q(V) is the charge moved for a voltage step from a given holding potential to V;

$Q_{max}$ is the total displaceable charge;

$Q_{hyp}$ is the charge at the hyperpolarizing extreme;

$V_{0.5}$ is the voltage at which 50% of the total charge has been displaced;

*z* is the apparent valency for an equivalent charged entity that moves across the whole membrane field;

k, e and T have their usual meanings.

The usual interpretation of the single Boltzmann function in this context is that the carrier protein's mobile charges are lumped into one equivalent charged entity of valency *z* that moves across the whole transmembrane electric field. This lumped charge can occupy one of two states, depending on *V,* which confers the energy to the charge to change state.

The three parameters obtained from the fit, $Q_{max}$, $V_{0.5}$ and *z*, can be determined as a function of the substrates present in the extracellular solution. In particular, their dependence on $[Na^+]$ can be used to obtain information about the interaction of $Na^+$ ions with the protein. As shown in Fig. 17, all three parameters decreased significantly for $Na^+=0$, whereas for $[Na^+]>10$mM, z and $Q_{max}$ are relatively constant. In contrast, $V_{0.5}$ is strongly dependent on the $[Na^+]$ and when plotted on a logarithmic scale, $V_{0.5}$ correlates linearly with $[Na^+]$.

As mentioned above, the Boltzmann model assumes a two state system but the observation that that the presteady-state relaxations are not totally suppressed in absence of $Na^+$ (as expected for a two state system) suggests that presteady-state currents observed cannot arise from such a simple system. Nevertheless, the parameterization of the *Q-V* data, and in particular the analysis of the relationship between $V_{0.5}$ and $[Na^+]$ has proven useful for subsequent development of a model for NaPi-II electrogenicity.

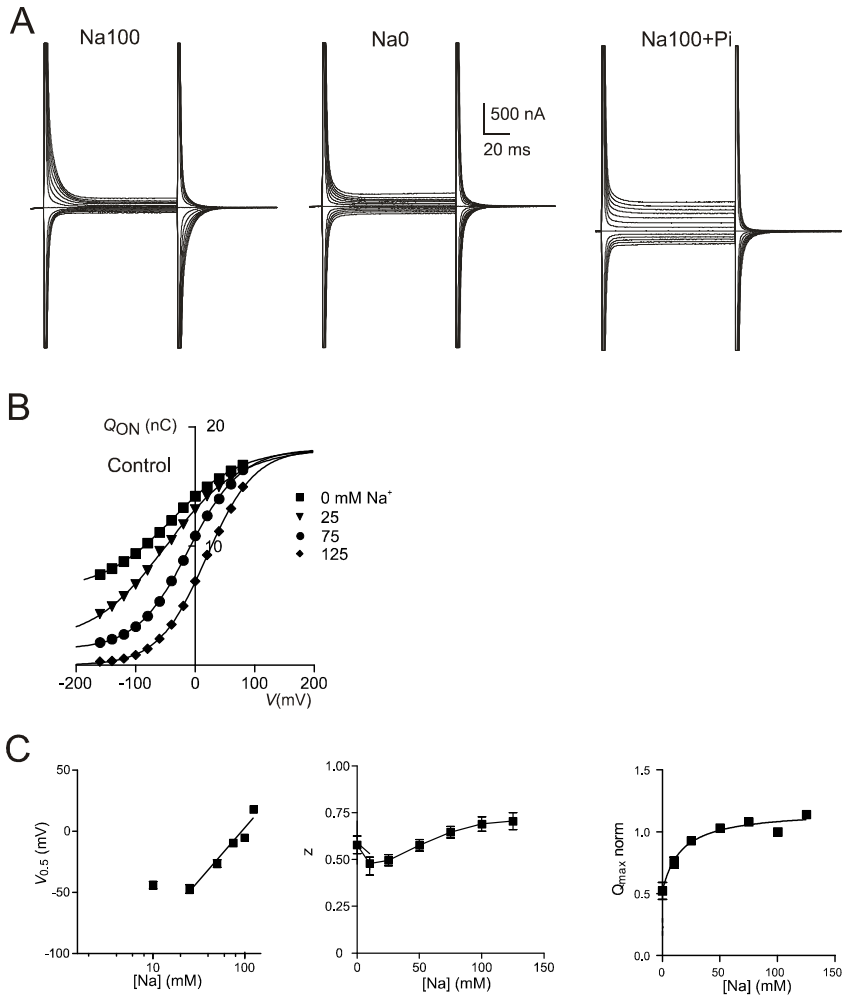


*Figure 17. A) Representative current recorded from a X.laevis oocyte expressing the flNaPi-IIb isoform under different superfusion conditions. B) Q-V data obtained from analysis of presteady-states currents in different $Na^+$ concentrations. C) Dependence of the Boltzmann parameters on external [$Na^+$]. Modified from [74].*

## 2.5 Kinetic characterization of NaPi-IIc

NaPi-IIc was cloned in the laboratory of Professor Miyamoto [64] in 2002 and in contrast to the other two members of the family, the translocation of the substrate is electroneutral.
Oocytes expressing NaPi-IIc display no change in holding current when voltage clamped and superfused with NaCl 100mN, which indicates that no net charge is translocated during each transport cycle. Activity of transporters can be assayed using uptake: oocytes are incubated with radiotracer (i.e. $^{32}P$, $^{22}Na$ ) and is monitored the amount of tracer inside the cell. These

experiments showed that NaPi-IIc activity is strictly dependent on the presence of $Na^+$ with an apparent affinity ($K_m^{Na}$ ) of ~ 50 mM. The preferred $P_i$ species is, as for the electrogenic isoforms, the divalent form with an apparent affinity ($K_m^{Pi}$) of ~0.060 mM.

Moreover, consistent with electroneutral co-transport and a preference for divalent phosphate the $Na^+$:$P_i$ stoichiometry is found to be 2:1 (Fig. 18) [75].

The fact that $K_m^{Na}$ and $K_m^{Pi}$ calculated for NaPi-IIc are very similar to the values calculated for electrogenic isoforms suggests, moreover, that the partial reactions that determine these parameters are the same for both electrogenic and electroneutral transporters and the major difference is due to electrogenicity itself and the interaction of one $Na^+$ ion with the empty carrier. This $Na^+$ ion, in absence of $P_i$, is in fact translocated in the leak mode and its movement within the electric field to its binding site constitutes part of the presteady-state relaxations (see above). These observations and the prediction that the second $Na^+$ interaction is electroneutral, offer significant insight into the fundamental difference between the electroneutral NaPi-IIc and its electrogenic cousins, NaPi-IIa/b: i.e. the former lacks the first $Na^+$ interaction.

Analysis of the primary sequence of NaPi-IIa and NaPi-IIc show a high degree of similarity particularly in the transmembrane domains regions. This suggests that only small changes in the amino acid sequence may be required to switch from electrogenic to electroneutral transport activity. In particular, a bioinformatic approach revealed the presence of three residues in the third transmembrane domain that are conserved in all electrogenic NaPi-II. When Asp-224, Ser-189 and Ser-191 were substituted with the equivalent residues found in NaPi-IIa (alanine, alanine and aspartic acid respectively), the NaPi-IIc triple mutant (AAD-IIc) displayed a $P_i$-induced, $Na^+$-dependent electrogenic response (Fig. 18)

As observed for electrogenic isoforms, AAD-IIc displayed presteady-state relaxations superimposed on the capacitive transient, a $Na^+$:$P_i$ stoichiometry of 3:1 and PFA sensitive current.

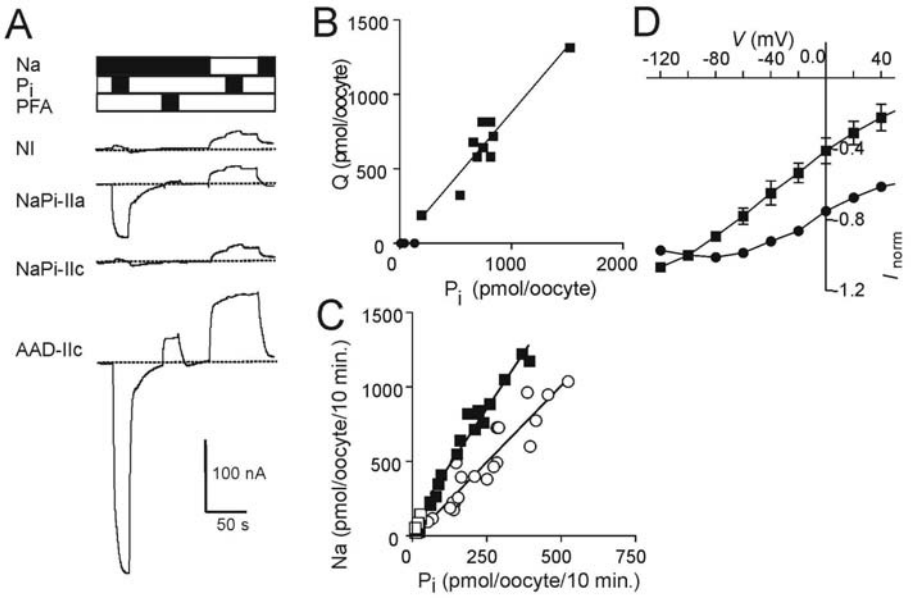


***Figure 18 The electrogenic AAD NaPi-IIc triple mutant.***

***A)*** *Representative current recorded from oocytes injected with NaPi-IIa, NaPi-IIc or the triple mutant AAD-IIc under the superfusion condition indicated. B) Net charge translocated plotted as a function of Pi uptake for individual oocytes expressing AAD-IIc. C) Dual uptake for AAD-IIc (black squares), control (white square) and NaPi-IIc wt (white circles) from the same donor frog. D) Normalized I-V plots to compare NaPI-IIa (black squares) and AAD-IIc (black circles)[75]*

## 2.6 Structure-function studies: SCAM

The structure-function studies performed on SLC34 family gene products have both increased information regarding structural organization of the protein and also deepened our knowledge of transport mechanism.

As already described in the Section 1.5, in absence of a crystal structure, one way of obtaining information about structure and correlate it to function, is the SCAM approach. The assumption in all the SCAM studies applied to NaPi-II proteins is that none of the 12 or more native cysteines is directly or indirectly involved in determining the protein functional behavior (i.e. any change in transport, leak or presteady-state currents was observed after application of MTS reagent to the WT isoforms).

The first application of SCAM was the validation of the topology model predicted from Skyte-Doolittle analysis (Magagnin et al). Novel cysteines were introduced at the interface between the linker regions and their associated TMDs and the change in accessibility

of each position was analyzed. (e.g. Forster et al 2002, Lambert et al., 2001). According to these experiments, for example, cyclic variation in accessibility of the predicted TMD9 suggests an α-helical organization, consistent with the idea that the region is a membrane spanning segment (Lambert 2001).

A second application of SCAM was the identification of important functional residues and the role of the two re-entrant loops. This was particularly important in the context of structure-function studies.

Two novel cysteines were introduced: one in each re-entrant loop and the $P_i$-induced current and the PFA-sensitive current were analyzed before and after the application of MTS reagents (Fig. 19) [71].

Introduction of a cysteine at the top of TMD9 (Ser460Cys) (Fig.19) resulted in a mutated transporter that displayed normal kinetic properties, but the functional importance of this residue was underscored by the fact that application of MTS caused a suppression of $P_i$-induced current, whereas PFA-sensitive current was un-affected.

In agreement with the idea of linker regions forming re-entrant loops deep inside the membrane, a cysteine introduced in the TMD4 (Ala203Cys) was found to be poorly accessible from the extracellular solution based on the observation that the $P_i$-induced current is only marginally affected. An unexpected feature of this mutant was the remarkable increase in the PFA-sensitive current (i.e. leak current).

The double mutant A203C-S460C was shown to combine the behavior of the two cysteine mutants. Before modification, A203C-S460C showed an increased PFA-sensitive current relative to the $P_i$-induced current as observed for the A203C. After modification with MTSA, PFA-sensitive current was increased even more and the response to PFA and $P_i$ are equivalent, as for S460C alone.

Moreover, by quantifying the loss of co-transport activity and increase in leak current during the modification process, it was shown that they follow closely the same time course. This behavior suggested that the two re-entrant loops are involved in the formation of the central pathway that is common to both transport and leak modes.

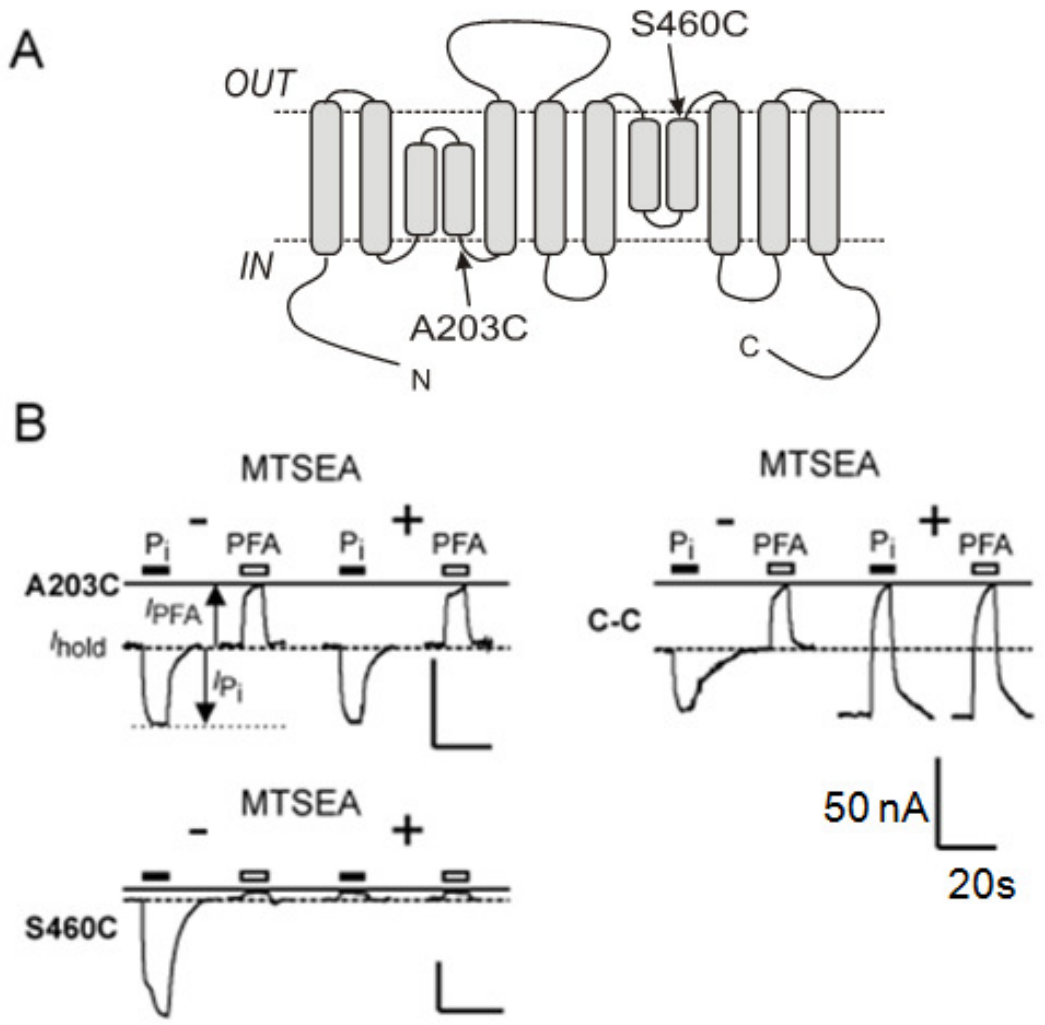


***Figure 19. A203C-S460C double mutant***

*A) Topology model of the rNaPi-IIa which indicates the position of the novel cysteines in S460C and A203C. B) Representative recording at -50mV showing response to $P_i$ (1mM) and PFA (3mM) under control condition and after exposure to MTSEA (1mM for 3 min)for A203C, S460C and A203C-S460C [71] .*

## 2.7 Structure function studies: VCF

The behavior of the presteady-state charge movements recorded from oocytes expressing NaPi-IIa and NaPi-IIb are consistent with the notion that electrogenic isoforms undergo conformational changes during transport cycle in response to change in membrane potential. More information regarding conformational changes induced not only by changes in membrane potential but also to substrate interactions can be obtained using Voltage Clamp Fluorometry (VCF) (Fig. 10).

The first study analyzed the behavior of a single cysteine mutant, (S448C) that was equivalent to S460C mutant in the rNaPi-IIa isoform, showed the typical electrogenical behavior. Incubation with the fluorophore MTS-TAMRA resulted in the suppression of $P_i$-induced current whereas the leak current remained un-affected [74].

Voltage steps caused changes in fluorescence that was voltage- and substrate-dependent (Fig. 20). Of particular interest was the finding that the dependence of fluorescence quenching on $[Na^+]$ was best fit with the Hill equation with $n_H \sim 1.8$. This indicated that the $Na^+$ interaction was cooperative and that > 1 $Na^+$ ion interact with the transporter before binding of $P_i$ (see Section 2.7 for a more detailed description of the substrate binding order).

In the presence of $Na^+$ ions, the addition of $P_i$ to the superfusate also induced fluorescent quenching. Quenching is dependent on the $P_i$ concentration with an estimated $n_H \sim 1$, consistent with one $P_i$ interacting with the protein per transport cycle. Moreover the apparent $K_{0.5}^{Pi}$ obtained from the Hill fits to the F-V data was similar to that obtained before labeling (fit to $I_{Pi}$-V data). This strongly suggested that fluorescence data truly reflect substrate interactions with the protein. In contrast $K_{0.5}^{Na}$ after labeling is higher compared to that calculated before labeling. A possible explanation of this observation is that before labeling $K_{0.5}^{Na}$ is determined on the basis of all three sodium ions interacting with the protein, whereas after labeling $K_{0.5}^{Na}$ is determined by partial reactions associated only with the two first interaction steps.

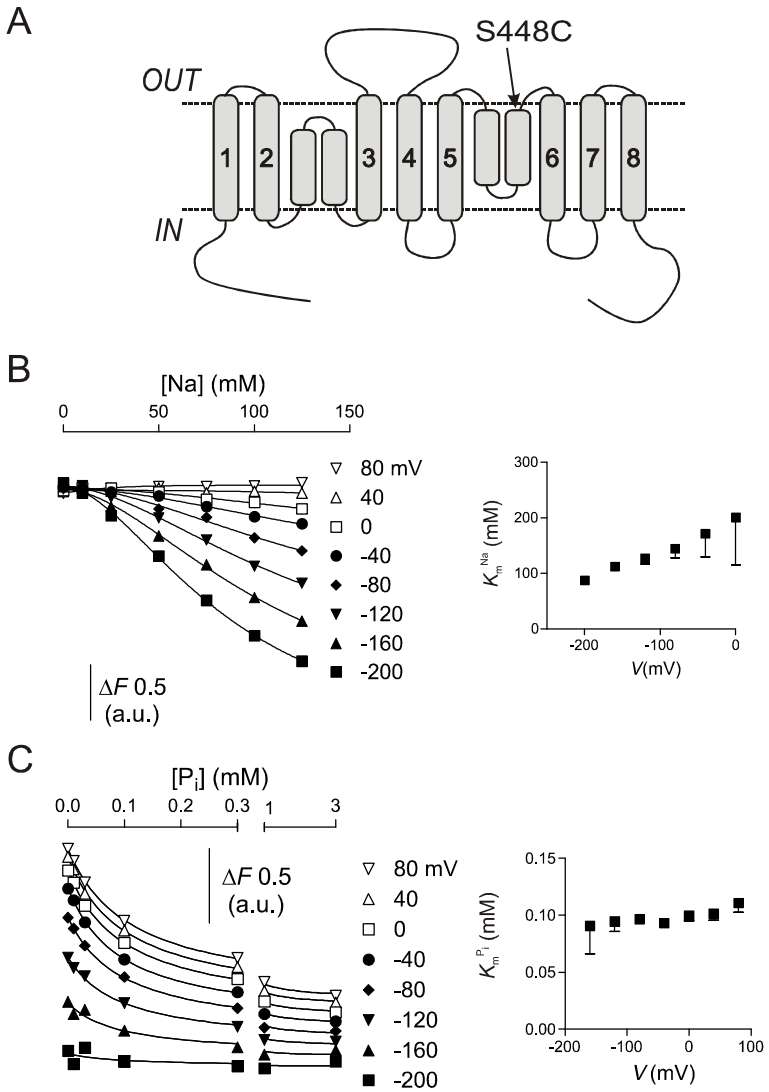


***Figure 20. Voltage dependent change in fluorescence of the S448C mutant***

*A) Topology model of the fNaPi-IIb isoform showing the position of Cys-448 to which the fluorophore is covalently linked. B) $Na^+$ dependence of fluorescence quenching for different membrane potentials (left) and voltage dependence of the apparent affinity for $Na^+$ ($K_{0.5}^{Na}$)(right). C) $P_i$ dependence of fluorescence quenching for different membrane potentials (left) and voltage dependence of the apparent affinity for $P_i$ ($K_{0.5}^{Pi}$)(right) [74].*

In the second study performed using VCF, novel cysteines were introduced in different parts of the flNaPi-IIb isoform with the aim of mapping conformational changes of the protein during the normal transport cycle. A pre-requisite for this study was that the introduction of novel cysteines or labeling with the fluorophore (MTS 5(6)-carboxytetramethylrhodamine or MTS-TAMRA) did not result in an alteration of the kinetic

properties. Four sites were found to satisfy this criteria: Ser155 and Ser226 in the N-terminal half of the protein and Gln319 and Glu415 in the C-terminal half of the protein [76]. Fluorescence was recorded in presence of different substrate in the extracellular solution ($Na^+$ 100mM, $Na^+$ 0mM and $Na^+$ 100mM + $P_i$ 1mM) and plotted as a function of the membrane potential (Fig. 21). In particular, it was observed that in presence of 100mM $Na^+$ the fluorescence quenching was opposite in the two halves of the protein. For S155C and S226Cmembrane depolarization causes an increase in F whereas for Q319C and E415C it causes a decrease in F. Based on these findings, it was speculated that complementary changes in the voltage dependence of the fluorescence reflect complementary rearrangements in the two halves of the protein.

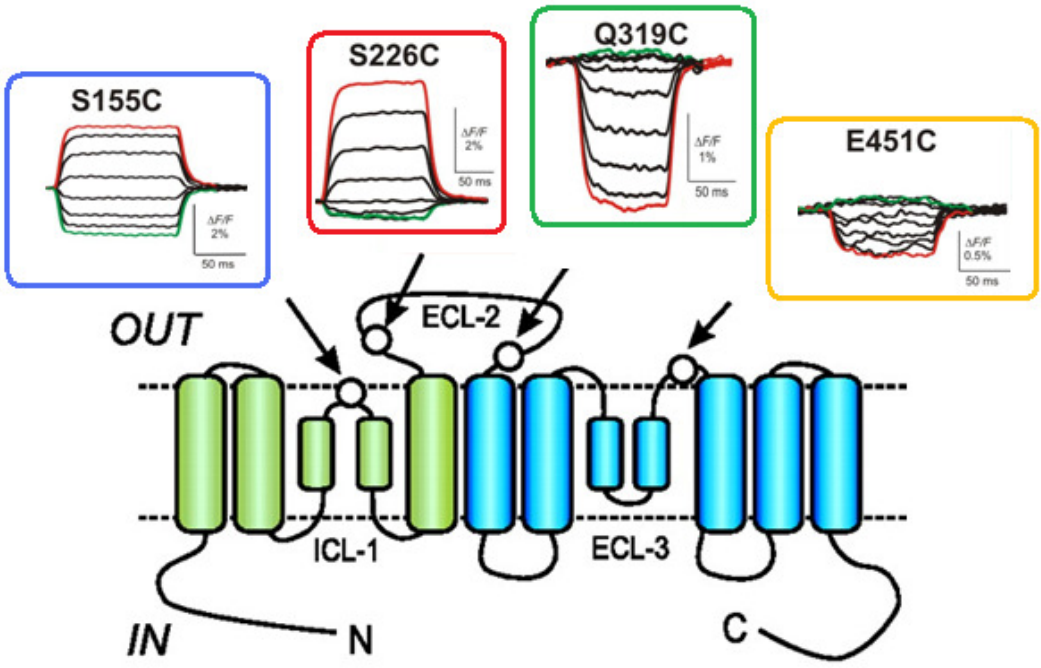


*Figure 21.* ***Complementary F-V changes observed in two halves of NaPi-II.***
*Topological scheme of flNaPi-IIb isoform which shows the purported positions of the novel cysteines for S155C, S226C, Q319 and E451C. The original F-V recordings made for the corresponding mutant in presence of $Na^+$100mM in the extracellular solution in response to the change in the membrane potential (voltage was stepped from the holding potential of -60 mV to test potentials ranging between -200 to +100 mV in 40mV increments for a duration of 100-200ms and averaged over 10-15 sweep )[76]*

.

## 2.8 The 10-state kinetic scheme and the substrate binding order

Based on electrophysiological assays (analysis of both steady state and presteady-state currents) the substrate binding order was assumed to be Na-Pi-Na-Na (Forster et al., 1998). This model has been revised based on (i) the behavior of the fluorescently labeled S448C mutant (Virkki et al 2006) and (ii) a reassessment of presteady-state data (Forster 2009) to Na-Na-Pi-Na.

The fluorescently labeled S448C mutant was a useful tool to understand substrate binding order. As noted above, dependence of fluorescence on $Na^+$ concentration resulted in quench dependence on [$Na^+$] consistent with the interaction of 2 $Na^+$ ions before $P_i$.

Binding of $P_i$ is then followed by the interaction of the last $Na^+$ as suggested by the observation that the rate limiting step for translocation of the substrates is dependent on $Na^+$ concentration in the extracellular solution (Forster et al 1997, 1998).

This finding can be incorporated into a kinetic model that describes the co-transport cycle as a sequence of partial reactions between 10 hypothetical conformational states of the protein (Fig. 21).

Five states are considered to be "outward" facing (1, 2a, 2b, 3, 4) and correspond to conformations in which the substrate binding sites to the extracellular side of the membrane are exposed. The remaining five states correspond to "inward" facing conformations but transitions between these states are not characterized due to the difficulty in changing substrate concentration inside the oocytes.

Voltage dependence is conferred to the complete co-transport cycle by transitions that precede $P_i$ interaction. Two partial reactions, the empty carrier transition (8↔1) and first $Na^+$ binding partial reaction (1↔2) are electrogenic and involve movement of mobile charges within transmembrane field: charge associated with the protein itself and one $Na^+$ respectively. The second $Na^+$ interaction (2a↔2b) is assumed to be electroneutral.

Transitions 1↔2 and 2a↔2b are considered to be responsible of the leak current that can be blocked applying PFA (transition 2b→3*).

The interaction of the 2 $Na^+$ ions is fundamental for the co-transport to occur as it allows the subsequent interaction of divalent $P_i$ with the protein (transition 2b↔3). The last transition is the binding of the 3$^{rd}$ $Na^+$ ion (transition 3↔4) which leads to the formation of the fully

loaded carrier complex that can undergo the conformational change required to translocate the substrates inside the cell (transition 4↔5).

The three currents recorded from the NaPi-II protein can also be included in the above kinetic scheme:

- presteady-state charge movements: are generated by conformational changes occurring in the electrogenic transitions 8↔1 and 1↔2a;
- $P_i$-induced cotransport current: results from a complete cycle through all 10 conformational states that define the kinetic scheme;
- Substrate-independent leak current: in the absence of Pi, the protein cycles between 1-2a-8a-8-1.

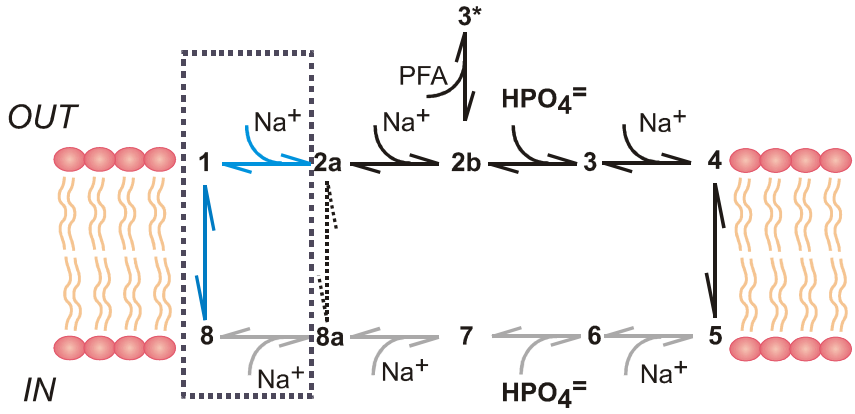


***Figure 21. Kinetic scheme for the electrogenic co-transport cycle.***

*Partial reactions that involve charge movement are indicated (blue). All other partial reactions are assumed to be electroneutral [63].*

## 2.9 Open questions

In absence of 3-D structure of NaPi-II proteins or their bacterial homologs and despite the extensive characterization already performed using both TEVC and VCF, many issues remained to be addressed at the start of the dissertation period. The two that were specifically investigated were:

1) *The substrate binding order of NaPi-IIc*:

2) *The interaction of reentrant loops during the transport cycle*:

*The substrate binding order of NaPi-IIc*: A fundamental difference between NaPi-IIa/IIb and NaPi-IIc is stoichiometry. As already noted above, dual uptake experiments showed that NaPi-IIa/IIb have a 3:1 $Na^+$: $P_i$ stoichiometry, which indicates that one net charge is translocated per transport cycle (assuming divalent Pi is transported), whereas NaPi-IIc displays a 2:1 $Na^+$: $P_i$ stoichiometry that results in an electroneutral transport cycle. Analysis of the primary sequence shows that electrogenic and electroneutral isoforms have a highly conserved sequence, particularly in the predicted transmembrane domains that are assumed to define the basic transport characteristics (substrate binding sites, substrate specificity, translocation pathway) and lead moreover to the determination of critical residue that when mutated confer electrogenicity to NaPi-IIc.

Based on the findings from TEVC and VCF it was initially hypothesized that the electroneutral NaPi-IIc was simply missing one of the $Na^+$ binding sites postulated for the electrogenic isoform, but direct experimental evidence to support this conclusion was lacking. Moreover, due to fact that transport can be assayed only by means of radiotracer uptake, kinetic characterization was just limited to the apparent affinity for $Na^+$ ($K_m^{Na}$) or for $P_i$ ($K_m^{Pi}$).

The importance of having a more precise knowledge of how NaPi-IIc works in terms of substrate interactions is underlined by the recent observation that mutations on NaPi-IIc are directed linked to a severe hereditary disease [77]. Hypophosphatemic rickets with hypercalciuria is a rare autosomal recessive disease that is characterized by hypophosphatemia, renal phosphate wasting, enhanced intestinal absorption of calcium that lead to increased urinary calcium excretion, limb deformities, bone pain and radiographic and/or histological evidence of rickets. The genetic analysis of some patients affected by HHRH has mapped the pathology to the region on chromosome 9 (9q34) that code for NaPi-IIc. Moreover, a genetic screen on patients affected by HHRH has led to the identification of certain point mutations that may cause a loss of function of NaPi-IIc that are localized in a region that is an important determinant of the stoichiometry and electroneutrality of the mouse ortholog Npt2c (i.e. S192L and G196R) (ref).

*The interaction of reentrant loops during the transport cycle*: Due to the lack of a 3-D model, all the information regarding the structure of NaPi-II proteins relies on the interpretation of findings from techniques such as SCAM or VCF. As described above NaPi-

II proteins are characterized by the presence of two highly conserved regions that are believed to form two re-entrant loops. As already shown these two regions most likely form the pathway along which both $Na^+$ and $P_i$ are translocated inside the cell [71].

According to the recent crystallization of different membrane proteins belonging to the SLC family [78] a common structural organization for carrier proteins with different substrate specificity and function has emerged. In particular, it appears that proteins are characterized by an internal two-fold symmetry.

On the basis of these two observations (namely a functional role of the two re-entrant loops and a possible structural similarity with already crystallized proteins), we investigated if the two re-entrant loops can physically interact and if this interaction is influence by composition of extracellular solution.

# CHAPTER 3

# METHODS AND RESULTS

## 3.1 Publications that contribute to this work:

### Paper 1:

"Substrate interactions of the electroneutral $Na^+$-coupled inorganic phosphate cotransporter (NaPi-IIc)".

**Methods used:**

- Single point mutagenesis
- Two electrode voltage clamp (TEVC)
- Radiotracer uptake
- Voltage clamp fluorometry (VCF)

### Paper 2:

"Amino acid interactions in the putative transport pathway of flNaPi-IIb observed by Voltage Clamp Fluorometry"

**Methods used:**

- Single point mutations
- Substituted cysteine accessibility method
- Two electrode voltage clamp(TEVC)
- Radiotracer uptake
- Voltage clamp fluorometry (VCF)
- Crosslinking assays

## Paper 3:

"The leak mode of type II $Na^+$-$P_i$ cotransporters."

**Methods used:**

- Two electrode voltage clamp (TEVC)
- Radiotracer uptake

The Journal of Physiology

J Physiol 587.17 (2009) pp 4293–4307



# Substrate interactions of the electroneutral $Na^+$-coupled inorganic phosphate cotransporter (NaPi-IIc)

Chiara Ghezzi, Heini Murer and Ian C. Forster

*Institute of Physiology and Center for Integrative and Molecular Physiology, University of Zurich, Zurich, Switzerland*

**The SLC34 solute carrier family comprises the electrogenic NaPi-IIa/b and the electroneutral NaPi-IIc, which display $Na^+ : P_i$ cotransport stoichiometries of 3 : 1 and 2 : 1, respectively. We previously proposed that NaPi-IIc lacks one of the three $Na^+$ interaction sites hypothesised for the electrogenic isoforms, but, unlike NaPi-IIa/b, its substrate binding order is undetermined. By expressing NaPi-IIc in *Xenopus* oocytes, isotope influx and efflux assays gave results consistent with $Na^+$ being the first and last substrate to bind. To further investigate substrate interactions, we applied a fluorometry-based technique that uses site-specific labelling with a fluorophore to characterize substrate-induced conformational changes. A novel Cys was introduced in the third extracellular loop of NaPi-IIc that could be labelled with a reporter fluorophore (MTS-TAMRA). Although labelling resulted in suppression of cotransport as previously reported for the electrogenic isoforms, changes in fluorescence were induced by changes in extracellular $Na^+$ concentration in the absence of $P_i$ and by changes in extracellular $P_i$ concentration in presence of $Na^+$. These data, combined with $^{32}P$ uptake data, also support a binding scheme in which $Na^+$ is the first substrate to interact. Moreover, the apparent $P_i$ affinity from fluorometry agreed with that from $^{32}P$ uptake, confirming the applicability of the fluorometric technique for kinetic studies of electroneutral carriers. Analysis of the fluorescence data showed that like the electrogenic NaPi-IIb, 2 $Na^+$ ions interact cooperatively with NaPi-IIc before $P_i$ binding, which implies that only one of these is translocated. This result provides compelling evidence that SLC34 proteins share common motifs for substrate interaction and that cotransport and substrate binding stoichiometries are not necessarily equivalent.**

(Received 19 May 2009; accepted after revision 7 July 2009; first published online 13 July 2009)
**Corresponding author** I. C. Forster: Institute of Physiology, University of Zurich, Winterthurerstrasse 190, CH-8057 Zurich, Switzerland. Email: iforster@access.uzh.ch

**Abbreviations** BBMV, brush border membrane vesicle; MTS, methanethiosulfonate; MTSEA, 2-aminoethyl methanethiosulfonate hydrobromide; MTSET, 2-(trimethylammonium)ethyl methanethiosulfonate bromide; MTS-TAMRA, 2-((5(6)-tetramethylrhodamine)carboxylamino)ethyl methanethiosulfonate; NaPi-IIc, type IIc $Na^+$-coupled $P_i$ cotransporter; PFA, phosphonoformic acid; SLC34, solute carrier family 34 (www.genenames.org).

Renal reabsorption of inorganic phosphate ($P_i$) is mediated by secondary active $P_i$ cotransporters that catalyse uphill $P_i$ transport using the prevailing electrochemical $Na^+$ gradient (Murer *et al.* 2008). Two gene products of the SLC34 family, NaPi-IIa (or SLC34A1) and NaPi-IIc (or SLC34A3) (Murer *et al.* 2004, 2008) are expressed at the renal brush border membrane of proximal tubules. A third member of the SLC34 family, NaPi-IIb (SLC34A2), is probably not expressed in the kidney (Hilfiker *et al.* 1998) but is present in several other organs such as the small intestine, where it is involved in the absorption of dietary phosphate, as well as lung, testis and liver. The importance of NaPi-IIa/c for renal $P_i$ transport in the kidney is underscored by studies on knockout mouse models (Beck *et al.* 1998) and the pathophysiology of naturally occurring mutations (Bergwitz *et al.* 2006; Jaureguiberry *et al.* 2008).

All three SLC34 isoforms preferentially transport divalent $P_i$ ($HPO_4^{2-}$). NaPi-IIa and NaPi-IIb are electrogenic: they show a strict $Na^+ : P_i$ cotransport stoichiometry of 3 : 1, which results in the translocation of one net positive charge per transport cycle (Forster *et al.* 1999). In contrast, NaPi-IIc has a $Na^+ : P_i$ cotransport stoichiometry of 2 : 1 and is electroneutral (Segawa *et al.* 2002; Bacconi *et al.* 2005). Based on the electrogenic kinetics of NaPi-IIa/b expressed in *Xenopus* oocytes (Forster *et al.* 1997; Forster *et al.* 1998), we proposed an ordered substrate binding model in which one $Na^+$ ion



DOI: 10.1113/jphysiol.2009.175596

interaction precedes $P_i$ binding, followed by the binding of the remaining two $Na^+$ ions (Forster *et al.* 1998). This model was recently revised, based on data obtained from voltage clamp fluorometry (VCF) (Virkki *et al.* 2006*b*), a technique which combines electrophysiology and time-resolved fluorescence microscopy (e.g. Cha *et al.* 1998). That study, using the electrogenic NaPi-IIb, yielded compelling evidence for the cooperative binding of two $Na^+$ ions before $P_i$ binding and consequently implied that the binding of only one $Na^+$ would be the last event before carrier translocation.

In this study, we ask the following question: what is the substrate binding order of the electroneutral NaPi-IIc? As no transport-related electrogenic activity (either steady-state or presteady-state) is detectable with NaPi-IIc, until now its kinetics have only been studied exclusively using radio-labelled isotopes (Segawa *et al.* 2002; Bacconi *et al.* 2005). Indeed, the 2 : 1 $Na^+ : HPO_4^-$ stoichiometry would suggest that NaPi-IIc lacks one of the three $Na^+$ interactions proposed for NaPi-IIa/IIb; however direct experimental evidence to support this conclusion is lacking. Moreover, only limited kinetic information, such as apparent substrate affinities, is available (Segawa *et al.* 2002) and, in particular, the substrate binding order is unknown. We therefore addressed these issues, first by determining the substrate binding order on the extracellular side using traditional tracer uptake methods and second by using a fluorometric technique to study putative conformational changes during substrate interactions on individual *Xenopus* oocytes. In this latter technique, the protein is site-specifically labelled with fluorophore. As the fluorescence emitted by the fluorophore depends on its environment, a change in the fluorescence, induced by changes in membrane potential (in the case of electrogenic interactions) or different substrate concentrations, reflects local potential- or concentration-sensitive conformational changes in the protein. Here we demonstrate the use of fluorometry to document steady-state conformational changes of an electroneutral carrier induced by substrate interactions. Our flux and fluorescence data have allowed us to propose a kinetic scheme for electroneutral NaPi-IIc, which suggests that electrogenic and electroneutral SLC34 proteins share the same cation interactions despite having different transport stoichiometries.

## Methods

### Solutions and reagents

Standard extracellular solution (ND100) contained (in mM): 100 NaCl, 2 KCl, 1.8 $CaCl_2$, 10 Hepes, pH 7.4 adjusted with Tris. In $Na^+$ substitution experiments NaCl was equimolarly replaced with choline chloride (ND0), whereas for $Li^+$ replacing experiments NaCl was replaced with LiCl (LD100). Solutions with intermediate $[Na^+]$ or $[Li^+]$ were obtained by mixing ND100 or LD100 with ND0 in appropriate portions to maintain a constant overall molarity. $P_i$ was added from a 1 M $K_2HPO_4/KH_2PO_4$ stock premixed to give pH 7.4. Phosphonoformic acid (PFA) was added to the test solution from 100 mM stock in water. Modified Barth's solution for storing oocytes contained (in mM): 88 NaCl, 1 KCl, 0.41 $CaCl_2$, 0.82 $MgSO_4$, 2.5 $NaHCO_3$, 2 $Ca(NO_3)_2$, 7.5 Hepes, pH 7.5 adjusted with Tris and supplemented with 5 mg $l^{-1}$ doxycyclin and 5 mg $l^{-1}$ gentamicin.

All standard reagents were obtained from either Sigma-Aldrich or Fluka (Buchs, Switzerland). 2-Aminoethyl methanethiosulfonate hydrobromide (MTSEA) and 2-(trimethylammonium)ethyl methanethiosulfonate bromide (MTSET) were obtained from Toronto Research Chemicals (North York, Ontario, Canada); 2-((5(6)-tetramethylrhodamine) carboxylamino)ethyl methanethiosulfonate (MTS-TAMRA) was obtained from Biotium (Hayward, CA, USA); tetramethylrhodamine-6-maleimide and tetramethylrhodamine-5-maleimide were obtained from Molecular Probes (Invitrogen/Life Technologies, Carlsbad, CA, USA).

### Site-directed mutagnesis and cRNA preparation

The S437C mutation was introduced in mNaPi-IIc WT using the Quickchange site-directed mutagenesis kit (Stratagene Inc., La Jolla, CA, USA). In brief, 10 ng of plasmid (pT7T3D-Pac) containing the WT mouse NaPi-IIc cDNA was amplified using 2.5 U of Pfu Turbo DNA polymerase (Stratagene Inc.), in the presence of primers (200 nM) containing the mutated codon sequence: GGCTGCCTTAGCCTGCCCTGCAGACATG. After PCR amplification, 10 U of DpnI was added to the amplification reaction and the sample was incubated at 37°C for 1 h to digest parental DNA. XL1-blue competent cells were transformed with the reaction mixture and then plated on LB plates supplemented with Ampicillin. The sequence was verified by sequencing (Microsynth, Balgach, Switzerland) and linearized with *Not*I, and cRNA was synthesized in the presence of Cap analogue using the T7 Message Machine kit (Ambion, Inc., Austin, TX, USA).

### Animal handling and ethical approval

Female *X. laevis* frogs were purchased from Xenopus Express (Vernassal, France) or African Xenopus Facility (South Africa). Frogs were anaesthetized in 0.1% MS222 (tricaine methansulphonate) in water and portions of ovaries were surgically removed by making a small incision in the abdomen. After suturing the incision, the frog was placed in a separate tank to recover fully and then returned

to a larger tank that contained all postoperative animals. A minimum of 8 weeks was allowed before re-operation on the same animal. All animal handling was in full compliance with regulations and recommendations of the University of Zurich (Institut für Labortierkunde) and the Swiss Federal Veterinary Office (FVO, Berne) from whom written approval was obtained. The authors have read the article by Drummond on reporting ethical matters and confirm that the experiments comply with the relevant policies and regulations (Drummond, 2009).

### Expression in *Xenopus laevis* oocytes

Ovaries were cut into small pieces and treated for 45 min with collagenase (crude type 1A) 1 mg ml$^{-1}$ in ND100 solution (without $Ca^{2+}$) in the presence of 0.1 mg ml$^{-1}$ trypsin inhibitor type III-O. Healthy stage V–VI oocytes were selected, maintained in modified Barth's solution at 16°C and injected with 10 ng of cRNA. Experiments were performed 4–7 days after injection.

### Uptake experiments

**Influx assays.** Control oocytes and oocytes expressing NaPi-IIc (6–10 oocytes/group) were first allowed to equilibrate in ND100 solution without tracer. After aspiration of this solution, oocytes were incubated in ND100 solution containing 1 mM cold $P_i$ and $^{32}P$ (specific activity 10 mCi mmol$^{-1}$ $P_i$). Uptake proceeded for 10 min and then oocytes were washed 3 or 4 times with ice-cold ND0 solution containing 2 mM $P_i$, and lysed individually in 10% SDS. The amount of radioactivity in each oocyte was measured by scintillation counting. The uptake time was chosen to be short enough to assume that initial rate conditions were satisfied so that uptake per unit time is a direct measure of transport velocity, without compromising measurement reliability, based on previous studies (Magagnin *et al.* 1993). Where indicated, oocytes were incubated with MTSET or MTSEA (1 mM in ND100) or MTS-TAMRA (0.4 mM in ND100) for 15 min prior to the uptake assay.

To determine the effective rate of labelling, oocytes were pre-incubated with ND100 containing MTS-TAMRA 0.4 mM for 5, 10, 15, 20, 30 for 45 min. $^{32}P$ uptake that remained after each successive application of MTS reagent was normalized to the value measured at $t = 0$ and plotted as a function of the exposure time. The data were fitted with a single decaying exponential to determine the effective second order reaction constant using an equation of the form:

$$v^t = (v^0 - v^\infty)\exp(-ctk) + v^\infty \qquad (1)$$

where $v^t$ is the transport rate (pmol oocyte$^{-1}$ min$^{-1}$) after incubation in the MTS reagent for a given a cumulative exposure time $t$, $v^\circ$ is the $^{32}P$ uptake rate without exposure to the MTS reagent, $v^\infty$ is the $^{32}P$ uptake rate at infinite time, c is the concentration of MTS reagent and $k$ is the effective second order rate constant (e.g. Virkki *et al.* 2006*b*).

For kinetic analysis, $[P_i]$ was varied from 0.1 to 1 mM and $[Na^+]$ was varied from 0 to 125 mM. Data were plotted as a function of $[P_i]$ or $[Na^+]$ and fitted with the Hill equation:

$$v = v^{\max}\left([S]^H/\left([S]^H + \left(K_{0.5}^S\right)^H\right)\right) \qquad (2)$$

where [S] is the concentration of variable substrate ($Na^+$ or $P_i$), $v^{\max}$ is the maximal velocity of transport, $K_{0.5}^S$ is the apparent affinity constant for substrate $S$, which in general depends on the invariant substrate and $H$ is the Hill coefficient.

**Efflux assays.** Control and injected oocytes were injected with 50 nl of a solution containing 0.5 M NaCl, 10 mM Hepes (pH 7.4 adjusted with Tris), 10 mM $P_i$ and $^{32}P$. Taking the typical oocyte volume of 450 nl, based on our estimates of the diameter, which varied from 0.8 to 1.1 mm between individual oocytes and between batches, and assuming spherical geometry, injection would result in an intracellular $[Na^+]$ of >50 mM and $[P_i] > 1$ mM depending on the distribution of these solutes between free aqueous compartment and organelles that can account for up to 63% of the oocyte volume (e.g. Zeuthen *et al.* 2002).

After washing in ND0 solution, single oocytes were incubated in 100 $\mu$l of ND100 or ND0 with or without cold $P_i$. Oocytes were gently shaken manually in the vial containing the specified external solution to ensure adequate mixing before sampling. Aliquots (10 $\mu$l) were collected at the indicated times and radioactivity was determined by liquid scintillation counting. The values were corrected for the volume of the incubation solution and divided by the total amount of radioactivity present in the oocyte. This amount was calculated for each oocyte by adding the radioactivity in the extracellular sample of the last time point and the radioactivity remaining in the oocyte.

### Fluorometry experiments

**Equipment.** The apparatus for simultaneous voltage clamp and fluorometry of *Xenopus* oocytes has been described in detail elsewhere (Virkki *et al.* 2006*b*). It comprises a two-electrode voltage clamp (OC725C, Warner Instruments, LLC, Hamden, CT, USA) with a laboratory-built fluorescence microscope based on a 10× fluorescence objective (CFI S Fluor, 0.5 N.A., 1.2 mm W.D., Nikon, Switzerland), and a filter set (XF33cube, comprising a 535DF35 excitation filter, 570DRLP dichroic mirror and 605DF50 emission filter; Omega Optical

Inc.). Emitted light was measured using a silicon photodiode (S1336-18BQ, Hammatsu, Switzerland) connected to the input of an integrating patch clamp headstage (CV 201, Molecular Devices, Sunnyvale, CA, USA) and processed by a patch clamp amplifier (Axopatch 200A, Molecular Devices). The output of the Axopatch 200A was processed by a differential amplifier/filter unit (LPF-8, Warner Instruments) before digitalization. Fluorescence was excited by a 100 W halogen light source. To avoid photobleaching when not recording, an electronic shutter (VS252T1, Uniblitz, Vincent Associates, Rochester, NY, USA) was mounted between the light source and the optical unit. Oocytes where pre-incubated for 1 h in ND100 solution with MTS-TAMRA, TMR6M or TMR5M 0.4 mM at 20°C.

**Protocols.** Changes in fluorescence were recorded in response to changing substrate concentration and changing membrane potential. Changes in steady state fluorescence, $\Delta F$, were measured in response to changes in: [$Na^+$] (from 0 to 125 mM), [$Li^+$] (from 0 to 125 mM), [$P_i$] (from 0.1 to 1 mM in ND100) or [PFA] (1 mM in ND100 or ND0). Each test substrate concentration application was bracketed with a control solution application (ND100) to allow for correction of a loss of fluorescence (see below). After application of the superfusate the oocyte was allowed to stabilize in the recording chamber for ∼2 min and then the shutter was opened for seven successive 230 ms intervals, to reduce photobleaching. For each change in solution, this protocol was applied 2–3 times. During the shutter opening time, the membrane potential was kept constant at −60 mV (to monitor substrate-dependent $\Delta F$) or was stepped from $V_h = -60$ mV to −120 mV (to monitor voltage dependent $\Delta F$).

**Data analysis.** During the course of the experiment, we observed two losses of fluorescence: (i) a systematic decrease in $F$ that occurred even if the oocyte was only exposed once briefly at the start of an experiment, which was attributable to wash out of unbound dye and the internalization of previously labelled membrane protein; (ii) light-dependent photobleaching that was reduced by using the pulsed protocol described above. These losses in $F$ necessitated off-line data correction, as follows. We corrected the light-independent decrease in fluorescence by plotting $F$ at each application of the control solution (ND100) as a function of exposure time after the start of the experiment. These data were best fitted with a single decaying exponential to yield a standardized time course of loss of $F$ in ND100. Interpolation of these data at the time point when we applied the test solution then allowed us to rescale the test measurement according to the predicted loss of $F$. We corrected the light-dependent decrease in $F$ by determining the change in fluorescence ($\Delta F$) for a defined solution change (ND100 to ND0 for the $Na^+$ and $Li^+$ dose dependence and ND100 to ND100 + $P_i$ (1 mM) for the $P_i$ dose dependence), plotting $\Delta F$ as a function of time and fitting with a single decaying exponential as for the light-independent loss component. These data were interpolated and the test $\Delta F$ rescaled appropriately according to the predicted $\Delta F$ at application time of the test solution. The underlying assumption for the validity of this second correction is that the photobleaching is a function of light exposure only and does not depend on the chemical composition of the perfusate.

After correction, $\Delta F$ obtained in response to changes in substrate concentration was plotted as a function of substrate concentration and fitted with the Hill equation:

$$\Delta F = \Delta F_{max}[S]^H/\left([S]^H + (K_{0.5}^S)^H\right) + K \qquad (3)$$

where [S] is the substrate concentration ($Na^+$, $Li^+$, $P_i$), $\Delta F_{max}$ is the extrapolated maximum fluorescence, $K_{0.5}^S$ is the concentration of S that gives half-maximum response, $H$ is the Hill coefficient and $K$ is an offset constant. All curve fitting was performed using GraphPad Prism v 3.02/4.02 for Windows (GraphPad Software, San Diego, CA, USA). All data are given as mean ± S.E.M.

## Results

### Substrate binding order of WT NaPi-IIc determined by $^{32}P$ flux assays

We characterized the wild-type (WT) NaPi-IIc by heterologous expression in *Xenopus laevis* oocytes using standard $^{32}P$ uptake assays. In the first report of NaPi-IIc kinetics (Segawa *et al.* 2002), estimates of the apparent substrate affinities for $P_i$ ($K_{0.5}^{P_i}$) and $Na^+$ ($K_{0.5}^{Na}$) were determined under saturating conditions for the invariant substrates; however from these data alone it is not possible to infer the binding order. To address this issue, we extended these influx assays by determining the substrate dependence at two concentrations of the invariant substrate. For the WT, the $P_i$ dependence in presence of 100 mM or 50 mM $Na^+$ showed the expected Michaelian characteristics with saturation for [$P_i$] > 0.3 mM (Fig. 1*A*). We fitted both data sets with the Michaelis–Menten equation (eqn (1), $H = 1$) to give estimates for $V_{max}$ and $K_{0.5}^{P_i}$. There was a clear '$V_{max}$' dependence on external [$Na^+$]: a reduction in [$Na^+$] from 100 mM to 50 mM led to a concomitant reduction of $V_{max}$ from 112 ± 11 to 64 ± 10 pmol oocyte$^{-1}$ min$^{-1}$. This behaviour accords with a substrate binding model in which $Na^+$ is the last substrate to bind, assuming rapid equilibrium of substrate binding (e.g. Stein, 1990). Consistent with this finding, the estimated $K_{0.5}^{P_i}$ increased from 0.08 mM to 0.12 mM, which would also be expected for an ordered substrate

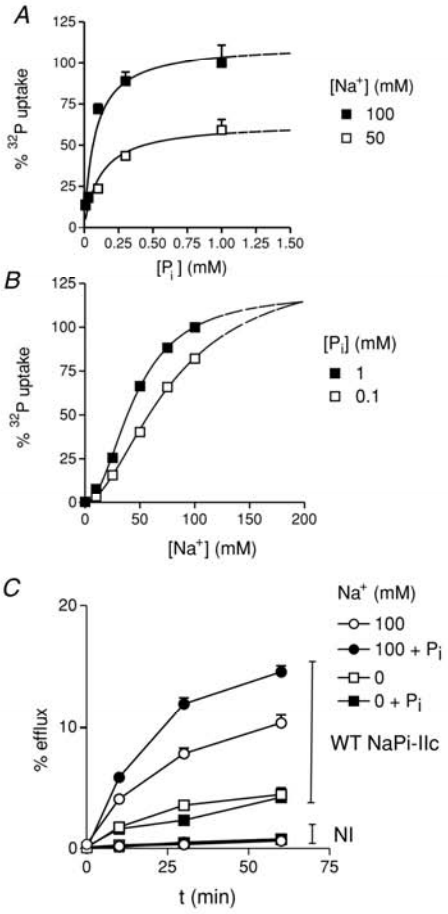


**Figure 1. Substrate dependence of $^{32}$P influx for WT NaPi-IIc**
*A*, $P_i$ dependence of WT mediated $^{32}$P-uptake for different [$Na^+$]. $^{32}$P uptake was measured at 0.01, 0.03, 0.1, 0.3 and 1 mM $P_i$ in the presence of ND100 or ND50 (50 mM NaCl and 50 mM choline chloride) and plotted as a function of [$P_i$]. Data points were fitted with eqn (2) (continuous line). The fit parameters were: $K_{0.5}^{P_i} = 0.08 \pm 0.03$ mM, $V_{max} = 112 \pm 11$ pmol oocyte$^{-1}$ min$^{-1}$ (100 mM $Na^+$) and $K_{0.5}^{P_i} = 0.12 \pm 0.06$ mM, $V_{max} = 64 \pm 10$ pmol oocyte$^{-1}$ min$^{-1}$ (50 mM $Na^+$). Values are means ± S.E.M. ($n$ = 6–8). Data for different oocytes were normalized to the mean uptake rate measured at 1 mM $P_i$ (ND100) and expressed as a percentage. The dashed lines indicate the extrapolated fit beyond the measurement points. *B*, $Na^+$ dependence of WT mediated $^{32}$P-uptake for different phosphate concentrations. $P_i$ uptake was measured at 0, 10, 25, 50, 75 and 100 mM $Na^+$ in the presence of 1 mM and 0.1 mM $P_i$ and plotted as a function of [$Na^+$]. The fit parameters were: $K_{0.5}^{Na} = 43 \pm 3$, $V_{max} = 114 \pm 5$ pmol oocytes$^{-1}$ min$^{-1}$ (1 mM $P_i$); $K_{0.5}^{Na} = 67 \pm 9$, $V_{max} = 125 \pm 19$ pmol oocytes$^{-1}$ min$^{-1}$ (0.1 mM $P_i$). Values are means ± S.E.M. ($n$ = 6–8). Data for different oocytes were normalized to the mean uptake rate measured at 1 mM $P_i$ (ND100) and expressed as a percentage. The dashed lines indicate the extrapolated fit beyond the measurement points. *C*, efflux assays for WT NaPi-IIc and non-injected (NI) oocytes from the same donor frog for different conditions in the external medium (filled symbols, + 1 mM $P_i$; open symbols, 0 mM $P_i$: circles, ND100; squares, ND0). Efflux was measured in ND100 or ND0 solution with or without $P_i$ (1 mM) and plotted as a function of time. Points have been joined by lines for visualising purposes only. Values are means ± S.E.M. ($n$ = 9).

interaction (Stein, 1990), although the results were not significant because of uncertainties in the fit (Table 1).

To further support this conclusion, we measured $Na^+$-dependent $^{32}$P uptake for NaPi-IIc at two [$P_i$]: close to the expected $K_{0.5}^{P_i}$ (0.1 mM) and close to saturation (1 mM). We varied the [$Na^+$] in the extracellular uptake solution from 0 mM to 100 mM. These data showed the expected sigmoidicity predicted for a system in which more than one $Na^+$ ion interacts with the carrier and we found the most satisfactory fit using the Hill equation (eqn (1)) with the Hill coefficient, $H > 1$ (Fig. 1*B*). With 1 mM $P_i$, the fit gave $K_{0.5}^{Na} = 46 \pm 3$ mM, which is close to the value ($48 \pm 9$ mM) previously reported (Segawa *et al.* 2002) and $H = 2.1 \pm 0.2$. By decreasing [$P_i$] from 1 mM to 0.1 mM, we observed that the predicted $V_{max}$ did not change significantly (1 mM $P_i$: $115 \pm 6$ pmol oocyte$^{-1}$ min$^{-1}$; 0.1 mM $P_i$: $125 \pm 19$ pmol oocyte$^{-1}$ min$^{-1}$), which was also consistent with $Na^+$ being the last ion that interacts with the transporter before translocation. Moreover, as predicted for an ordered binding model, $K_{0.5}^{Na}$ increased to ~80 mM (Table 1), whereas the Hill coefficient remained reasonably constant ($1.7 \pm 0.2$).

Although these experiments strongly suggest that $Na^+$ is the last substrate to bind before translocation, there are, however, at least two possibilities for the order of the preceding partial reactions: they could be strictly ordered, in which $Na^+$ precedes $P_i$ (or vice versa) or random, in which either $Na^+$ or $P_i$ interacts depending on the relative activity of the substrate. To investigate these possibilities, we examined the effect of external substrate on $^{32}$P efflux. We injected oocytes with 50 nl aliquots of an injection buffer containing $^{32}$P, so that after ~10 : 1 dilution in the cytosol, the internal [$Na^+$] would be at least 50 mM, which would thereby facilitate establishing an outward $Na^+$ gradient. We then examined the effect of four combinations of external substrates on $P_i$ efflux (Fig. 1*C*) at three time points after incubation in the respective medium. The efflux rates based on the 10 min measurement point were significantly smaller than the corresponding influx rates with comparable driving force. For NaPi-IIc injected oocytes, we measured an efflux rate of $0.18 \pm 0.03$ pmol oocyte$^{-1}$ min$^{-1}$ ($n$ = 4) when incubated in ND0 solution alone compared with typically 40 pmol oocyte$^{-1}$ min$^{-1}$ for influx measurements in ND50. Moreover, insignificant efflux was measured from non-injected oocytes under the same external conditions. For NaPi-IIc expressing oocytes, the efflux rate was

**Table 1. Comparison of phenomenological constants obtained from $^{32}P$ assays, fluorescence ($\Delta F$) and electrophysiology (TEVC)**

| Fit parameter | $K_{0.5}^{P_i}$ (mM) | | $K_{0.5}^{Na}$ (mM) | | $V_{max}^{50}/V_{max}^{100}$ |
|---|---|---|---|---|---|
| Measurement condition | 100 mM $Na^+$ | 50 mM $Na^+$ | 1 mM $P_i$ | 0.1 mM $P_i$ | 100 mM/50 mM $Na^+$; 1 mM $P_i$ |
| **WT NaPi-IIc ($^{32}P$)** | **0.08 ± 0.03** | **0.12 ± 0.06** | **46 ± 8** | **79 ± 9** | **0.57 ± 0.06** |
| **S437C ($^{32}P$)** | **0.08 ± 0.02** | **0.10 ± 0.03** | **46 ± 3** | **79 ± 9** | **0.42 ± 0.04** |
| **S437C ($\Delta F$)** | **0.07 ± 0.01** | **nd** | **79 ± 8** | **nd** | **na** |
| WT NaPi-IIc ($^{32}P$)[1] | 0.07 | nd | 48 ± 3 | nd | nd |
| WT NaPi-IIa (TEVC)[2] | 0.054 | 0.27 | 50.1 | 89 | 0.67 |

Data determined in this study are shown bold; na = not applicable, nd = not determined. [1]Segawa *et al.* (2002). [2]Forster *et al.* (1998).

non-linear for all the conditions and suggested that saturation would occur at times > 60 min. This may result from substrate accumulation due to unstirred layer effects at the external face of the oocyte membrane.

Under all three incubation conditions, the $^{32}P$ efflux by control oocytes was negligible (< 1%) compared to those expressing NaPi-IIc (Fig. 1*C*), which established that the efflux was a direct result of expression of NaPi-IIc. In the absence of external $Na^+$, a significant efflux was measured that was unaffected by external $P_i$. The lack of trans-inhibition of efflux by external $P_i$ in the absence of external $Na^+$ is consistent with a scheme that requires $Na^+$ to bind before $P_i$ (see Discussion). In contrast, the presence of external $Na^+$ (100 mM) in the external medium stimulated efflux approximately 2-fold (at 60 min) and there was a further ~25% stimulation when $P_i$ was also present in the external medium.

### Introducing a Cys at Ser-437 does not alter basic transport properties

To gain further insight into the interactions of substrates with NaPi-IIc, we used a fluorometric approach in which a change in emitted fluorescence that results from changes in a fluorophore's micro-environment are assumed to reflect local, substrate-induced conformational changes. This approach requires introducing a novel cysteine in the protein at a functionally important site that can be conveniently covalently labelled with the fluorophore from the external medium. Based on previous studies, we chose the site Ser-437 at the C-terminal end of the putative, extracellularly oriented, re-entrant segment comprising transmembrane domains 8 and 9 (Fig. 2*A*). This site is predicted to be a region highly accessible from the extracellular solution and is close to the predicted substrate translocation pathway (Lambert *et al.* 2001; Kohler *et al.* 2002). The equivalent Ser–Cys substitution in the electrogenic isoforms (NaPi-IIa, NaPi-IIb) is well-tolerated with only minor changes in transport properties. After incubation in methanethiosulfonate (MTS) reagents, including MTS conjugated with the fluorophore rhodamine, electrogenic cotransport activity and $P_i$ transport are significantly suppressed, yet substrate interactions are retained (Lambert *et al.* 1999; Virkki *et al.* 2006*b*).

As for WT NaPi-IIc, $P_i$ transport by S437C was $Na^+$ dependent, and moreover, the $Na^+$-dependent transport activity of oocytes expressing WT NaPi-IIc and S437C for oocytes from the same donor animal was very similar (Fig. 2*A*). This indicated that under these assay conditions, the mutation most likely had not altered the turnover rate. We next repeated the $P_i$ dependence and $Na^+$ dependence assays (Fig. 1*A* and *B*) and obtained similar estimates for the apparent substrate affinities to the WT (see Table 1). Finally, we investigated the effect on cotransport activity of the $Na^+/P_i$ cotransport inhibitor, phosphonoformic acid (PFA), which is a competitive inhibitor of $P_i$ transport mediated by SLC34 proteins (Busch *et al.* 1995; Villa-Bellosta *et al.* 2007). We confirmed that PFA also inhibits uptake mediated by NaPi-IIc and S437C by performing radio-labelled $P_i$ uptake assays on oocytes incubated with $P_i$ (0.3 mM) or both $P_i$ (0.3 mM) and PFA (1 mM), and a significant decrease in $^{32}P$ uptake was documented (Fig. 2*C*). Taken together, these data confirmed that the Ser–Cys substitution had not affected the basic characteristics of the protein.

### Changes in fluorescence reported by mutant S437C after labelling with MTS-TAMRA

We next investigated the properties of S437C after labelling with MTS reagents. Oocytes that expressed either the WT or S437C were assayed for $Na^+$-dependent $^{32}P$ uptake after incubation with MTSEA, MTSET or MTS-TAMRA (15 min, 1 mM). For the WT, uptake was unaltered (Fig. 3*A*), as we have previously reported for the WT NaPi-IIa (Lambert *et al.* 1999; Ehnes *et al.* 2004). This confirmed that there are no functionally important Cys residues accessible in the WT. In contrast, $^{32}P$ for S437C was significantly reduced after preincubation in all three reagents (Fig. 3*A*). This finding agrees with the behaviour that we have previously reported for the equivalent mutants in the electrogenic rat NaPi-IIa (S460C) (Lambert *et al.* 1999) and flounder NaPi-IIb (S448C) (Virkki

*et al.* 2006*b*). It supports our conclusion that this site is critical among all SLC34 gene products. For incubation in MTS-TAMRA, we observed that there was approximately 25% transport activity remaining after Cys modification. This might indicate that the concentration/exposure time was insufficient to complete the modification of all expressed proteins, or that the Cys modification does not cause a complete loss of activity of the protein, as we have previously observed for some Cys mutants (e.g. Lambert *et al.* 2001; Ehnes *et al.* 2004).

To investigate the underlying reasons for this behaviour, we exposed oocytes expressing WT or S437C for longer times and assayed the uptake. WT NaPi-IIc showed no significant alteration in activity for incubation periods up to 45 min, whereas the activity of S437C decreased progressively and reached a plateau corresponding to approximately 10% of the initial response at each test exposure (Fig. 3*B*). By assuming the MTS reagent to be in excess, we can consider the decrease in activity to result from a pseudo first order reaction and by fitting these data with a decaying exponential (eqn (1)) an effective second order rate constant, $k = 0.055 \pm 0.001$ mM$^{-1}$ s$^{-1}$, was obtained (e.g. Karlin & Akabas, 1998). This is an indirect measure of the accessibility of the Cys-437 by MTS-TAMRA and is at least two orders of magnitude smaller than values we have previously reported for the rat NaPi-IIa S460C (Lambert *et al.* 2001) and the flounder NaPi-IIb S448C (Virkki *et al.* 2006*b*). The apparent reduced accessibility may result from the larger size of the conjugated fluorophore compared with the other MTS reagents or a lower accessibility of the site for NaPi-IIc compared with the electrogenic isoforms. The baseline activity for long exposure may result from the insertion of unlabelled protein that we have also observed in the case of the electrogenic isoforms (I. C. Forster and L. V. Virkki, unpublished observations). From these data we decided to routinely incubate S437C in 1 mM MTS-TAMRA for 60 min.

Oocytes incubated with MTS-TAMRA showed a reversible increase in fluorescence when the superfusion solution was changed from ND100 to ND0 (i.e. removal of external $Na^+$). We observed no changes of background fluorescence in response to changes in the external medium in non-injected or water-injected control oocytes, which indicated that the fluorescence response is unique to oocytes that express S437C (data not shown). A representative recording (Fig. 4*A*) shows two additional features. First, there was a decrease in change in fluorescence ($\Delta F$), which we attribute to photobleaching. Although this could be reduced by limiting the time the shutter was open (230 ms), it still accounted for up 50% of the decrease in $\Delta F$. Second, we observed another type of fluorescence loss that was independent of exposure to light (dashed line, Fig. 4*A*). This fluorescence

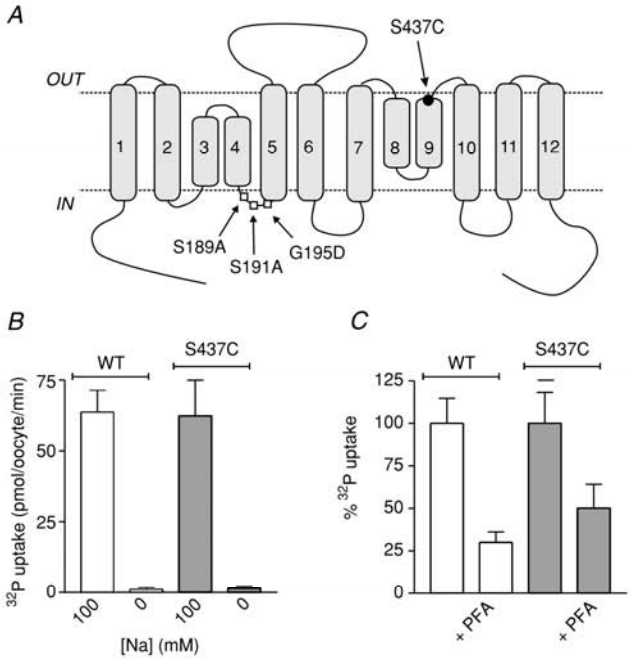


**Figure 2. Mutant S437C shows similar transport properties to WT NaPi-IIc**
*A*, topological model of SLC34 proteins indicating the site of the Ser–Cys substitution for mutant S437C (filled square). The model proposes 12 transmembrane domains (numbered), 2 opposed reentrant loops and intracellular C- and N- termini (e.g. Virkki *et al.* 2007). The sites substituted in the AAD mutant that resulted in a NaPi-IIc electrogenic transporter are also indicated (open squares) (Bacconi *et al.* 2005) (see Discussion). *B*, oocytes injected with cRNA of WT (open bars) or S437C mutant (filled bars) were assayed 3 days after injection for $^{32}$P uptake in the presence of standard uptake solution (ND100) or $Na^+$-free uptake solution (equimolar replacement of $Na^+$ by choline). Values are means ± S.E.M. ($n = 5$–6). *C*, $^{32}$P uptake measured for WT and S437C using standard uptake solution (ND100) in the absence or presence of PFA (1 mM). Values are means ± S.E.M. ($n = 6$–7). Data for different oocytes were normalized to the mean uptake rate measured at 1 mM $P_i$ in the absence of PFA and expressed as a percentage.

loss is probably due to the wash-out of unbound dye or to the internalization of labelled protein and it follows a mono-exponential decay.

As described in Methods, we calculated $\Delta F$ in response to a solution change from the standard [$Na^+$] (ND100) to the test solution as the difference between the value recorded and that predicted from the fit when the oocyte was superfused with ND100. Figure 4*B* shows the same data replotted as mean $F$ of the individual seven measurements plotted on an absolute time scale. The same time-dependent decrease in $F$ was also found in the absence of $Na^+$ (ND0), which confirmed that the effect was not due to substrate interaction with the fluorophore itself (data not shown).

We performed these pilot experiments using MTS-TAMRA that we have previously used for VCF studies on the flounder NaPi-IIb mutants (Virkki *et al.* 2006*a*,*b*). As MTS-TAMRA is a mixed isomer and may therefore result in a reduced $\Delta F$, we compared the response with that from separate labelling with single isomers (tetramethylrhodamine-6-maleimide

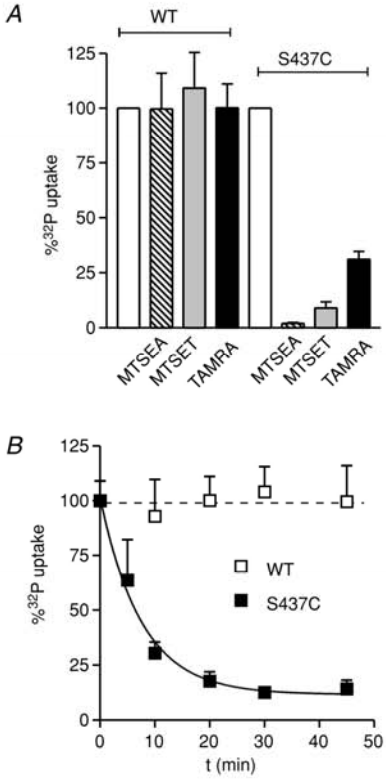


**Figure 3. Effect of MTS on WT and S437C transport activity**
*A*, oocytes expressing WT or S437C were incubated for 15 min with MTSEA, MTSET or MTS-TAMRA (1 mM) and then $^{32}P$ uptake was assayed. Values are means ± S.E.M. ($n \geq 6$). *B*, groups of 6–8 oocytes expressing WT (open squares) or S437 (filled squares) were pre-incubated for different times (5, 10, 20, 30, 45 min) in MTS-TAMRA (0.4 mM) and $^{32}P$ uptake was measured in the control solution (ND100). $^{32}P$ uptake after each MTS-TAMRA exposure was normalized to the value at $t = 0$ and expressed as a percentage. Data points were fitted with a single decaying exponential (continuous line) to obtain the effective second-order rate constant for Cys modification. For WT, data points are connected by a dotted line to better visualize the absence of effect of MTS-TAMRA on $P_i$ uptake.

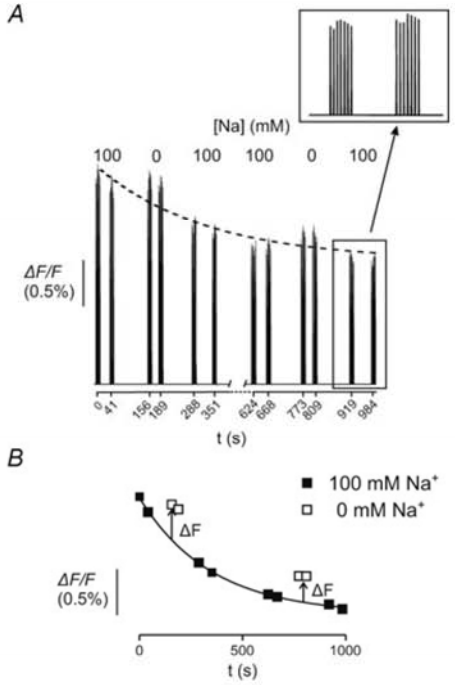


**Figure 4. Fluorescence measurements in the steady state**
*A*, original fluorescence traces recorded in presence of different $Na^+$ concentrations at the holding potential of −60 mV recorded with a Minidigi 1A (Molecular Devices). The ordinate is the change in fluorescence expressed as a percentage of the initial background fluorescence signal when the shutter was first opened. $V_h$ was kept constant at −60 mV and the shutter was open for 7 successive 230 ms pulses followed by a 2 s closed time. For each [$Na^+$] concentration, the protocol was repeated 2 or 3 times and to control for loss of $F$ in each test solution (ND0, in this case) the assay was bracketed by ND100. To better visualize the progressive loss of fluorescence, the signal (mean of the 7 samples) recorded in the presence of ND100 is connected by a dashed line. Note that the change in fluorescence ($\Delta F$) induced is smaller for the second set of measurements in ND0 because of photobleaching (see Methods). *B*, $F$ measured in ND100 (filled squares) is plotted as a function of time and fitted with a single decaying exponential (continuous line) to quantify loss of fluorescence. The effective change in fluorescence ($\Delta F$) induced by a change in substrate concentration is calculated as the difference between the value experimentally obtained and the value predicted from the fit. Error bars smaller than symbol size are not shown.

and tetramethylrhodamine-5-maleimide). Oocytes were incubated with each of the fluorophores (final concentration 0.4 mM) in the presence of ND100 for 1 h. The main difference among the three fluorophores was the value of background fluorescence: for tetramethylrhodamine-6-maleimide and tetramethylrhodamine-5-maleimide the background fluorescence, taken as the steady-state photodiode current relative to the dark condition, was respectively 6.4-fold and 5.3-fold higher than that observed for MTS-TAMRA (data not shown). This higher background fluorescence was probably due to unspecific interaction with endogenous protein expressed in the oocyte and the consequence is a lower $\Delta F/F$ ratio. Therefore, we performed all subsequent experiments with the mixed isomer.

### Voltage and cation dependence of fluorescence

$P_i$ translocation mediated by SLC34 proteins is coupled to the electrochemical gradient of $Na^+$. Our finding that a change in $F$ accompanies a change in external $[Na^+]$ provided compelling evidence that $Na^+$ ions interact with NaPi-IIc before $P_i$ binding, as we have previously reported for the electrogenic NaPi-IIb isoform (Virkki *et al.* 2006*b*). In that study, we showed that the dependence of $F$ on external $[Na^+]$ is cooperative, which indicated that more than one $Na^+$ ion interacts with the protein before $P_i$ binding. Given that NaPi-IIc is electroneutral and involves translocation of two $Na^+$ ions per divalent $P_i$, and if we assume that the last substrate interaction before translocation is $Na^+$ dependent (Fig. 1*A*), we would therefore predict that for an ordered binding scheme, only one $Na^+$ ion should interact with S437C in the absence of $P_i$.

To test this hypothesis, we examined $\Delta F$ with increasing $[Na^+]$ in the absence of $P_i$ (Fig. 5*A*). We recorded the highest fluorescence in 0 mM $Na^+$ (ND0), which was then progressively quenched as $[Na^+]$ increased. There was clear evidence of saturating behaviour, although we did not increase $[Na^+]$ above 125 mM because the oocytes did not generally tolerate higher $[Na^+]$, particularly for long exposure times. These data reveal a sigmoidal relationship between $\Delta F$ and $[Na^+]$ and when fitted with the Hill equation (eqn (2)) the fit predicted an apparent affinity for $Na^+$, $K_{0.5}^{Na} = 78.7 \pm 7.7$ mM and a Hill coefficient, $H = 1.8 \pm 0.1$. Thus, although the MTS-TAMRA-labelled S437C no longer transports $P_i$, $Na^+$ ions interact with S437C and in a cooperative manner: the Hill coefficient indicated the cooperative binding of more than one $Na^+$ ion in the absence of $P_i$.

For electrogenic NaPi-IIb, we have also shown that the dependence of $\Delta F$ on $[Na^+]$ is voltage dependent (Virkki *et al.* 2006*a*,*b*). As it is possible that one or more partial reactions in the transport cycle of electroneutral carrier may still be electrogenic (e.g. Lester *et al.* 1994), we next investigated if this was the case for S437C. We compared $\Delta F$ obtained in ND0 solution at three potentials: 0 mV, −60 mV and −120 mV. We were unable to detect any significant difference in $\Delta F$, which strongly suggested that the partial reactions that reflect the

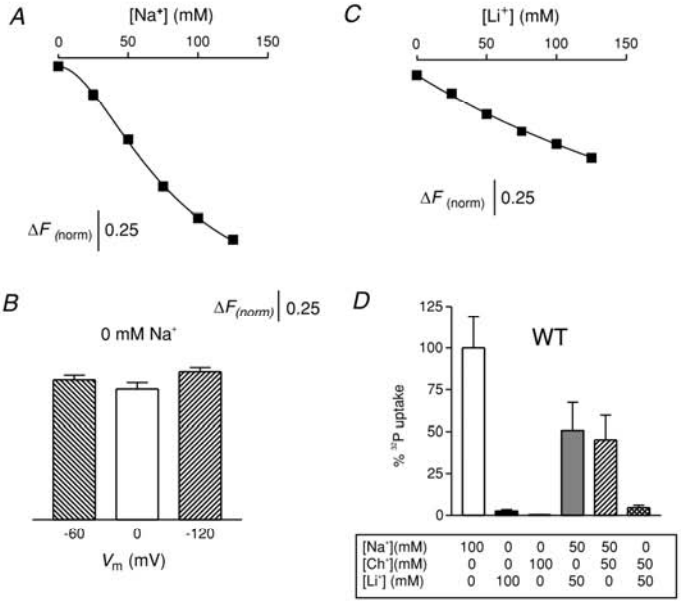


**Figure 5. Sodium and lithium dependence of fluorescence change ($\Delta F$) in oocytes expressing S437C**
*A*, $Na^+$ dependence of fluorescence ($\Delta F$). Fluorescence was recorded at different $[Na^+]$ and data were fitted with eqn (3) (continuous line). Values are given as means ± S.E.M. ($n = 4$ for $[Na^+] = 125$ mM and 75 mM; $n \geq 7$ for $[Na^+] = 100$ mM, 0 mM, 25 mM and 50 mM). Error bars smaller than symbol size are not shown. *B*, voltage dependence of fluorescence ($\Delta F$). Fluorescence was recorded at $V_h = -60$ mV, 0 mV and −120 mV and normalized to the value obtained at −60 mV. Values are means ± S.E.M. ($n = 5$). *C*, $Li^+$ dependence of fluorescence ($\Delta F$). Fluorescence was recorded at different $Li^+$ concentrations and data were fitted with eqn (3) (continuous line). The fit gave an apparent affinity constant for $Li^+$, $K_{0.5}^{Li} = 377 \pm 111$ mM. Values are means ± S.E.M. ($n \geq 4$). Error bars smaller than symbol size are not shown. *D*, $^{32}P$ uptake was measured for NaPi-IIc WT in presence of different superfusates as indicated (concentrations in mM). Values are means ± S.E.M. ($n = 8$). There was no statistical significance between the uptake for 50 mM $Na^+$ + 50 mM $Li^+$ and 50 mM $Na^+$ + 50 mM Chol.

localized conformational changes near Cys-437 are voltage independent (Fig. 5*B*).

Sodium is the only cation that acts as a cosubstrate for NaPi-II isoforms, although previous studies have shown that $H^+$ (Forster *et al.* 2000; Virkki *et al.* 2005*b*) and $Li^+$ (Virkki *et al.* 2006*a*,*b*) interact. We therefore examined the effect of replacing $Na^+$ with equimolar $Li^+$ and we found that $\Delta F$ decreased with increasing $[Li^+]$ (Fig. 5*C*). We fitted the $Li^+$ dependence with the Hill equation (eqn (3)). The unconstrained fit predicted a Hill coefficient, $H = 1.07 \pm 0.23$, which suggested, as we have previously shown, that only one $Li^+$ interacts with the electrogenic NaPi-IIb (Virkki *et al.* 2006*b*). When we constrained $H = 1$ (Fig. 5*C*) to reduce the fit uncertainty, this procedure yielded an apparent affinity constant for $Li^+$, $K_{0.5}^{Li} = 377 \pm 111$ mM which, given the fit error, is comparable to the value reported using VCF (Virkki *et al.* 2006*b*). These results indicated that, as observed for NaPi-IIb (Virkki *et al.* 2006*b*), $Li^+$ ions can also interact with NaPi-IIc, but in an apparently non-cooperative manner.

If $Li^+$ ions interact with the transporter as suggested by the above fluorometric findings, can this interaction alter $Na^+$-dependent transport rate? To answer this question, we performed $^{32}P$ uptake at 50 mM $Na^+$, close to the predicted $K_{0.5}^{Na}$ and compared having either choline or $Li^+$ as the remaining cation (Fig. 5*D*). As expected, complete replacement of $Na^+$ with either $Li^+$ or choline resulted in insignificant transport activity for the WT. Moreover, we observed no significant difference in uptake in the presence of 50 mM $Na^+$ when $Li^+$ or choline constituted 50% of the main monovalent cations. S437C showed similar behaviour (data not shown). These findings established that $Li^+$ appears to have no direct effect on the cotransport activity with saturating $P_i$.

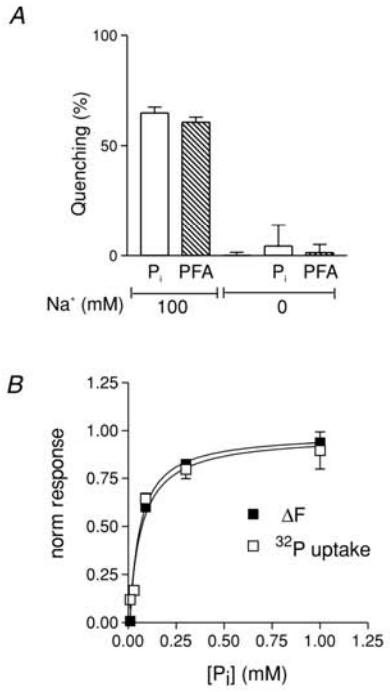


**Figure 6. $P_i$ and PFA dependence of fluorescence change ($\Delta F$) in oocytes expressing S437C**

*A*, comparison of the effect of substrate on fluorescence quenching in ND100 and in ND0, in the presence of $P_i$ (1 mM) (open bars) or PFA (1 mM) (hatched bars). Data are expressed as a percentage of the total fluorescence quench when changing from ND0 to ND100 measured in the absence of substrate. Values are means ± S.E.M. ($n \geq 5$). *B*, $\Delta F$ was recorded at different $P_i$ concentrations (0, 0.1, 0.3 and 1 mM) and data were fitted with eqn (3) ($H = 1$). The fit gave an apparent affinity constant, $K_{0.5}^{P_i} = 0.066 \pm 0.003$ mM. Values are means ± S.E.M. ($n \geq 5$). Error bars smaller than the symbol size are not shown.

### $P_i$ and PFA induce fluorescence changes in presence of $Na^+$ ions

We analysed $\Delta F$ due to the presence in the extracellular solution of 1 mM $P_i$ in ND100 or ND0. In the absence of $Na^+$ ions in the external medium (ND0), $P_i$ induced no change in $F$ relative to the control condition (ND0). However, in ND100, when we added 1 mM $P_i$ to the superfusate, we observed an increase of $F$ relative to ND100 alone (Fig. 6*A*). This increase was approximately 30% of the maximal change in fluorescence observed in ND0 alone relative to $F$ in ND100.

As PFA is a competitive inhibitor of $Na^+$–$P_i$ cotransport, we would expect it to interact at the same site as $P_i$. Therefore, we would predict that PFA would cause a similar $\Delta F$ as $P_i$. To test this prediction, we recorded $\Delta F$ in the presence of 1 mM PFA, by superfusing in ND100 or ND0, and the data were compared with $\Delta F$ recorded in the presence of $P_i$. Here, we observed that 1 mM of either PFA or $P_i$ in ND100 gave a similar percentage quench of fluorescence and this accounted for approximately 65% of the total quench observed when changing from ND0 to ND100 (Fig. 6*A*). This suggested that the conformational change induced by the interaction of either substrate with the carrier, in the micro-environment of Cys-437, is the same, in support of our prediction. When the same experiment was performed in the absence of external $Na^+$ (ND0), no significant fluorescence quenching was observed apart from the normal loss of $F$ (see Methods). Taken together, these results indicate that both $P_i$ and PFA require $Na^+$ in the extracellular solution to interact with the transporter and suggest that they share a common binding site.

Finally, we observed that the change in fluorescence induced by $P_i$ showed a dose dependence that was well

described by fitting the data with the Michaelian form of eqn (3) ($H = 1$) (Fig. 6*B*). The fit predicted an apparent affinity constant for $P_i$, $K_{0.5}^{P_i} = 0.066 \pm 0.003$ mM, which is close to that estimated by means of uptake for the WT or S437C before MTS incubation (Table 1). The similarity of the $P_i$ dose dependence for the normal and modified protein can be readily seen by superimposing the normalized fluorescence and uptake data (Fig. 6*B*). Taken together, these findings suggested that after incubation with MTS-TAMRA, $P_i$ still interacts with the mutant in a similar manner to the fully functional protein, although $P_i$ cotransport is blocked in the former case.

## Discussion

Solute cotransport involves the interaction of one or more cations with the carrier to initiate and facilitate substrate binding and translocation. Ideally there is tight coupling between the driving cations and the driven solute, and translocation can only take place when the carrier is fully loaded. This implies no 'uncoupled' leak of any substrate, a fixed number of substrate binding/interaction sites on the protein and strict 'rules' for occupancy and accessibility to these sites (e.g. Rudnick, 2006), which accord with the canonical alternating access model for cotransport. It follows that the nature of the substrate–carrier interactions that precede translocation of the loaded carrier is essential to characterise the cotransport mechanism of a given carrier. Several generalised models have been proposed to account for coupled transport and to distinguish between, for example, simultaneous and consecutive translocation of substrates and random or ordered binding. Here, we provide evidence, by integrating the findings from isotope flux assays and a novel fluorometric technique, which supports a kinetic scheme in which $Na^+$ is the first and last substrate to interact and bind to the outward facing conformations of the carrier before translocation.

First, based on our influx experiments on the WT NaPi-IIc, our data are consistent with $Na^+$ being the last to bind before translocation of the fully loaded carrier because the maximum transport velocity ($V_{max}$) shows a $Na^+$ dependence under saturating $P_i$. This conclusion is further supported by the results of the complementary experiment in which the external [$Na^+$] was varied at two [$P_i$] and no '$V_{max}$' effect was observed. This behaviour is also consistent with rapid equilibrium conditions applying to at least the $P_i$ interaction with NaPi-IIc (for discussion, see Berteloot, 2003). As summarized in Table 1, for the $P_i$ dependence assays, the ratio of $V_{max}$ in ND50 to that in ND100 for the WT NaPi-IIc, and mutant S437C were similar whereas, for the equivalent measurement using the electrogenic NaPi-IIa, the ratio was higher (Forster *et al.* 1998). This may reflect the presence of an additional driving force (−50 mV) and 3 : 1 stoichiometry with respect to $Na^+$ ions or isoform-specific differences.

The influx experiments are consistent with at least two ordered kinetic schemes illustrated in Fig. 7*A* (left panel), in which the empty carrier (state 1) is sequentially loaded with substrates (state 4), and translocates and releases them to assume an inward facing empty carrier conformation (state 6) before returning to state 1. To determine which of these two schemes is the more likely using only influx assays would necessitate differentiating between the predicted dependencies of $V_{max}$ on [$Na^+$] for each scheme. This may be difficult to achieve as the range of [$Na^+$] possible with the oocyte system is limited, thereby leading to ambiguous interpretations.

Our second experimental strategy involved preloading oocytes with substrate and observing the effect of external substrate interactions on efflux rates (e.g. Turner, 1981, 1984; Beliveau & Strevey, 1988). The efflux rates were at least two orders of magnitude smaller than influx rates with comparable driving force conditions. This may indicate that NaPi-IIc is asymmetrical and optimised for forward mode transport: the apparent substrate affinities on the internal side are low and one or more partial reactions in the reverse cycle are rate limiting. On the other hand, we cannot exclude that the amount of injected $P_i$ (and $^{32}P$) that remains free for transport is significantly reduced due to intracellular sequestering and buffering.

Our findings strongly suggest that $Na^+$ is also the first substrate to interact with the empty carrier on the extracellular side. With no external substrates (i.e. zero *trans*), NaPi-IIc will proceed anticlockwise around the transport cycle, thereby effluxing $^{32}P$ (Fig. 7*A*, right panel, boxed). If $P_i$ were the first substrate to interact with the empty carrier, in the absence of external $Na^+$, we would predict that the addition of $P_i$ to the external medium would increase the proportion of transporters in 'locked' in state 2 so that the overall efflux rate should decrease. Note that for completion of either the influx or efflux cycles starting arbitrarily at state 1, release of all substrates implies that the carrier returns to state 1, independent of the concentration of substrates on the release side. As we observed no significant difference in efflux whether or not external $P_i$ was present, our data favour a model in which external $Na^+$ is required to interact with the carrier before $P_i$ can bind. However, when both $Na^+$ and $P_i$ are present, the transporter will favour occupancy of states 4 and 5, thereby exchanging $^{32}P$ with cold $P_i$ in the external medium (*trans* stimulation). This simple scheme nevertheless fails to explain the stimulatory effect of external $Na^+$ on $^{32}P$ efflux (Fig. 1*C*). For the ordered model, addition of external $Na^+$ in the absence of $P_i$ should result in a *trans*-inhibition of efflux as a fraction of the transporters will favour occupancy of state 2. The discrepancy between the predicted model behaviour and measured data can be resolved if we assume that an

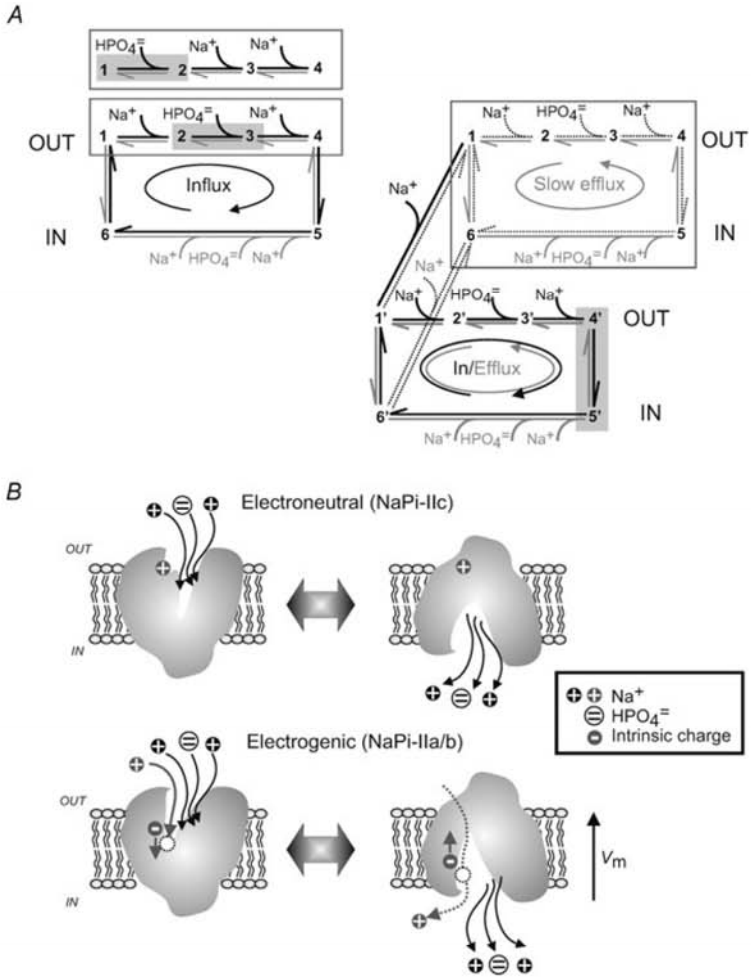


**Figure 7. Evolution of a kinetic scheme for NaPi-IIc**
*A*, influx and efflux experiments suggest an ordered binding scheme for substrate interactions on the outside. Each number represents a conformation (state) that the carrier occupies in sequence during the transport cycle. Preferred partial reactions: bold (influx: black; efflux: grey); unfavourable reactions: dotted. Influx experiments (left panel) allow discrimination between the boxed binding schemes and are consistent with $Na^+$ being the last substrate interaction before translocation (lower box). The $P_i$ interaction ($2 \rightleftharpoons 3$) is in rapid equilibrium (shaded). We cannot readily distinguish between the two schemes so that first substrate interaction remains undefined. Efflux experiments (right panel) are consistent with $Na^+$ being the first substrate to bind. In the absence of external $Na^+$, the addition of $P_i$ to the outside does not affect the efflux rate because transition $2 \rightarrow 3$ cannot occur. The low efflux rate under zero *trans* conditions occurs via the 'unprimed' cycle (boxed). The 'primed' cycle occurs when external $Na^+$ is available and first involves partial reaction $1 \rightarrow 1'$ to bind the 'catalytic' $Na^+$ ion (see text). With external $Na^+$ and $P_i$ available, the carrier adopts an exchange mode ($4' \rightleftharpoons 5'$) (shaded). *B*, scheme comparing the essential differences in substrate interactions for the electroneutral NaPi-IIc (upper) and electrogenic NaPi-IIa/b (lower) isoforms. Two conformations are shown: binding sites externally oriented (left) and internally oriented (right). For NaPi-IIc, the first $Na^+$ to interact is postulated to be immobile during the whole cotransport cycle, but acts as a catalytic activator for subsequent substrate binding to give a 2 : 1 cotransport stoichiometry. For NaPi-IIa/b, an additional intrinsic mobile charge establishes a binding site and translocation pathway for the first $Na^+$ ion within the transmembrane electric field. In the absence of external $P_i$, this $Na^+$ ion can leak through the protein (uncoupled leak mode), whereas in the presence of external $P_i$, it participates in the transport cycle and is released along with $P_i$ and 2 more $Na^+$ ions to give a 3 : 1 cotransport stoichiometry. Upon release of substrates on the inside, the intrinsic charge senses the transmembrane field and its movement causes a voltage-dependent reorientation of the empty carrier to expose the activating $Na^+$ ion binding site once more to the external medium.

additional $Na^+$ ion interacts with the empty carrier with high affinity in the outward oriented conformation (state 1) so that the efflux transport cycle proceeds at a faster rate, as observed experimentally. Evidence for this hypothesis was obtained from the fluorometry data and the properties of the electrogenic isoforms as follows.

We previously applied the fluorometric technique under voltage clamp conditions to the electrogenic NaPi-IIb (Virkki *et al.* 2006*b*). In that study, we obtained evidence that two $Na^+$ ions interact cooperatively with the empty carrier prior to $P_i$ binding and that one of these interactions is most likely electroneutral (Virkki *et al.* 2006*a*). This led to the proposal of a binding sequence for NaPi-IIa/b of $Na^+$–$Na^+$–$P_i$–$Na^+$ that contrasted with our previously proposed $Na^+$–$P_i$–$Na^+$–$Na^+$ scheme (Forster *et al.* 1998). For the electroneutral NaPi-IIc with a 2 : 1 $Na^+$ : $P_i$ cotransport stoichiometry, it follows that in accordance with the $Na^+$–$P_i$–$Na^+$ binding order (Fig. 7*A*),we would predict that only one $Na^+$ ion should interact before $P_i$ binding and the fluorescence quenching should show a hyperbolic dependence on external [$Na^+$].

Like the electrogenic NaPi-IIb (Virkki *et al.* 2006*b*), we could label the equivalent site in NaPi-IIc (Cys-437) with a fluorophore and record changes in fluorescence in response to changes in the external substrates. In the absence of external $P_i$, increasing the external [$Na^+$] quenched the fluorescence as we have previously documented for the labelled Cys-448 in NaPi-IIb (Virkki *et al.* 2006*b*), but for the electroneutral S437C mutant, this effect was independent of the membrane potential. The $Na^+$-dependent fluorescence quenching in the absence of $P_i$ corroborates the efflux studies on the WT NaPi-IIc by showing that under these conditions $Na^+$ ions can induce conformational changes of the protein that are reported by the fluorophore linked to Cys-437. The fluorescence data therefore provide independent support for a kinetic scheme in which $Na^+$ is the first substrate to interact with the empty carrier (Fig. 7*A*). Unexpectedly, we found that the change in fluorescence induced by changes in external [$Na^+$] reflected a cooperative interaction of $>1$ $Na^+$ ion. The Hill coefficient of $\sim$2 therefore suggests that at least two $Na^+$ ions interact with both electroneutral and electrogenic SLC34 proteins in a similar cooperative manner.

To account for this behaviour in our model, we therefore postulate that in the forward (clockwise) cycle of NaPi-IIc, an additional $Na^+$ ion first binds to the empty carrier state 1 (partial reaction 1–1′, Fig. 7*A*) with high affinity from the external solution. This ion remains bound throughout the 'primed' cotransport cycle (1′–2′–3′–4′–5′–6′–1′), thereby acting as a catalytic activator for cotransport (Turner, 1983); however it does not contribute to overall stoichiometrically coupled cotransport. Its presence can then explain the stimulatory effect that external $Na^+$ ions have on $^{32}P$ efflux (Fig. 1*C*). In the absence of external $Na^+$, with the catalytic site unoccupied, efflux takes place via the less favourable 'unprimed' efflux cycle that involves a reorientation of the empty carrier (1→6, Fig. 7*A*). In contrast, in the presence of external $Na^+$, the catalytic $Na^+$ binding site is now occupied and we predict that the carrier will then efflux at a higher rate, i.e via the 'primed' cycle that now involves a reorientation of the 'primed' empty carrier (1′–6′) after substrate release. The identity of the partial reaction(s) in the 'unprimed' cycle altered by the presence of this $Na^+$ ion remains to be determined. As indicated in Fig. 7*A*, the binding at the catalytic site by a $Na^+$ ion from the internal side (partial reaction 6→6′) is assumed to be unfavourable.

Thus, it is only in the electrogenic isoforms that the first $Na^+$ ion binds to a site *within* the transmembrane field, as evidenced by $Na^+$-dependent pre-steady-state relaxations (e.g. Forster *et al.* 2002). This $Na^+$ ion is subsequently translocated – either in the absence of $P_i$ (uncoupled leak mode) (Forster *et al.* 1998; Andrini *et al.* 2008) or together with $P_i$ and two additional $Na^+$ ions (cotransport mode), as depicted in Fig. 7*B*. In both cases the translocation within the protein is an electroneutral event. Therefore, in terms of substrate interactions, the electrogenic isoforms (e.g. Virkki *et al.* 2006*b*) and the electroneutral NaPi-IIc differ only with respect to the mobility of the first $Na^+$ ion. So far, structure–function studies on SLC34 proteins have revealed one key structural difference between the electrogenic and electroneutral isoforms: the absence of a charged aspartic acid at the equivalent site in NaPi-IIc (Gly-195) (Fig. 2*A*): removal of this charge in NaPi-IIa results in electroneutral cotransport (Virkki *et al.* 2005*a*), whereas introduction of this charge in NaPi-IIc restores electrogenic behaviour, including PFA-sensitive leak, presteady-state relaxations and 3 : 1 $Na^+$ : $P_i$ stoichiometry (Bacconi *et al.* 2005).

Although the fluorescence data were obtained from a protein that has been modified and cannot complete the full cotransport cycle, our finding that the apparent $K_{0.5}^{P_i}$ obtained from fluorescence measurements was close to that obtained using uptake assays with the whole transport cycle (Table 1) strongly suggests that the partial reactions that determine this phenomenological parameter are unchanged in the labelled S437C. Moreover, we can exclude translocation of the fully loaded carrier as a kinetic determinant of $K_{0.5}^{P_i}$. On the other hand, the apparent affinity for $Na^+$ interactions ($K_{0.5}^{Na}$) determined by fluorescence was significantly larger than that determined using flux assays (Table 1). As $K_{0.5}^{Na}$ obtained from fluorescence only relates to the first two $Na^+$ interactions, the higher apparent $K_{0.5}^{Na}$ for partial reactions suggests that the final $Na^+$ interaction is a strong determinant of the overall apparent $K_{0.5}^{Na}$. Consistent with our previous studies on electrogenic NaPi-IIa/b in which Cys substitution was made at the equivalent site in NaPi-IIa (Ser-460) (Lambert *et al.* 1999; Kohler *et al.* 2002) and NaPi-IIb (Ser-448) (Virkki *et al.* 2006*b*), this finding would

also suggest that the modified Cys-437 in NaPi-IIc limits conformational changes to those associated with the same partial reactions. However, we are unable to determine if the last $Na^+$ interaction ($3 \rightleftharpoons 4$) can occur and the Cys modification blocks the final translocation of the fully loaded carrier ($4 \rightleftharpoons 5$) (Fig. 7*A*). The fluorometric measurements on S437C also establish that like $P_i$, the interaction of the inhibitor PFA with the carrier requires $Na^+$. As the increase in fluorescence relative to ND100 alone by both substrates was very similar, this would be consistent with its established competitive inhibitory properties (Szczepanska-Konkel *et al.* 1986) and it most likely interacts directly at the $P_i$ binding site. Finally, in contrast to $Na^+$, $Li^+$ ions do not drive $P_i$ cotransport, yet we observe a change in $F$ when $[Li^+]$ is changed that was qualitatively similar that reported for the electrogenic NaPi-IIb isoform (Virkki *et al.* 2006*b*). The lack of a significant change in uptake rate at 50 mM $Na^+$, when $Li^+$ was substituted for choline, may indicate that there is no direct interaction between these cations in NaPi-IIc.

### Conclusions

Our findings suggest that electrogenic and electroneutral SLC34 isoforms probably share a common functional architecture, which includes substrate coordination sites and translocation pathway. These structural features are reflected in the identical transport characteristics (similar $K_m^{P_i}$, $K_m^{Na}$, pH dependence) for these isoforms. They differ only with respect to the role played by the catalytically activating first $Na^+$ interaction, which in the case of the electrogenic isoforms will serve to increase the electrochemical driving force for cotransport and the concentrating capacity of the carrier. This study also underscores the notion that transport stoichiometry and substrate binding stoichiometry may not be equivalent among members of the same transporter family and this may be a feature common to coupled transport systems (e.g. Rudnick, 2006; Shi *et al.* 2008).

## References


Andrini O, Ghezzi C, Murer H & Forster IC (2008). The leak mode of type II $Na^+$-$P_i$ cotransporters. *Channels (Austin)* **2**, 346–357.

Bacconi A, Virkki LV, Biber J, Murer H & Forster IC (2005). Renouncing electrogenicity is not free of charge: switching on electrogenicity in a $Na^+$-coupled phosphate cotransporter. *Proc Natl Acad Sci U S A* **102**, 12606–12611.

Beck L, Karaplis AC, Amizuka N, Hewson AS, Ozawa H & Tenenhouse HS (1998). Targeted inactivation of Npt2 in mice leads to severe renal phosphate wasting, hypercalciuria, and skeletal abnormalities. *Proc Natl Acad Sci U S A* **95**, 5372–5377.

Beliveau R & Strevey J (1988). Kinetic model for phosphate transport in renal brush-border membranes. *Am J Physiol Renal Physiol* **254**, F329–336.

Bergwitz C, Roslin NM, Tieder M, Loredo-Osti JC, Bastepe M, Abu-Zahra H, Frappier D, Burkett K, Carpenter TO, Anderson D, Garabedian M, Sermet I, Fujiwara TM, Morgan K, Tenenhouse HS & Juppner H (2006). SLC34A3 mutations in patients with hereditary hypophosphatemic rickets with hypercalciuria predict a key role for the sodium-phosphate cotransporter NaPi-IIc in maintaining phosphate homeostasis. *Am J Hum Genet* **78**, 179–192.

Berteloot A (2003). Kinetic mechanism of $Na^+$-glucose cotransport through the rabbit intestinal SGLT1 protein. *J Membr Biol* **192**, 89–100.

Busch AE, Wagner CA, Schuster A, Waldegger S, Biber J, Murer H & Lang F (1995). Properties of electrogenic $P_i$ transport by a human renal brush border $Na^+/P_i$ transporter. *J Am Soc Nephrol* **6**, 1547–1551.

Cha A, Zerangue N, Kavanaugh M & Bezanilla F (1998). Fluorescence techniques for studying cloned channels and transporters expressed in *Xenopus* oocytes. *Methods Enzymol* **296**, 566–578.

Drummond GB (2009). Reporting ethical matters in *The Journal of Physiology*: standards and advice. *J Physiol* **587**, 713–719.

Ehnes C, Forster IC, Kohler K, Bacconi A, Stange G, Biber J & Murer H (2004). Structure-function relations of the first and fourth predicted extracellular linkers of the type IIa $Na^+/P_i$ cotransporter: I. Cysteine scanning mutagenesis. *J Gen Physiol* **124**, 475–488.

Forster I, Hernando N, Biber J & Murer H (1998). The voltage dependence of a cloned mammalian renal type II $Na^+/P_i$ cotransporter (NaPi-2). *J Gen Physiol* **112**, 1–18.

Forster IC, Biber J & Murer H (2000). Proton-sensitive transitions of renal type II $Na^+$-coupled phosphate cotransporter kinetics. *Biophys J* **79**, 215–230.

Forster IC, Kohler K, Biber J & Murer H (2002). Forging the link between structure and function of electrogenic cotransporters: the renal type IIa $Na^+/P_i$ cotransporter as a case study. *Prog Biophys Mol Biol* **80**, 69–108.

Forster IC, Loo DD & Eskandari S (1999). Stoichiometry and $Na^+$ binding cooperativity of rat and flounder renal type II $Na^+$-$P_i$ cotransporters. *Am J Physiol Renal Physiol* **276**, F644–649.

Forster IC, Wagner CA, Busch AE, Lang F, Biber J, Hernando N, Murer H & Werner A (1997). Electrophysiological characterization of the flounder type II $Na^+/P_i$ cotransporter (NaPi-5) expressed in *Xenopus laevis* oocytes. *J Membr Biol* **160**, 9–25.

Hilfiker H, Hattenhauer O, Traebert M, Forster I, Murer H & Biber J (1998). Characterization of a murine type II sodium-phosphate cotransporter expressed in mammalian small intestine. *Proc Natl Acad Sci U S A* **95**, 14564–14569.

Jaureguiberry G, Carpenter TO, Forman S, Juppner H & Bergwitz C (2008). A novel missense mutation in SLC34A3 that causes hereditary hypophosphatemic rickets with hypercalciuria in humans identifies threonine 137 as an important determinant of sodium-phosphate cotransport in NaPi-IIc. *Am J Physiol Renal Physiol* **295**, F371–379.

Karlin A & Akabas MH (1998). Substituted-cysteine accessibility method. *Methods Enzymol* **293**, 123–145.

Kohler K, Forster IC, Stange G, Biber J & Murer H (2002). Transport function of the renal type IIa $Na^+/P_i$ cotransporter is codetermined by residues in two opposing linker regions. *J Gen Physiol* **120**, 693–703.

Lambert G, Forster IC, Stange G, Biber J & Murer H (1999). Properties of the mutant Ser-460-Cys implicate this site in a functionally important region of the type IIa $Na^+/P_i$ cotransporter protein. *J Gen Physiol* **114**, 637–652.

Lambert G, Forster IC, Stange G, Kohler K, Biber J & Murer H (2001). Cysteine mutagenesis reveals novel structure-function features within the predicted third extracellular loop of the type IIa $Na^+/P_i$ cotransporter. *J Gen Physiol* **117**, 533–546.

Lester HA, Mager S, Quick MW & Corey JL (1994). Permeation properties of neurotransmitter transporters. *Annu Rev Pharmacol Toxicol* **34**, 219–249.

Magagnin S, Werner A, Markovich D, Sorribas V, Stange G, Biber J & Murer H (1993). Expression cloning of human and rat renal cortex $Na/P_i$ cotransport. *Proc Natl Acad Sci U S A* **90**, 5979–5983.

Murer H, Forster I & Biber J (2004). The sodium phosphate cotransporter family SLC34. *Pflugers Arch* **447**, 763–767.

Murer H, Forster IC, Hernando N & Biber J (2008). Proximal tubular handling of phosphate: $Na/P_i$-cotransporters and their regulation. In *Seldin and Giebisch's The Kidney*, 3rd ed. Alpern RJ & Hebert SC, pp. 1979–1988. Acdemic Press.

Rudnick G (2006). Serotonin transporters – structure and function. *J Membr Biol* **213**, 101–110.

Segawa H, Kaneko I, Takahashi A, Kuwahata M, Ito M, Ohkido I, Tatsumi S & Miyamoto K (2002). Growth-related renal type II $Na/P_i$ cotransporter. *J Biol Chem* **277**, 19665–19672.

Shi L, Quick M, Zhao Y, Weinstein H & Javitch JA (2008). The mechanism of a neurotransmitter:sodium symporter–inward release of $Na^+$ and substrate is triggered by substrate in a second binding site. *Mol Cell* **30**, 667–677.

Stein WD (1990). *Channels, Carriers and Pumps. An Introduction to Membrane Transport*. Academic Press, San Diego.

Szczepanska-Konkel M, Yusufi AN, VanScoy M, Webster SK & Dousa TP (1986). Phosphonocarboxylic acids as specific inhibitors of $Na^+$-dependent transport of phosphate across renal brush border membrane. *J Biol Chem* **261**, 6375–6383.

Turner RJ (1981). Kinetic analysis of a family of cotransport models. *Biochim Biophys Acta* **649**, 269–280.

Turner RJ (1983). Quantitative studies of cotransport systems: models and vesicles. *J Membr Biol* **76**, 1–15.

Turner RJ (1984). Sodium-dependent sulfate transport in renal outer cortical brush border membrane vesicles. *Am J Physiol Renal Physiol* **247**, F793–798.

Villa-Bellosta R, Bogaert Y, Levi M & Sorribas V (2007). Toxicity of phosphonoformic acid in vascular smooth muscle cells: relationship to vascular calcification. *FASEB J* **21**, 905.25.

Virkki LV, Biber J, Murer H & Forster IC (2007). Phosphate transporters: a tale of two solute carrier families. *Am J Physiol Renal Physiol* **293**, F643–654.

Virkki LV, Forster IC, Bacconi A, Biber J & Murer H (2005*a*). Functionally important residues in the predicted 3rd transmembrane domain of the type IIa sodium-phosphate co-transporter (NaPi-IIa). *J Membr Biol* **206**, 227–238.

Virkki LV, Forster IC, Biber J & Murer H (2005*b*). Substrate interactions in the human type IIa sodium-phosphate cotransporter (NaPi-IIa). *Am J Physiol Renal Physiol* **288**, F969–F981.

Virkki LV, Murer H & Forster IC (2006*a*). Mapping conformational changes of the type IIb $Na^+/P_i$ cotransporter by voltage clamp fluorometry. *J Biol Chem* **281**, 28837–28849.

Virkki LV, Murer H & Forster IC (2006*b*). Voltage clamp fluorometric measurements on a type II $Na^+$-coupled $P_i$ cotransporter: shedding light on substrate binding order. *J Gen Physiol* **127**, 539–555.

Zeuthen T, Zeuthen E & Klaerke DA (2002). Mobility of ions, sugar, and water in the cytoplasm of *Xenopus* oocytes expressing $Na^+$-coupled sugar transporters (SGLT1). *J Physiol* **542**, 71–87.

## Author contributions

Experimental work: C.G., I.C.F; conception and design, analysis and interpretation of data: C.G., H.M., I.C.F.; drafting and revision of manuscript: C.G., I.C.F.; approval of final manuscript: C.G., H.M., I.C.F. Experiments were performed in the Institute of Physiology at the University of Zurich, Zurich, Switzerland.

## Acknowledgements

We thank Dr Raimund Dutzler for helpful comments and suggestions on the manuscript and Eva Hänsenberger for the oocyte preparation. This work was funded by the Swiss National Science Foundation (to H.M.) and Gebert-Rüf Foundation (to C.G.).

# Functional interactions between sites in putative re-entrant domains of a $Na^+$-coupled phosphate cotransporter

Chiara Ghezzi, Heini Murer and Ian C. Forster

Institute of Physiology and ZIHP, University of Zurich

Correspondence: Ian C. Forster, PhD

Institute of Physiology

University of Zurich

Winterthurerstrasse 190

CH-8057 Zurich, Switzerland.

FAX: +41 (0) 44 635 6814

TEL: +41 (0) 44 635 5059

EMAIL: iforster@access.uzh.ch

## Abstract

Sodium-coupled inorganic phosphate cotransporters of the SLC34 family (NaPi-IIa/b/c) are characterized by a common structural feature: a pair of inverted regions in the N- and C-terminal halves of the protein. These regions are hypothesised to contain re-entrant domains that associate to allow alternating access of the substrates from either side of the membrane. To investigate if these domains interact during the NaPi-II transport cycle, we introduced novel cysteines at 3 functionally important sites associated with the predicted re-entrant domains of the flounder NaPi-IIb for the purpose of fluorescent labeling and cross-linking. Single and double mutants were expressed in *Xenopus* oocytes and their function analysed by electrophysiology and voltage clamp fluorometry. The substitution at the cytosolic end of the first re-entrant domain induced a large hyperpolarizing shift in the voltage dependence of steady-state and presteady-state kinetics, whereas the two substitutions at the external face were less critical. Voltage-dependent fluorescence data suggested that a localized interaction between the two domains takes place dependent on the membrane potential and substrate present: we found that the fluorescence intensity reported by a labelled cysteine in one domain was dependent on the side chain substituted at a functionally critical site in the opposed domain. Moreover, by using Cu-phenanthroline to induce disulfide bridge formation, we observed a loss of transport activity that depended on the presence of sodium in the incubation medium. This suggested that external sodium increased the probability of NaPi-IIb occupying a conformation that favors interaction between sites in the re-entrant domains.


Key words: phosphate cotransport, electrophysiology, fluorometry, cross-linking

# Introduction

Type II sodium/phosphate cotransporters (NaPi-II[1]) belong to a unique class of $Na^+$-dependent carrier proteins (SLC34A family, according to the Solute Carrier classification: www.bioparadigms.com or 2.1.58/ PNAS class, according to the Transporter Classification Database, www.tcdb.org ) and show no sequence homology to other known cotransporter families. The family includes 3 isoforms that can be further classified according to their tissue localization: the electrogenic NaPi-IIa and electroneutral NaPi-IIc are localized exclusively in the renal proximal tubule and the electrogenic NaPi-IIb is expressed in non-renal epithelial-like tissues [52]. All isoforms share an overall amino acid similarity of ~57%, which is even higher in the predicted transmembrane domain regions [79]; therefore all isoforms most likely share a common 3-D structure. However, the current lack of a crystal structure of bacterial homologs of NaPi-II proteins and the weak sequence homology with other Na-dependent cotransporters, have so far precluded successful homology modeling. It follows that indirect approaches must be used to determine the structure-function relationships of these proteins.

Based on cysteine (Cys) scanning mutagenesis and *in vitro* transcription/translation assays a topology model was proposed for NaPi-IIa that is most likely also valid for NaPi-IIb and NaPi-IIc [57]. This model predicts 12 transmembrane-spanning domains (TMDs), with intracellular $NH_2$ and COOH termini (Fig. 1A). A large extracellular loop between TMDs 5 & 6 links the C- and N-terminal halves of the protein. Analysis of the primary sequence of the 3 NaPi-II isoforms from different species reveals two regions in each half, 89 residues long, which contain repeated sequences with typically >30% identity (Fig. 1B). Topology predictions indicate that these regions include two membrane spanning domains that we have postulated to form re-entrant domains localized between TMDs 2 & 5 and TMDs 7 &10 respectively [57, 63]. From functional studies using Cys substitutions, we proposed that these putative re-entrant domains may associate to form the $P_i$ transport pathway and, by implication, are also involved in the translocation of the co-substrate ($Na^+$) in the functionally associated leak mode that operates in the absence of external $P_i$ [70, 71]. Moreover, recent voltage clamp fluorometry (VCF) studies on mutants in which cysteines were substituted at sites in linker regions accessible from the extracellular medium, offer compelling evidence that the parts of the NaPi-II protein associated with the opposed re-entrant domains may move in a complementary manner during the transport cycle. These findings offer a first glimpse into the dynamics of the NaPi-II transport cycle [76]. However, evidence of a direct association of the

[1] Footnote 1

re-entrant domains is still lacking: the findings of our previous study [71] could result from the Cys substitution in each domain indirectly acting on a structurally separate transport pathway; moreover as that study was performed at a fixed holding potential of -50 mV the validity of the data is limited to one experimental condition.

To obtain more functional evidence of interactions, we have extended our previous study over a wide voltage range to quantitate the leak and cotransport modes so that conformational states are better defined and substrate interactions more easily identified. In addition to conventional steady-state and presteady-state analysis, we have applied voltage clamp fluorometry (VCF) assays to examine substrate- and voltage-dependent local interactions with reporter fluorophores and we have investigated the effect of inducing disulfide bridge formation using *Xenopus laevis* oocytes expressing functional flounder NaPi-IIb transporters. Sites were chosen for Cys substitution for fluorophore labeling or to test for disulfide bridge formation that corresponded to the equivalent sites described in our previous studies on the rat NaPi-IIa and flounder NaPi-IIb isoforms. Two sites (Ser155, Ala175) were located in the 1$^{st}$ (outward facing) re-entrant domain in the N-terminal half of the protein and one site (Ser448) was located in the C-terminal half of the protein at end of the 2$^{nd}$ (inward facing) re-entrant domain (Fig. 1A).

Our data provide new evidence that supports the involvement of these regions in voltage-dependent, substrate interactions. Moreover, we show that sites associated with the domains come in close contact during substrate translocation, which suggests that SLC34 proteins may share an inverted *trans* re-entrant architecture analogous to that found, for example, in the bacterial $Glt_{Ph}$ , (e.g.[27, 28]).

# Methods

### Solutions and reagents

Standard extracellular solution (100Na) contained (in mM): 100 NaCl, 2 KCl, 1.0 $MgCl_2$, 1.8 $CaCl_2$, 10 HEPES, pH 7.4 adjusted with TRIS base. In $Na^+$ substitution experiments NaCl was equimolarly replaced with choline Cl (0Na) and solutions with intermediate [$Na^+$] were obtained by mixing 100Na with 0Na in appropriate portions to maintain a constant molarity. $P_i$ was added from a 1M $K_2HPO_4$/ $KH_2PO_4$ stock premixed to give pH 7.4. PFA was added from a 100 mM stock to give the final concentration of 1 mM. Modified Barth's solution for storing oocytes contained (in mM): 88 NaCl, 1 KCl, 0.41 $CaCl_2$, 0.82 $MgSO_4$, 2.5 $NaHCO_3$, 2 $Ca(NO_3)_2$, 7.5 HEPES, pH 7.5 adjusted with Tris and supplemented with 5 mg/l doxycyclin and 5 mg/l gentamicin. All standard reagents were obtained from either Sigma-Aldrich or Fluka (Buchs, Switzerland). [2-(trimethylammonium) ethylmethanethiosulfonate bromide (MTSET) was obtained from Toronto Research Chemicals or Biotium (USA); 2-((5(6)-tetramethylrhodamine)carboxylamino) ethyl methanethiosulfonate (MTS-TAMRA) was obtained from Biotium (USA).

### Site-directed mutagnesis and cRNA preparation

cDNA encoding wild-type (WT) flounder (fl) NaPi-IIb (GenBank/EMBL/DDBJ accession n. AAB16821) was subcloned into a vector containing the 5' and 3' UTRs from *Xenopus* β-globin to improve its expression in oocytes [80]. Novel cysteines were introduced using the Quickchange site-directed mutagenesis kit (Stratagene Inc.). The sequence was verified by sequencing (Microsynth, Switzerland), linearized with *Xba*I and cRNA was synthesized in presence of Cap analog using the T3 Message Machine kit (Ambion).

### Expression in *Xenopus laevis* oocytes

Female *X. laevis* frogs were purchased from *Xenopus* Express (France) or African *Xenopus* Facility (R. South Africa). Portions of ovaries were surgically removed from frogs anesthetized in MS222 (tricaine methansulphonate) and cut in small pieces. Oocytes were treated for 45 min with collagenase (crude type 1A) 1 mg/ml in 100Na solution (without $Ca^{2+}$) in presence of 0.1 mg/ml trypsin inhibitor type III-O. Healthy stage V-VI oocytes were selected, maintained in modified Barth's solution at 16°C and injected with 10 ng of cRNA. Experiments were performed 4-7 days after injection. All animal procedures were conducted in accordance with the Swiss Cantonal and Federal legislation relating to animal experimentation.

**Two-electrode voltage clamp**

The standard two-electrode voltage clamp technique was used as previously described [69, 73]. For recordings at constant holding potential, currents were acquired at >20 samples/s and filtered at 10 Hz. Faster sampling rates (up to 20k samples/s) were used for voltage step recordings with filtering adjusted accordingly. Steady state $P_i$ activation was determined by varying the $P_i$ concentration in presence of 100Na and subtracting the respective currents in 100Na from those in 100Na+ $P_i$. Steady state $Na^+$ activation was similarly determined by subtracting the respective responses in XNa from those in XNa+ $P_i$ (1mM), where X is the test $Na^+$ concentration (in mM). Steady state $P_i$-induced currents ($I_{Pi}$) were fit with a form of the modified Hill Equation:

$$I_{Pi} = I_{Pi}^{\max} \left( [S]^H / \left( [S]^H + (K_{0.5}^S)^H \right) \right) + K \qquad (1)$$

where [S] is the concentration of variable substrate ($Na^+$ or $P_i$), $I_{Pi}^{\max}$ is the maximal electrogenic activity, $K_{0.5}^S$ is the apparent affinity constant for substrate *S*, *H* is the Hill coefficient and k is a constant that take in account of uncoupled leak effects [81]. For $P_i$ activation, the Michaelian form of Eqn 1 was used with $H$=1. Leak current ($I_{leak}$) in the absence of $P_i$ was determined from the response to 1 mM PFA (in 100Na) such that $I_{leak} = -I_{PFA}$.

Pre-steady state relaxations were recorded using voltage steps from $V_h$=-60 mV to voltages in the range of -180 to +80 mV. Relaxations were quantified by fitting with a two-component exponential function. The faster component, which represents the endogenous linear capacitive charging of the oocyte membrane, was subtracted from the total relaxation to obtain the NaPi-II dependent component. This was numerically integrated to obtain the charge moved ($Q$) for a step from the holding potential to the test potential. The $Q$-$V$ data were fitted with a Boltzmann function of the form given by Equation 2:

$$Q = Q_{hyp} + Q_{\max} / \left(1 + \exp(ze(V_{0.5} - V)/kT)\right) \qquad (2)$$

where $V_{0.5}$ is the voltage at which the charge is distributed equally between two hypothetical states, z is the apparent valence of an equivalent charge that moves through the whole of the

membrane field, $Q_{max}$ is the total charge available to move, $Q_{hyp}$ is the charge of the hyperpolarizing limit and is a function of $V_h$, and $e$, $k$ and $T$ have their usual meanings.

## $^{32}$P uptake

Oocytes expressing flNaPi-IIb Cys mutants (6-10 oocytes/group) were first allowed to equilibrate in 100Na solution without tracer. After aspiration of this solution, oocytes were incubated in 100Na solution containing 1mM cold $P_i$ and $^{32}P$ (specific activity 10 mCi/mmol $P_i$). Uptake proceeded for 10 min and then oocytes were washed 3-4 times with ice-cold 0Na solution containing 2 mM $P_i$, and lysed individually in 10% SDS for 1 hour before addition of scintillation cocktail. The amount of radioactivity in each oocyte was measured by scintillation counting.

**Simultaneous voltage clamp and fluorometry**

The apparatus for simultaneous VCF has been described in detail elsewhere [74, 76]. Cysteine mutants were labelled in 100Na in presence of MTS-TAMRA (0.4 mM) at room temperature. Voltage dependent changes in fluorescence ($\Delta F$) were determined using a voltage step protocol. The membrane voltage was stepped from $V_h$=-60 mV to test potentials ranging between -200 mV and +200 mV in 40 mV increments for a duration of 100-200 ms, and averaged over 20-64 sweeps. $\Delta F$ was measured in 100Na, 0Na and 100Na +1$P_i$ (100 mM $Na^+$+1mM $P_i$); each test substrate concentration application was bracketed with a control solution application (100Na) to allow for correction of a loss of fluorescence. After application of the superfusate the oocyte was allowed to stabilize in the recording chamber for ~2 min and then fluorescence was recorded. Recordings were baseline corrected relative to the value at $V_h$= -60 mV. After correction for photobleaching, the data from single oocytes were normalized to the predicted maximum change in fluorescence ($\Delta F_{max}$) recorded in 100Na and then pooled. $\Delta F_{max}$ was obtained from the $\Delta F$-$V$ data were fitted with the Boltzmann equation (Eqn. 2, where $Q$ was substituted with $\Delta F$).

**Thiol modification by MTSET**

MTSET were prepared from dry stock in water to give 1 M stock solution, which was kept at -20°C until required and added to 100Na solution to give a final concentration of 1 mM. MTSET was applied to the chamber with gravity feed via a 0.5-mm-diameter cannula positioned near the cell. Incubation time was 3

minutes and was followed by a 1 minute wash out period. During superfusion with MTSET, oocytes were kept at $V_h$= -50 mV. After washout, the $P_i$-induced current measured.

**Inhibition by copper(II)(1,10-phenanthroline)$_3$**

The Cu(II) (1,10-Phenanthroline)$_3$ ($CuPh_3$) stock solution was prepared for each experiment by mixing 40 µl of 1.25M 1,10-Phenanthroline (dissolved in water: ethanol 1:1) and 60 µl of 250 mM $CuSO_4$. For $^{32}P$ uptake, groups of 12 oocytes from two different batches were pre-incubated in 0.2 mM $CuPh_3$ for 5 min and then washed in 100Na. Half of these were further incubated in DTT (10 mM) for 10 minutes and washed again in 100Na (5 min). After washing, 100Na was replaced with the uptake solution. Uptake was performed as described above. For TEVC experiments, $P_i$ induced current was first measured in control condition (100Na). $P_i$ induced current was measured again after incubation of the oocytes in $CuPh_3$ 0.2 mM for 5 minutes (in 100Na or 0Na). For DTT treatment, oocytes, after incubation with $CuPh_3$ were treated for 10 minutes with freshly prepared 12 mM DTT (in 100Na) and then washed and tested. Oocytes were removed from the recording chamber for incubation to avoid irreversible deterioration of electrodes by DTT.

**Software and data analysis.**

Simulations of a 10 state model describing electrogenic cotransport were performed by solving a set of differential equations using Berkeley Madonna V8.0.2a8 software (www.berkeleymadonna.com). All curve fitting was performed using GraphPad Prism version 3.02/ 4.02 for Windows, (GraphPad Software, San Diego California USA, www.graphpad.com). Data points are shown as mean±sem. Error bars are not displayed if smaller than symbol.

# Results

**Cysteine substitutions and thiol modification alter transport kinetics**

*Steady-state behavior*: After expression in *X. laevis* oocytes, the single (S155C, A175C, S448C) and double (S155C-S448C, A175C-S448C and A175S-S448C) mutants, gave robust $P_i$-induced currents in the presence of external $Na^+$ (100Na solution) in the range -50 nA to -300 nA, when voltage clamped to $V_h$=-50 mV. To determine if and how the Cys substitution affected the cotransport activity, we estimated the apparent affinity constants for $P_i$-activation (with 100Na as control) ($K_{0.5}^{Pi}$) and $Na^+$-activation ($K_{0.5}^{Na}$ with 1 mM $P_i$) by measuring the $P_i$-induced current ($I_{P_i}$) under different superfusing conditions as previously described (e.g. [73, 82]). The data in both cases were reliably fitted using Eqn 1. The Cys substitution did not significantly affect $K_{0.5}^{Pi}$ for any of the constructs, whereas we observed a significant increase in $K_{0.5}^{Na}$ for A175C at 0 mV and -100 mV (Table I).

To investigate the effect of Cys substitution and subsequent modification of the introduced cysteines on voltage dependent kinetics, we first determined the steady-state voltage dependence of the leak current ($I_{leak}$) and the cotransport current ($I_{cot}$) before and after exposure to the membrane impermeable MTSET (1 mM, 3 min or until the change in $I_{P_i}$ reached a steady-state). $I_{leak}$ was estimated by measuring the change in holding current induced by 1 mM PFA ($I_{leak}$=-$I_{PFA}$) and $I_{cot}$ was obtained from ($I_{cot}$ = $I_{P_i}$ + $I_{leak}$). The determination of the cotransport activity by this procedure assumed that 1 mM $P_i$ or 1 mM PFA were sufficient to suppress the leak mode completely (e.g. [70, 81]). Fig. 2 shows *I-V* data normalized to $I_{P_i}$ at -100 mV before MTSET application to facilitate comparison of the voltage dependences.

To quantify changes in voltage dependence on cotransport activity caused by mutagenesis itself, we compared the normalised $I_{cot}$ at $V$= 0 relative to $V$= -100 mV. The ratio was used as a steady-state voltage dependence index (indicated in each panel of Fig. 2). For the single mutants (Fig. 2A), these data show that although Cys substitution at 175 was tolerated, the voltage dependence was significantly altered, whereby $I_{cot}^{0}/I_{cot}^{-100}$ was reduced from 0.41 (WT) to 0.10 (A175C). This behavior was also observed in the voltage dependence of $I_{leak}$ for this mutant. In contrast, Cys substitution at sites 155 or 448 had a small and opposite effect on the voltage dependence of $I_{cot}$ as indicated by the increase in $I_{cot}^{0}/I_{cot}^{-100}$ compared to the WT: both S155C and S448C showed more saturation of $I_{cot}$ at hyperpolarizing potentials, which was reflected in their larger $I_{cot}^{0}/I_{cot}^{-100}$ (Fig. 2A).

The *I-V* data of S155C-S448C and A175C-S448C (Fig. 2B) showed mixed behavior, depending on the site of substitution in the first re-entrant domain. For S155C-S448C, $I_{cot}^{0}/I_{cot}^{-100}$ lay close to the values for the corresponding single mutants, whereas for A175C-S448C, $I_{cot}^{0}/I_{cot}^{-100}$ was significantly larger than that of A175C.

The altered voltage dependences of A175C and A175C-S448C compared to the WT prompted us to investigate in more detail the role site 175 might play in determining this kinetic parameter. We replaced Ala175 with Ser, Leu, Asp and Arg in the S448C background. Only one double mutant (A175S-S448C) gave measurable $I_{P_i}$. For A175S-S448C, analysis of substrate activation data in the cotransport mode gave apparent affinity constants $K_{0.5}^{Pi}$ and $K_{0.5}^{Na}$ that were indistinguishable from the WT (Table I), which indicated that the Ser substitution was well tolerated, and its $I_{cot}^{0}/I_{cot}^{-100}$ approached the WT value.

Of the 3 single mutants, only S448C showed a significant change in behavior after MTSET incubation, as previously reported [74]) and is consistent with that of the equivalent mutation (S460C) in the rat NaPi-IIa isoform [83]. After Cys modification, $I_{P_i}$ was fully suppressed and was outwardly directed, whereas, $I_{leak}$ remained unchanged. $I_{cot}$ was therefore close to zero, consistent with only the leak mode being active after Cys modification; i.e. with suppressed cotransport activity, the action of $P_i$ and PFA are indistinguishable [71]. For S155C, as previously reported [76], we observed no significant change in $I_{P_i}$ , even though this site is considered accessible to MTS reagents [57, 76]. A175C showed only a small decrease in $I_{P_i}$ and no change in $I_{leak}$.

The double mutants containing Cys-448 showed qualitatively similar behavior after MTSET incubation: like S448C their cotransport activity was suppressed (Fig. 2B). In accord with our earlier study using the rat NaPi-IIa isoform [71], A175C-S448C, showed an increased $I_{leak}$ with an apparent outward $I_{P_i}$ that had approximately the same magnitude as $I_{leak}$ after MTSET exposure, whereas both S155C-S448C and A175S-S448C showed no resolvable change $I_{leak}$.

*Pre-steady state behavior:* To identify the partial reactions in the transport cycle responsible for the shifts in steady-state voltage dependence, we investigated the presteady-state kinetics. Voltage dependence of NaPi-II proteins is proposed to arise from partial reactions in the transport cycle that involve charge translocation, specifically from the binding/release of substrates ($Na^+$ ions) and intrinsic voltage-dependent conformational changes of the protein (e.g. [69, 73]). These partial reactions can be investigated by applying

voltage steps under different superfusate conditions and analysing the resulting presteady-state relaxations, after elimination of the linear capacitive charging transient.

For a representative oocyte expressing the WT and superfused in 100Na (Fig. 3A), the transient currents in response to equal but opposite voltage-steps, showed a characteristic asymmetry that depended on the direction of the voltage step from the holding potential ($V_h$=-60 mV). More charge was displaced for a depolarizing step than for the same magnitude hyperpolarizing step. The single mutants S448C and S155C as well as S155C-S448C showed similar behavior to the WT (data not shown). In contrast, A175C and A175C-S448C (Fig. 3A) showed relaxations with the opposite behavior, whereby more charge was displaced for the hyperpolarizing step compared with the depolarizing step. This behavior matched the shift in steady-state voltage dependence of $I_{P_i}$ towards hyperpolarizing potentials (Fig. 2). A175S-S448C gave presteady-state relaxations similar to the WT (not shown).

To determine if the altered voltage-dependence arose from changes to the kinetics of the empty carrier, $Na^+$ ion interaction or both, we examined the $Na^+$-dependence of presteady-state currents by exposing the oocytes to solutions with different $Na^+$ concentrations. For each condition, the charge ($Q_{ON}$) displaced from -60 mV to each test potential ($V$) was separated from the linear oocyte capacitive charge movement (see Materials and Methods) and plotted as function of $V$. To facilitate comparison, the $Q$-$V$ data were normalized to the depolarizing limit estimated from the Boltzmann fit (see below). For the WT (Fig. 3B), $Q_{ON}$ tended to saturate at positive and negative potentials for all [$Na^+$] as we have previously shown [73, 74] and there was a characteristic hyperpolarizing shift in the charge distribution as $Na^+$ was progressively replaced by choline. For A175C and A175C-S448C (Fig. 3B), saturation at hyperpolarizing potentials was less apparent except at low [$Na^+$]. We were unable to step to potentials more negative than -180 mV because the transient currents became contaminated by activating endogenous $Cl^-$ currents or the oocyte became irreversibly leaky, thereby making the presteady-state analysis more error prone.

To further characterize the presteady-state data, we fitted them with a form of the Boltzmann equation (Eq.2, continuous lines (Fig. 3B)) to obtain 3 parameters: $Q_{max}$, the maximum charge displaced; $V_{0.5,}$ the midpoint voltage and $z$, the apparent valence (Fig. 3C). For the WT, the estimated $Q_{max}$ at 100 mM $Na^+$ decreased by 20% at 25 mM and then more rapidly to approximately 50% of the maximum in 0Na; $V_{0.5}$ showed the characteristic hyperpolarizing shift that we have previously reported for NaPi-IIb [74] and $z$ reported by the fit lay in the range 0.4-0.6 for all superfusion conditions. For A175C and A175C-S448C the derivation of the Boltzmann parameters

was less certain due to the lack of saturation of the charge movement at hyperpolarizing potentials. In particular, for A175C, we constrained $z$ to 0.4 to reduce fit uncertainties. Under these conditions, the dependence of $Q_{max}$ and $V_{0.5}$ on [$Na^+$] contrasted significantly with that of the WT for both mutants: $Q_{max}$ increased almost linearly with [$Na^+$] and, unexpectedly, $V_{0.5}$ decreased with increasing [$Na^+$] (Fig. 3C). In 0 mM $Na^+$, $V_{0.5}$ was shifted for both A175C and A175C-S448C to more hyperpolarizing potentials, which indicated that the substitution at site 175 had changed the steady-state empty carrier occupancy. At 100mM $Na^+$, the shift of $V_{0.5}$ relative to the WT for all mutants correlated with the direction of of shift of $I_{cot}^0/I_{cot}^{-100}$ (Fig. 3D). This result underscored the importance of the presteady-state charge movement kinetics in determining the voltage dependence of the cotransport mode. Presteady-state relaxations were also resolved after Cys-modification by MTSET. Neither S155C nor A175C showed significant deviation from the behavior before MTSET application (data not shown). In contrast, all constructs containing Cys448 showed a significant decrease in the estimated total amount of mobile charge ($Q_{max}$) for superfusion in 0Na and 100Na and shifts in $V_{0.5}$ that depended on the site mutated in the 1$^{st}$ re-entrant domain (Table II).

**Substrate- and voltage-dependent changes in fluorescence**

To investigate possible interactions between the two re-entrant domains, we applied voltage clamp fluorometry (VCF), which we have previously demonstrated to be useful in observing local conformational changes of NaPi-II proteins [74, 76, 84]. The rationale for these experiments was that if the two re-entrant domains interact, structural changes induced by mutagenesis in one domain may directly alter the microenvironment of the reporter fluorophore in the other domain. Oocytes expressing single or double mutants were incubated in MTS-TAMRA (0.4 mM, 5 min.) and we measured changes in fluorescent intensity ($\Delta F$) in response to step changes in the membrane potential. As substrates are assumed to place the protein in different conformational states that may alter the relative position of the re-entrant domains, we compared the fluorescence with superfusion in 0Na, 100Na and 100Na+1$P_i$.

Fig. 4 compares the fluorescence recorded from representative oocytes expressing the respective mutant transporters in response to voltage steps from $V_{h=}$ -60 mV to 3 test potentials: -160, 0, +80 mV. These data show that $\Delta F$-$V$ varied, depending on the construct and the superfusion conditions. The direction of $\Delta F$ was the same as the direction of change of $V$ for all constructs. With the notable exception of A175C, all constructs gave robust $\Delta F$ in 100Na of comparable magnitude, whereas the responses of the same oocyte in 0Na and 100Na+1$P_i$ were different. For example, oocytes expressing S448C showed no detectable $\Delta F$ in 0Na, whereas $\Delta F$ was

resolved in 100Na or 100Na+1$P_i$. In contrast, oocytes expressing A175C-S448C showed a robust $\Delta F$ in 0Na and 100Na but no detectable $\Delta F$ in 100Na+1$P_i$. It should be noted that the functional consequences of labelling with the fluorophore (e.g. suppression of $I_{P_i}$ in the case of S448C) were the same as found for incubation in MTSET (data not shown). Moreover, we also observed that no $\Delta F$ could be resolved if oocytes were pre-incubated in MTSET before labelling with the fluorophore, which confirmed that the target Cys was most likely the same as for MTSET. After correcting for the loss of fluorescence due to bleaching or washout (Materials and Methods), the magnitude of $\Delta F$ observed for each superfusate was found to be independent of the order of application of the particular superfusate, thereby confirming that we were observing a memoryless process. The absence of detectable $\Delta F$ for oocytes expressing A175C suggested either that the site was also inaccessible to MTS-TAMRA, consistent with the insensitivity of $I_{P_i}$ to MTSET exposure (Fig. 2B) or if labelled, that the microenvironment of the fluorophore at this site did not change sufficiently to yield detectable fluorescence changes.

We obtained further insight into the voltage- and substrate-dependence of fluorescence by recording $\Delta F$ for voltage steps over a wide voltage range and used extensive signal averaging to improve the signal-to-noise ratio (see Materials and Methods). To aid comparison of the voltage dependence of fluorescence, $\Delta F$-$V$ data (Fig. 5) pooled from several batches of oocytes were normalized to $\Delta F_{max}$ predicted from fits using Eqn 2. Fit data are summarized in Table II.

*S155C and S155C-S448C* (Fig. 5A)*:* In 0Na, S155C and S155C-S448C showed similar $\Delta F$–$V$ with no saturation at the hyperpolarizing extreme. This behavior suggested that the fluorophores reported $\Delta F$ consistent with both Cys155 and Cys448 being successfully labelled in the double mutant, in contrast to the lack of detectable $\Delta F$ for S448C under the same conditions. For superfusion in 100Na, S155C-S448C showed similar behavior to S448C with no saturation at the hyperpolarizing extreme. This contrasted with the behavior of S155C, which yielded a sigmoidal $\Delta F$-$V$ relationship within the voltage range explored. Finally, with 100Na+1$P_i$, the $\Delta F$-$V$ relation for S155C-S448C resembled that of S448C; compared to S155C, there was reduced $\Delta F$ over the same voltage range and no obvious sigmoidicity in its voltage dependence.

*A175C-S448C and A175S-S448C* (Fig. 5B): $\Delta F$ recorded from oocytes expressing A175C-S448C showed a substrate- and voltage-dependence very different from S448C: for 0Na and 100Na, its $\Delta F$ –$V$ relation was sigmoidal, and adding $Na^+$ to the medium caused a ~20 mV depolarizing shift in the midpoint voltage ($V_{0.5}^F$)

(Table II). In 100Na+1$P_i$, we resolved no $\Delta F$ over the range of potentials explored. $\Delta F$ was also detectable with the double mutant A175S-S448C, which depended on the superfusion conditions. Like S448C, no $\Delta F$ was detectable for superfusion in 0Na, whereas superfusion in 100Na gave a sigmoidal $\Delta F$-$V$ relationship similar to A175C-S448C, but with a larger $z^F$ and a hyperpolarizing shift of ~40 mV in $V_{0.5}{}^F$ (Table II). In 100Na+1$P_i$, its $\Delta F$ -$V$ relation was similar to that of S448C.

**$CuPh_3$ promotes disulfide bridge formation between pairs of cysteines**

Finally, we investigated the functional behavior of the double Cys mutants after inducing disulfide bond formation between the introduced cysteines. This can be catalyzed using $O_2$/Cu(II)(1,10-phenanthroline)$_3$ ($CuPh_3$), whereby the dissolved dioxygen acts as an oxidant and $CuPh_3$ as a redox catalyst [85]. Moreover, the bond formation should be reversible by incubation in a reducing medium, e.g. dithiothrietol (DTT). We reasoned that if the two re-entrant domains associate to form the pathway for the translocation of the substrate, formation of a disulphide bond should interfere with the normal conformational changes associated with translocation of the substrate and therefore result in a change in $I_{P_i}$.

We first analysed the effect of incubation with $CuPh_3$ on single and double mutants using $^{32}P$ uptake (Fig. 6A). Neither $CuPh_3$ nor incubation in DTT affected $P_i$ uptake mediated by A175C, S155C and S448C (Fig. 6A) or the WT (data not shown). This finding confirmed that the introduced cysteines did not interact with any of the 11 endogenous cysteines that are present in flNaPi-IIb. Nevertheless, we cannot exclude the possibility that such disulfide bonds were formed but had no effect on transport function. In contrast, for S155C-S448C and A175C-S448C, treatment with $CuPh_3$ caused reductions in $^{32}P$ uptake of 50% and 40% respectively. Moreover, this inhibition could be reversed by subsequent incubation of the oocytes with DTT (Fig. 6A, *grey bars*) in support of the hypothesis that the inhibition of the transport was due to disulfide bridge formation between the pairs of introduced cysteines.

From this and other studies there is strong evidence obtained from presteady-state and voltage clamp fluorometric assays that NaPi-II proteins undergo conformation changes dependent on the substrate availability that involves the re-entrant domains. We therefore investigated if the presence or absence of substrate could affect the likelihood disulfide bridge formation by changing the state of the protein during the $CuPh_3$ incubation. Individual oocytes were assayed under voltage clamp before and after exposure to $CuPh_3$ and DTT in 0Na or

100Na. We did not perform these assays with preincubation in 100Na+1$P_i$ due to a loss of transport activity, which results from internalization of transporters following repeated and extended application of $P_i$ (e.g. [21]).

Consistent with uptake data, the single mutants showed no significant change in $I_{P_i}$ after preincubation in $CuPh_3$ with either 0Na or 100Na (Fig. 6B). In contrast, when S155C-S448C or A175C-S448C was incubated in 100Na+ $CuPh_3$, we observed a decrease of $I_{P_i}$ of ~50% and 40%, respectively. Longer incubation periods did not result in a further decrease in current, whereas subsequent application of MTSET suppressed $I_{P_i}$ (data not shown). Moreover, for incubation with 0Na+$CuPh_3$, no significant change in $I_{P_i}$ was measured for S155C-S448C, whereas there was a small decrease for A175C-S448C at hyperpolarizing potentials. To confirm that the loss of function observed for the double mutants occurred as a result of cross-linking within each NaPi-II monomer, and not between adjacent monomers, we coexpressed the A175C or S155C together with S448C and incubated the oocytes in $CuPh_3$ as above. No change in function was observed. Despite the obvious loss of transport function after $CuPh_3$ treatment, we detected no significant change in the presteady-state charge movement ($Q_{max}$, $V_{0.5}$ and $z$) (data not shown) for the double mutants. This result indicated that the disulfide bridge formation had neither altered the voltage dependence of the empty carrier nor $Na^+$ interactions.

# Discussion

The identification of the transport pathway and sites of substrate binding in membrane carrier proteins is of crucial importance to understand cotransport mechanisms at the molecular level. 3-D structures of crystallized bacterial homologs of mammalian $Na^+$-dependent cotransporters that belong to different gene families reveal a common structural motif: an inverted repeat topology in which the respective elements are structurally associated through an apparent twofold symmetry around an axis through the membrane plane. This common architecture defines a central substrate translocation pathway with the substrate binding sites located approximately halfway through the membrane and accessible from either side of the membrane, consistent with the alternating access model for carrier-mediated transport [28, 86, 87]. Pairs of discontinuous helices play a key structure-functional role in this architecture [88]. These can be either transmembrane spanning, as found in $LeuT_{Aa}$ [29] and *v*SGLT [89] or hairpin (re-entrant) as found in ClC [90] and $GlT_{Ph}$ [27]. The short peptide linkers between the helices are critical for substrate recognition and coordination. The ubiquity of these common architectures among genetically unrelated transporters is underscored by studies comparing hydropathies of the core regions that propose classification based on similarity of structural folds [91, 92].

Given that many transporters share a common functionality-i.e. coupling to the electrochemical gradient of $Na^+$ to catalyze uphill movement of a specific substrate-it follows that the same architecture may be present in transport proteins whose 3-D structures have yet to be resolved. For the SLC34 family and related bacterial homologs, no crystal structure is currently available and their low homology with proteins of known structure has so far precluded successful homology modelling. Nevertheless, the existence in all members of the SLC34 family of the common repeat region in the N- and C-terminal halves of the proteins (Fig. 1B) offers compelling evidence that these regions may also be involved in the formation of transport pathway. This conclusion has been the basis of a number of functional studies focussing on these regions [71, 72, 93]. For example, evidence that the re-entrant domains play a functional role in co-determining the transport mode (leak or cotransport) was found for the rat NaPi-IIa isoform, based on the behavior of a double Cys mutant (corresponding to A175C-S448C in the present study) [71].

Here we have taken a functional approach to: (i) characterise the role these putative re-entrant domains play in defining the kinetics of the transport cycle and (ii) test for interactions between the domains for a representative member of the SLC34 $Na^+$-coupled $P_i$ transporter family. We have focussed on changes in substrate- and voltage- dependence of the transport function because these are considered strong determinants of

implied conformational changes. In the context of structure-function relationships it is helpful to consider the transport properties of electrogenic SLC34 proteins in terms of a 10 state kinetic scheme to which our experimental findings can be referred (Fig. 7). This model depicts the two modes of electrogenic activity, leak and cotransport as a cyclic sequence of partial reactions, some of which (empty carrier and $Na^+$-interaction partial reactions) are common to both modes [70]. A feature of this model is that the electrogenicity of both the leak and cotransport cycles arises only from mobile charges associated with the empty carrier transition (1↔8), assumed to be intrinsic to the protein, and the 1$^{st}$ $Na^+$ interaction (1↔2a, 8↔7a). All other partial reactions are assumed electroneutral in this scheme. One aim of structure-function studies is to determine the relationship between structural elements and the partial reactions in such a scheme.

***Cysteine mutagenesis: identification of a site in putative re-entrant domain 1 implicated in $Na^+$ interactions and voltage dependence.***

Single Cys substitutions affected the voltage dependence at all 3 sites, but to varying degrees. Substitutions at 155 and 448, sites predicted to be exposed to the external medium had relatively small effects: both shifted the steady-state voltage dependence of $I_{P_i}$ towards depolarizing potentials relative to the WT. For these mutants, any small changes in the voltage dependence of $I_{leak}$ relative to the WT, which we would predict according to our kinetic scheme, were not easily resolved due to the small magnitude of this current. In contrast, Cys substitution at 175, a site predicted to be deep in the protein, which led to a strong hyperpolarizing shift in $I_{cot}$ and $I_{leak}$, was also only resolved at hyperpolarizing potentials (Fig. 2A). The changes in steady-state voltage dependence were reflected in the altered presteady-state charge distribution, which reports the result of partial reactions that precede $P_i$ binding (Fig. 7). The unique behavior of A175C (and A175C-S448C) may arise from the close proximity of site 175 to three residues (Ala190, Ala192, Asp196) that we have previously shown to be critical determinants of both $Na^+$ interaction and electrogenicity in the mammalian NaPi-IIa isoforms [75, 94] (Fig. 1A).

These findings suggested that the residue at this site was an important determinant of voltage dependence and $Na^+$ interaction. In contrast, the weak effect of Cys substitutions at the external facing sites (155, 448) suggested that these sites were not critical determinants of $Na^+$ interactions. Moreover, our finding that the voltage dependence of A175C could be partly restored to the WT behavior by the Ser-Cys substitution at 448 in the double mutant (A175C-S448C) supports the notion of the putative re-entrant domains forming an integral

core region of the protein that defines its transport kinetics. Like A175C, A175C-S448C also showed a large $I_{leak}$ at hyperpolarizing potentials (Fig. 2B), whereby its voltage dependence mirrored that of $I_{cot}$. This would be expected if the voltage dependence of the leak and cotransport modes was codetermined by common partial reactions in the kinetic scheme (Fig. 7).

The effect of Cys substitutions on the voltage dependent kinetics was confirmed by performing numerical simulations of the cotransport cycle according to our kinetic scheme. We began with a set of rate constants and intrinsic charges that described the steady-state and presteady-state behavior of the WT (Table III) and adjusted the rates to best match the experimental findings. We found that the effect of Cys substitution at 155 or 448 could be simulated by simply adjusting the forward rate constant ($k_{18}$) of the empty carrier transition (1↔ 8). In contrast, to simulate the effect of Cys substitution at 175, it was necessary to alter the rate constants ($k_{12a}$, $k_{2a1}$) that define the 1$^{st}$ $Na^+$ interaction from the external membrane face (1↔2a) (Table III). Changes to the 2$^{nd}$ $Na^+$ interaction rates ($k_{2a3}$, $k_{32a}$) alone did not result in a satisfactory match to the experimental data.

The simulated steady-state *I-V* relationships (Fig. 8A) predicted the shifts in voltage dependence of $I_{cot}$ observed experimentally (Fig. 2A). In particular, they offer a mechanistic explanation for the effect of the Cys substitution at 175, whereby at a given membrane potential, state 8 (inward facing, empty carrier) became more favored as the dissociation constant for the 1$^{st}$ $Na^+$ binding partial reaction was increased: to attain the same forward transport rate as the WT therefore required a stronger membrane hyperpolarization. The simulations also predicted that $K_{0.5}^{Pi}$ was relatively insensitive to the changes in the rate constants, whereas $K_{0.5}^{Na}$ increased for the simulated A175C case, as found experimentally (Table I) (not shown).

The presteady-state relaxations in the absence of $P_i$ for the simulated WT and A175C case also recapitulated the experimental data (compare Fig. 3A and Fig. 8B) and the corresponding *Q-V* data for different [$Na^+$] gave different steady-state charge distributions (Fig. 8C). It was significant that the *Q-V* data for the simulated A175C revealed two distinct Boltzmann distributions, which become more apparent at low [$Na^+$] if the voltage range was extended to hyperpolarizing potentials, well beyond what would be experimentally feasible. If the simulated data were fit with a single Boltzmann within the experimental voltage range, the predicted Boltzmann parameters (Fig. 8D) showed qualitatively the same behavior as the experimental data (Fig. 3C). In particular, $V_{0.5}$ obtained from a single Boltzmann fit to the simulated *Q-V* data decreased with increasing [$Na^+$] and reached a plateau close to 100 mM (Fig. 8C), which was in agreement with the Boltzmann analysis of the experimental data (Fig. 3B).

These data explain our difficulty in applying a free fit to the experimental data because of the lack of saturation at negative test potentials and, moreover, underscores the influence the experimental voltage window may have on data interpretation. For A175C in the experimental potential range (-180 mV to +80 mV), charge movement is mainly contributed by the empty carrier and the $Na^+$-dependent partial reactions contribute significantly to overall charge movement only at hyperpolarizing potentials. In contrast, for the WT (and S448C and S155C), the contributions to the *Q-V* from the empty carrier and electrogenic $Na^+$ interactions become merged within the experimental voltage range. Our fitting strategy using a single Boltzmann function represents a compromise dictated by experimental and analytical constraints.

***Cys modification alters transport mode and mobile charge movement***

Using MTS reagents to effect *in situ* thiol modification of cysteines is a widely used method to identify functionally important sites and determine topological features of membrane transport proteins. We have applied this strategy extensively to SLC34 proteins [71, 72, 81, 83, 93-95]. In the present study after MTSET incubation all constructs containing Cys448 showed suppression of $I_{cot}$, but $I_{leak}$ remained detectable. We assume this behavior resulted specifically from modification of Cys448 and that native cysteines of flNaPi-IIb are not involved, based on our finding that introduction of a Cys at the equivalent site in the Cys-reduced rat NaPi-IIa shows the same behavior with respect to cotransport and leak [96]. We also observed a reduced mobile charge movement after thiol modification (Table II), which we have previously interpreted as evidence of a reduction in the apparent electrical distance $Na^+$ must move to its binding site [74]. Despite this altered $Na^+$ interaction, modification of Cys448 provided us with a means to investigate the protein as it underwent transitions between a restricted number of states, thereby facilitating data interpretation.

In contrast to the behavior of constructs with Cys448, the absence of significantly altered steady-state and presteady-state activity for A175C and S155C suggested that the introduced cysteines were either inaccessible from the external medium or, if modified, were functionally unimportant. Previous studies have shown that S155C can indeed be labelled [57, 76]. The lack of a functional change due to Cys modification of Cys155, which for MTSET would add both bulk and positive charge at this site, therefore suggests that the side chain at 155 is not itself a critical determinant of transport kinetics. On the other hand, Cys175 is most likely inaccessible from the external medium based on evidence obtained from the rat NaPi-IIa isoform with a Cys introduced at the equivalent site (A203C) [93].

From previous studies on the equivalent site to 448 in the rat NaPi-IIa protein (S460C), we concluded that after Cys modification of this site, the remaining NaPi-II electrogenic activity represents the leak mode ($I_{leak}$). This conclusion was based on the findings that: (i) $^{32}P$ uptake was suppressed after MTS treatment, indicating suppression of the cotransport mode; (ii) the PFA response was the same before and after treatment indicating that the leak mode was unchanged and (ii) the response to $P_i$ after MTS treatment was identical to the PFA response [71, 83], i.e. after MTS treatment $I_{cot}$ =0, $I_{leak}$= - $I_{P_i}$. $Na^+$ and $P_i$ interactions still occur, however completion of the cotransport cycle is blocked. Under these conditions, state 3 with $P_i$ bound is functionally equivalent to state 3* with PFA bound (Fig. 7). Of the 3 double mutants containing Cys448, the behavior of A175C-S448C was consistent with this model: $I_{cot}$=0 was valid over the range of test potentials applied (Fig. 2B). For S155C-S448C and A175S-S448C, resolution of the leak current was hampered by the presence of endogenous PFA and $P_i$-sensitive currents that partially masked the exogenous response, depending on the expression level. It was significant that the shifted voltage dependence of A175C was also observed in $I_{leak}$ for A175C-S448C, before and after Cys modification, and in $I_{P_i}$ after treatment. This supported the notion that voltage dependence of the leak and cotransport modes are codetermined by the same elements in the protein. However, we found that the magnitude of $I_{leak}$ for A175C-S448C approximately doubled, in contrast to S448C, S155C-S448C and A175S-S448C, for which there was no resolvable change in $I_{leak}$ after thiol modification. This suggested that Cys175 can modulate the phenotype of the S448C and hinted at a possible interaction between the 1$^{st}$ re-entrant domain and Cys448.

***Evidence for substrate- and voltage-dependent interactions between re-entrant domains from voltage clamp fluorometry***

In contrast to presteady-state relaxations that reflect global conformational changes that involve the concerted movement of perhaps many charges as the protein undergoes transitions between states in response to rapid changes in membrane potential, VCF offers a means of detecting local conformational changes in the microenvironment of a fluorophore [24, 35, 74, 76, 97-99]. The difference in the voltage dependent parameters obtained by the two methods is seen by comparing $V_{0.5}$ and $z$ obtained from the $Q$-$V$ analysis (after MTSET treatment) and fluorescence (Table II).

We compared the changes in fluorescent intensity ($\Delta F$) induced by voltage steps under 3 superfusion conditions that allow investigation of the empty carrier alone and the carrier with one or both substrates present. The following interpretations can be made:

*−ΔF reported by the labelled single mutants depends on the site of Cys substitution*. For labelled S448C, only the leak mode operates, and any Δ*F* should only result from transitions involved in the leak cycle (Fig. 7). For S448C, it is significant that no Δ*F* was detected in 0Na (empty carrier) [74]. In contrast, the labelled S155C reports Δ*F* for the 3 superfusion conditions with different magnitude and voltage dependences [76]: this suggests that the microenvironment of the fluorophore at site155 is influenced by molecular rearrangements associated with partial reactions between all states in the transport cycle. As labelling Cys155 only marginally affected the electrogenic properties of S155C (Fig. 2A and [76]), we assume that changes in the microenvironment of this fluorophore reflect conformational changes of the normal transport cycle. In contrast, for A175C, consistent with lack of any change in electrogenic kinetics observed after MTSET exposure, we also observed no Δ*F*. We therefore conclude that this site must either be poorly accessible or if labelled, the added bulk of the MTS reagent does not alter the transport properties. The latter seems unlikely considering the change the Ala-Cys substitution alone had on the voltage dependence. Moreover, have previously shown for the equivalent site (Ala203) in the rat NaPi-IIa isoform that it is poorly accessible from the external medium [71].

- *The side chain at site 175 in re-entrant domain 1 influences the microenvironment of the fluorophore at 448*. For S448C, A175C-S448C and A175S-S448C the protein operates in the leak mode. In 0Na, labelled Cys448 does not respond to potential in 0Na, therefore the Δ*F* measured from A175C-S448C suggested that Cys175 had altered the microenvironment of the labelled Cys448 such that it responded to voltage dependent reorientation of the empty carrier. Alternatively, if Cys175 were also labelled, Δ*F* would reflect changes in the microenvironment of its fluorophore. Although we favor the former scenario, we are unable to distinguish between these two possibilities from the present data. When the non-polar Ala175 was substituted with a polar Ser, the labelled Cys448 reported no Δ*F* for 0Na and in 100Na, the Δ*F* –*V* that lay between that of the S448C and the A175C-S448C. This behavior underscores the importance of the side chain at this site in determining voltage dependence. If both substrates were present, Δ*F* reported by the A175S-S448C was very similar to that for S448C alone, whereas with a Cys at 175, no Δ*F* was reported. These findings suggest that the structural changes induced by changing the side chain at 175 can influence how the fluorophore at 448 responds to changes in its microenvironment.

-*Cys448 influences the microenvironment of the fluorophore at 155 in re-entrant domain 1*. For S155C-S448C, Δ*F* in 0Na was nearly identical to that of labelled S155C and as labelled S448C show no Δ*F* in 0Na, this suggested that Δ*F* from S155C-S448C arises only from changes to the microenvironment of the fluorophore at

Cys-155. In 100Na, S155C and S448C report Δ*F*, but with significantly different voltage dependences (Table II). According to our kinetic scheme (Fig. 7), Δ*F* obtained from labelled S155C should reflect contributions from $Na^+$ binding and the empty carrier, whereas the labelled S448C only reports $Na^+$ interactions. Therefore, if both cysteines were labelled in S155C-S448C, we would predict that its Δ*F*-*V* should reflect the combined response of the two single mutants under the same conditions. Instead, we observed a Δ*F*-*V* with a weak voltage dependence, similar to Δ*F*-*V* for S448C in 100Na ($z^F$ in 100Na reduced to 0.2, Table II), and also when both substrates were present. These findings suggest that Cys448 altered the microenvironment of the fluorophore at Cys155, but this was conditional on the presence of one or both substrates.

Without more structural information it is not possible to interpret the Δ*F*-*V* data in terms of specific local molecular rearrangements in the environment of the fluorophores, nevertheless our data demonstrate how the change in fluorescence intensity reported by a labelled Cys in one domain can be influenced by the side chain substituted at a functionally critical site in the opposed domain. Moreover, they show how the presence or absence of substrate can determine the structural rearrangements that occur in different parts of the protein.

***Promoting disulfide bridge formation: evidence for a state-dependent association of re-entrant domains***

The strategy of chemical cross-linking between pairs of cysteines is a common approach to elucidate the functional association of helices and re-entrant regions in several membrane transport proteins (e.g. [100-103]. The cross-linking data provided compelling evidence that the association of the novel cysteines depended on the state of the protein: in 0Na, one or both cysteines in S155C-S448C were unable to cross link, whereas for A175C-S448C, cross-linking was more favourable, possibly due to a different orientation or closer proximity of the novel cysteines. Three assumptions were implicit in the interpretation of our results: (i) disulfide bridge formation would have detectable functional consequences; (ii) only the introduced cysteines were involved and (iii) the disulfide bridges were intra- and not inter-molecular due to association between adjacent NaPi-II proteins or their oligomeric state. Although NaPi-II proteins are considered to be functional monomers [104], there is also indirect evidence that they may dimerize [105]. It is therefore possible that the oxidizing treatment may result in disulfide bridge formation between cysteines (novel or native) in adjacent monomers of dimers. Our finding that there was no loss of function after $CuPh_3$ incubation for the single Cys mutants, whether singly or co-expressed confirmed that bridge formation occurred only between the introduced Cys in each monomer.

By assuming that the formation of a disulfide bridge in any monomer results in full inhibition of cotransport, our finding that the reduction of $I_{P_i}$ for S155-S448C was greater than for A175C-S448C suggests that in the former construct, the two cysteines are closer and therefore bridge formation was more favourable. This would accord with the predicted topology for TMD4 (Fig. 1A). That the suppression of the $I_{P_i}$ was also dependent on the $CuPh_3$ incubation conditions further supports the notion that $Na^+$ effects a conformational change in the core region composed of the re-entrant domains and implicates them in $Na^+$ coordination. For $CuPh_3$ incubation of A175C-S448C in 0Na, the small loss of cotransport activity indicated that even in the absence of substrate, Cys175 and Cys448 may associate, albeit rarely. In contrast, for S155C-S448C loss of activity was only seen after incubation in 100Na. We also observed no significant change in the total mobile charge movement, which contrasts with the effect of thiol modification of the introduced cysteines. This suggested that the cross-linking had neither immobilized the empty carrier nor interfered with the ability of Na ions to enter the electric field. Finally, our finding of only partial inhibition of the electrogenic response after $CuPh_3$ treatment indicates that not all transporters were affected and this was confirmed by subsequent exposure to MTSET. The amount of inhibition could then be taken as a measure of the probability of finding the respective Cys within a distance of 15.2 Å of one another [85].

**Conclusion**s

We have identified a site in the 1$^{st}$ putative re-entrant domain that is a critical determinant of voltage dependence and $Na^+$ interaction. Moreover, we provide evidence from fluorometry and cross-linking that sites associated with the re-entrant domains can interact. Our findings lend functional support to the importance of the *trans* repeat architecture in cation-coupled cotransporters.

**Acknowledgements**

We gratefully acknowledge Eva Hänsenberger for oocyte preparation and Dr Anne-Kristine Meinild for expert comments on the manuscript. We also thank Dr Leila Virkki for generating the A175C-S448C mutant. This work was supported by the Swiss National Science Foundation grants to HM and ICF.

**Footnote**

1 *Abbreviations used in this paper*: 100Na: 100 mM $Na^+$ buffer, 0Na: 0 mM $Na^+$ choline buffer; au, arbitrary unit, fluorescence; $CuPh_3$, Cu(II) (1,10-Phenanthroline)$_3$; $I_{P_i}$, change in oocyte holding current induced by $P_i$; $I_{PFA}$, change in holding current induced by PFA; $I_{leak}$, leak current, $I_{cot}$, cotransport current; MTSET, 2-(trimethylammonium)ethyl MTS bromide; MTS-TAMRA, 2-((5(6)-tetramethylrhodamine)carboxylamino) ethyl methanethiosulfonate NaPi-II, type II sodium phosphate cotransporter; PFA phosphonoformic acid; $P_i$, inorganic phosphate; TMDn: transmembrane domain, n; $V_h$, holding potential; WT, wild type.

**References**

Abramson J, S.I., Kasho V, Verner G, Kaback HR, Iwata S. 2003. Structure and mechanism of the lactose permease of Escherichia coli. *Science*. 301:610-615.

Abramson, J., and E.M. Wright. 2009. Structure and function of $Na^+$-symporters with inverted repeats. *Curr Opin Struct Biol*. 19:425-432.

Andrini, O., C. Ghezzi, H. Murer, and I.C. Forster. 2008. The leak mode of type II $Na^+$-$P_i$ cotransporters. *Channels (Austin)*. 2:346-357.

Bacconi, A., L.V. Virkki, J. Biber, H. Murer, and I.C. Forster. 2005. Renouncing electrogenicity is not free of charge: switching on electrogenicity in a $Na^+$-coupled phosphate cotransporter. *Proceedings of the National Academy of Sciences of the United States of America*. 102:12606-12611.

Careaga C.L., F.J.J. 1992. Thermal motions of surface alpha-helices in the D-galactose chemosensory receptor. Detection by disulfide trapping. *J Mol Biol.* 226:1219-1235.

Castagna, M., A. Soragna, S.A. Mari, M. Santacroce, S. Bette, P.G. Mandela, G. Rudnick, A. Peres, and V.F. Sacchi. 2007. Interaction between lysine 102 and aspartate 338 in the insect amino acid cotransporter KAAT1. *Am J Physiol Cell Physiol*. 293:C1286-1295.

Cha, A., and F. Bezanilla. 1998. Structural implications of fluorescence quenching in the Shaker $K^+$ channel. *Journal of General Physiology*. 112:391-408.

Dutzler, R., E.B. Campbell, M. Cadene, B.T. Chait, and R. MacKinnon. 2002. X-ray structure of a ClC chloride channel at 3.0 A reveals the molecular basis of anion selectivity. *Nature*. 415:287-294.

Ehnes, C., I.C. Forster, A. Bacconi, K. Kohler, J. Biber, and H. Murer. 2004a. Structure-function relations of the first and fourth extracellular linkers of the type IIa $Na^+/P_i$ cotransporter: II. Substrate interaction and voltage dependency of two functionally important sites. *Journal of General Physiology*. 124:489-503.

Ehnes, C., I.C. Forster, K. Kohler, A. Bacconi, G. Stange, J. Biber, and H. Murer. 2004b. Structure-function relations of the first and fourth predicted extracellular linkers of the type IIa $Na^+/P_i$ cotransporter: I. Cysteine scanning mutagenesis. *Journal of General Physiology*. 124:475-488.

Forrest, L.R., and G. Rudnick. 2009. The rocking bundle: a mechanism for ion-coupled solute flux by symmetrical transporters. *Physiology (Bethesda)*. 24:377-386.

Forster, I., N. Hernando, J. Biber, and H. Murer. 1998. The voltage dependence of a cloned mammalian renal type II $Na^+/P_i$ cotransporter (NaPi-2). *Journal of General Physiology*. 112:1-18.

Forster, I.C., C.A. Wagner, A.E. Busch, F. Lang, J. Biber, N. Hernando, H. Murer, and A. Werner. 1997. Electrophysiological characterization of the flounder type II $Na^+/P_i$ cotransporter (NaPi-5) expressed in Xenopus laevis oocytes. *Journal of Membrane Biology*. 160:9-25.

Ghezzi, C., H. Murer, and I.C. Forster. 2009. Substrate interactions of the electroneutral $Na^+$-coupled inorganic phosphate cotransporter (NaPi-IIc). *J Physiol*. 587:4293-4307.

Gisler, S.M., S. Kittanakom, D. Fuster, V. Wong, M. Bertic, T. Radanovic, R.A. Hall, H. Murer, J. Biber, D. Markovich, O.W. Moe, and I. Stagljar. 2008. Monitoring protein-protein interactions between the mammalian integral membrane transporters and PDZ-interacting partners using a modified split-ubiquitin membrane yeast two-hybrid system. *Mol Cell Proteomics*. 7:1362-1377. d

Hilfiker, H., O. Hattenhauer, M. Traebert, I. Forster, H. Murer, and J. Biber. 1998. Characterization of a murine type II sodium-phosphate cotransporter expressed in mammalian small intestine. *Proceedings of the National Academy of Sciences of the United States of America*. 95:14564-14569.

Huang X., M.M. 1991. A time-efficient, linear-space local similarity algorithm. *Adv. Appl. Math*. 12:337-357

Kohler, K., I.C. Forster, G. Lambert, J. Biber, and H. Murer. 2000. The functional unit of the renal type IIa $Na^+/P_i$ cotransporter is a monomer. *Journal of Biological Chemistry*. 275:26113-26120.

Kohler, K., I.C. Forster, G. Stange, J. Biber, and H. Murer. 2002a. Identification of functionally important sites in the first intracellular loop of the NaPi-IIa cotransporter. *American Journal of Physiology*. 282:F687-696.

Kohler, K., I.C. Forster, G. Stange, J. Biber, and H. Murer. 2002b. Transport function of the renal type IIa $Na^+/P_i$ cotransporter is codetermined by residues in two opposing linker regions. *Journal of General Physiology*. 120:693-703.

Kohler, K., I.C. Forster, G. Stange, J. Biber, and H. Murer. 2003. Essential cysteine residues of the type IIa $Na^+/P_i$ cotransporter. *Pflugers Archiv. European Journal of Physiology*. 446:203-210.

Krishnamurthy H, P.C., Gouaux E. 2009. Unlocking the molecular secrets of sodium-coupled transporters. *Nature*. 459:347-355.

Lambert, G., I.C. Forster, G. Stange, J. Biber, and H. Murer. 1999. Properties of the mutant Ser-460-Cys implicate this site in a functionally important region of the type IIa $Na^+/P_i$ cotransporter protein. *Journal of General Physiology*. 114:637-652.

Lambert, G., I.C. Forster, G. Stange, K. Kohler, J. Biber, and H. Murer. 2001. Cysteine mutagenesis reveals novel structure-function features within the predicted third extracellular loop of the type IIa $Na^+/P_i$ cotransporter. *Journal of General Physiology*. 117:533-546.

Larkin M.A., B.G., Brown N.P., Chenna R., McGettigan P.A., McWilliam H.*, Valentin F.*, Wallace I.M., Wilm A., Lopez R.*, Thompson J.D., Gibson T.J. and Higgins D.G. 2007. ClustalW and ClustalX version 2. *Bioinformatics*. 23:2947-2948.

Larsson, H.P., A.V. Tzingounis, H.P. Koch, and M.P. Kavanaugh. 2004. Fluorometric measurements of conformational changes in glutamate transporters. *Proceedings of the National Academy of Sciences of the United States of America*. 101:3951-3956.

Li, M., and H.A. Lester. 2002. Early fluorescence signals detect transitions at mammalian serotonin transporters. *Biophysical Journal*. 83:206-218.

Lolkema, J.S., and D.J. Slotboom. 2003. Classification of 29 families of secondary transport proteins into a single structural class using hydropathy profile analysis. *J Mol Biol*. 327:901-909.

Lolkema, J.S., and D.J. Slotboom. 2008. The major amino acid transporter superfamily has a similar core structure as $Na^+$-galactose and $Na^+$-leucine transporters. *Mol Membr Biol*. 25:567-570. doi:905963464

Loo, D.D., S. Eskandari, B.A. Hirayama, and E.M. Wright. 2002. A kinetic model for secondary active transport. *In* Membrane Transport and Renal Physiology. H.E. Layton and A.M. Weinstein, editors. Springer. 65-84.

Loo, D.D., B.A. Hirayama, E.M. Gallardo, J.T. Lam, E. Turk, and E.M. Wright. 1998. Conformational changes couple $Na^+$ and glucose transport. *Proceedings of the National Academy of Sciences of the United States of America*. 95:7789-7794.

Meinild, A.K., B.A. Hirayama, E.M. Wright, and D.D. Loo. 2002. Fluorescence studies of ligand-induced conformational changes of the $Na^+$/glucose cotransporter. *Biochemistry*. 41:1250-1258.

Radanovic, T., S.M. Gisler, J. Biber, and H. Murer. 2006. Topology of the type IIa $Na^+/P_i$ cotransporter. *J Membr Biol*. 212:41-49. doi:10.1007/s00232-006-0033-2.

Ravera, S., L.V. Virkki, H. Murer, and I.C. Forster. 2007. Deciphering PiT transport kinetics and substrate specificity using electrophysiology and flux measurements. *American Journal of Physiology-Cell Physiology*

Ryan, R.M., A.D. Mitrovic, and R.J. Vandenberg. 2004. The chloride permeation pathway of a glutamate transporter and its proximity to the glutamate translocation pathway. *J Biol Chem*. 279:20742-20751.

Screpanti, E., and C. Hunte. 2007. Discontinuous membrane helices in transport proteins and their correlation with function. *J Struct Biol*. 159:261-267. Tao, Z., Y.W. Zhang, A. Agyiri, and G. Rudnick. 2009. Ligand effects on cross-linking support a conformational mechanism for serotonin transport. *J Biol Chem*.

Virkki, L.V., J. Biber, H. Murer, and I.C. Forster. 2007. Phosphate transporters: a tale of two solute carrier families. *Am J Physiol Renal Physiol*. 293:F643-654.

Virkki, L.V., I.C. Forster, A. Bacconi, J. Biber, and H. Murer. 2005a. Functionally important residues in the predicted 3rd transmembrane domain of the type IIa sodium-phosphate co-transporter (NaPi-IIa). *Journal of Membrane Biology*. 206:227-238.

Virkki, L.V., I.C. Forster, J. Biber, and H. Murer. 2005b. Substrate interactions in the human type IIa sodium-phosphate cotransporter (NaPi-IIa). *American Journal of Physiology*. 288:F969-F981.

Virkki, L.V., I.C. Forster, N. Hernando, J. Biber, and H. Murer. 2003. Functional characterization of two naturally occurring mutations in the human sodium-phosphate cotransporter type IIa. *Journal of Bone and Mineral Research*. 18:2135-2141.

Virkki, L.V., H. Murer, and I.C. Forster. 2006a. Mapping conformational changes of the type IIb $Na^+/P_i$ cotransporter by voltage clamp fluorometry. *Journal of Biological Chemistry*. 281:28837-28849.

Virkki, L.V., H. Murer, and I.C. Forster. 2006b. Voltage clamp fluorometric measurements on a type II $Na^+$-coupled $P_i$ cotransporter: shedding light on substrate binding order. *Journal of General Physiology*. 127:539-555.

Werner, A., and R.K. Kinne. 2001. Evolution of the Na-$P_i$ cotransport systems. *American Journal of Physiology*. 280:R301-312.

Yamashita A., S.S.K., Kawate T., Jin Y., Gouaux E. 2005. Crystal structure of a bacterial homologue of $Na^+/Cl^-$-dependent neurotransmitter transporters. *In* Nature. 215-223.

Yernool D, B.O., Jin Y, Gouaux E. 2004. Structure of a glutamate transporter homologue from Pyrococcus horikoshii. *Nature*. 431:811-818.

Zomot, E., Y. Zhou, and B.I. Kanner. 2005. Proximity of transmembrane domains 1 and 3 of the gamma-aminobutyric acid transporter GAT-1 inferred from paired cysteine mutagenesis. *J Biol Chem*. 280:25512-25516.

**Figure legends**

**Fig. 1. Re-entrant domains of NaPi-IIb.**

A. Topology model of NaPi-II proteins predicts 12 transmembrane domains (TMDs) and intracellular C- and N-termini [57]. Residues that were replaced with a cysteine are indicated as well as 3 sites at the cytosolic end of TMD5 that are determinants of voltage dependence (see Discussion). Numbering is according to flounder NaPi-IIb sequence.

B. Comparison of amino acid sequences from 3 isoforms of NaPi-IIa/b/c from different species (fl= flounder, h= human, m = mouse, r = rat) and the bacterial homolog from *vibrio cholera* (npt) using Clustalw [106] for the two repeat regions predicted using the Lalign tool [107]. For fl NaPi-IIb, Lalign identifies two regions from the N-terminal and C-terminal halves of the protein with an 89 amino acid overlap that show 31.9% identity. Vertical bars indicate identical (*black*) and similar (*grey*) residues in each. Shaded bars at top and bottom indicate predicted TMDs (numbered). The sites of start and termination of the TMDs were obtained from predictions based on rat NaPi-IIa [57]. A conserved proline is present in the linker regions of each domain, consistent with a putative re-entrant topology. Sites mutated to cysteines in the present study are colored magenta according to the flNaPi-IIb sequence.

**Fig. 2. Cysteine substitution alters NaPi-IIb voltage dependence.**

A. Normalized current-voltage (*I-V)* data for single mutants: S448C (*left*); S155C (*center*) and A175C (*right*). Voltage dependence of leak (*diamonds*) and cotransport mode (*circles*) before (*filled symbols*) and after MTSET incubation (*open symbols*). *Upper panels*: leak current, given by $-I_{PFA}$. *Lower panels*: cotransport-related currents: $P_i$-induced current ($I_{P_i}$) and predicted cotransport mode ($I_{cot}= I_{P_i}-I_{PFA}$).

B. Current-voltage (*I-V*) curves for double mutants S155C-S448C (*left*), A175C-S448C (*center*) and A175S-S448C (*right*) showing the leak and transport mode related currents before and after exposure to MTSET. All symbols and nomenclature as in A.

Each data point represents the mean of ≥5 oocytes, and data were normalized to $I_{P_i}$ at -100mV before MTSET incubation. Data points joined for visualization. Normalized $I_{P_i}$ data for NaPi-IIb WT are superimposed on data sets to show the effect of mutagenesis and cys-modification on the voltage dependence. The steady-state voltage dependence index ($I_{cot}^{0}/I_{cot}^{-100}$) (see text) is indicated for each construct (WT = 0.41). Different ordinates are used for S175C and S175C-S448C to account for the larger relative currents at hyperpolarizing potentials compared with the other mutants.

**Fig. 3. Presteady-state charge movements indicate that Cys-175 imposes a dominant effect on voltage dependence of $Na^+$ interaction.**

A. Representative current recordings from WT (*left*), A175C (*center*) and A175C-S448C (*right*) for superfusion in 100 mM $Na^+$ in response to symmetrical 100 mV depolarizing (*red*) and hyperpolarizing (*green*) steps from the holding potential (-60 mV).

B. Charge ($Q_{ON}$) for voltage steps from -60 mV to test potential ($V$) determined from curve fits to presteady-state relaxations, plotted as function of $V$ for different external [$Na^+$] : WT (*left*); A175C (*center*); A175C-S448C (*right*). Continuous lines are fits with Eq.2. To better visualize the effect of [$Na^+$] on the midpoint voltage ($V_{0.5}$), the data were offset so that each data set and curve are superimposed at the depolarizing limit predicted from the fit to the 100Na data and normalized**.**

C. $Na^+$ dependence of Boltzmann parameters predicted from fits to $Q$-$V$ data plotted as a function of [$Na^+$]. Each panel shows data for WT (*open squares*); A175C (*filled circles*) and A175C-S448C (*filled squares*). Data points are shown as mean ± SEM ($n$ >4) and joined for visualization.

D. Comparison of steady-state voltage dependence ($I_{cot}^{0}/I_{cot}^{-100}$) and $V_{0.5}$ with 100 Na superfusion, for each construct. Dotted lines indicate WT mean values.

**Fig. 4. Voltage dependent changes in fluorescence intensity depend on superfusate.**

Representative data recorded for voltage steps from -60 mV to -160 (*green*), 0 (*black*) and +80 mV (*red*) for the constructs indicated. Each data set represents recordings from the same oocyte expressing the respective mutant

under different superfusion conditions. Note that for A175C, the same data with two scale factors are shown to indicate that no detectable $\Delta F$ was observed for this mutant.

**Fig. 5. Substrate and voltage dependent changes in fluorescence intensity.**

A. Voltage-dependent change in fluorescence intensity ($\Delta F$) for S448C (*filled squares*), S155C (*open circles*) and A155C-S448C (*open diamonds*) compared for three superfusion conditions: 0 mM $Na^+$ (*left panel*), 100 mM $Na^+$ (*center panel*) and 100 mM $Na^+$+ 1 mM $P_i$ *(right panel*). Data points and fits were adjusted so that they superimposed at the depolarizing limit. For each construct, $\Delta F$ data were normalized to $\Delta F_{max}$ in100 mM $Na^+$ predicted from a fit using a single Boltzmann function (Eqn 2). Each data point represents mean±SEM with $n \geq$ 3 cells. Error bars were smaller than symbols.

B. Voltage-dependent change in fluorescence intensity ($\Delta F$) for S448C (*filled squares*) compared with A175C-S448C (*filled circles*) and A175S-S448C (*open diamonds*) for three superfusion conditions as in A.

**Fig. 6. Effect of $CuPh_3$ on cotransport activity for single and double mutants.**

A. $^{32}P$ uptake was measured on groups of oocytes ($n$>5) in control condition (*empty bars*), after incubation in $CuPh_3$ (*cross hatched bars*) and after incubation in $CuPh_3$ followed by incubation in DTT (*gray bar*s). Data are shown as mean ± SEM.

B. *I-V* data showing $I_{P_i}$ for mutants indicated was measured in control condition (*filled squares*), after incubation in $CuPh_3$ in 100 mM $Na^+$ (*filled circles*) or after incubation in 0 mM $Na^+$ (*empty squares*). Data were normalized to $I_{P_i}$ at -100 mV for control. Points are joined for visualisation.

**Fig. 7. Ten state kinetic scheme for the electrogenic leak and cotransport modes for SLC34 proteins.**

Each state is assumed to represent a unique conformation of the protein. Transitions between states are described in terms of forward and backward rate constants that for certain transitions are substrate or voltage dependent (Table III). This model assumes only the empty carrier (1↔8) and 1$^{st}$ Na binding partial reactions (1↔2a; 8 ↔7a) involve charge movement (*blue*). The two transport modes (leak and cotransport) share these transitions.

PFA is assumed to place in the protein in a dead-end state. A set of 1st order differential equations can be solved for the steady-state occupancies of each state and time-dependent charge movements from which the steady-state $P_i$-induced current and presteady-state relaxations respectively, are obtained (e.g. [69, 73, 108]). The two transport cycles (leak-*dashed line* ; cotransport-*continuous line*) are indicated.

**Fig. 8. Simulations predict voltage dependent kinetics of single Cys substitutions.**

A. Voltage dependence of steady-state $P_i$-induced current ($I_{P_i}$) obtained from simulations using parameters (Table III) corresponding to the WT (*filled squares*), S448C or S155C (*open squares*) and A175C (*filled squares*). Data were normalized to $I_{P_i}$ at -100 mV to aid comparison with experimental data (Fig. 2A).

B. Presteady-state relaxations predicted by model in 100 mM $Na^+$ in response to symmetrical voltage steps from -60 mV for WT and A175C.

C. *Q-V* as a function of [Na] obtained by integrating the simulated relaxations for the simulated WT and A175C. Note that for the experimental situation, the voltage window is restricted to the data points within the shaded area and therefore the fit with a single Boltzmann function (*colored, continuous lines*) does not accurately describe the true charge distribution, especially for the simulated A175C.

D. Boltzmann parameters derived from fitting the shaded region in C (-180 to +80 mV) with Eqn 2. WT (*empty squares*); A175C (*filled squares*). These data can be compared with the corresponding panels in Fig. 3B.

**Table I. Steady-state apparent affinity constants at -100 mV and 0 mV**

Apparent affinity constants for $P_i$ ($K_{0.5}^{Pi}$) or $Na^+$ ($K_{0.5}^{Na}$) determined from fits using Eqn 1 to $P_i$- or Na-dose dependence of $I_{P_i}$.

| | -100 mV | | 0 mV | |
|---|---|---|---|---|
| | $K_{0.5}^{Pi}$ [a] | $K_{0.5}^{Na}$ [b] | $K_{0.5}^{Pi}$ [a] | $K_{0.5}^{Na}$ [b] |
| **WT** | **0.048 ± 0.015** | **35.3 ± 4.5** | **0.043 ± 0.011** | **58.0 ± 6.3** |
| A175C | 0.050 ± 0.005 | 57.3 ± 4.8 * | 0.048 ± 0.001 | 91.7 ± 3.2* |
| A175C-S448C | 0.055 ± 0.005 | 42.9 ± 4.2 | 0.049 ± 0.001 | 60.6 ± 8.7 |
| A175S-S448C | 0.066 ± 0.012 | 38.9 ± 8.6 | 0.057 ± 0.030 | 48.4 ± 3.5 |
| S155C[c] | 0.068 ± 0.012 | n.d. | 0.052 ± 0.009 | n.d. |
| S155C-S448C | 0.040 ± 0.002 | 37.1 ± 3.8 | 0.037 ± 0.004 | 48.3 ± 3.5 |
| S448C[d] | 0.047 ± 0.009 | 25.9 ± 2.5 | 0.039 ± 0.008 | 53.8 ± 3.9 |

n.d.: not determined. [a] determined in 100Na; [b] determined with 1 mM $P_i$; [c]Values from [76]; [d]values from [74]; * indicates statistically significant compared to WT (Student's *t-test*, $p \leq 0.01$). Values are given as mean ± sem as reported by fitting algorithm from pooled, normalized data ($n \geq 5$).

**Table II. Comparison of Boltzmann parameters for presteady-state and fluorescence**

| Construct | $Q_{max}^{+MTSET}/Q_{max}^{-MTSET}$ | | $V_{0.5}$ (mV)[b] | | $V_{0.5}^{F}$ (mV)[b] | $z^{b}$ | | $z^{F\,b}$ |
|---|---|---|---|---|---|---|---|---|
| | **0Na** | **100Na** | ***-MTSET*** | ***+MTSET*** | ***+MTS-TAMRA*** | ***-MTSET*** | ***+MTSET*** | ***+MTS-TAMRA*** |
| WT | 1.00 | 1.00 | -17 ± 3 | -15 ± 2 | - | 0.68 ± 0.05 | 0.69 ± 0.05 | - |
| S448C | 0.45 | 0.56 | 8 ± 2 | -6 ± 9 | -197 ± 17 | 0.60 ± 0.03 | 0.42 ± 0.06 | 0.30 ± 0.02 |
| S155C | 0.91 | 1.00 | 6 ± 3 | -8 ± 2 | -38 ± 1 | 0.61 ± 0.03 | 0.56 ± 0.04 | 0.49 ± 0.01 |
| S155C-S448C | 0.40 | 0.45 | 3 ± 3 | -28 ± 4 | -230± 5 | 0.67 ± 0.05 | 0.59 ± 0.05 | 0.20 ± 0.01 |
| A175C | 0.91 | 0.91 | -198 ± 16 | -178 ± 10 | n.a | 0.4[a] | 0.4[a] | n.a |
| A175C-S448C | 0.48 | 0.59 | -112 ± 4 | -52 ± 5 | -42 ± 5 | 0.64 ± 0.02 | 0.56 ± 0.04 | 0.26 ± 0.02 |
| A175S-S448C | 0.42 | 0.43 | -13 ± 9 | 4 ± 9 | -81 ± 4 | 0.67 ± 0.07 | 0.57 ± 0.12 | 0.4 ± 0.02 |

[a] *z* constrained to 0.4 for fit; [b] values determined in100Na; n.a. not applicable

**Table III. Rate constants for simulations using the 10-state model for electrogenic NaPi-IIb cotransport cycle.**

| *Forward* | | *Backward* | |
|---|---|---|---|
| $k_{12a}$[a,b] ($M^{-1} s^{-1}$) | | $k_{2a1}$[a] ($s^{-1}$) | |
| WT | 2e3 $e^{-0.4V/50}$ | WT | 4e2 $e^{0.4V/50}$ |
| A175C | 4e2 $e^{-0.4V/50}$ | A175C | 2e3 $e^{-0.4V/50}$ |
| S155C/S448C | 2e3 $e^{-0.4V/50}$ | S155C/S448C | 4e2 $e^{-0.4V/50}$ |
| $k_{2a2b}$[b] ($M^{-1} s^{-1}$) | 6e3 | $k_{2b2a}$ ($s^{-1}$) | 2e2 |
| $k_{2b3}$[b] ($M^{-1} s^{-1}$) | 4e6 | $k_{32b}$ ($s^{-1}$) | 8e3 |
| $k_{34}$[b] ($M^{-1} s^{-1}$) | 4e5 | $k_{43}$ ($s^{-1}$) | 1e3 |
| $k_{87a}$[a,b] ($M^{-1} s^{-1}$) | 1e3 $\exp^{-0.2V/50}$ | $k_{7a8}$[a] ($s^{-1}$) | 1e3 $\exp^{0.2V/50}$ |
| $k_{7a7b}$[b] ($M^{-1} s^{-1}$) | 1e3 | $k_{7b7a}$ ($s^{-1}$) | 1e3 |
| $k_{7b6}$ | -[c] | $k_{67b}$ ($s^{-1}$) | 1e3 |
| $k_{65}$[b] ($M^{-1} s^{-1}$) | 1e5 | $k_{56}$ ($s^{-1}$) | 1e3 |
| $k_{45}$ ($s^{-1}$) | 25 | $k_{54}$ ($s^{-1}$) | 25 $s^{-1}$ |
| $k_{81}$[a] ($s^{-1}$) | | $k_{18}$[a] ($s^{-1}$) | 150 $\exp^{0.4V/50}$ |
| WT | 50 $\exp^{-0.4V/50}$ | | |
| A175C | 50 $\exp^{-0.4V/50}$ | | |
| S155C/S448C | 100 $\exp^{-0.4V/50}$ | | |

[a] voltage dependent transitions were modeled using Eyring barrier model assuming sharp, symmetrical barriers. One net charge is assumed to move across the entire transmembrane electric field. The apparent valence of the empty carrier = 0.4; the charge movement contributed by a single $Na^+$ binding = 0.4 from the outside and = 0.2 from the inside.

[b] pseudo first order kinetics were assumed for all partial reactions involving substrate interaction.

[c] free parameter to satisfy microscopic reversibility given by:

$$k_{7b6} = \frac{k^{o}_{67b}\, k^{o}_{7b7a}\, k^{o}_{7a8}\, k^{o}_{81}\, k^{o}_{12a}\, k^{o}_{2a2b}\, k^{o}_{2b3}\, k^{o}_{34}\, k^{o}_{45}\, k^{o}_{56}}{k^{o}_{65}\, k^{o}_{54}\, k^{o}_{43}\, k^{o}_{32b}\, k^{o}_{2b2a}\, k^{o}_{2a1}\, k^{o}_{18}\, k_{87a}\, k_{7a7b}}$$

Figure 1

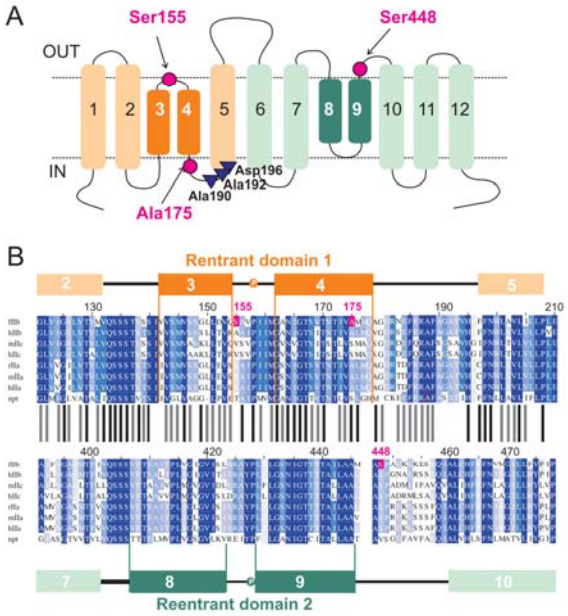
A
Ser155
Ser448
OUT
IN
1
2
3
4
5
6
7
8
9
10
11
12
Asp196
Ala192
Ala190
Ala175
B
Rentrant domain 1
Reentrant domain 2

Figure 2

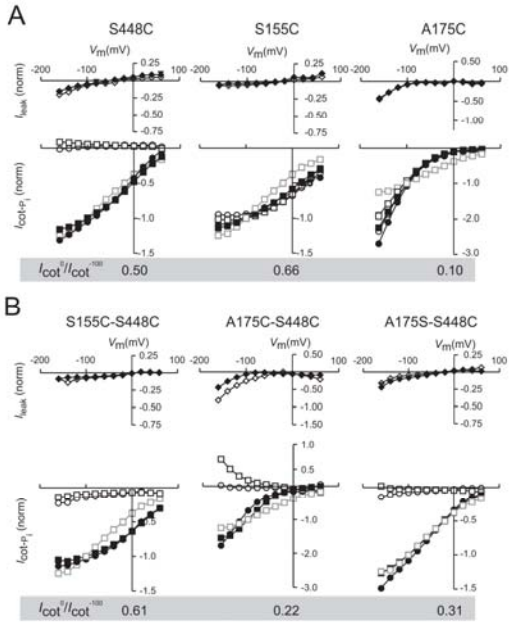
A
S448C
S155C
A175C
$V_m$(mV)
$I_{leak}$ (norm)
$I_{cot-P_i}$ (norm)
$I_{cot}^{+}/I_{cot}^{-100}$ 0.50 0.66 0.10
B
S155C-S448C
A175C-S448C
A175S-S448C
$I_{cot}^{+}/I_{cot}^{-100}$ 0.61 0.22 0.31

Figure 3

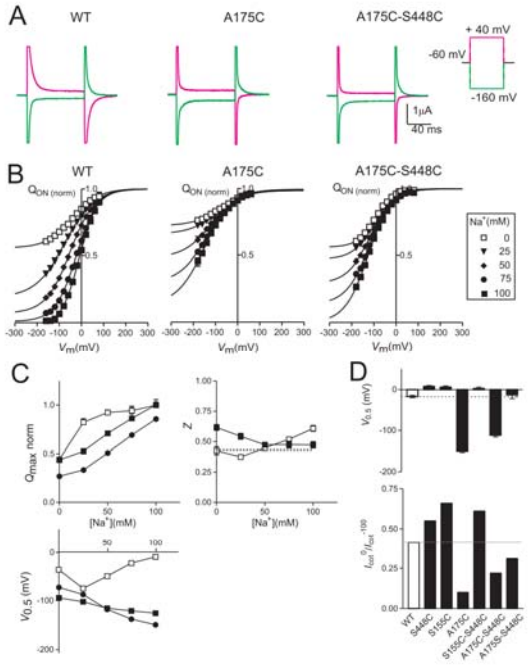
A
WT
A175C
A175C-S448C
+ 40 mV
-60 mV
-160 mV
1µA
40 ms
B
WT
A175C
A175C-S448C
$Q_{ON\ (norm)}$
$V_m$(mV)
Na+(mM)
0
25
50
75
100
C
$Q_{max}$ norm
[Na+](mM)
Z
$V_{0.5}$ (mV)
D
$V_{0.5}$ (mV)
$I_{Ca}^0/I_{Ca}^{-100}$
WT
S448C
S155C
A175C
S155C-S448C
A175C-S448C
A175S-S448C

Figure 4

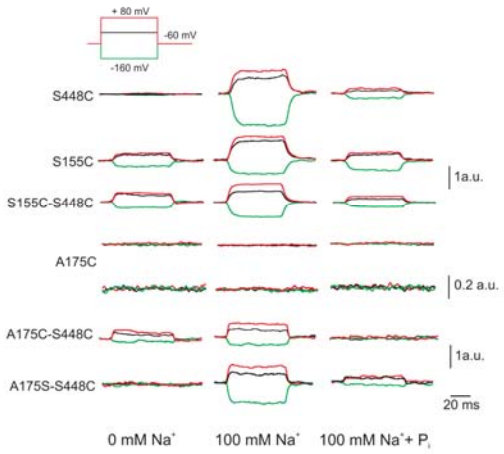
+ 80 mV
-60 mV
-160 mV
S448C
S155C
S155C-S448C
A175C
A175C-S448C
A175S-S448C
1a.u.
0.2 a.u.
1a.u.
20 ms
0 mM Na+
100 mM Na+
100 mM Na+ + Pi

Figure 6

Figure 5

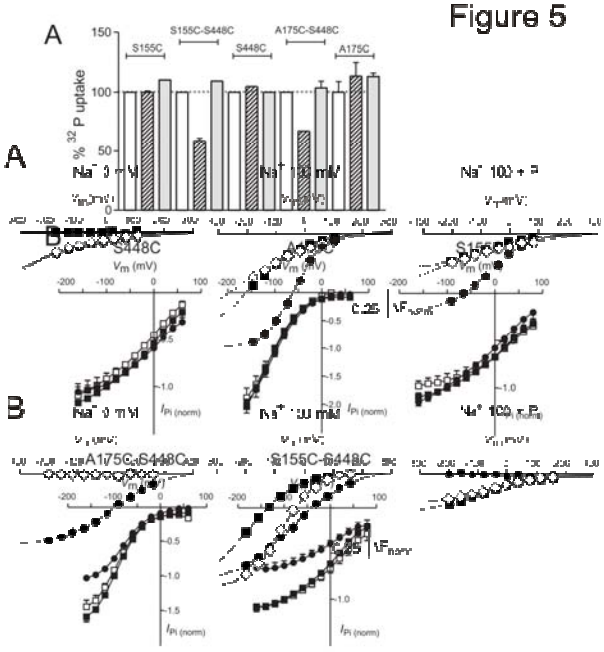

Figure 7

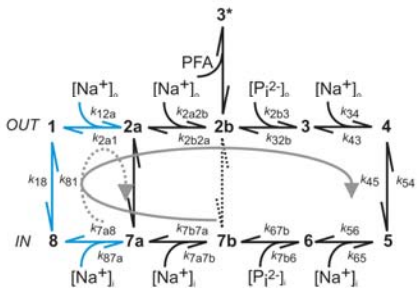
3*
PFA
[Na+]o
[Na+]o
[Pi2-]o
[Na+]o
OUT 1
2a
2b
3
4
k12a
k2a1
k2a2b
k2b2a
k2b3
k32b
k34
k43
k18
k81
k45
k54
IN 8
7a
7b
6
5
k7a8
k87a
k7b7a
k7a7b
k67b
k7b6
k56
k65
[Na+]i
[Na+]i
[Pi2-]i
[Na+]i

Figure 8

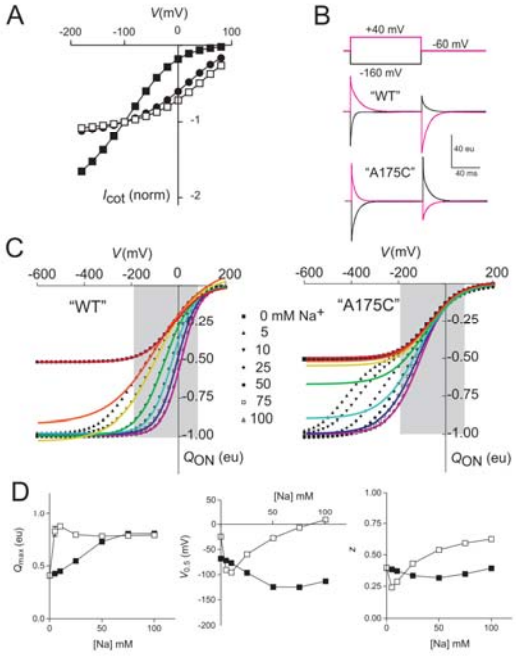
A
V(mV)
-200
-100
0
100
-1
-2
$I_{cot}$ (norm)
B
+40 mV
-60 mV
-160 mV
"WT"
40 eu
40 ms
"A175C"
C
V(mV)
-600
-400
-200
0
200
"WT"
"A175C"
0 mM Na+
5
10
25
50
75
100
-0.25
-0.50
-0.75
-1.00
$Q_{ON}$ (eu)
D
$Q_{max}$ (eu)
$V_{0.5}$ (mV)
z
[Na] mM

[Channels 2:5, 346-357; September/October 2008]; ©2008 Landes Bioscience

Review

# The leak mode of type II $Na^+$-$P_i$ cotransporters

Olga Andrini, Chiara Ghezzi, Heini Murer and Ian C. Forster*

Institute of Physiology and Center of Integrative Human Physiology; University of Zurich; Zurich Switzerland

**Abbreviations:** $I_{Pi}$, $P_i$-dependent change in holding current; $I_{PFA}$, PFA-dependent change in holding current; MTS, methanethiosulfonate; MTSEA, 2-aminoethyl MTS hydrobromide; MTSES, (MTS ethylsulfonate); MTSET, 2-(triethylammonium)ethyl MTS bromide; NaPi-IIa/b/c, type IIa/b/c sodium phosphate cotransporter; PFA, phosphonoformic acid; $P_i$, inorganic phosphate; SCAM, substituted cysteine accessibility method; TMD, transmembrane domain; WT, wild-type; SLC34, solute carrier family 34

**Key words:** phosphate, sodium, cotransport, leak current, *Xenopus* oocyte, electrophysiology

**$Na^+$-coupled phosphate cotransporters of the SLC34 gene family catalyze the movement of inorganic phosphate ($P_i$) across epithelia by using the free energy of the downhill electrochemical $Na^+$ gradient across the luminal membrane. Electrogenic (NaPi-IIa/b) and electroneutral (NaPi-IIc) isoforms prefer divalent $P_i$ and show strict $Na^+$:$P_i$ stoichiometries of 3:1 and 2:1, respectively. For electrogenic cotransport, one charge is translocated per transport cycle. When NaPi-IIa or NaPi-IIb are expressed in *Xenopus* oocytes, application of the $P_i$ transport inhibitor phosphonoformic acid (PFA) blocks a leak current that is not detectable in the electroneutral isoform. In this review, we present the experimental evidence that this transport-independent leak originates from a $Na^+$-dependent uniport carrier mode intrinsic to NaPi-IIa/b isoforms. Our findings, based on the characteristics of the PFA-inhibitable leak measured from wild type and mutant constructs, can be incorporated into an alternating access class model in which the leak and cotransport modes are mutually exclusive and share common kinetic partial reactions.**

## Introduction

Secondary-active cotransporters catalyze uphill solute movement across membranes by using the free energy available from the electrochemical gradient of the driving substrate, usually a monovalent cation ($Na^+$, $H^+$ or $K^+$). The transport cycles of many members of this class are electrogenic, whereby net charge transfer accompanies cotransport and the partial reactions that constitute the transport cycle show voltage dependent kinetics. We can investigate the kinetics of these carriers by electrophysiological techniques, as ideally the substrate-induced current is an indirect measure of the transport rate for a constant number of charges translocated per cycle. Uncoupled currents give rise to deviations from the tightly coupled electrogenicity and strict stoichiometry between driving and driven substrates that is expected of the ideal secondary-active carrier. They are also referred to as leak or slippage currents (reviewed in refs. 1 and 2) and are intimately associated with the heterologous expression of the carrier protein. Their co-existence alongside the coupled transport electrogenic activity has led to a reassessment of the traditional view of channels and carriers as unique molecular entities (reviewed in ref. 3).

Uncoupled currents are commonly sub-classified as transport-dependent and transport-independent currents, depending on whether they are detectable in the absence or presence of substrate. Cotransporters can exhibit one or both types of uncoupled current with different contributing ions. Uncoupled currents appear to be ubiquitous among electrogenic carriers and they have been described for gene products of at least nine solute carrier families identified in the human genome[4] (Table 1). Within a given solute carrier family, the properties of the uncoupled currents can also vary considerably for different isoforms, measured under the same experimental conditions. For example, in the biogenic amine transporter subgroup of the SLC6 family, GAT4 is reported to have two transport independent, mutually exclusive $Na^+$-dependent conductances that are permeable to $Li^+$ or $Cl^-$, both of which are present only in the absence of external $Na^+$ and GABA.[5] In contrast, the human GAT1 isoform displays only a $Li^+$-dependent uncoupled leak [Uncoupled currents are not exclusively associated with electrogenic transport. Electroneutral transporters show uncoupled currents, for example, $Na^+$-coupled glutamine transporter (SNAT3)].[5]

Transport-dependent uncoupled currents are observed in the *presence* of both driven and driving substrates and manifest themselves as currents in excess of those associated with the stoichiometric charge translocation. The most notable examples are members of the excitatory amino acid transporter family (EAAT's of the SLC1 family) that catalyze transport of glutamate driven by two $Na^+$ ions. For these carriers, experimental manipulations allow separation of the transport-dependent current to be separated into a stoichiometric component and a thermodynamically uncoupled anion selective component that is only activated in the presence of $Na^+$ and the amino acid (e.g., glutamate, aspartate).[10] This uncoupled current has been likened to that of ligand-gated channel that is gated by the driven substrate.[2,11] Although the presence of $Cl^-$ is not essential for cotransport, it is accelerated by $Cl^-$ ions[12,13] and studies suggest

*Correspondence to: Ian C. Forster; Institute of Physiology; University of Zurich; Winterthurerstrasse 190; Zurich CH-8057 Switzerland; Tel.: +41.44.635.5059; Fax: +41.44.635.5025; Email: IForster@access.unizh.ch

Submitted: 10/20/08; Accepted: 10/20/08

Previously published online as a *Channels* E-publication:
http://www.landesbioscience.com/journals/channels/article/6900

Table 1 **Examples of gene products of the solute carrier families[1] that mediate uncoupled currents**

| SLC | Example proteins | Coupled substrates | Un-coupled current[2] | Ions carried by uncoupled currents | Selected references[3] |
|---|---|---|---|---|---|
| 1 | EAAT1,2,3,4 | $Na^+/H^+/K^+$/Glu | T | $Cl^-$ | (11, 69) |
| | EAAC1 | | L | $Na^+$ | (70) |
| | ASCT1,2 | $Na^+$/neutral amino acids (exch) | T | $Cl^-$ | (8, 9) |
| 5 | SGLT1 | $Na^+$/glucose | L | $Na^+$ | (17, 67, 71) |
| | NIS | $Na^+/I^-$ | L | $Na^+$ | (15) |
| | SMIT | $Na^+$/myoinositol | L | $Na^+$ | (72) |
| | SMCT | $Na^+$/monocarboxylate | L | Anions | (73) |
| | CHT | $Na^+$/choline | L | $Na^+$ | (74) |
| 6 | GAT-1,4 | $Na^+/Cl^-$/GABA | L | $Li^+$,$Cs^+$, $Cl^-$ | (5, 19, 75) |
| | SERT | $Na^+/Cl^-/K^+$/5HT | T/L | $Na^+$, $Li^+$, $K^+$, $H^+$ | (7, 75, 76) |
| | hDAT | $Na^+/Cl^-$/DA$^+$ | T/L | $Na^+$, $Li^+$, $K^+$, H, $Cl^-$ | (20, 77) |
| 11 | DMT1 | $H^+$/divalent cations | L | $H^+$ | (34, 49) |
| 13 | NaD (NaC) | $Na^+$/dicarboxylates | L | $Na^+$ | (78) |
| 15 | PepT2 | $H^+$/peptides | L | $H^+$ | (79) |
| 23 | SVCT1,2 | $Na^+$/ascorbic acid | L | $Na^+$ | (16, 80) |
| 34 | NaPi-IIa/b | $Na^+/P_i$ | L | $Na^+$ | (41, 45) |
| 38 | SNAT3 | $Na^+$/glutamine | T | $K^+$, $H^+$, $Na^+/H^+$ exch. | (6) |
| | | | L | Cations | |

[1]Nomenclature according to Human Genome Organisation Database (4). [2]According to the nomenclature of Sonders and Amara (2): L(eak) = transport-independent currents, T(ransport) = transport-dependent currents respectively. [3]Only studies using the *Xenopus* oocyte expression system are cited.

that the negative charge acts as a counterbalance to the excess charge associated with cotransported $Na^+$ ions.[14]

In contrast, transport-independent uncoupled currents are observed in the *absence* of the driven substrate and represent a constitutive leak that may or may not involve the driving substrate. In some cases, for example the $Na^+/I^-$ cotransporter (NIS)[15] and the $Na^+$/L-ascorbic acid transporters (SVCT1,2),[16] the leak currents measured when the transporter is heterologously expressed in *Xenopus* oocytes are significantly larger than those observed for control oocytes and comparable in magnitude to the substrate-induced current. For other cotransporters, the currents can only be quantified with confidence by the application of substrates or blockers that bind specifically to the transporter, but which themselves are not transported. Characterization is further complicated by the finding that the cation species contributing to the leak current can either be the same or different from the cation that preferentially drives cotransport. For example, the leak associated with the sodium glucose cotransporter (SGLT1) is mediated by $Na^+$ ions,[17,18] whereas for GAT1 from the same gene family, alkali metal cations such as $K^+$ and $Li^+$, which do not drive transport, can nevertheless permeate.[2,5,19-21]

Several questions arise with respect to the identity and underlying mechanism of uncoupled currents:

(i) Are they an intrinsic property of the carrier or an artifact of the heterologous expression system?

(ii) Given that they are constitutive to the carrier, do they share either the same permeation pathway as the cotransported substrates, or are the ions conducted via a separate pathway, for example through a pore established by oligomerization of functional subunits?

(iii) Is the leak better described as a channel (gated pore) or a uniport (carrier) type mechanism?

(iv) Do they play mechanistic or physiological roles?

It has been challenging to answer these questions unambiguously, in part because of possible artifacts of the expression systems, the small size of the currents compared with the cotransport mode currents and given that the same ions are cotransported and permeate the leak pathway. Evidence from structure-function studies on heterologously expressed, as well as functionally reconstituted carriers, together with 3-D crystallographic data from bacterial homologs, is helping to provide clearer answers to these questions.

Indirect support that uncoupled currents are intrinsic to carriers comes from the observation that their magnitude correlates strongly with that of the substrate-induced electrogenic response, which should reflect the number of active transporters expressed in the membrane. However, it has been reported that heterologous expression of proteins in *Xenopus* oocytes can lead to the upregulation of endogenous $Cl^-$ and non-specific hyperpolarization-activated cation channels (reviewed in refs. 22–25). Therefore, the number of upregulated endogenous channels might still correlate with the activity of the heterologously expressed protein. More compelling evidence that leak currents are intrinsic to the carrier protein comes from studies in which the leak is modified or even "uncoupled" from the cotransport mode activity through mutations of the protein, or by in situ modification of specific residues. These studies establish a direct link at the molecular level between the leak current and the heterologously expressed protein (reviewed in refs. 26–34). The most convincing approach to confirm the intrinsic nature of the leak current is to purify and reconstitute the protein in a membrane preparation. Transport assays can then be performed to identify the leak and transport related fluxes. For example, compelling evidence for a constitutive $Cl^-$ conductance was found for the bacterial glutamate transporter homolog ($Glt_{Ph}$) reconstituted in proteoliposomes.[12]

As some cotransporters are known to form homo-oligomers, there has been speculation that leak pathways could be created at the interface between the subunits analogous to the structure of multimeric ionotropic proteins (reviewed in ref. 35). However, recent studies on the neuronal EAAT3,[36] and its bacterial homolog $Glt_{Ph}$ [12] suggest that the translocation pathways for the substrate itself and transport-dependent leak are colocalized to individual subunits and function independently. On the other hand, direct structural evidence concerning the localization of the permeation pathway for transport-independent uncoupled currents is lacking.

## The Uncoupled Leak of SLC34 Proteins

**Introduction.** Members of the SLC34 family of $Na^+$-coupled inorganic phosphate ($P_i$) transporters play a vital physiological role in $P_i$ homeostasis, particularly in the kidney, where they are responsible for $P_i$ reabsorption from the glomerular filtrate across the apical membrane of proximal tubule epithelia. They are also expressed in epithelial membranes in the small intestine and other organs (testes, lung, liver), where their physiological function is less well understood (reviewed see ref. 37). The family comprises three isoforms that prefer divalent $P_i$ as the driven substrate: NaPi-IIa, NaPi-IIb catalyze electrogenic transport with a $Na^+$:$P_i$ stoichiometry of 3:1 and one net charge is translocated per transport cycle;[38,39] NaPi-IIc is electroneutral and therefore cotransports with a $Na^+$:$P_i$ stoichiometry of 2:1.[40]

Based on kinetic studies of WT isoforms and structure-function studies of mutant constructs, we have developed a kinetic scheme for the cotransport cycle (Fig. 1A) that comprises a sequence of partial reactions representing the transitions between unique conformational states of the protein.[37,41-43] Under normal physiological conditions, the cotransport cycle begins in the outward facing conformation of the empty carrier (state 1), which favors ordered binding of two $Na^+$ ions, followed by binding of one divalent $P_i$ and a 3$^{rd}$ $Na^+$ ion from the external medium. A translocation partial reaction of the fully loaded carrier (transition 4↔5) occurs, followed by release of substrates to the cytosol to leave the carrier in state 8. The normally negative intracellular potential is now sensed by the now free mobile charges intrinsic to the empty carrier, the movement of which effects a conformational change from state 8 to state 1. In its simplest form, only two electrogenic partial reactions (8↔1, 1↔2a) are sufficient for the model to account for voltage dependent kinetics and translocation of one net charge/cycle: the empty carrier and 1$^{st}$ $Na^+$ interaction. In this model, the translocation of the fully loaded carrier is electroneutral. The scheme is consistent with an alternating access mechanism that excludes translocation of substrates from intermediate states. In this scheme, membrane potential contributes a source of free energy to drive cotransport, but is not essential: the cycle can also proceed with membrane potentials ≥0, albeit at a lower turnover rates, driven by the difference in free energy for $Na^+$ ions between the external and internal mediums. Support for this prediction was first provided by studies on renal brush border membrane vesicles, in which the initial rate of $^{32}P$ uptake by renal brush border membrane vesicles is reduced, but not eliminated, when the vesicle membrane potential is changed from hyperpolarizing to depolarizing in the presence of an inward $Na^+$ gradient.[44] Experimental evidence also strongly supports the ordered substrate binding for the outward facing conformations (1↔4), however evidence is lacking with respect to order of substrate interaction for the inward facing conformations (5↔8).

Although the cotransport cycle is probably the normal physiologically relevant transport process, electrogenic NaP-IIa/b isoforms also exhibit a leak current in the absence of $P_i$ when expressed in *Xenopus* oocytes. This is incorporated in the kinetic scheme as second transport cycle that resembles a $Na^+$-dependent uniporter and shares three of the partial reactions of the cotransport cycle (Fig. 1A). In this model, both the cotransport and leak modes mediate the net movement of one charge per cycle (Fig. 1A, *inset*). For the cotransport mode, this has been established by simultaneous isotope flux and electrophysiological recording.[38,39] For NaPi-IIa/b isoforms, it has not been feasible to apply the same approach to establish the stoichiometry of the leak because the corresponding cation flux is at the limit of experimental resolution using isotopes. Therefore, our current understanding of the leak mechanism and the evidence to support of its inclusion in the kinetic scheme as a uniporter has come from the integration of findings from electrophysiological studies using both WT and mutant constructs as described below.

**Properties of the uncoupled leak for WT NaPi-IIa/b.** We have found no evidence of significant electrogenic activity in excess of the stoichiometrically coupled components for three electrogenic isoforms of the SLC34 family[38,39] when expressed in *Xenopus* oocytes. However, a transport-independent leak current was postulated by comparing the electrogenic responses of oocytes heterologously expressing NaPi-IIa or NaPi-IIb isoforms to $P_i$ or the $P_i$-transport inhibitor phosphonoformic acid (PFA). Figure 1B depicts a representative recording from an oocyte expressing rat NaPi-IIa when voltage was clamped to -50 mV using a two-electrode voltage clamp (*inset*). In contrast to the electrogenic response to a saturating concentration of $P_i$ (1 mM), which results in a downward deflection in the holding current corresponding to the inward movement of charge ($I_{Pi}$, Fig. 1B), 3 mM PFA induces a small upward deflection of the steady-state holding current ($I_{PFA}$). This is interpreted as evidence of block of an intrinsic leak,[41] analogous to the phlorizin-dependent block of the leak intrinsic to the $Na^+$-coupled glucose transporter (SGLT1), first described by Umbach et al.[17] The holding current level reached during PFA superfusion is not zero, but is given by the endogenous leak current of the oocyte ($I_{Endog}$), which at a membrane potential of -50 mV, is usually inward but its magnitude can vary widely both between and within batches of oocytes. In the absence of external $Na^+$, PFA like $P_i$, does not induce a change in holding current, which underscores the $Na^+$-dependence for the electrogenic responses to $P_i$ and PFA. At -50 mV, $I_{PFA}$ accounts for approx 10–20% of $I_{Pi}$, although we have documented larger PFA-induced changes in holding current for constructs that contain point mutations at sites associated with the putative transport pathway (see below). We have also observed a PFA-dependent block of holding current in all characterized electrogenic NaPi-II isoforms, however at a given membrane potential its magnitude relative to $I_{Pi}$ can vary, which is also reflected in differences in steady-state voltage dependence of the cotransport mode (see Fig. 5C).

As we first reported,[41] the magnitude of $I_{PFA}$ correlates with $I_{Pi}$ under the same voltage clamp conditions (Fig. 1C). For the rat NaPi-IIa isoform $I_{Pi}$ is typically < -200 nA at -100 mV, whereas the magnitude of the leak current is comparable to $I_{Endog}$ and therefore could not be easily detectable without using PFA as a blocking substrate. As illustrated for a representative oocyte expressing rat NaPi-IIa (lower, Fig. 1D), the current-voltage (*I-V*) relation for

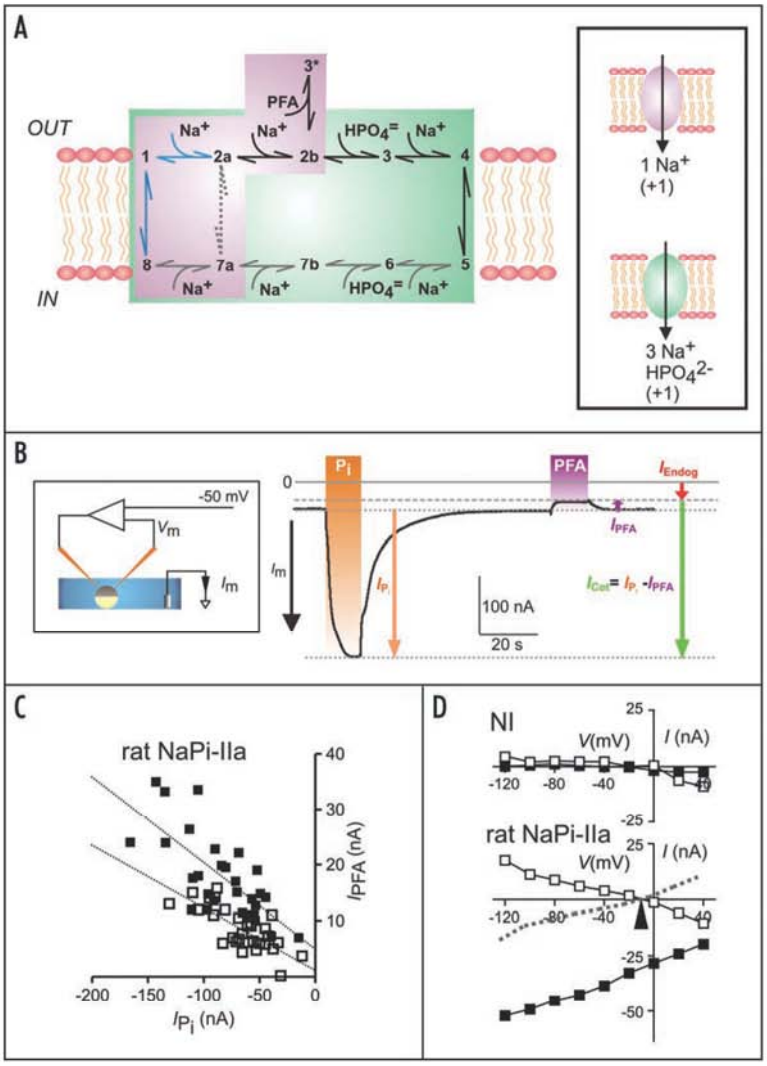


Figure 1. The transport modes of electrogenic SLC34 proteins. (A) Kinetic scheme showing the ordered sequence of partial reactions that result in net charge translocation for the cotransport mode (green shading) and leak mode (violet shading). Two electrogenic partial reactions (blue) account for the voltage dependence of transport. All other partial reactions are assumed to be electroneutral. Inset shows the two modes of electrogenic transport: cotransport and leak. Both involve the translocation of one net charge per cycle. Only the stoichiometry of the cotransport mode has been determined experimentally by simultaneous uptake and voltage clamp.[38] (B) Electrogenic responses of an oocyte expressing the rat NaPi-IIa isoform to saturating $P_i$ (1 mM) ($I_{Pi}$) and PFA (3 mM) ($I_{PFA}$) in the presence of 100 mM $Na^+$. Oocyte is voltage clamped using a two-electrode voltage (inset) and the membrane clamped to -50 mV. $I_{Endog}$ represents the endogenous oocyte current. If the leak is fully suppressed by saturating $P_i$, the predicted electrogenic cotransport activity is given by $I_{Cot}$. (Forster IC, unpublished data). (C) Correlation of $I_{PFA}$ with $I_{Pi}$ shown for oocytes harvested from >5 donor frogs at two holding potentials (-100 mV, filled squares; -60 mV, open squares). Linear regression lines have slopes -0.16 ± 0.03 (-100 mV); -0.11 ± 0.02 (-60 mV) but were not statistically significant (n = 29). (D) Typical steady-state voltage dependence of $I_{Pi}$ and $I_{PFA}$ for a representative oocyte expressing rat NaPi-IIa (lower) and a non-injected (NI) oocyte from the same donor frog as control (upper). Each data point is obtained by subtracting the oocyte holding current in the control solution from the current with 1 mM $P_i$ or 1 mM PFA added to the control solution. Note that $I_{PFA}$ reverses at ~-10 mV for the NaPi-IIa expressing oocyte (arrow). Dotted line indicates the apparent PFA-inhibitable leak current ($-I_{PFA}$, see text). An endogenous response to PFA is also observed for NI for $V > 0$ mV (filled squares: $I_{Pi}$; open squares: $I_{PFA}$). (Andrini O and Forster IC, unpublished data).

$I_{Pi}$ shows an inward current for all test potentials, consistent with cotransport cycling clockwise in Figure 1A. In contrast, $I_{PFA}$ is outward for hyperpolarizing potentials and typically reverses at potentials between -30 mV to -10 mV (arrowed, Fig. 1D). This apparently anomalous *I-V* behavior for a substrate-dependent current is simply a result of subtracting the holding current at each potential in the absence of PFA from the response in the presence of PFA to eliminate $I_{Endog}$ [We adopt the convention that $I_{Pi}$ and $I_{PFA}$ indicate the change in holding current caused by the addition of $P_i$ or PFA to the control superfusate. For steady-state *I-V* curves, data points were obtained by subtracting currents recorded in response to voltage steps in the presence of substrate, from the corresponding records in the control solution, thereby eliminating endogenous currents. The validity of this method rests on the assumption that substrates do not modulate endogenous currents]. The apparent leak current, which we assume PFA fully inhibits, is therefore $-I_{PFA}$ (dotted line, Fig. 1D). Non-injected or $H_2O$-injected oocytes showed either no response to PFA or a consistently smaller change in holding current for holding potentials <0 mV, (upper, Fig. 1D). Thus, the scatter in the $I_{PFA}$ - $I_{Pi}$ correlation most likely arises from contamination from endogenous responses to either $P_i$ or PFA.[41,45] For $V > 0$ mV, control (non-injected or $H_2O$ injected) oocytes sometimes also show an endogenous response to PFA, which resembles the response of injected oocytes in the same voltage range (Fig. 1D) (see below).

Our original analysis of $I_{PFA}$ using the rat NaPi-IIa isoform documented a Nernstian shift in its reversal potential with external [$Na^+$]

from which we concluded that $-I_{PFA}$ is a measure of the permeation of $Na^+$ ions through the transporter. Furthermore, the dependence of $-I_{PFA}$ on external [$Na^+$] shows Michaelian kinetics (apparent $K_m$ = 128 mM), which suggests that one $Na^+$ ion interacts with the carrier.[41] Taken together, these findings offer compelling evidence that the underlying transport mechanism is more akin to that of a uniport class of carrier rather than a channel.

Under the tacit assumption that $I_{PFA}$ reflects the inhibition of an intrinsic transport-independent leak mode of NaPi-IIa, we postulated an electroneutral $Na^+$ translocation partial reaction (2a↔7a) takes place in the absence of $P_i$ (Fig. 1A). The leak and cotransport modes share common partial reactions (empty carrier and $Na^+$ binding/debinding on the external and internal faces of the membrane) and this model predicts that at saturating $P_i$, when the forward partial reaction 2b→3 is favored, the leak mode will be inactive. When PFA is bound, the protein occupies a unique blocked conformation ($3^*$). This is similar to schemes proposed for the $Na^+$ glucose cotransporter SGLT1 (reviewed in refs. 18 and 46). Importantly, if the leak and cotransport modes are mutually exclusive, the true baseline for quantitating the electrogenic activity of the cotransport mode for saturating $P_i$ ($I_{Cot}$,) is given by the holding current in the presence of PFA and *not* the holding current in the control solution (Fig. 1B).

In this model, the rate of translocation of $Na^+$ via the leak pathway is also predicted to be very slow. We have estimated the turnover rates for the cotransport cycle of electrogenic SLC34 proteins to lie in the range 4–13 $s^{-1}$ (47). Therefore, if one net charge is translocated in the leak mode, the magnitude of $I_{PFA}$ suggests that the leak turnover rate will be <1 $s^{-1}$.

The carrier mechanism for the leak mode has gained further support from a study on the temperature dependence of $I_{Pi}$ and $I_{PFA}$ of the flounder NaPi-IIb isoform, which was chosen because of its large transport activity, up to 5-fold greater than mammalian isoforms.[40] As illustrated in Figure 2A, both $I_{Pi}$ and $I_{PFA}$ show strong temperature dependencies that when fit with the Arrhenius equation yield activation energies ($E_a$) at -100 mV of ~16 kcal $mol^{-1}$ and ~11 kcal $mol^{-1}$ for $I_{Pi}$ and $I_{PFA}$ , respectively (Fig. 2B). The estimate of $E_a$ for $I_{PFA}$ is consistent with that expected for a carrier type mechanism involving large conformational changes, rather than a channel. The latter should have an activation energy closer to that for free diffusion of ions (e.g., reviewed in ref. 48), for example, as reported for the $Cl^-$ leak of GAT4.[5] The activation energy for $I_{PFA}$ is the same as that reported for the $H^+$-mediated leak of the divalent metal ion transporter DMT1,[49] but significantly less than 26 kcal $mol^{-1}$ reported for the $Li^+$-activated leak of GAT1,[21] and 21 kcal $mole^{-1}$ for the $Na^+$-activated leak of SGLT1.[50] These data show that among members of different solute carrier families there is varying complexity of conformation changes that accompany the uncoupled leak mode. Furthermore, we found that $E_a$ for both cotransport and leak modes is only weakly sensitive to membrane potential (Fig. 2B), which supports the assumption that the rate-limiting substrate translocation partial reactions for each mode (2a↔7a; 4↔5) are electroneutral.[51] Analysis of the temperature dependence of the partial reactions associated with the empty carrier and lumped $Na^+$ binding interactions, which are manifest experimentally as presteady-state charge movements (see below), also revealed activation energies >10 kcal $mol^{-1}$.[51] It is therefore conceivable that the temperature dependence of $I_{PFA}$ reflects molecular rearrangements

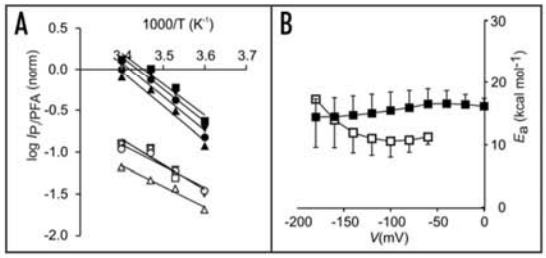


Figure 2. Temperature dependence of $I_{PFA}$ suggests that it arises from a carrier-mediated conductance. (A) Arrhenius plots of the normalized magnitude of $I_{Pi}$ (filled symbols) and $I_{PFA}$ (open symbols) for the membrane potentials indicated. Straight lines represent linear regression fits to the data points to yield the apparent activation energy ($E_a$) given by: log [$I_{Pi,PFA}$] = $-E_a/(2.303\ R)\ (1/T)$ + log A, where $E_a$ is the activation energy, R the gas constant, T temperature (K) and A a constant. (Squares: -180 mV; *inverted triangles:* -140 mV; circles: -100 mV; triangles: -60 mV). (B) $E_a$ plotted as a function of membrane potential, $I_{Pi}$ (filled squares) and $I_{PFA}$ (open squares). Modified from ref. 51 with permission.

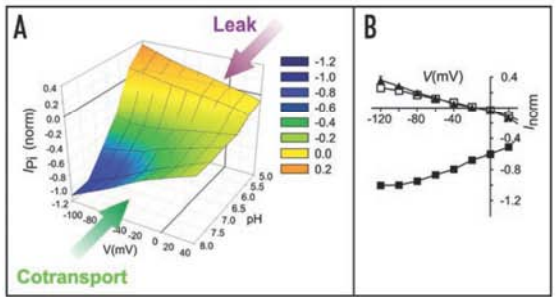


Figure 3. Acidification transforms the electrogenic transport modes of rat NaPi-IIa. (A) Evidence for "mode" switching from cotransport to leak as the external medium is acidified. Steady-state pH-V profile of WT showing $I_{Pi}$ (1 mM total $P_i$) as a function of external pH and V. Currents were normalized to the magnitude of $I_{Pi}$ at -100 mV, pH 7.4 and pooled (n = 4). Error bars omitted for clarity. Legend indicates color and corresponding normalised $I_{Pi}$. (B) Normalized, pooled (n = 5) I-V data for WT that compares $I_{Pi}$ at pH 5.0 (open squares) with $I_{PFA}$ at pH 7.4 (filled triangles), normalized to the magnitude of $I_{Pi}$ at -100 mV, pH 7.4 (filled squares). The superposition of $I_{Pi}$ at pH 5.0 and $I_{PFA}$ at pH 7.4 suggests that at pH 5.0 only the leak mode is operational. © Ehnes et al., adapted from Figure 3 originally published in The J Gen Physiol 2004;124: 489–503.

associated with the empty carrier and $Na^+$ binding events and not translocation per se.

In other studies, we have documented the insensitivity of $I_{PFA}$ to changes in external pH.[45,52] As illustrated in Figure 3A, when the external medium is acidified, $I_{Pi}$ at all potentials decreases, in part due to the reduced availability of the preferred divalent $P_i$ and also because protons interact with partial reactions in the transport cycle.[39,45] It is noteworthy that at pH 5, $I_{Pi}$ closely matches $I_{PFA}$ at pH 7.4 (Fig. 3B), which suggests that there is a progressive pH-dependent shift from the cotransport mode to the leak mode. Moreover, these data indicate that even in its monovalent form at pH 5.0, $P_i$ can interact with the carrier to inhibit both leak and

cotransport modes.[52] The robust nature of $I_{PFA}$ is also underscored by its insensitivity to the arginine modifying reagent, phenolglyoxal, which typically reduces $I_{Pi}$ by 50%.[53]

**Leak and electrogenicity go hand in hand in SLC34 proteins.** Although PFA inhibits $Na^+$-coupled $P_i$ cotransport mediated by both electrogenic and electroneutral SLC34 isoforms (Ghezzi C and Stange G, unpublished data), a PFA-dependent change in holding current is only detectable in electrogenic NaPi-IIa/b isoforms (Fig. 4A and B). This suggests that the putative $Na^+$-leak pathway is absent in NaPi-IIc. Evidence to support this conclusion comes from studies on the WT NaPi-IIc and the WT NaPi-IIc backbone engineered to restore electrogenicity.

First, WT NaPi-IIc is proposed to lack a $Na^+$-binding site within the transmembrane electric field, consistent with its $Na^+$:$P_i$ stoichiometry of 2:1,[40] (lower, Fig. 4B). Binding of one $Na^+$ ion at this site would correspond to the 1st $Na^+$ interaction of the transport cycle (1↔2a) (Fig. 1A). For electrogenic NaPi-IIa/b, voltage steps induce presteady-state charge movements in 0 mM $P_i$. These are considered to originate in part from the movement of one $Na^+$ ion per transporter with the transmembrane electric field, as well as the movement of mobile charges associated with the empty carrier, observed in the absence of external $Na^+$.[42,43] As neither component of charge movement is detectable in oocytes that express functioning NaPi-IIc, this may indicate that in the electroneutral transport cycle, partial reaction 1↔2a is absent, and the reorientation of the empty carrier is electroneutral. Moreover, voltage clamping NaPi-IIc oocytes at different potentials does not alter the rate $P_i$ uptake, which indicates that the electroneutral isoform lacks voltage-dependent partial reactions in its transport cycle.[40]

Second, by comparing the sequences of the electrogenic and electroneutral isoforms, we identified a critical three amino acid motif conserved in all electrogenic isoforms that includes an aspartic acid (Fig. 6), which is absent in all electroneutral isoforms. When the residues comprising this motif, are substituted at the equivalent sites in the electroneutral backbone, the resulting mutant (AAD-IIc) displays electrogenic behavior (Fig. 4A). One net charge is transported per $P_i$ (Fig. 4B, upper) and the $Na^+$:$P_i$ stoichiometry of cotransport is increased from 2:1 to 3:1 (Fig. 4B, lower).[40] Moreover, presteady-state charge movements are detectable, both in the presence and absence of external $Na^+$ (data not shown). The former finding is consistent with the re-establishment of a $Na^+$ binding site within the transmembrane field.[40] The latter finding indicates that the effective mobile charge, which confers voltage dependence to the empty carrier partial reaction (Fig. 1A), is present in AAD-IIc, possibly contributed by the substituted Asp-224. Application of PFA induces an upward deflection of the steady-state holding current (arrowed, Fig. 4A) similar to that observed for the WT electrogenic isoforms, however the *I-V* relationship (Fig. 4C) reveals a weaker voltage dependence for both $I_{Pi}$ and $I_{PFA}$ compared to the WT over the same voltage range. Thus, the substituted motif is essential, but not exclusively involved in determining the voltage dependence.[40] Like the WT, for AAD-IIc the magnitude of $I_{PFA}$ correlates with $I_{Pi}$ (Fig. 4D), which supports our view that $I_{PFA}$ reflects electrogenic activity intrinsic to the expressed protein.

In summary, these findings offer compelling evidence that the presence of a leak current and the electrogenic interaction of one $Na^+$ ion with the empty carrier are not coincidental. As this $Na^+$ interaction is absent in the electroneutral isoform, the leak current displayed by electrogenic isoforms seems to be a direct consequence of their electrogenic transport kinetics.

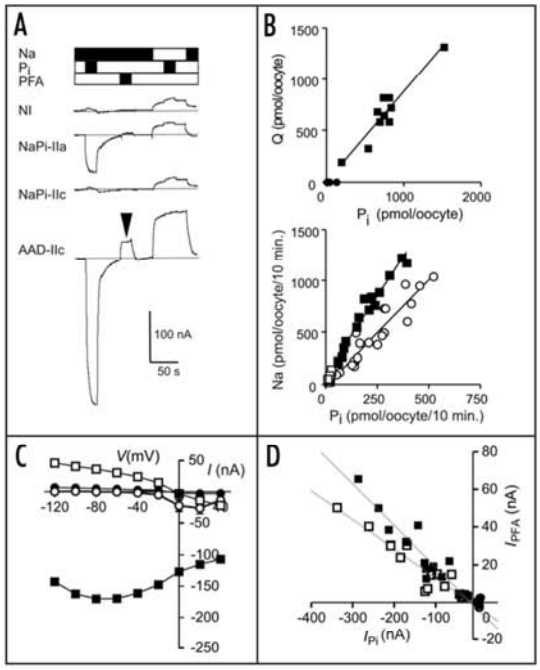


Figure 4. Conferring electrogenicity and leak to the electroneutral NaPi-IIc. (A) Representative current tracings of oocytes from the same donor frog, comparing non-injected (NI), mouse NaPi-IIa, mouse NaPi-IIc and AAD-IIc under different superfusion conditions as indicated. Na: Control buffer; $P_i$: Control + 1 mM $P_i$; PFA: Control + 1 mM PFA. Control buffer contains either 100 mM NaCl (filled bar) or 100 mM CholineCl (empty bar). Oocytes were voltage clamped at -50 mV. Arrow indicates response of AAD-IIc to 1 mM PFA in 100 mM NaCl buffer. (B) Upper: Charge translocation (Q) correlates with $P_i$ uptake for AAD-IIc. Each point is from an individual oocyte. AAD-IIc (filled squares); NI (filled circles) from same donor frog. Slope of linear regression line (0.9 ± 0.1) indicates that one charge is translocated per $P_i$ molecule as for WT NaPi-IIa/b.[38] Lower: Dual uptake ($^{22}Na$, $^{32}P_i$) for WT NaPi-IIc and AAD-IIc demonstrate that the $Na^+$:$P_i$ stoichiometry is increased in the AAD-IIc. AAD-IIc (filled squares); NaPi-IIc (open circles); NI (open squares) from the same donor frog. Data points for NaPi-IIc and AAD-IIc are fit with linear regression lines that give slopes of: 3.0 ± 0.2 (AAD-IIc) and 2.0 ± 0.2 (NaPi-IIc). Figure 4A and B are adapted from © Bacconi et al., Figure 3 originally published in Proc Natl Acad Sci USA 2005; 102:489–503. (C) Representative *I-V* data for AAD-IIc (squares) and WT NaPi-IIc (circles). $I_{Pi}$ (filled symbols; $I_{PFA}$ (open symbols). (Bacconi A, Forster IC, unpublished data). (D) Correlation between $I_{PFA}$ and $I_{Pi}$. Data for oocytes expressing AAD-IIc (squares, n = 15) and NI (circles, n = 4) from different donor frogs for currents measured for the same oocyte at two holding potentials (-60 mV: open symbols; -100 mV: filled symbols). Lines are linear regression fits with slopes: -0.154 ± 0.015 (-60 mV) and -0.221 ± 0.021 (-100 mV). (Bacconi A, Forster IC, unpublished data).

**Anion replacement experiments.** The small magnitude of $I_{PFA}$ and potential for contamination by endogenous currents that are also modulated by the specific substrates of the SLC34 family proteins

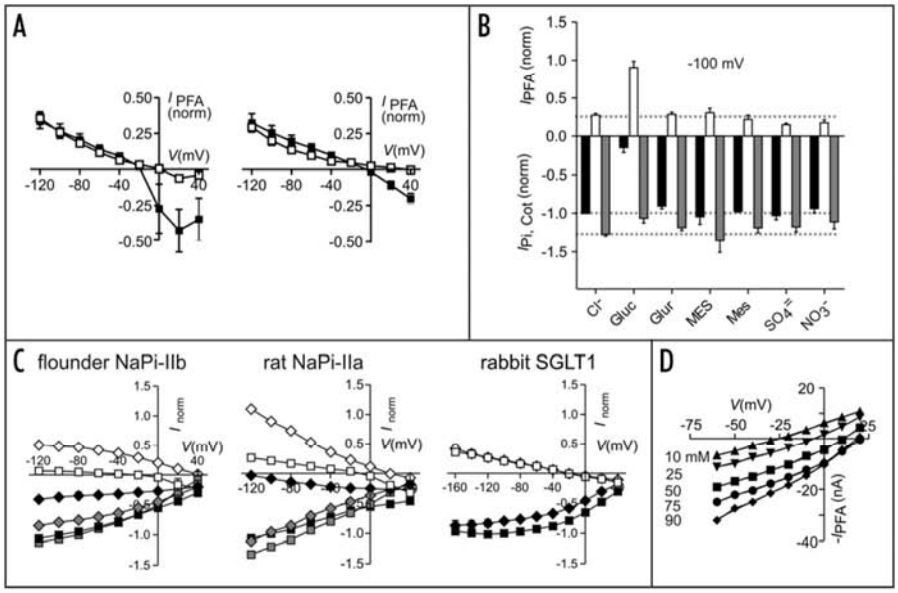


Figure 5. Effect of external anion substitution on $I_{Pi}$ and $I_{PFA}$. (A) Upper: Steady-state *I-V* data for rat NaPi-IIa expressing oocytes showing $I_{PFA}$ with external $Cl^-$ = 107 mM (filled squares) and morpholineethanesulfonate (MES) (100 mM) + 7 mM $Cl^-$ (open squares) in the external solution. Data were normalized to $I_{Pi}$ (1 mM $P_i$, 107 mM $Cl^-$, -100 mV) and pooled (n = 3). Lower: Steady-state *I-V* data for rat NaPi-IIa expressing oocytes, showing $I_{PFA}$ with external $Cl^-$ = 107 mM (filled squares) and glucuronate (100 mM) + 7 mM $Cl^-$ (open squares) in the external solution. Data were normalized to $I_{Pi}$ (1 mM $P_i$, 107 mM $Cl^-$, -100 mV) and pooled (n = 5). (Andrini O and Forster IC, unpublished data). (B) Summary of substituting 100 mM of external $Cl^-$ with indicated anions showing $I_{Pi}$ (filled bars); $I_{PFA}$ (open bars) and $I_{Cot}$ (= $I_{Pi}$ - $I_{PFA}$) (grey bars) at -100 mV, normalized to $I_{Pi}$ in 107 mM $Cl^-$ at -100 mV. Gluc, gluconate, Glur, glucuronate; Mes, methanesulfonate; MES, morpholineethansulfonate. Data are pooled using oocytes expressing rat NaPi-IIa (n ≥ 5). (Andrini O and Forster IC, unpublished data). (C) Left: Steady-state *I-V* data for flounder NaPi-IIb (n = 3); center: rat NaPi-IIa (n = 4); right: rabbit SGLT1 (n = 5). In each case, normalized data are shown for superfusion in 107 $Cl^-$ (*squares*) and 100 mM gluconate + 7 mM $Cl^-$ (*diamonds*). For flounder NaPi-IIb, rat NaPi-IIa: $I_{Pi}$ (1 mM)—filled symbols; $I_{PFA}$ (1 mM)—open symbols, $I_{Cot}$ (= $I_{Pi}$ - $I_{PFA}$)—grey symbols; for rabbit SGLT1: $I_{\alpha\text{-MDG}}$ (1 mM) (filled symbols), phlorizin (100 μM) (open symbols). (Ghezzi C and Forster IC, unpublished data). (D) Dependence of the PFA-inhibitable current on external [$Na^+$] in 100 mM gluconate superfusate confirms the [$Na^+$]-dependent shift in reversal potential. Data are from a representative oocyte expressing the human NaPi-IIa isoform. $Na^+$ was replaced equimolarly with $Li^+$. The hyperpolarizing shift in reversal potential followed a Nernstian relation with a slope 54.2 ± 4.0 mV/log[$Na^+$] (Forster IC, unpublished data).

has prevented its full characterization over a wide range of experimental conditions, particularly for membrane potentials close to 0 mV, unless cells with high expression ($I_{Pi}$) are selected. One feature of $I_{PFA}$ that was not fully resolved in the above studies was thatif the PFA-inhibitable leak reflects the activity of a $Na^+$-dependent conductance, equilibrium thermodynamics predicts that its reversal potential ($E_r$) should be given by the Nernst potential. For example, if we assume a typical oocyte cytosolic [$Na^+$] <10 mM (reviewed in ref. 54), with an external [$Na^+$] = 100 mM, $E_r$ > +60 mV. In practice, we consistently document $E_r$ in the range -10 to -30 mV (for example see Fig. 1D), which might be expected for a $Cl^-$ conductance and suggests that PFA inhibits more than one permeating ion species. Interestingly, the reversal potential for $I_{PFA}$ was similar to that of phlorizin-inhibitable leak current of $Na^+$-coupled glucose transporter (SGLT-1) (see Fig. 5C), which was shown to be dependent on internal sugar.[17] Initially, we therefore adopted a similar strategy for simulations using the kinetic model for NaPi-IIa/b, by assuming a finite internal $P_i$ (reviewed in refs. 45 and 53).

Experiments in which we replaced ~90% of external $Cl^-$ with other anions have now shed new light on the origin of the negative $E_r$. Substitution with the large polyatomic anions like morpholineethanesulfonate (MES) (upper, Fig. 5A) and glucuronate (lower, Fig. 5A) cause a depolarizing shift of $E_r$ and suppression of $I_{PFA}$ for $V$ > 0 mV. This behaviour is consistent with the partial suppression of an inward $Cl^-$ flux (in all anion replacement experiments, the external [$Cl^-$] = 7 mM). Moreover, a comparison of the responses of non-injected or $H_2O$-injected oocytes to PFA indicates that it suppresses an endogenous outward rectifying current that varies considerably between oocyte batches and according to the number of days after retrieval from the ovary. This endogenous current, which can be larger than the transporter-associated leak could therefore account for the negative $E_r$ in NaPi-IIa/b expressing oocytes. In contrast, for $V$ < 0 mV we observe only a small change in the $I_{PFA}$ when $Cl^-$ is removed from the external medium. Moreover, $I_{PFA}$ was little affected when oocytes were dialysed in a low $Cl^-$ medium to reduce the internal [$Cl^-$] (reviewed in ref. 10) compared to non-dialysed oocytes, thereby confirming that outward movement of $Cl^-$ ions does not contribute significantly for hyperpolarizing potentials.

With the notable exception of gluconate, equimolar replacement of 100 mM external chloride with a selection of anions

(Fig. 5B) had only minor effects on the magnitude of $I_{Pi}$ and $I_{PFA}$ at hyperpolarizing potentials, and the variations in $I_{PFA}$ for the different conditions therefore most likely reflect the influence of endogenous currents. Gluconate substitution resulted in a significant increase in $I_{PFA}$, a concomitantly smaller $I_{Pi}$ relative to the holding current in the gluconate control solution, yet only a small reduction (17% at -100 mV) in the apparent cotransport activity ($I_{Cot} = I_{Pi} - I_{PFA}$) (Fig. 5B). The increased $I_{PFA}$ with gluconate superfusion was documented also for human NaPi-IIb and flounder NaPi-IIb. Significantly, its voltage dependence mirrors that of $I_{Pi}$ in 107 mM $Cl^-$, as illustrated in Figure 5C for the flounder NaPi-IIb (left) and rat NaPi-IIa (center). These isoforms show characteristically different voltage dependencies for $I_{Pi}$ (1 mM) (e.g., Forster 2006): for hyperpolarizing potentials down to -120 mV, rat NaPi-IIa shows no rate-limiting behavior compared with the flounder NaPi-IIb. The similarity of the voltage dependence of $I_{Pi}$ and $I_{PFA}$ for each isoform supports our notion that the leak and cotransport modes share common voltage dependent processes (Fig. 1A). Moreover, in both cases, the reduced $I_{Pi}$ in gluconate superfusion appears as a direct consequence of the subtraction procedure used to eliminate endogenous currents in which the leak is, in effect, subtracted from the response to $P_i$. The increase in leak with gluconate superfusion appears to be a unique property of NaPi-IIa/b proteins expressed in *Xenopus* oocytes. We examined the effect of gluconate substitution on the intrinsic leak of SGLT1, using phlorizin to block its uncoupled leak.[17] Here, we documented no significant difference between the phlorizin-dependent currents in 107 mM $Cl^-$ or with 100 mM gluconate and no shift in the reversal potential (right, Fig. 5C) unlike the behavior observed for NaPi-IIa/b expressing oocytes from the same donor frog. Gluconate replacement slightly reduced the α-MNG-dependent cotransport mode current, as previously reported and indicates that $Cl^-$ ions can interact with SGLT1 and alter its voltage dependent kinetics.[55] However, the negative $E_r$ for SGLT1 cannot be explained simply by the involvement of $Cl^-$ ions. Finally, we also confirmed that PFA-inhibitable current measured with gluconate replacement has the properties of $Na^+$-dependent conductance (Fig. 5D). Equimolar replacement of $Na^+$ with $Li^+$, which does not drive transport in SLC34 transporters, shifted the $E_r$ of $-I_{PFA}$ according to the Nernstian relationship with slopes of 54.9 ± 6.5 mV/log[$Na^+$] (rat NaPi-IIa, n = 3) and 51.9 ± 2.4 mV/log[$Na^+$] (human NaPi-IIa, n = 3) (Forster IC, unpublished data). These data strongly suggest that the main permeating ion in the leak mode is $Na^+$, in agreement with our earlier findings.[41]

The mechanism by which gluconate increases the PFA-inhibitable leak of NaPi-IIa/b is unclear and will require further investigation. As gluconate is a known chelator of divalent cations,[56] we confirmed that the appropriate reduction of free [$Ca^{2+}$] and [$Mg^{2+}$] in the external buffer, to simulate chelation by gluconate, was not the underlying cause. The main effect of gluconate substitution on NaPi-IIa/b kinetics is to increase the leak current, most likely by altering the rate of the $Na^+$-translocation step 2a↔7a (Fig. 1A), whereas the predicted cotransport activity is only marginally affected. In this respect, the behaviour of NaPi-IIa/b with gluconate superfusion supports the notion that $P_i$ induces a switch from the leak to cotransport cycle.

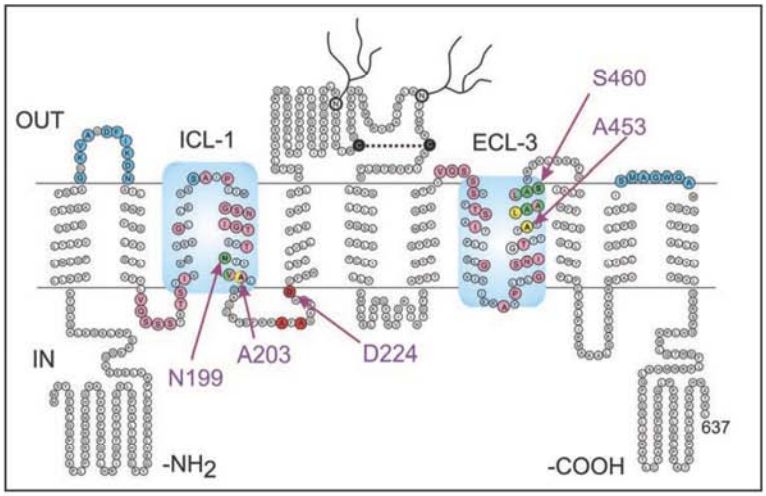


Figure 6. Secondary topology of SLC34 family proteins. Topology is based on the rat NaPi-IIa sequence and predicted according to (81). One essential cysteine bridge (black, dashed line) links the N- and C-terminal halves of the protein and there are two N-glycosylation sites in the large extracellular loop. The two re-entrant loops, proposed to form the transport pathway, are shaded (light blue) contain repeat residues (pink). Selected sites, relevant to leak and cotransport modes, which have been identified from structure-function studies, in which either the leak mode or cotransport mode or both are affected by MTS incubation are indicated as follows; blue: leak unchanged; green: cotransport fully suppressed, leak unchanged; yellow: cotransport fully suppressed, leak increased. In addition, sites critical for electrogenicity are shown (red). © Virkki et al., adapted from Figure 3 originally published in AJP-renal Physiol 2007; 293:643–54.

**New insights from structure-function studies- evidence that leak and cotransport share the same pathway.** The current secondary topology of SLC34 proteins (Fig. 6) is based on prediction algorithms and structure-function studies (reviewed in refs. 37 and 43). The functional unit of NaPi-IIa is a monomer,[57] however there is also evidence that it may dimerize in the membrane.[58] Each monomer comprises a core backbone of eight transmembrane domains interspersed with two repeat regions in the C- and N-terminal halves of the protein. We propose that they form two reentrant loops that associate to constitute the transport pathway. Cysteine scanning studies have confirmed that parts of loop ECL-3 and ICL-1 are accessible from the external and internal sides of the membrane, respectively. In ECL-3, evidence of a partial α-helical structure was obtained from cysteine scanning,[27] however no detailed topological features have been identified for the outwardly oriented ICL-1. As no 3-D structure for members of the SLC34 family or its bacterial homologs currently exist and there is no homology with available 3-D structures of other $Na^+$-dependent cotransporters, this functional assignment of

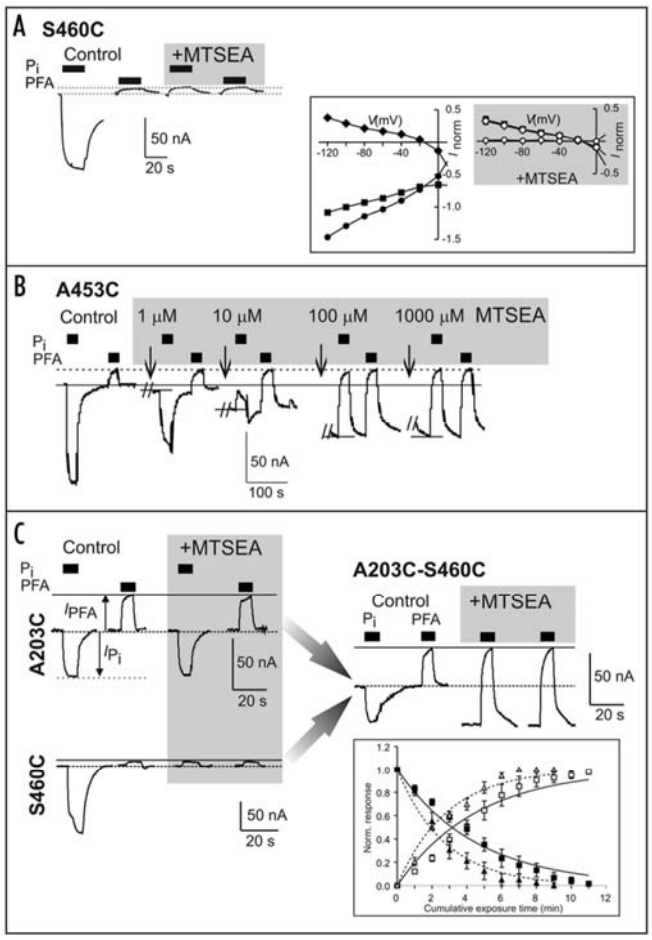


Figure 7. Structure function studies separate leak from cotransport activity. (A) S460C mutant. Representative current recording at -50 mV showing response to $P_i$ (1 mM) and PFA (3 mM) under control conditions. The oocyte was then exposed to the methanethiosulfonate reagent MTSEA (1 mM) for 3 minutes and then the measurement was repeated. © Lambert et al., adapted from Figure 6 originally published in The J Gen Physiol 1999; 114:637–51. Inset shows *I-V* data for S460C and establishes that $I_{Pi}$ after and $I_{PFA}$ before and after MTSEA exposure are almost identical over a wide range of test potentials. Data points normalised to $I_{Pi}$ at -100 mV before MTSEA exposure (n = 4). Filled symbols: control; empty symbols: after MTSEA exposure; squares: $I_{Pi}$; diamonds: $I_{PFA}$; circles: $I_{Cot}$. (Forster IC, unpublished data). (B) A453C mutant. Representative recording at -50 mV showing response to $P_i$ (1 mM) and PFA (3 mM) under control conditions and after exposure to MTSEA for 3 min at the indicated concentrations. Only the baseline that immediately preceded application and washout of the test substrates is shown. The dashed line indicates holding current reached during control PFA application. Continuous line indicates initial holding current in control superfusate. No external adjustment of current offset was made during the recording. After 100 μM MTSEA application there is little change in the responses to $P_i$ and PFA. © Lambert et al., adapted from Figure 3 originally published in The J Gen Physiol 2001; 117:533–46. (C) The double mutant A203C-S460C. Representative recording at -50 mV showing response to $P_i$ (1 mM) and PFA (3 mM) under control conditions and after exposure to MTSEA (1 mM for 3 min) for mutant A203C (upper) and S460C (lower) and A203C-S460C. Inset shows the reciprocity of transport mode activity as A203C-S460C is progressively modified using MTS reagents MTSEA (squares) and MTSES (triangles). Loss of cotransport function (filled symbols) and gain in leak (open symbols) follow reciprocal time courses suggesting that the two processes are linked. Continuous (MTSEA) and dotted (MTSES) lines are fits to the data with a single exponential function to give modification rates for MTSEA (leak gain: $7.3 \times 10^{-4}$ $s^{-1}$ $\mu M^{-1}$; cotransport loss: $7.2 \times 10^{-4}$ $s^{-1}$ $\mu M^{-1}$) an MTSES (leak gain: $1.1 \times 10^{-3}$ $s^{-1}$ $\mu M^{-1}$; cotransport loss: $1.2 \times 10^{-3}$ $s^{-1}$ $\mu M^{-1}$). Each data point represents mean ± SEM (n = 6). (For further details see ref. 29.) © Kohler et al., adapted from Figures 2 and 6 originally published in The J Gen Physiol 2002; 120:693–705.

the reentrant segments remains speculative. Nevertheless, the repeat regions are also conserved in the prokaryotic homolog from *Vibrio cholera*.[43,59] Moreover, recent 3-D structures of $Na^+$-driven cotransporters[60-63] have highlighted the importance of the inverted repeat structure that defines the substrate binding region and which could well apply to SLC34 proteins.

Insights into the nature and localization of the leak pathway for SLC34 proteins have come from structure-function studies in which cysteine residues are substituted at functionally important sites. This involves determining accessibility by methanethiosulfonate (MTS) reagents of the novel cysteine and characterizing the effect of the cys-substitution and MTS-modification on the $I_{Pi}$ and $I_{PFA}$.[26-29,64,65] In these studies, a number of mutants show full suppression of cotransport activity after MTS modification, which confirms their accessibility. These can be further distinguished according to the effect cys-modification has on the PFA-inhibitable leak: constructs in which the leak is unchanged after cys-modification and those in which the leak activity is increased.

Mutant S460C exemplifies the first type of behavior, which has a Ser-Cys substitution at a site in the C-terminal end of reentrant loop ECL-3 (Fig. 6). The substitution alone does not alter the basic kinetic properties compared to the WT.[26] However, after exposure to MTS reagents that increase the residue bulk and alter the charge at the substitution site, cotransport activity is inhibited, and the electrogenic responses to $P_i$ (1 mM) and PFA (3 mM) are identical (Fig. 7A). This behavior can readily be understood in terms of the kinetic scheme (Fig. 1A), whereby $P_i$ and PFA compete for the same binding site, thus blocking the leak mode. In the case of S460C, after MTS exposure, the substrate binding partial reactions for binding of $Na^+$ (1-2a, 2a-2b) and $P_i$ (2b-3) still occur, however subsequent partial reactions in the transport cycle are excluded because the modified cysteine restricts the possible conformational states the protein can occupy. With respect to

the leak mode, state 3* (PFA bound) and state 3 ($P_i$ bound) are therefore indistinguishable, in agreement with the equivalence of $I_{Pi}$ and $I_{PFA}$ over a wide range of test potentials(inset, Fig. 7A). At least one site has also been identified that shows similar behavior to S460C in the predicted reentrant loop ICL-1.[28] The cotransport activity of this mutant N199C (Fig. 6) is modified using the partially membrane permeable reagent MTSEA, whereas the impermeable MTSET has no effect. In addition to providing confirmation of the predicted topology, this finding is a first, albeit indirect hint that these reentrant loops might contribute to a common transport pathway for both the leak and cotransport modes. The critical importance of Asn-199 was demonstrated by making other substitutions at this site. Mutants in which the native Asn is substituted with the amide derivative of glutamate (Gln) or other basic or acidic amino acids (Asp, His, Arg) show only leak (PFA response), whereas substituting with Cys, Ala and Thr is tolerated and the corresponding mutants show both leak and cotransport activity.[28]

Mutant A453C also with a cys-substitution in ECL-3, exemplifies the second type of behavior. MTSEA treatment induces a large $Na^+$-dependent leak that, like S460C, is equally suppressed by both PFA and $P_i$ (Fig. 7B).[27] As the MTSEA concentration is increased, a progressively greater fraction of transporters is modified and $I_{Pi}$ changes from the initial downward deflection, characteristic of cotransport, to an upward deflection, which represents inhibition of the leak current. Note that the holding current reached during PFA application remains the same and corresponds to $I_{Endog}$ (Fig. 1A). In the GABA transporter GAT1 a similar phenotype of increased leak after MTS modification of Cys-74 in the first reentrant loop region[33] which, according to the 3-D structure of the bacterial homolog $LeuT_{Aa}$, forms part of the substrate binding domain.[63,66]

These findings provide compelling evidence for an interaction between ICL-1 and ECL-3, which was further investigated by examining the effect on the Cys-Ser substitution at site 460 by making a second cys substitution at site Ala-203 in ICL-1.[29] The single mutant (A203C) exhibits a significantly larger $I_{PFA}$ compared with the WT[28] (Fig. 7C). As expected, the double mutant (A203C-S460C) displays the phenotype of A203C, which indicates that the Cys-460 does itself alter the electrogenic activity. However, after exposure to MTSEA, the leak increases and $P_i$ induces the same change in holding current as PFA,[29] thus recapitulating the phenotype observed for Ala-Cys substitution in ECL3 (Fig. 7B). Based on the behavior of this and other mutants, our current view is that the leak and cotransport pathways share common structural elements. Whether one or both novel Cys in A203C-S460C are modified remains to be determined, however we currently favor a steric interaction between Cys-203 and Cys-460, in which only Cys-460 is modified, based on the behavior of other substitutions at these sites and a comparison of the rates of modification (Fig. 7C, inset).[29] The A203C-S460C double mutant also provides a useful tool to demonstrate the close interrelationship between leak and cotransport modes. The progressive growth in leak and decrease in cotransport activity over the time course of cys-modification is reciprocal (Fig. 7C, inset). This is the behavior expected of two populations of transporters: those that are modified and mediate only leak and those that are unmodified and can still mediate cotransport.[29]

**Transport kinetics and leak.** Transport-independent leak currents can introduce a source of error and lead to data misinterpretation when characterizing the transport kinetics of electrogenic carriers. As noted above, some WT cotransporters display leak currents that are comparable in magnitude to the substrate-induced change in holding current, (e.g., NIS,[15] and SVCT1,-2, [ref. 16]). If our model of mutual exclusivity of the leak and cotransport modes is valid also for other electrogenic carriers, large leak currents should be taken into account when deriving phenomenological kinetic parameters, such as apparent substrate affinities. Errors will arise when the substrate-induced currents are measured relative to the leak current (i.e., the baseline current in the absence of substrate, see Fig. 1A), which would substantially underestimate the magnitude of the cotransport mode current.[43] At non-saturating [$P_i$], the overall electrogenic activity will be contributed by both leak and cotransport modes: depending on the probability of occupancy of the associated states, a fraction of the transporters will translocate charge in the leak mode and others in the cotransport mode.

For cotransporters like NaPi-IIa/b, and SGLT1, where the leak typically accounts for ≤20% of substrate induced current, this error is small. For SGLT1, it was estimated that the leak contribution to electrogenic activity is negligible for glucose concentrations well below the apparent affinity for glucose cotransport[18] and a similar analysis has yet to be undertaken for NaPi-IIa/b. However, for NaPi-IIa/b, the error can become larger under specific conditions, such as low pH (Fig. 2A) or gluconate perfusion (Fig. 5C), where the relative contribution of the two transport modes to electrogenic activity changes significantly. This could account a significant deviation in stoichiometry of NaPi-IIa/b observed at pH < 6.8 determined by simultaneous uptake and charge measurements on single oocytes. Here, the transported charge is quantified by integrating the steady-state response to substrate (e.g., $I_{Pi}$ in Fig. 1B), using the control solution as baseline (reviewed in refs. 15, 38 and 67). At pH 7.4 and 6.8, the Q:$P_i$ ratio for rat NaPi-IIa expressing oocytes is ~1.0,[38] whereas at pH 6.2, where $I_{Pi}$ is significantly smaller but the leak is unchanged, Q:$P_i$ = 0.5 ± 0.1 (n = 13) (Forster IC, Loo DDF, Eskandari S, unpublished experiments). It may also explain the non-integer estimate of stoichiometry reported for the $Na^+$-coupled iodide cotransporter (NIS).[15]

## Conclusions

The physiological significance the NaPi-IIa/b leak is unclear: for example, along the length of the renal proximal tubule, NaPi-IIa in the brush border membrane is mostly exposed to Pi levels that exceed $K_m^{Pi}$ and therefore we would not expect the substrate-independent leak to contribute to a significant inward $Na^+$ flux. However, in the context of structure-function investigations, the leak mode offers a useful phenotype for gaining insight into transport mechanisms. Whereas many transporters exhibit channel-like (gated pore) behavior with complex permeation phenotypes (see Table 1), the $Na^+$-dependent leak current of SLC34 proteins appears to result from the intrinsic translocation of one charge per transport cycle and is specific for $Na^+$. Although we cannot exclude a leak mechanism in which $Na^+$ itself gates a thermodynamically uncoupled $Na^+$-selective pore, the evidence we have obtained so far from WT and mutant constructs is consistent with the leak being intimately associated with the electrogenic interaction of a single $Na^+$ ion, and its subsequent translocation via a uniport mechanism. In this respect, the term "uncoupled" leak should be used with reservation. Importantly, the leak and cotransport modes of NaPi-IIa/b appear to be mutually

exclusive: the behavior of the Cys mutants provides strong evidence that the leak mode is fully suppressed when substrate is bound. Here, we assume that the mutant behavior reflects the transitions between a subset of conformational states also occupied in the WT. Therefore, according to the transport scheme (Fig. 1A), for a given external [$Na^+$], the concentration of $P_i$ will determine whether the protein translocates only $Na^+$ ions via the leak loop (transition 2↔7), or binds $P_i$ and cotransports 3 $Na^+$ ions and $P_i$ (transition 4↔5), with the same $Na^+$ ion common to both modes.

Finally, we note that our data are based exclusively on experiments with intact oocytes and constant intracellular environment. To test the validity of the alternating access model implied by the kinetic scheme of Figure 1A, further investigations would benefit from the cut-open oocyte technique, to allow access to the intracellular medium (reviewed in ref. 68).

**Acknowledgements**

This work was supported by the Swiss National Science Foundation and the Gebert-Ruf Foundation. The rabbit SGLT1 cDNA was a kind gift of Professor Ernest M. Wright, UCLA.

**References**

1. Nelson N, Sacher A, Nelson H. The significance of molecular slips in transport systems. Nat Rev Mol Cell Biol 2002; 3:876-81.
2. Sonders MS, Amara SG. Channels in transporters. Curr Opin Neurobiol 1996; 6:294-302.
3. DeFelice LJ, Goswami T. Transporters as channels. Ann Rev Physiol 2007; 69:87-112.
4. Hediger MA, Romero MF, Peng JB, Rolfs A, Takanaga H, Bruford EA. The ABCs of solute carriers: physiological, pathological and therapeutic implications of human membrane transport proteinsIntroduction. Pflugers Archiv Eur J Physiol 2004; 447:465-8.
5. Karakossian MH, Spencer SR, Gomez AQ, et al. Novel properties of a mouse gamma-aminobutyric acid transporter (GAT4). J Memb Biol 2005; 203:65-82.
6. Schneider HP, Broer S, Broer A, Deitmer JW. Heterologous expression of the glutamine transporter SNAT3 in *Xenopus* oocytes is associated with four modes of uncoupled transport. J Biol Chem 2007; 282:3788-98.
7. Cao Y, Mager S, Lester HA. $H^+$ permeation and pH regulation at a mammalian serotonin transporter. J Neurosci 1997; 17:2257-66.
8. Zerangue N, Kavanaugh MP. ASCT-1 is a neutral amino acid exchanger with chloride channel activity. J Biol Chem 1996; 271:27991-4.
9. Broer A, Wagner C, Lang F, Broer S. Neutral amino acid transporter ASCT2 displays substrate-induced $Na^+$ exchange and a substrate-gated anion conductance. Biochem J 2000; 346:705-10.
10. Wadiche JI, Amara SG, Kavanaugh MP. Ion fluxes associated with excitatory amino acid transport. Neuron 1995; 15:721-8.
11. Fairman WA, Vandenberg RJ, Arriza JL, Kavanaugh MP, Amara SG. An excitatory amino-acid transporter with properties of a ligand-gated chloride channel. Nature 1995; 375:599-603.
12. Ryan RM, Mindell JA. The uncoupled chloride conductance of a bacterial glutamate transporter homolog. Nat Struct Mol Biol 2007; 14:365-71.
13. Miller C. A leak in the EAATs. Nat Struct Mol Biol 2007; 14:356-7.
14. Zomot E, Bendahan A, Quick M, Zhao Y, Javitch JA, Kanner BI. Mechanism of chloride interaction with neurotransmitter:sodium symporters. Nature 2007; 449:726-30.
15. Eskandari S, Loo DD, Dai G, Levy O, Wright EM, Carrasco N. Thyroid $Na^+/I^-$ symporter. Mechanism, stoichiometry and specificity. J Biol Chem 1997; 272:27230-8.
16. Tsukaguchi H, Tokui T, Mackenzie B, et al. A family of mammalian $Na^+$-dependent L-ascorbic acid transporters. Nature 1999; 399:70-5.
17. Umbach JA, Coady MJ, Wright EM. Intestinal $Na^+$/glucose cotransporter expressed in *Xenopus* oocytes is electrogenic. Biophys J 1990; 57:1217-24.
18. Chen XZ, Coady MJ, Jalal F, Wallendorff B, Lapointe JY. Sodium leak pathway and substrate binding order in the $Na^+$-glucose cotransporter. Biophys J 1997; 73:2503-10.
19. Mager S, Kleinberger-Doron N, Keshet GI, Davidson N, Kanner BI, Lester HA. Ion binding and permeation at the GABA transporter GAT1. J Neurosci 1996; 16:5405-14.
20. Sonders MS, Zhu SJ, Zahniser NR, Kavanaugh MP, Amara SG. Multiple ionic conductances of the human dopamine transporter: the actions of dopamine and psychostimulants. J Neurosci 1997; 17:960-74.
21. MacAulay N, Zeuthen T, Gether U. Conformational basis for the $Li^+$-induced leak current in the rat gamma-aminobutyric acid (GABA) transporter-1. J Physiol 2002; 544:447-58.
22. Shimbo K, Brassard DL, Lamb RA, Pinto LH. Viral and cellular small integral membrane proteins can modify ion channels endogenous to *Xenopus* oocytes. Biophys J 1995; 69:1819-29.
23. Tzounopoulos T, Maylie J, Adelman JP. Induction of endogenous channels by high levels of heterologous membrane proteins in *Xenopus* oocytes. Biophys J 1995; 69:904-8.
24. Buyse G, Voets T, Tytgat J, et al. Expression of human pICln and ClC-6 in *Xenopus* oocytes induces an identical endogenous chloride conductance. J Biol Chem 1997; 272:3615-21.
25. Broer S, Schuster A, Wagner CA, et al. Chloride conductance and Pi transport are separate functions induced by the expression of NaPi-1 in *Xenopus* oocytes. J Memb Biol 1998; 164:71-7.
26. Lambert G, Forster IC, Stange G, Biber J, Murer H. Properties of the mutant Ser-460-Cys implicate this site in a functionally important region of the type IIa $Na^+/P_i$ cotransporter protein. J Gen Physiol 1999; 114:637-52.
27. Lambert G, Forster IC, Stange G, Kohler K, Biber J, Murer H. Cysteine mutagenesis reveals novel structure-function features within the predicted third extracellular loop of the type IIa $Na^+/P_i$ cotransporter. J Gen Physiol 2001; 117:533-46.
28. Kohler K, Forster IC, Stange G, Biber J, Murer H. Identification of functionally important sites in the first intracellular loop of the NaPi-IIa cotransporter. Am J Physiol 2002; 282:687-96.
29. Kohler K, Forster IC, Stange G, Biber J, Murer H. Transport function of the renal type IIa $Na^+/P_i$ cotransporter is codetermined by residues in two opposing linker regions. J Gen Physiol 2002; 120:693-703.
30. Ryan RM, Mitrovic AD, Vandenberg RJ. The chloride permeation pathway of a glutamate transporter and its proximity to the glutamate translocation pathway. J Biol Chem 2004; 279:20742-51.
31. Borre L, Kavanaugh MP, Kanner BI. Dynamic equilibrium between coupled and uncoupled modes of a neuronal glutamate transporter. J Biol Chem 2002; 277:13501-7.
32. Ryan RM, Vandenberg RJ. Distinct conformational states mediate the transport and anion channel properties of the glutamate transporter EAAT-1. J Biol Chem 2002; 277:13494-500.
33. Yu N, Cao Y, Mager S, Lester HA. Topological localization of cysteine 74 in the GABA transporter, GAT1, and its importance in ion binding and permeation. FEBS Letters 1998; 426:174-8.
34. Mackenzie B, Ujwal ML, Chang MH, Romero MF, Hediger MA. Divalent metal-ion transporter DMT1 mediates both $H^+$-coupled $Fe^{2+}$ transport and uncoupled fluxes. Pflugers Archiv. Eur J Physiol 2006; 451:544-58.
35. Eskandari S, Kreman M, Kavanaugh MP, Wright EM, Zampighi GA. Pentameric assembly of a neuronal glutamate transporter. Proc Natl Acad Sci USA 2000; 97:8641-6.
36. Leary GP, Stone EF, Holley DC, Kavanaugh MP. The glutamate and chloride permeation pathways are colocalized in individual neuronal glutamate transporter subunits. J Neurosci 2007; 27:2938-42.
37. Virkki LV, Biber J, Murer H, Forster IC. Phosphate transporters: a tale of two solute carrier families. Am J Physiol Renal Physiol 2007; 293:643-54.
38. Forster IC, Loo DD, Eskandari S. Stoichiometry and $Na^+$ binding cooperativity of rat and flounder renal type II $Na^+$-$P_i$ cotransporters. Am J Physiol 1999; 276:644-9.
39. Virkki LV, Forster IC, Biber J, Murer H. Substrate interactions in the human type IIa sodium-phosphate cotransporter (NaPi-IIa). Am J Physiol 2005; 288:969-81.
40. Bacconi A, Virkki LV, Biber J, Murer H, Forster IC. Renouncing electrogenicity is not free of charge: switching on electrogenicity in a $Na^+$-coupled phosphate cotransporter. Proc Natl Acad Sci USA 2005; 102:12606-11.
41. Forster I, Hernando N, Biber J, Murer H. The voltage dependence of a cloned mammalian renal type II $Na^+/P_i$ cotransporter (NaPi-2). J Gen Physiol 1998; 112:1-18.
42. Virkki LV, Murer H, Forster IC. Voltage clamp fluorometric measurements on a type II $Na^+$-coupled $P_i$ cotransporter: shedding light on substrate binding order. J Gen Physiol 2006; 127:539-55.
43. Forster IC, Kohler K, Biber J, Murer H. Forging the link between structure and function of electrogenic cotransporters: the renal type IIa $Na^+/P_i$ cotransporter as a case study. Prog Biophys Mol Biol 2002; 80:69-108.
44. Beliveau R, Ibnoul-Khatib H. Electrogenicity of phosphate transport by renal brush-border membranes. Biochem J 1988; 252:801-6.
45. Forster IC, Biber J, Murer H. Proton-sensitive transitions of renal type II $Na^+$-coupled phosphate cotransporter kinetics. Biophys J 2000; 79:215-30.
46. Parent L, Supplisson S, Loo DD, Wright EM. Electrogenic properties of the cloned $Na^+$/glucose cotransporter: II. A transport model under nonrapid equilibrium conditions. [erratum appears in J Membr Biol 1992; 130:203]. J Memb Biol 1992; 125:63-79.
47. Forster IC, Virkki LV, Bossi E, Murer H, Biber J. Electrogenic kinetics of a mammalian intestinal $Na^+/P_i$-cotransporter. J Memb Biol 2006; 212:177-90.
48. van Winkle L. Biomembrane Transport. San Diego: Academic 1999.
49. Mackenzie B, Takanaga H, Hubert N, Rolfs A, Hediger MA. Functional properties of multiple isoforms of human divalent metal-ion transporter 1 (DMT1). Biochem J 2007; 403:59-69.
50. Loo DD, Hirayama BA, Meinild AK, Chandy G, Zeuthen T, Wright EM. Passive water and ion transport by cotransporters. J Physiol 1999; 518:195-202.
51. Bacconi A, Ravera S, Virkki LV, Murer H, Forster IC. Temperature-dependency of steady-state and presteady-state kinetics of a type IIb $Na^+/P_i$ cotransporter. J Memb Biol 2007; 215:81-92.
52. Ehnes C, Forster IC, Kohler K, et al. Structure-function relations of the first and fourth predicted extracellular linkers of the type IIa $Na^+$/Pi cotransporter: I. Cysteine scanning mutagenesis. J Gen Physiol 2004; 124:475-88.

53. Forster IC, Kohler K, Stange G, Biber J, Murer H. Modulation of renal type IIa $Na^+/P_i$ cotransporter kinetics by the arginine modifier phenylglyoxal. J Memb Biol 2002; 187:85-96.
54. Sciortino CM, Romero MF. Cation and voltage dependence of rat kidney electrogenic $Na^+$-HCO(-)(3) cotransporter, rkNBC, expressed in oocytes. Am J Physiol 1999; 277:611-23.
55. Loo DD, Eskandari S, Boorer KJ, Sarkar HK, Wright EM. Role of $Cl^-$ in electrogenic $Na^+$-coupled cotransporters GAT1 and SGLT1. J Biol Chem 2000; 275:37414-22.
56. Kenyon JL, Gibbons WR. Effects of low-chloride solutions on action potentials of sheep cardiac Purkinje fibers. J Gen Physiol 1977; 70:635-60.
57. Kohler K, Forster IC, Lambert G, Biber J, Murer H. The functional unit of the renal type IIa $Na^+$/Pi cotransporter is a monomer. J Biol Chem 2000; 275:26113-20.
58. Forster IC, Hernando N, Biber J, Murer H. Proximal tubular handling of phosphate: A molecular perspective. Kidney Intl 2006; 70:1548-59.
59. Werner A, Kinne RK. Evolution of the Na-$P_i$ cotransport systems. Am J Physiol 2001; 280:301-12.
60. Boudker O, Ryan RM, Yernool D, Shimamoto K, Gouaux E. Coupling substrate and ion binding to extracellular gate of a sodium-dependent aspartate transporter. Nature 2007; 445:387-93.
61. Faham S, Watanabe A, Besserer GM, et al. The crystal structure of a sodium galactose transporter reveals mechanistic insights into $Na^+$/sugar symport. Science 2008; 321:810-4.
62. Yernool D, Boudker O, Jin Y, Gouaux E. Structure of a glutamate transporter homologue from Pyrococcus horikoshii. Nature 2004; 431:811-8.
63. Yamashita A, Singh SK, Kawate T, Jin Y, Gouaux E. Crystal structure of a bacterial homologue of $Na^+/Cl^-$-dependent neurotransmitter transporters. Nature 2005; 437:215-23.
64. Kohler K, Forster IC, Stange G, Biber J, Murer H. Essential cysteine residues of the type IIa $Na^+/P_i$ cotransporter. Pflugers Archiv. Eur J Physiol 2003; 446:203-10.
65. Virkki LV, Forster IC, Bacconi A, Biber J, Murer H. Functionally important residues in the predicted 3rd transmembrane domain of the type IIa sodium-phosphate co-transporter (NaPi-IIa). J Memb Biol 2005; 206:227-38.
66. Kanner BI. Structure and function of sodium-coupled GABA and glutamate transporters. J Memb Biol 2006; 213:89-100.
67. Mackenzie B, Loo DD, Wright EM. Relationships between $Na^+$/glucose cotransporter (SGLT1) currents and fluxes. J Memb Biol 1998; 162:101-6.
68. Adams SV, DeFelice LJ. Ionic currents in the human serotonin transporter reveal inconsistencies in the alternating access hypothesis. Biophys J 2003; 85:1548-59.
69. Wadiche JI, Arriza JL, Amara SG, Kavanaugh MP. Kinetics of a human glutamate transporter. Neuron 1995; 14:1019-27.
70. Kanai Y, Nussberger S, Romero MF, Boron WF, Hebert SC, Hediger MA. Electrogenic properties of the epithelial and neuronal high affinity glutamate transporter. J Biol Chem 1995; 270:16561-8.
71. Chen XZ, Coady MJ, Jackson F, Berteloot A, Lapointe JY. Thermodynamic determination of the $Na^+$: glucose coupling ratio for the human SGLT1 cotransporter. Biophys J 1995; 69:2405-14.
72. Coady MJ, Wallendorff B, Gagnon DG, Lapointe JY. Identification of a novel $Na^+$/myo-inositol cotransporter. J Biol Chem 2002; 277:35219-24.
73. Coady MJ, Wallendorff B, Bourgeois F, Charron F, Lapointe JY. Establishing a definitive stoichiometry for the $Na^+$/monocarboxylate cotransporter SMCT1. Biophys J 2007; 93:2325-31.
74. Iwamoto H, Blakely RD, De Felice LJ. $Na^+$, $Cl^-$ and pH dependence of the human choline transporter (hCHT) in *Xenopus* oocytes: the proton inactivation hypothesis of hCHT in synaptic vesicles. J Neurosci 2006; 26:9851-9.
75. Mager S, Min C, Henry DJ, et al. Conducting states of a mammalian serotonin transporter. Neuron 1994; 12:845-59.
76. Galli A, Petersen CI, deBlaquiere M, Blakely RD, DeFelice LJ. Drosophila serotonin transporters have voltage-dependent uptake coupled to a serotonin-gated ion channel. J Neurosci 1997; 17:3401-11.
77. Meinild AK, Sitte HH, Gether U. Zinc potentiates an uncoupled anion conductance associated with the dopamine transporter. J Biol Chem 2004; 279:49671-9.
78. Yao X, Pajor AM. The transport properties of the human renal $Na^+$-dicarboxylate cotransporter under voltage-clamp conditions. Am J Physiol Renal Physiol 2000; 279:54-64.
79. Chen XZ, Zhu T, Smith DE, Hediger MA. Stoichiometry and kinetics of the high-affinity $H^+$-coupled peptide transporter PepT2. J Biol Chem 1999; 274:2773-9.
80. Mackenzie B, Illing AC, Hediger MA. Transport model of the human $Na^+$-coupled L-ascorbic acid (vitamin C) transporter SVCT1. Am J Physiol Cell Physiol 2008; 294:451-9.
81. Radanovic T, Gisler SM, Biber J, Murer H. Topology of the type IIa $Na^+$/P(i) cotransporter. J Memb Biol 2006; 212:41-9.

# CHAPTER 4

# DISCUSSION

## 4.1 Studying $Na^+$-dependent $P_i$ cotransporters

In the last 15 years transport activity of NaPi-II proteins have been extensively studied by heterologous expression in *Xenopus laevis* oocytes and different techniques such as two electrode voltage clamp, radiotracer uptake and voltage clamp fluorometry. When taken together, the data obtained using these tools have significantly advanced our understanding of the mechanism of transport.

Studies on SLC34 proteins have focused initially on the behavior of WT proteins with the aim of characterizing their transport kinetics and elucidating a mechanism for cotransport [69, 109]. These studies have revealed similarities and differences in the underlying transport mechanisms for each isoform. For example, it has been shown that apparent affinity for $Na^+$ and $P_i$ are not significantly different between the three different isoforms. This indicates that the partial reactions that determine these parameters are probably the same for both electrogenic and electroneutral transporters. On the other hand, there is a clear difference in the electrogenicity and the binding of one "extra" $Na^+$ in the electrogenic isoforms. This first substrate interaction step is considered electrogenic and responsible for the presence of leak and pre-steady state currents exclusively in NaPi-IIa/IIb. In particular, analysis of pre-steady state currents has allowed insight into the voltage-dependent kinetics and has led to the postulation of a binding scheme in which binding of $P_i$ require the binding of one $Na^+$ ion before and two $Na^+$ ions after [66, 69]). The fully loaded carrier can, then, undergoes the conformational change, release the substrates inside the cells and be ready for a new transport cycle.

This binding scheme was more recently revised on the basis of experiments performed on a Cys mutant of the flNaPi-IIb isoform and the use of voltage clamp fluorometry [74]. Using VCF (Fig. 10) a novel cysteine was introduced in position S448C of the fNaPi-IIb and labelled with the specific fluorophore (MTS-TAMRA). Emitted fluorescence was dependent on membrane potential and on the composition of the extracellular solution and in particular analysis of $Na^+$-dependent quenching revealed the interaction of 2 $Na^+$ ions before binding of

$P_i$. According to these data, the model initially proposed for the electrogenic isoforms [69] was revised to a $Na^+$-$Na^+$-$P_i$-$Na^+$ binding order [74](Fig. 21).

## 4.2 Binding order for the electroneutral NaPi-IIc

Determination of the stoichiometry of NaPi-IIc revealed that for each divalent $P_i$ only 2 $Na^+$ ions are translocated inside the cell [75]. This suggested that the difference between electroneutral and electrogenic isoforms was the absence, of one of the $Na^+$ binding sites proposed for the electrogenic isoforms. This was further support by the lack of two typical currents recorded in the electrogenic isoforms and directed linked to the first $Na^+$ interaction : leak and pre-steady state currents [64, 75].

For the electrogenic isoforms, in the absence of $P_i$, the first $Na^+$ ion is translocated in the leak mode and its movement within the transmembrane field to its binding site gives rise to part of the pre-steady state relaxations induced by voltage steps. In the absence of external $Na^+$, the relaxations arise from the movement of charges intrinsic to the protein and are proposed to reflect voltage-dependent conformational changes associated with the binding site of the first $Na^+$ ion. Moreover, experimental data and simulations suggest that the second $Na^+$ ion interaction is electroneutral and thus preserved also in NaPi-IIc. Based on these considerations, the NaPi-IIc kinetic scheme would be the same as that of NaPi-IIa/b without the leak and first $Na^+$ ion partial reactions (Fig. 21).

To experimentally test the validity of this binding scheme we applied conventional techniques, such as radiotracer influx and efflux experiments, combined with VCF on a NaPi-IIc wt and S437C mutant.

$^{32}P$ uptake was measured for different $P_i$ concentrations (in $Na^+$ 100 mM or 50 mM) or for different $Na^+$ concentrations (in presence of $P_i$ 1 mM or 0.1 mM). Analysis of the data showed a reduction of $V_{max}$ when [$Na^+$] was reduced from 100 mM to 50 mM. This indicated that $Na^+$ is the last substrate to bind. The absence of effect on the $V_{max}$ due to the decrease of [$P_i$] from 1 mM to 0.1 mM was also consistent with $Na^+$ being the last ion that interacts with the transporter before translocation (Fig 22 A).

Determination of the first partial reaction of the transport cycle required an additional experiment: $^{32}P$ efflux. We injected oocytes with 50 nl aliquots of an injection buffer containing $^{32}P$ and $Na^+$, so that after ~10 : 1 dilution in the cytosol the internal [$Na^+$] would

be at least 50 mM, thereby facilitating the establishment of an outward $Na^+$ gradient so that reverse cycling of the transporter should occur.

We then monitored over time the amount of radiotracer translocated out of the cell in different extracellular conditions: 100Na, 100Na +$P_i$, 0Na and 0Na +$P_i$.

In absence of external $Na^+$ we measured a small but significant efflux. This was unaffected by presence of external $P_i$ consistent with a scheme that requires $Na^+$ to bind before $P_i$. When 100 mM $Na^+$ is present in the external medium we observed a stimulation of efflux (~2-fold) that was further increase when $P_i$ was also present in the external medium (Fig. 22B). These data are consistent with a binding scheme in which $Na^+$ is the first ion to interact with the transporter and moreover they demonstrated that NaPi-IIc can work in reverse.

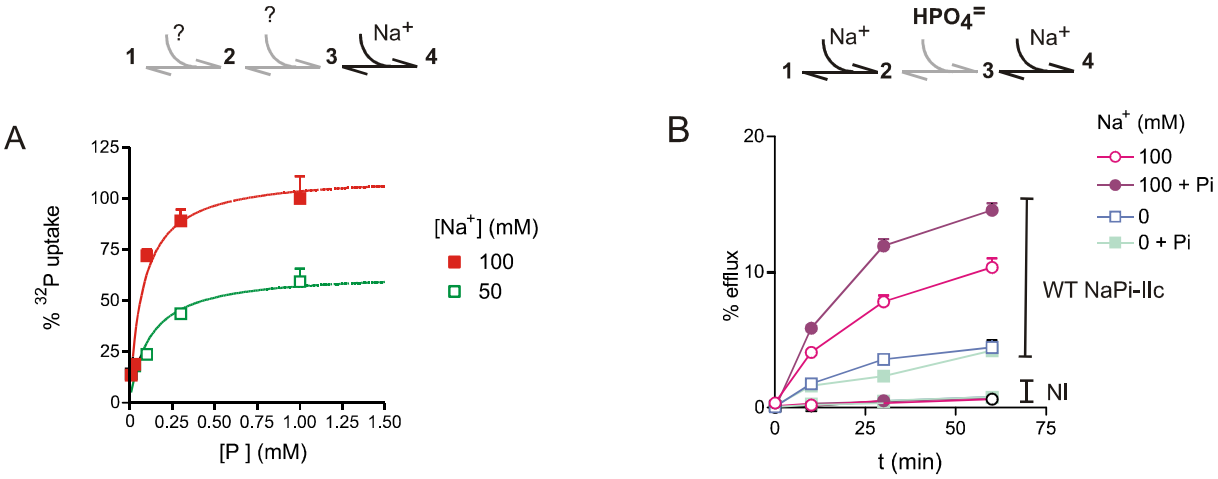


***Figure 22. Uptake and efflux experiments on NaPi-IIc wt***

*A) $P_i$-dependence of WT mediated $^{32}P$ -uptake for different [$Na^+$]. $^{32}P$ uptake was measured at 0.01, 0.03, 0.1, 0.3, 1 mM $P_i$ in presence of $Na^+$ 100mM or $Na^+$ 50 mM and plotted as a function of [$P_i$]. B) Efflux was measured in ND100 or ND0 solution with or without $P_i$ (1mM) and plotted as a function of time. Points have been joined by lines for visualising purposes only. Values are mean ± S.E. (n = 9). Data adapted from [110]*

To further confirm our data we applied fluorometry to test the hypothesis that only one $Na^+$ ion should interact with NaPi-IIc in the absence of $P_i$.

For the proposed fluorescence measurements it was necessary to introduce a novel cysteine that could be easily labelled from the extracellular medium, and which was in a functionally important area of the protein. Based on previous studies, we chose the site Ser-437 in the putative 3rd extracellular loop (corresponding mutation of the S460C in the rNAPi-IIa shown in Figure 19) that is predicted to be a region highly accessible from the extracellular solution.

The S437C mutant was labelled with MTS-TAMRA and we examined $\Delta F$ with increasing [$Na^+$] in the absence of $P_i$. The highest fluorescence was recorded in 0 mM $Na^+$ and this was then progressively quenched as [$Na^+$] increased. These data revealed a sigmoidal relationship between $\Delta F$ and [$Na^+$] and when fitted with the Hill equation the fit predicted a Hill coefficient, $H = 1.8 \pm 0.1$.

Moreover we analysed $\Delta F$ due to the presence in the extracellular solution of 1mM $P_i$ or PFA in 100Na or 0Na. In the absence of $Na^+$ ions in the external medium, both $P_i$ and PFA induced no change in *F* relative to the control condition (0Na). However, in 100Na, when we added 1 mM $P_i$ or 100 mM PFA to the superfusate, we observed an increase of *F* relative to 100Na alone. This suggest that $P_i$ can still bind to the transporters even though the transporter cannot undergo the conformational change necessary to the release of the substrate inside the cells. The fact that $P_i$ and PFA induce the same fluorescence change suggests that the two substrates bind to the same binding site and induce the same conformational change in the protein.

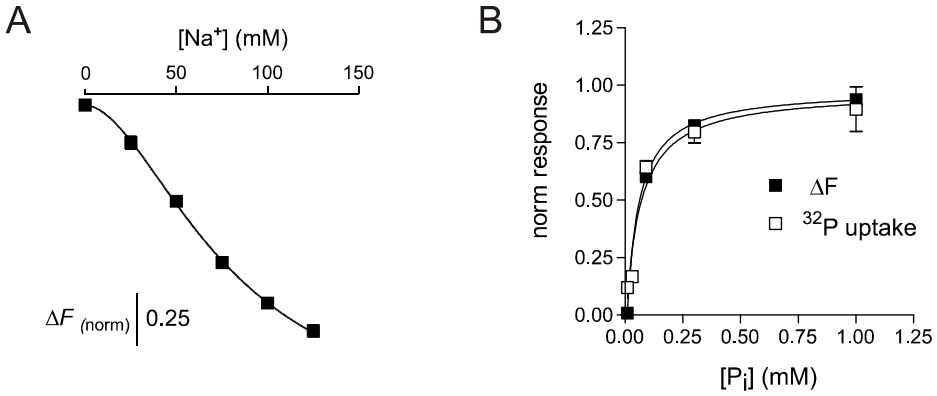


***Figure 23. Substrate dependency of fluorescence changed observed for the S437C mutant.***

*A) Sodium dependence of fluorescence change, B)* $\Delta F$ and $^{32}P$ uptake was recorded at different $P_i$ concentrations (0, 0.1, 0.3 and 1 mM).

On the basis of uptake, efflux and VCF data, we were able to propose the kinetic scheme shown in Fig. 23. Uptake and efflux experiment predict an ordered binding scheme in which $Na^+$ is the first and the last ion that interact with the protein: $Na^+$-Pi- $Na^+$. Fluorescence data confirm this hypothesis but moreover, unexpectedly indicate that more than one $Na^+$ ions interact with the transporter in a cooperative manner. In particular, the Hill coefficient of 1.8 suggests that at least 2 $Na^+$ interact also with the electroneutral NaPi-IIc before $P_i$.

To account for this "extra" $Na^+$ we therefore postulate that the first $Na^+$ ion, which would normally interact with a binding site created by intrinsic charge of the electrogenic isoforms that is lacking in NaPi-IIc, still can bind to the protein (see Fig.). It will remain insensitive to changes in the transmembrane electric field and moreover it will not participate in the stoichiometry coupled cotransport. Interaction of the first $Na^+$ ion with the protein appears to be a necessary condition for the subsequent partial reactions to take place and it can be thought of as a catalytic interaction.

In conclusion, we provide strong evidence that all SLC34 proteins possess the same number of $Na^+$ interaction sites and the principle difference between the electrogenic and electroneutral isoforms is the presence of the charged aspartic acid (indicated with a minus in the cartoon in Fig. 24) that in the former case allows $Na^+$ to interact with the empty carrier in a voltage-dependent manner, thereby conferring voltage dependence to the overall cotransport cycle. The intrinsic mobile negative charge ensures that the outward facing empty carrier conformation is favoured after all substrates are released on the internal face and together with the 1st $Na^+$ interaction represents the "interface" that couples the free energy of the transmembrane electric field to the cotransport cycle. In terms of the cotransport thermodynamics, the electrogenic partial reactions increase the potential concentrating capacity of the protein by two orders of magnitude under physiological conditions compared to the electroneutral isoform.

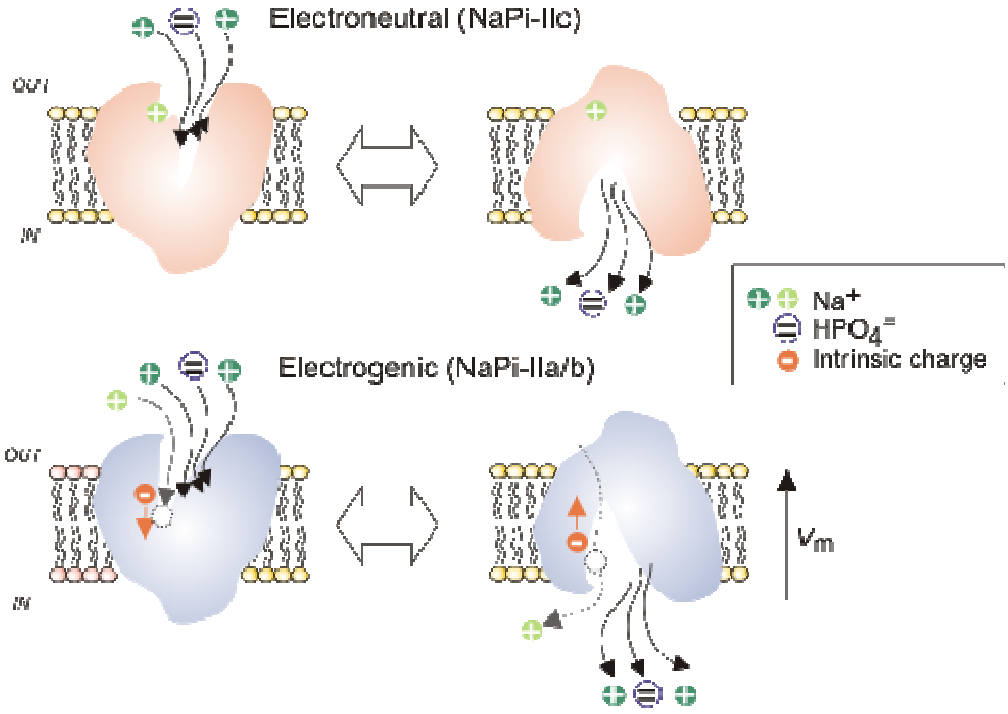

**Figure 24. Cartoon that compares the substrate interactions of NaPi-II electroneutral and electrogenic isoforms.**

## 4.3 Amino acid interactions in the putative transport pathway

After the crystallization of LeuT [29], identification of structure of several other transporter proteins belonging to un-related families [78] [30] [111] has revealed the presence of a common inverted topology motif: an inverted repeat topology in which the respective elements are structurally associated through an apparent twofold symmetry around an axis through the membrane plane. This common architecture defines a central substrate translocation pathway with the substrate binding sites located approximately halfway through the membrane and accessible from either side of the membrane, consistent with the alternating access model for carrier-mediated transport [78] [112] [28]. Pairs of discontinuous helices play a key structure-functional role in this architecture [88] appearing to be involved in substrate recognition and coordination.

Given that many transporters share a common functionality-i.e. coupling to the electrochemical gradient of $Na^+$ to catalyze uphill movement of a specific substrate-it follows that the same architecture may be present in proteins whose 3-D structures have yet to be resolved.

In absence of a crystal structure for the members of the SLC34 family and of sequence similarity with any of the crystallized proteins, predictions of NaPi-II structure are based *ab inititio* prediction algorithms and the application of indirect biophysical techniques (to probe structural accessibility and conformational changes). Analysis of the primary sequence of the different members of the SLC34 family has shown that these proteins can be divided in two halves with high intra-sequence homology [93]. Organization of the protein in two semi-halves was further confirmed by voltage clamp fluorometry studies. Introduction of novel cysteines in the two halves of the protein in fact showed that they undergo complementary conformational changes that lead to the exposure of the binding sites [76].
Identification of the structure of the bacterial aspartate transporter GltPh from *Pryococcus horokoshii* [27] has provided key insight into various aspects of transport. The GltPh structure contains 8 transmembrane domains and two helix-turn-helix motifs, HP1 and HP2, which point toward the center of the membrane from opposite sides. The substrate and ion binding

sites are located close to the point where the tips of HP1 and HP2 meet. Transport is generally believed to involve a mechanism in which the central binding site for the substrate becomes accessible alternately from one side of the membrane or the other during the transport cycle [113]. It was shown the presence of two loops with particular high homology localized between TM 2-3 and TM 7-10 in the three NaPi-II isoforms (Fig. 15). These regions are believed to form two re-entrant loops and they been shown to contain functionally important sites [83] [83, 93]. Modification of novel cysteines with MTS reagents in both loops cause the inhibition of NaPi-IIa mediated co-transport activity, suggesting their role in the formation of the $P_i$ pathway. In accord with this hypothesis, the introduction of two novel cysteines, one in each re-entrant loop, results in the inhibition of $P_i$ induced current, but an unexpected increase in the leak current [71].

To better understand not only the structure but also conformational changes occurring in the protein, we investigated a possible interaction between a pair of cysteines inserted in the re-entrant loop. We have focussed on changes in substrate- and voltage- dependence of the transport function because these are considered strong determinants of implied conformational changes.

A novel cysteine was introduced in the first re-entrant loop at either Ser-155 orAla-175 and this was paired with one in the second re-entrant loop (Ser448) of the fNaPi-IIb isofom. The behavior of single substitutions (S155C, A175C, S448C) and the double mutant (S155C-S448C, A175C-S448C) was analyzed with TEVC and VCF.

*Identification of site involved in the voltage dependence and $Na^+$ interaction*

We focused our initial analysis on the effect of introducing novel cysteines on the normal transport behavior and the consequence of application of MTS reagents. We observed that introduction of single cysteine affected voltage dependence at all three sites. Substitutions at 155 and 448 (S155C, S448C and S155C-S448C mutants) had relatively small effects: in all cases the voltage dependence of $I_{P_i}$ towards resulted shifted toward depolarizing potentials relative to the WT. In contrast, Cys substitution at 175 caused a strong hyperpolarizing shift in $I_{Pi}$ and a reduction of the apparent $Na^+$ affinity compared to the WT and other constructs. The voltage dependence of A175C could be partly restored to the WT behavior by the Ser-Cys substitution at 448 in the double mutant (A175C-S448C).

The changes in steady-state voltage dependence were reflected in the altered pre-steady state charge distribution. Taken together these findings suggested that the residue at this site was an important determinant of voltage dependence and $Na^+$ interaction. In contrast, the weak effect of Cys substitutions at the external facing sites (155, 448) suggested that these sites are not critical determinants of $Na^+$ interactions. The fact that the voltage dependence of A175C could be partly restored to the WT behavior by introducing a Cys in position 448 supports the notion of the putative re-entrant loops forming an integral core region of the protein that defines its transport kinetics.

To understand the functional importance of the selected sites we incubated each mutant in MTS reagents and test for effects on the $P_i$-induced and leak currents. After MTSET incubation all constructs containing Cys448 showed suppression of the co-transport current ($I_{cot}$) but the same leak current ($I_{leak}$). In contrast, the absence of significantly altered steady-state and presteady-state activity for A175C and S155C suggested that the introduced cysteines were either inaccessible from the external medium (A175C) or, if modified, were functionally unimportant (S155C).

Our interpretation of the results obtained with the single mutants containing Cys 448 is that after thiol modification of this site, the remaining NaPi-II electrogenic activity represents the leak mode ($I_{leak}$). $Na^+$ and $P_i$ interactions still occur, however completion of the cotransport cycle is blocked. For all the 3 double mutants containing Cys448, the behavior after MTS treatment was consistent with this model: $I_{cot}$=0 over the range of test potentials applied.

Moreover we observed that, in contrast to S448C, S155C-S448C and A175S-S448C, the magnitude of $I_{leak}$ for A175C-S448C approximately doubled after thiol modification. This suggested that Cys175 can modulate the phenotype of the S448C and hinted at a possible interaction between the 1$^{st}$ re-entrant loop and Cys448.

*Evidence for substrate- and voltage-dependent interactions between re-entrant loops*

In contrast to presteady-state relaxations that reflect global conformational changes as the protein undergoes transitions between states in response to rapid changes in membrane potential, VCF offers the potential to observe local conformational changes in the microenvironment of the fluorophore [34] [35] [24] [98] [97] [99] [76] [74]. In this study we have obtained evidence of interaction of re-entrant loops by comparing the changes in fluorescence under 3 superfusion conditions that allow investigation of the empty carrier

(0Na), empty carrier + $Na^+$ interactions (100Na) and empty carrier + $Na^+$ + $P_i$ interactions (100Na+1$P_i$) induced by voltage steps.

For S155C-S448C, $\Delta F$ in 0Na was nearly identical to that of labelled S155C. As labelled S448C shows no $\Delta F$ under these conditions, this behavior strongly suggested that $\Delta F$ measured for S155C-S448C arises from changes to the microenvironment of the fluorophore at Cys-155 only. In 100Na, both single mutants report $\Delta F$ but with significantly different voltage dependences: the S155C in fact shows a fluorescence signal that saturates at both positive and negative potentials, whereas for S448C $\Delta F$ saturates only at positive potentials. For the double mutant we observe $\Delta F$-$V$ similar S448C in 100Na, namely no saturation at negative potentials. Similarly, when both substrates were present, the behavior of S155C-S448C was also like S448C, which is consistent with the lack of cotransport mode activity for the labelled Cys-448. These findings indicate that the structural changes induced by the labelled Cys448 led to a profound change in the conformational changes reported by the fluorophore at Cys155 when one or both substrates are present, consistent with an interaction between the re-entrant loops.

Although we were unable to detect $\Delta F$ with the A175C under any superfusion conditions, A175C-S448C yielded significant $\Delta F$ that depended on the superfusate. Since we could not detect any fluorescence change from the A175C, we expected, in absence of interaction between the two re-entrant loops, to observe the same fluorescence change for the A175C-S448C as for the S448C. Unexpectedly, when oocytes expressing the double mutant where tested we observed a unique change in the voltage dependence of fluorescence. In 100 mM $Na^+$ the ΔF-V recorded from the S448C was shifted to the right (depolarizing potentials) by the introduction of the second Cys at position 175. Moreover, its behavior in 0Na and 100Na + Pi was the opposite of S448C.

To determine if in the double mutant Cys-448 was the only cysteine that was labeled or $\Delta F$ reflected changes also in the microenvironment of the fluorophore at Cys175, we substituted the Ala-175 with amino acids (Aspartic acid, glutamate, lysine and serine). The only substitution tolerated by the protein was Ala-Ser; for all other mutants, we could not detect any $P_i$-induced current[2].

[2] As no antibodies specific to the flounder NaPi-IIb are available, we were unable to determine if the lack of electrogenic response results from a dysfunction of expressed transporters, or a targeting error.

When tested with the VCF system the A175S-S448C mutant showed a robust change in fluorescence dependent on both the substrate in the extracellular solution and the voltage. When the non-polar Ala at 175 was substituted with a polar Ser, the labelled Cys-448 reported no $\Delta F$ for 0Na and in 100Na, $\Delta F$ $-V$ lay between that of the S448C and the A175C-S448C. This result points to the importance of the side chain at this site as a determinant of the voltage dependence

This observation indicated that substitution of an amino-acid in the first intracellular loop is sufficient to alter the fluorescence recorded from residues in the second reentrant loop.

Since our data strongly suggest a local interaction between the two re-entrant loops we decided to confirm this hypothesis using an independent methodology: crosslinking the two Cys by promoting the formation of a disulphide bridge. The rationale of this approach is that if the two Cys are close enough they can be linked in an oxidating environment. If the two re-entrant loops are involved in the formation of the $P_i$ pathway, cross-linking of the two cysteines should result in a decrease in the mobility of the region with a consequent effect on the $P_i$ induced current. One of the reagents normally used for promoting disulphide bridge formation is $O_2$/Cu(II)(1,10-phenanthroline)$_3$ ($CuPh_3$). The dissolved dioxygen acts as an oxidant and CuPh as a redox catalyst. The system is thought to oxidize by generation of an oxyradical that diffuses to the vicinity of a sulfhydryl and removes an electron, yielding a sulphur radical capable of disulfide formation upon collision with a second thiol or sulphur radical [85]. Disulfide bridges can then be reverted by incubation in a reducing medium like Dithiothreitol (DTT).

We first analysed the effect of incubation with $CuPh_3$ on single and double mutants using $^{32}P$ uptake. Groups of oocytes were incubated in $CuPh_3$ and either assayed functionally after washing or after further incubation in DTT. $CuPh_3$ did not affect $P_i$ uptake of A175C, S155C and S448C indicating that the novel cysteines cannot interact with any of the 11 endogenous cysteines that are present in fNaPi-IIb. $CuPh_3$ reduced $^{32}P$ uptake by 50% for the S155C-S448C and by 40% for the A175C-S448C (Fig.26A). This inhibition could be reversed by subsequent incubation of the oocytes with DTT in agreement with the idea that the inhibition of the transport was due to oxidative crossllinking of the cysteines.

The main limitation of uptake experiments is that membrane voltage cannot be controlled so we decide to investigate the effect of $CuPh_3$ over a wide range of membrane potentials using

TEVC. Since the two re-entrant loops are considered to be involved in substrate translocation we decide to investigate if the composition of the external medium can effect cross-linking. In particular, we compared the effect of incubating in 100Na or 0Na. We were not able to perform the same experiment in 100Na+Pi due to rundown. For the A175C, the S155C and the S448C we did not observe any effect on the $P_i$-induced current independent of the composition of the extracellular solution. In contrast, when we incubated the S155C-S448C and the A175C-S448C mutants in 100Na+$CuPh_3$ we observed a decrease of the $I_{Pi}$ of about 50% and 40% respectively (Fig. 26B). Absence of co-substrate (0Na) significantly protection against the cross-linking of the cysteines (open squares in Fig. 26B).

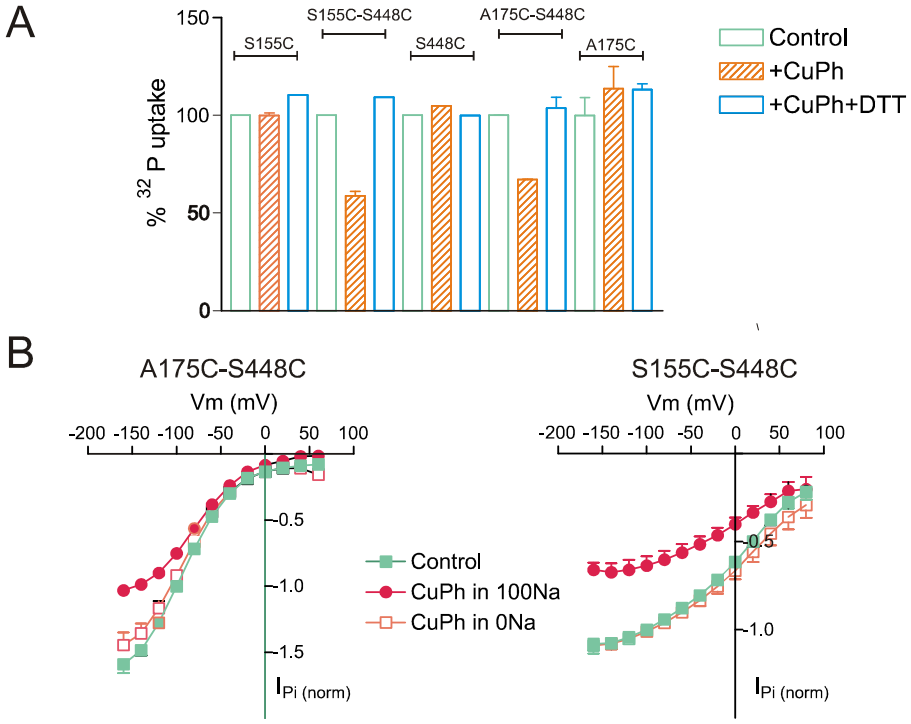


***Figure 26. Effect of CuPh on single and double mutants.***

*a. $^{32}P$ uptake on oocytes expressing flNaPi-IIb single and double mutants. Groups of 12 oocytes were pre-treated with $CuPh_3$ (orange bars) or $CuPh_3$ followed by application of DTT(blue bars) and the amount of 32P inside the single oocytes was compared with untreated oocytes (green bars); b. Effect of $CuPh_3$ was tested over wide range of membrane potentials using TEVC and different incubation solutions (100 mM $Na^+$ in red or 0 mM $Na^+$ in pink) and compared with untreated oocytes (control group in green).*

Taken together our data indicate that the two re-entrant loop can interact during the transport cycle. The interaction shows substrate dependence indicating an important role of the two loops in the formation of the substrate translocation pathway.

## 4.4 Future perspectives

*Determination of electrogenicity/electroneutrality:* one of the main differences among NaPi-II proteins is transport mode that result in electrogenicity or electroneutrality of the protein. The high sequence similarity between the three NaPi-II isoforms led to the obvious question: which residues are involved?

The sequence comparison of NaPi-IIc and NaPi-IIa [75] has shown that the amino acid differences between the electrogenic and electroneutral transporters cluster in 3 areas. Until now the analysis focused on cluster I, and as already described, the substitution of three residues (G195A, S191A and A224D) led to a functional electrogenic NaPi-IIc transporter (AAD NaPi-IIc). The kinetic analysis of the AAD NaPi-IIc had also shown that the properties of the wild type transporter are not completely restored (e.g. $K_{0.5}^{Pi}$, $K_{0.5}^{Na}$) and this means that mutagenesis of other sites would be necessary to establish the typical electrogenic behaviour.

*Structure-function studies on NaPi-IIc:* the discovery of a direct role of NaPi-IIc in the onset of the hereditary hypophosphatemic rickets with hypercalciuria highlighted the physiological role of this protein in the context of $P_i$ homeostasis and regulation. Identification of naturalyl occurring mutations in patients indicate that to better understand the dysfunction associated with them it is necessary to understand the mechanism of function of WT protein and its structural organization. One possible approach is in particular to compare the behavior of NaPi-IIc with that of the electrogenic isoform to obtain information about the conformational changes in the protein.

In the NaPi-IIc WT protein, cysteine scanning mutagenesis is limited by the lack of electrogenic activity that narrow the analysis to the use of radiotracer uptake. A useful tool for studying may be represented by the AAD mutant in which the characteristic of the NaPi-IIc protein are quite well preserved. Novel cysteines in the backbone of the AAD triple mutant can, first, be studied with TEVC to obtain information over a wider range of membrane potentials on $P_i$ and $Na^+$ apparent affinities, pH dependence, voltage dependence and PFA-sensitive currents. Second they can be analyzed with Voltage Clamp Fluorometry to obtain information about conformational changes induced by change in voltage and in substrate concentration.

*Dynamics of the fluorescence:* conformational changes in the protein can be analyzed using different approaches. Information about global conformational changes can be obtained from the analysis of the pre-steady states current whereas local conformational changes from the analysis of florescence emitted by fluorophore attached to specific sites of the protein. Are the two process correlated? To address this question we can introduce novel cysteine in different position of the fNaPi-IIb isoform and compare the fluorescence emitted by each position.

This will allow us to monitor conformational changes from different point of the protein but moreover the analysis of the time dependence of fluorescence change in response to step changes in membrane potential, analogous to pre-seady state charge relaxation, will give us information about the dynamics of the conformational changes.

# BIBLIOGRAPHY


1. Doyle DA, M.C.J., Pfuetzner RA, Kuo A, Gulbis JM, Cohen SL, Chait BT, MacKinnon R., *The structure of the potassium channel: molecular basis of K+ conduction and selectivity.* Science, 1998. **280**(5360): p. 69-77.
2. Aronson, P.S., *Identifying secondary active solute transport in epithelia.* Am J Physiol. , 1981. **240**(1): p. F1-11.
3. Widdas, W.F., *Inability of diffusion to account for placental glucose transfer in the sheep and*
   *consideration of the kinetics of a possible carrier transfer.* . J Physiol, 1952. **118**(1): p. 23–39.
4. Carvelli L, M.P., Blakely RD, Defelice LJ., *Dopamine transporters depolarize neurons by a channel mechanism.* Proc Natl Acad Sci U S A., 2004. **101**(45): p. 16046-51.
5. Galli, A., R.D. Blakely, and L.J. DeFelice, *Norepinephrine transporters have channel modes of conduction.* Proceedings of the National Academy of Sciences of the United States of America, 1996. **93**(16): p. 8671-6.
6. Lester HA, C.Y., Mager S., *Listening to neurotransmitter transporters.* Neuron, 1996. **17**(5): p. 807-10.
7. Petersen CI, D.L., *Ionic interactions in the Drosophila serotonin transporter identify it as a serotonin channel.* Nat. Neurosci., 1999. **2**(7): p. 605-10.
8. Maduke M, P.D., Miller C., *High-level expression, functional reconstitution, and quaternary structure of a prokaryotic ClC-type chloride channel.* J Gen Physiol,, 1999. **114**(5): p. 713-22.
9. Accardi A, M.C., *Secondary active transport mediated by a prokaryotic homologue of ClC Cl- channels.* Nature, 2004. **26**(427): p. 803-7.
10. Dutzler R, C.E., MacKinnon R., *Gating the selectivity filter in ClC chloride channels.* Science, 2003. **300**(5616): p. 108-12.
11. DeFelice, L.J. and T. Goswami, *Transporters as channels.* Annu Rev Physiol, 2007. **69**: p. 87-112.

12. Hediger, M.A., et al., *The ABCs of solute carriers: physiological, pathological and therapeutic implications of human membrane transport proteins. Introduction.* Pflugers Archiv. European Journal of Physiology, 2004. **447**(5): p. 465-8.
13. Wagner CA, F.B., Setiawan I, Lang F, Bröer S, *The Use of Xenopus laevis Oocytes for the Functional Characterization of Heterologously Expressed Membrane Proteins. .* Cell Physiol Biochem 2000. **10**: p. 1-12.
14. Mager, S., et al., *Steady states, charge movements, and rates for a cloned GABA transporter expressed in Xenopus oocytes.* Neuron, 1993. **10**(2): p. 177-88.
15. Wright, E.M., et al., *The sodium/glucose cotransporter (SGLT1).* Society of General Physiologists Series, 1993. **48**: p. 229-41.
16. Forster, I., J. Biber, and H. Murer, *Electrophysiological analysis of renal $Na^+$-coupled divalent anion transporters.* Pharmaceutical Biotechnology, 1999. **12**: p. 251-67.
17. Roux, M.J., R. Martinez-Maza, A. Le Goff, B. Lopez-Corcuera, C. Aragon, and S. Supplisson. , *The glial and the neuronal glycine transporters differ in their reactivity to sulfhydryl reagents. .* J. Biol. Chem., 2001. **276**: p. 17699–17705.
18. Ju, P., K. R. Aubrey, and R. J. Vandenberg., *Zn2+ inhibits glycine transport by glycine transporter subtype 1b.* J. Biol. Chem., 2004. **279**: p. 22983–22991.
19. Aubrey, K.R., A. D. Mitrovic, and R. J. Vandenberg, *Molecular basis for proton regulation of glycine transport by glycine transporter subtype 1b.* Mol. Pharmacol., 2000. **58**: p. 129-135.
20. Cherubino F., B.E., Miszner A, Ghezzi C, Peres A, *Transient Currents in the Glycine Cotransporter GlyT1 Reveal Different Steps in Transport Mechanism.* J Mol Neurosci, 2009.
21. Ravera, S., et al., *Deciphering PiT transport kinetics and substrate specificity using electrophysiology and flux measurements.* American Journal of Physiology-Cell Physiology 2007.
22. Loo, D.D., et al., *Role of Cl- in electrogenic Na+-coupled cotransporters GAT1 and SGLT1.* Journal of Biological Chemistry, 2000. **275**(48): p. 37414-22.
23. Mager, S., et al., *Ion binding and permeation at the GABA transporter GAT1.* Journal of Neuroscience, 1996. **16**(17): p. 5405-14.

24. Loo, D.D., et al., *Conformational changes couple Na+ and glucose transport.* Proceedings of the National Academy of Sciences of the United States of America, 1998. **95**(13): p. 7789-94.
25. Lester, H.A., Y. Cao, and S. Mager, *Listening to neurotransmitter transporters.* Neuron, 1996. **17**(5): p. 807-10.
26. Murakami S, N.R., Yamashita E, Yamaguchi A., *Crystal structure of bacterial multidrug efflux transporter AcrB.* Nature, 2002. **419**(6907): p. 587-93.
27. Yernool D, B.O., Jin Y, Gouaux E., *Structure of a glutamate transporter homologue from Pyrococcus horikoshii.* Nature, 2004. **431**(7010): p. 811-8.
28. Krishnamurthy H, P.C., Gouaux E., *Unlocking the molecular secrets of sodium-coupled transporters.* Nature, 2009. **459**(7245): p. 347-55.
29. Yamashita A., S.S.K., Kawate T., Jin Y., Gouaux E., *Crystal structure of a bacterial homologue of Na+/Cl--dependent neurotransmitter transporters.*, in *Nature*. 2005. p. 215-23.
30. Faham S., W.A., Besserer G.M., Cascio D., Specht A., Hirayama B.A., Wright E.M., Abramson J., *The crystal structure of a sodium galactose transporter reveals mechanistic insights into Na+/sugar symport.* Science 2008. **321**(5890): p. 810-4.
31. Weyand S, S.T., Yajima S, Suzuki S, Mirza O, Krusong K, Carpenter EP, Rutherford NG, Hadden JM, O'Reilly J, Ma P, Saidijam M, Patching SG, Hope RJ, Norbertczak HT, Roach PC, Iwata S, Henderson PJ, Cameron AD., *Structure and molecular mechanism of a nucleobase-cation-symport-1 family transporter.* Science, 2008. **322**(5902): p. 709-13.
32. Karlin, A. and M.H. Akabas, *Substituted-cysteine accessibility method.* Methods in Enzymology, 1998. **293**: p. 123-45.
33. Kaback HR, S.-T.M., Weinglass AB., *The kamikaze approach to membrane transport.* Nat Rev Mol Cell Biol, 2001. **2**(8): p. 610-20.
34. Mannuzzu, L.M., M.M. Moronne, and E.Y. Isacoff, *Direct physical measure of conformational rearrangement underlying potassium channel gating.* Science, 1996. **271**(5246): p. 213-6.
35. Cha, A. and F. Bezanilla, *Structural implications of fluorescence quenching in the Shaker K+ channel.* Journal of General Physiology, 1998. **112**(4): p. 391-408.

36. Andersen J, K.A., Bang-Andersen B and Strømgaard K, *Recent advances in the understanding of the interaction of antidepressant drugs with serotonin and norepinephrine transporters*

Chem. Commun, 2009: p. 3677 - 3692.

37. Su, A., et al., *A multi-substrate single-file model for ion-coupled transporters.* Biophysical Journal, 1996. **70**(2): p. 762-77.

38. Lu, C.C. and D.W. Hilgemann, *GAT1 (GABA:Na+:Cl-) cotransport function. Kinetic studies in giant Xenopus oocyte membrane patches.* Journal of General Physiology, 1999. **114**(3): p. 445-57.

39. Lu, C.C. and D.W. Hilgemann, *GAT1 (GABA:Na+:Cl-) cotransport function. Steady state studies in giant Xenopus oocyte membrane patches.* Journal of General Physiology, 1999. **114**(3): p. 429-44.

40. Hilgemann, D.W. and C.C. Lu, *GAT1 (GABA:Na+:Cl-) cotransport function. Database reconstruction with an alternating access model.* Journal of General Physiology, 1999. **114**(3): p. 459-75.

41. Singh SK, P.C., Yamashita A, Gouaux E., *A competitive inhibitor traps LeuT in an open-to-out conformation.* Science, 2008. **322**(5908): p. 1655-61.

42. Shils ME, S.M., Ross AC, Caballero B, Cousins RJ., *Modern Nutrition in Health and Disease.* , ed. t.e.B.L.W. Wilkins. 2006. 211-222.

.

43. Berndt T, K.R., *Novel mechanisms in the regulation of phosphorus homeostasis.* Physiology and Behavior, 2009. **24**: p. 17-25.

44. Berndt T, K.F.G., *Renal regulation of phosphate excretion* The Kidney. 2511-2532.

45. Takeda E, Y.H., Nashiki K, Sato T, Arai H, Taketani Y., *Inorganic phosphate homeostasis and the role of dietary phosphorus.* J Cell Mol Med, 2004. **8**(2): p. 191-200.

46. Biber J, H.N., Forster I, Murer H., *Regulation of phosphate transport in proximal tubules.* Pflugers Arch, 2009. **458**(1): p. 39-52.

47. Ullrich KJ, M.H., *Sulphate and phosphate transport in the renal proximal tubule.* Philos Trans R Soc Lond B Biol Sci., 1982. **299**(1097): p. 549-58.

48. Baumann K, d.R.C., Roinel N, Rumrich G, Ullrich KJ., *Renal phosphate transport: inhomogeneity of local proximal transport rates and sodium dependence.* Pflugers Archiv 1975. **356**

(4): p. 287-98.

49. Custer M, M.F., Schlatter E, Greger R, Garcia-Perez A, Biber J, Murer H, *Localization of NaPi-1, a Na-Pi cotransporter, in rabbit kidney proximal tubules. I. mRNA localization by reverse transcription/polymerase chain reaction.* Pflugers Archiv, 1993. **424**: p. 203-9.

50. Busch AE, S.A., Waldegger S, Wagner CA, Zempel G, Broer S, Biber J, Murer H, Lang F. , *Expression of a renal type I sodium/phosphate transporter (NaPi-1) induces a conductance in Xenopus oocytes permeable for organic and inorganic anions.* Proc Natl Acad Sci U S A., 1996. **93**(11): p. 5347-51.

51. Custer M, L.M., Biber J, Murer H, Kaisslling *Expression of Na/Pi cotransport in rat kidney: Localization by RT-PCR and immunohistochemistry.* Am J Physiol Renal Physiol, 1994. **266**: p. F767-F774

52. Hilfiker, H., et al., *Characterization of a murine type II sodium-phosphate cotransporter expressed in mammalian small intestine.* Proceedings of the National Academy of Sciences of the United States of America, 1998. **95**(24): p. 14564-9.

53. van Zeijl, M., et al., *A human amphotropic retrovirus receptor is a second member of the gibbon ape leukemia virus receptor family.* Proc Natl Acad Sci U S A, 1994. **91**(3): p. 1168-72.

54. Johann, S.V., J.J. Gibbons, and B. O'Hara, *GLVR1, a receptor for gibbon ape leukemia virus, is homologous to a phosphate permease of Neurospora crassa and is expressed at high levels in the brain and thymus.* J Virol, 1992. **66**(3): p. 1635-40.

55. Kavanaugh, M.P., et al., *Cell-surface receptors for gibbon ape leukemia virus and amphotropic murine retrovirus are inducible sodium-dependent phosphate symporters.* Proceedings of the National Academy of Sciences of the United States of America, 1994. **91**(15): p. 7071-5.

56. Villa-Bellosta, R., et al., *The Na+/Pi cotransporter piT-2 (SLC20A2) is expressed in the apical membrane of rat renal proximal tubules and regulated by dietary Pi.* American Journal of Physiology-Renal Physiology, 2008.

57. Radanovic, T., et al., *Topology of the type IIa Na+/P(i) cotransporter.* J Membr Biol, 2006. **212**(1): p. 41-9.

58. Hoffmann, N., M. Thees, and R. Kinne, *Phosphate transport by isolated renal brush border vesicles.* Pflugers Arch, 1976. **362**(2): p. 147-56.

59. Burckhardt, G., H. Stern, and H. Murer, *The influence of pH on phosphate transport into rat renal brush border membrane vesicles.* Pflugers Arch, 1981. **390**(2): p. 191-7.

60. Samarzija, I., V. Molnar, and E. Fromter, *pH--dependence of phosphate absorption in rat renal proximal tubule.* Proc Eur Dial Transplant Assoc, 1983. **19**: p. 779-83.

61. Forster, I.C., et al., *Forging the link between structure and function of electrogenic cotransporters: the renal type IIa $Na^+/P_i$ cotransporter as a case study.* Progress in Biophysics and Molecular Biology, 2002. **80**(3): p. 69-108.

62. Forster, I.C., et al., *Proximal tubular handling of phosphate: A molecular perspective.* Kidney Int, 2006. **70**(9): p. 1548-59.

63. Virkki, L.V., et al., *Phosphate transporters: a tale of two solute carrier families.* Am J Physiol Renal Physiol, 2007. **293**(3): p. F643-54.

64. Segawa, H., et al., *Growth-related renal type II Na/Pi cotransporter.* Journal of Biological Chemistry, 2002. **277**(22): p. 19665-72.

65. Busch, A., et al., *Electrophysiological analysis of $Na^+/P_i$ cotransport mediated by a transporter cloned from rat kidney and expressed in Xenopus oocytes.* Proceedings of the National Academy of Sciences of the United States of America, 1994. **91**(17): p. 8205-8.

66. Forster, I.C., D.D. Loo, and S. Eskandari, *Stoichiometry and $Na^+$ binding cooperativity of rat and flounder renal type II $Na^+$-$P_i$ cotransporters.* American Journal of Physiology, 1999. **276**(4 Pt 2): p. F644-9.

67. Szczepanska-Konkel, M., et al., *Phosphonocarboxylic acids as specific inhibitors of Na+-dependent transport of phosphate across renal brush border membrane.* Journal of Biological Chemistry, 1986. **261**(14): p. 6375-83.

68. Busch, A.E., et al., *Properties of electrogenic $P_i$ transport by a human renal brush border $Na^+/P_i$ transporter.* Journal of the American Society of Nephrology, 1995. **6**(6): p. 1547-51.

69. Forster, I., et al., *The voltage dependence of a cloned mammalian renal type II $Na^+/P_i$ cotransporter (NaPi-2).* Journal of General Physiology, 1998. **112**(1): p. 1-18.

70. Andrini, O., et al., *The leak mode of type II Na(+)-P(i) cotransporters.* Channels (Austin), 2008. **2**(5): p. 346-357.

71. Kohler, K., et al., *Transport function of the renal type IIa $Na^+/P_i$ cotransporter is codetermined by residues in two opposing linker regions.* Journal of General Physiology, 2002. **120**: p. 693-703.

72. Lambert, G., et al., *Cysteine mutagenesis reveals novel structure-function features within the predicted third extracellular loop of the type IIa $Na^+/P_i$ cotransporter.* Journal of General Physiology, 2001. **117**(6): p. 533-46.

73. Forster, I.C., et al., *Electrophysiological characterization of the flounder type II $Na^+/P_i$ cotransporter (NaPi-5) expressed in Xenopus laevis oocytes.* Journal of Membrane Biology, 1997. **160**(1): p. 9-25.

74. Virkki, L.V., H. Murer, and I.C. Forster, *Voltage clamp fluorometric measurements on a type II $Na^+$-coupled $P_i$ cotransporter: shedding light on substrate binding order.* Journal of General Physiology, 2006. **127**: p. 539-555.

75. Bacconi, A., et al., *Renouncing electrogenicity is not free of charge: switching on electrogenicity in a $Na^+$-coupled phosphate cotransporter.* Proceedings of the National Academy of Sciences of the United States of America, 2005. **102**: p. 12606-11.

76. Virkki, L.V., H. Murer, and I.C. Forster, *Mapping conformational changes of the type IIb $Na^+/P_i$ cotransporter by voltage clamp fluorometry.* Journal of Biological Chemistry, 2006. **281**: p. 28837-28849.

77. Bergwitz, C., et al., *SLC34A3 Mutations in Patients with Hereditary Hypophosphatemic Rickets with Hypercalciuria Predict a Key Role for the Sodium-Phosphate Cotransporter NaPi-IIc in Maintaining Phosphate Homeostasis.* Am J Hum Genet, 2006. **78**(2): p. 179-92.

78. Abramson J, W.E., *Structure and function of Na(+)-symporters with inverted repeats.* Curr Opin Struct Biol., 2009. **19**(4): p. Curr Opin Struct Biol.

79. Werner, A. and R.K. Kinne, *Evolution of the Na-$P_i$ cotransport systems.* American Journal of Physiology, 2001. **280**(2): p. R301-12.

80. Virkki, L.V., et al., *Functional characterization of two naturally occurring mutations in the human sodium-phosphate cotransporter type IIa.* Journal of Bone and Mineral Research, 2003. **18**(12): p. 2135-41.

81. Ehnes, C., et al., *Structure-function relations of the first and fourth extracellular linkers of the type IIa $Na^+/P_i$ cotransporter: II. Substrate interaction and voltage dependency of two functionally important sites.* Journal of General Physiology, 2004. **124**: p. 489-503.

82. Virkki, L.V., et al., *Substrate interactions in the human type IIa sodium-phosphate cotransporter (NaPi-IIa).* American Journal of Physiology, 2005. **288**: p. F969-F981.

83. Lambert, G., et al., *Properties of the mutant Ser-460-Cys implicate this site in a functionally important region of the type IIa $Na^+/P_i$ cotransporter protein.* Journal of General Physiology, 1999. **114**(5): p. 637-52.

84. Ghezzi, C., H. Murer, and I.C. Forster, *Substrate interactions of the electroneutral Na+-coupled inorganic phosphate cotransporter (NaPi-IIc).* J Physiol, 2009. **587**(Pt 17): p. 4293-307.

85. Careaga C.L., F.J.J., *Thermal motions of surface alpha-helices in the D-galactose chemosensory receptor. Detection by disulfide trapping.* J Mol Biol., 1992. **226**(4): p. 1219-1235.

86. Abramson, J. and E.M. Wright, *Structure and function of Na(+)-symporters with inverted repeats.* Curr Opin Struct Biol, 2009. **19**(4): p. 425-32.

87. Forrest, L.R. and G. Rudnick, *The rocking bundle: a mechanism for ion-coupled solute flux by symmetrical transporters.* Physiology (Bethesda), 2009. **24**: p. 377-86.

88. Screpanti, E. and C. Hunte, *Discontinuous membrane helices in transport proteins and their correlation with function.* J Struct Biol, 2007. **159**(2): p. 261-7.

89. Abramson J, S.I., Kasho V, Verner G, Kaback HR, Iwata S., *Structure and mechanism of the lactose permease of Escherichia coli.* Science, 2003. **301**(5633): p. 610-5.

90. Dutzler, R., et al., *X-ray structure of a ClC chloride channel at 3.0 A reveals the molecular basis of anion selectivity.* Nature, 2002. **415**(6869): p. 287-94.

91. Lolkema, J.S. and D.J. Slotboom, *Classification of 29 families of secondary transport proteins into a single structural class using hydropathy profile analysis.* J Mol Biol, 2003. **327**(5): p. 901-9.

92. Lolkema, J.S. and D.J. Slotboom, *The major amino acid transporter superfamily has a similar core structure as Na+-galactose and Na+-leucine transporters.* Mol Membr Biol, 2008. **25**(6-7): p. 567-70.

93. Kohler, K., et al., *Identification of functionally important sites in the first intracellular loop of the NaPi-IIa cotransporter.* American Journal of Physiology, 2002. **282**(4): p. F687-96.

94. Virkki, L.V., et al., *Functionally important residues in the predicted 3rd transmembrane domain of the type IIa sodium-phosphate co-transporter (NaPi-IIa).* Journal of Membrane Biology, 2005. **206**(3): p. 227-38.

95. Ehnes, C., et al., *Structure-function relations of the first and fourth predicted extracellular linkers of the type IIa $Na^+$/Pi cotransporter: I. Cysteine scanning mutagenesis.* Journal of General Physiology, 2004. **124**(5): p. 475-88.

96. Kohler, K., et al., *Essential cysteine residues of the type IIa $Na^+/P_i$ cotransporter.* Pflugers Archiv. European Journal of Physiology, 2003. **446**(2): p. 203-10.

97. Larsson, H.P., et al., *Fluorometric measurements of conformational changes in glutamate transporters.* Proceedings of the National Academy of Sciences of the United States of America, 2004. **101**(11): p. 3951-6.

98. Li, M. and H.A. Lester, *Early fluorescence signals detect transitions at mammalian serotonin transporters.* Biophysical Journal, 2002. **83**(1): p. 206-18.

99. Meinild, A.K., et al., *Fluorescence studies of ligand-induced conformational changes of the $Na^+$/glucose cotransporter.* Biochemistry, 2002. **41**(4): p. 1250-8.

100. Castagna, M., et al., *Interaction between lysine 102 and aspartate 338 in the insect amino acid cotransporter KAAT1.* Am J Physiol Cell Physiol, 2007. **293**(4): p. C1286-95.

101. Ryan, R.M., A.D. Mitrovic, and R.J. Vandenberg, *The chloride permeation pathway of a glutamate transporter and its proximity to the glutamate translocation pathway.* J Biol Chem, 2004. **279**(20): p. 20742-51.

102. Tao, Z., et al., *Ligand effects on cross-linking support a conformational mechanism for serotonin transport.* J Biol Chem, 2009. **284**(49): p. 33807-14.

103. Zomot, E., Y. Zhou, and B.I. Kanner, *Proximity of transmembrane domains 1 and 3 of the gamma-aminobutyric acid transporter GAT-1 inferred from paired cysteine mutagenesis.* J Biol Chem, 2005. **280**(27): p. 25512-6.

104. Kohler, K., et al., *The functional unit of the renal type IIa Na+/Pi cotransporter is a monomer.* Journal of Biological Chemistry, 2000. **275**(34): p. 26113-20.

105. Gisler, S.M., et al., *Monitoring protein-protein interactions between the mammalian integral membrane transporters and PDZ-interacting partners using a modified split-ubiquitin membrane yeast two-hybrid system.* Mol Cell Proteomics, 2008. **7**(7): p. 1362-77.

106. Larkin M.A., B.G., Brown N.P., Chenna R., McGettigan P.A., McWilliam H.*, Valentin F.*, Wallace I.M., Wilm A., Lopez R.*, Thompson J.D., Gibson T.J. and Higgins D.G., *ClustalW and ClustalX version 2.* Bioinformatics, 2007. **23**(21): p. 2947-2948.

107. Huang X., M.M., *A time-efficient, linear-space local similarity algorithm.* Adv. Appl. Math, 1991. **12**: p. 337-357

108. Loo, D.D., et al., *A kinetic model for secondary active transport*, in *Membrane Transport and Renal Physiology*, H.E. Layton and A.M. Weinstein, Editors. 2002, Springer. p. 65-84.

109. Murer, H., et al., *Proximal tubular phosphate reabsorption: molecular mechanisms.* Physiological Reviews, 2000. **80**(4): p. 1373-409.

110. Ghezzi C, M.H., Forster IC., *Substrate interactions of the electroneutral Na+-coupled inorganic phosphate cotransporter (NaPi-IIc).* J Physiol, 2009. **587**(Pt17): p. 4293-307.

111. Huang Y, L.M., Song J, Auer M, Wang DN., *Structure and mechanism of the glycerol-3-phosphate transporter from Escherichia coli.* Science, 2003. **301**(5633): p. 616-20.

112. Forrest L.R., R.G., *The Rocking Bundle: A Mechanism for Ion-Coupled Solute Flux by Symmetrical Transporters.* Physioogy, 2009. **24**: p. 377-386.

113. Jardetzky, *Simple allosteric model for membrane pumps.* Nature, 1966. **211**(5052): p. 969-70.

# CURRICULUM VITAE

## Personal Information

Date of birth: 12.12.1982
Place of birth: Cittiglio (VA), Italy
Nationality: Italian
Work address: University of Zürich, Institute of Physiology, Winterthurerstr. 190,
CH-8056, Zürich, Switzerland
Tel: 0041-(0)44635541
E-mail: chiara.ghezzi@access.uzh.ch

## Education

- 2006 (December) University of Zürich, Faculty of MNF, Institute of Physiology, PhD (in progress)
- 2006 (October) University of Insubria Varese, Faculty of Biology. Master degree in Biological Sciences. Supervisor Prof. Antonio Peres.
  Title: Transient currents in the glycine neuronal transporter GlyT2 reveal steps in transport mechanism.

  Mark: 110 cum laude/110.

- 2004 (December) University of Insubria Varese, Faculty of Biology. Bachelor degree in Biological Sciences. Supervisor Prof. Antonio Peres
  Title: Construction of vectors for the expression of fusion proteins between two high homologus transporters.

  Mark:110/110

- 2001 High School, Liceo Scientifico Istituto di Istruzione "Edith Stein" Gavirate (VA)

## Work Experience

- May-December 2004. 8 months course in the Laboratory of Cellular and Molecular Physiology Dept. of Structural and Functional Biology-University of Insubria-Varese.
  "Introduction of point mutations and constructon of vector expressing fusion proteins between KAAT1 and CAATCH1".

- January-October 2006. 9 months course in the Laboratory of Cellular and Molecular Physiology Dept. of Structural and Functional Biology-University of Insubria-Varese. "Electrophysiologycal characterization of the neuronal glycine transporter GlyT2".

## Publications

Cherubino F, Bossi E, Miszner A, Ghezzi C, Peres A. (2010) Transient currents in the glycine cotransporter GlyT1 reveal different steps in transport mechanism. *J Mol Neurosci; 41(2:243-51).*

Ghezzi C, Murer H, Forster IC. (2009) Substrate interactions of the electroneutral $Na^+$-coupled inorganic phosphate cotransporter (NaPi-IIc). *J. Physiol.* 587 (17): 4293-307.

Andrini O, Ghezzi C, Murer H, Forster IC. (2008) The leak mode of type II Na(+)-P(i) cotransporters. Channels (Austin). 2(5).

# ACKNOWLEDGEMENTS

Heini Murer for giving me the possibility to work in his lab and Ian Forster whose encouragement, guidance and support from the initial to the final level enabled me to develop an understanding of the subject,

The other members of my thesis committee, Bruno Stieger and Gerhard Burckhardt for the interesting discussions and support during and after thesis meetings,

All the present and past members of the J-floor for the nice environment.
In particular Soline, Stine/Alex and Gerti for the nice time spent in the office, Paola, Sonja and Simone for all the technical advises, Abhi for all the morning walks to the lab, Nadine and Tina for writing and correcting the German summary, Silvia and Daniel.

All the Italian friends: Sara, Fra, Ale, Maurizio, Valeria, Marta, Luca, Isa, Luca, Chiara, Erika, Paolo, Marco,

All the "Swiss" friends, Andrea, Andrea, Davide, Benoit, Sandra, Francois for all the lunches, dinners, apero shared. You have made my time in Zurich simply great!

Olga with whom I shared the dark and cold lab for many afternoons for all the working (and more important not working) discussions, the shared ideas and the nice time spent and Carlo for simply always been there.

Special thanks to my family, without whom I could not have gotten this far, for all the support and encouragement.